UNIVERSIDAD DE CHILE
FACULTAD DE CIENCIAS FÍSICAS Y MATEMÁTICAS
DEPARTAMENTO DE GEOLOGÍA.

"CENOZOIC UPLIFT AND EXHUMATION ABOVE THE SOUTHERN PART OF THE FLAT SLAB SUBDUCTION SEGMENT OF CHILE (28.5-32°S)"

TESIS PARA OPTAR AL GRADO DE DOCTORA EN CIENCIAS MENCIÓN GEOLOGÍA

MARÍA PÍA RODRÍGUEZ MONTECINOS

PROFESOR GUIA:
REYNALDO CHARRIER GONZÁLEZ
PROFESOR CO-GUIA:
SÉBASTIEN CARRETIER
MIEMBROS DE LA COMISION:
MARCELO FARÍAS THIERS
VICTOR MAKSAEV JURCHUC
RODRIGO RIQUELME SALAZAR

SANTIAGO DE CHILE
AÑO 2013

Resumen de la Tesis para optar al grado de Doctora en Ciencias mención Geología
Por: María Pía Rodríguez Montecinos
Fecha: 13/12/2013
Profesor Guía: Reynaldo Charrier González

"CENOZOIC UPLIFT AND EXHUMATION ABOVE THE SOUTHERN PART OF THE FLAT SLAB SUBDUCTION SEGMENT OF CHILE (28.5-32°S)"

The following dissertation presents the results of a tectonic geomorphology study in the Andes of north-central Chile (28.5-32°S), whose main goal is to reconstruct the landscape evolution in this region since the Neogene. The timing of main uplift is constrained by the geomorphological analysis of paleosurfaces, U-Pb zircon geochronology of tuffs overlying these surfaces and cosmogenic isotopes. The spatial and temporal variations of exhumation are determined through the combination of apatite fission track (AFT) and apatite (U-Th)/He (AHe) thermochronology and U-Pb zircon geochronology studies on both sides of the topographic front separating the Coastal from the Frontal Cordillera.

Mesozoic rocks from the Coastal Cordillera show AFT ages between ~ 60 and 40 Ma and AHe ages around 30 Ma, while Paleozoic and Cenozoic rocks in the Frontal Cordillera show AFT and AHe ages between ~ 40 and 8 Ma and ~ 20 to 6 Ma respectively. According to thermal models of AFT and AHe data, the Coastal Cordillera was accelerated exhumed at ~ 65-50 Ma and suffered little exhumation since ~ 45 Ma to, at least, ~ 30 Ma. Accelerated exhumation at ~ 65-50 Ma correlates with Late Mesozoic to Early Cenozoic compressive tectonic events. North of 31°S, thermal models indicate that exhumation started before ~ 30 at the foot of the topographic front. Here, exhumation was continuous until shortly after 20 Ma, whereas episodes of accelerated exhumation at ~ 22-18 Ma and around 7 Ma affected the areas to the east. Oligocene exhumation is correlated with the denudation of an Eocene mountain range located along the axis of the Frontal Cordillera, whereas episodes of accelerated exhumation during the Early and Late Miocene correlate with the progressive tectonic inversion of an Oligocene extensional intra-arc basin developed along the international border between Chile and Argentina. South of 31°S, accelerated exhumation at the foot of the front occurred around 22-16 Ma and extended until the Late Miocene in the areas to the east. Accelerated exhumation at 22-16 Ma in this area correlates with the tectonic inversion of an extensional volcano-sedimentary basin, known as the Abanico Basin, which developed from ~ 32°S to the south.

Prior to the Early Miocene, an extensive pediplain sloping down to sea-level dominated the landscape of the present-day Coastal Cordillera. North of 31°S, this surface developed west of the Eocene mountain range recognized by the thermochronometric data, whereas south of 31°S it developed to the west of an Eocene magmatic belt. The development of this pediplain is consistent with thermochronometric data indicating that the present-day Coastal Cordillera was little exhumed during the Eocene to Late Oligocene. The pediplain was offset during the Early Miocene, leading to uplift of ~ 1.1 km of the eastern Coastal Cordillera with respect to the western Coastal Cordillera. Later, during the Late Miocene, the entire Coastal Cordillera was uplifted ~ 1.2 km. A new planation surface formed by shore platforms along the coast and by strath terraces and pediments along the main river valleys in the western Coastal Cordillera developed between the Early to Middle Pleistocene and was finally uplifted post-500 ka.

The major uplift stages and/or patterns of accelerated exhumation identified for the Early Miocene, the Late Miocene and the Middle Pleistocene correlate with episodes of increased contractional deformation widely recognized throughout the entire Central Andes, starting after the break-up of the Farallon into the Nazca and Cocos Plate, at 25 Ma.

Resumen de la Tesis para optar al grado de Doctora en
Ciencias mención Geología
Por: María Pía Rodríguez Montecinos
Fecha: 13/12/2013
Profesor Guía: Reynaldo Charrier González

"ALZAMIENTO Y EXHUMACIÓN CENOZOICOS SOBRE LA ZONA SUR DEL SEGMENTO DE SUBDUCCIÓN PLANA DE CHILE (28,5-32°S)"

En esta tesis se incluyen los resultados y conclusiones de un estudio de geomorfología tectónica en los Andes del Norte Chico de Chile (28,5-32°S) orientado a reconstruir la evolución del relieve desde el Neógeno en esta región. Los periodos de alzamiento principales son determinados a través del análisis geomorfológico de paleosuperficies, la geocronología de U-Pb circón en niveles volcánicos sobreyacientes y la isotopía cosmogénica. A su vez, las variaciones espaciales y temporales en la exhumación son determinadas al combinar la termocronología de trazas de fisión en apatito (AFT) y de (U-Th)/ He en apatito (AHe) con geocronología de U-Pb circón a ambos lados del frente topográfico que separa la Cordillera de la Costa de la Cordillera Frontal.

Las rocas mesozoicas de la Cordillera de la Costa presentan edades AFT entre ~ 60 y 40 Ma y edades AHe alrededor de 30 Ma, mientras que las rocas Paleozoicas y Cenozoicas de la Cordillera Frontal presentan edades AFT y AHe entre ~ 40 y 8 Ma y ~ 20 y 6 Ma, respectivamente. El modelamiento termal de los datos termocronológicos indica que la Cordillera de la Costa fue exhumada de manera acelerada entre ~ 65-50 Ma y fue escasamente exhumada desde ~ 45 Ma hasta, al menos, ~ 30 Ma. La exhumación acelerada entre ~ 65-50 Ma se correlaciona con eventos tectónicos compresivos del Mesozoico Tardío al Cenozoico Temprano. Al norte de 31°S, los modelos termales indican que la exhumación comenzó antes de ~ 30 Ma al pie del frente topográfico. En este sector la exhumación fue continua hasta los 20 Ma, mientras que hacia el este, episodios de exhumación acelerada tuvieron lugar ~ 22-18 Ma y ~ 7 Ma. La exhumación Oligocena se correlaciona con la denudación de una cadena montañosa Eocena ubicada a lo largo del eje de la Cordillera Frontal, mientras que los episodios de exhumación durante el Mioceno Temprano y Tardío se correlacionan con la inversión tectónica progresiva de una cuenca extensional de intra-arco que se desarrolló durante el Oligoceno a lo largo del actual límite de Chile y Argentina. Al sur de los 31°S, el frente topográfico se habría desarrollado con posterioridad, comenzando con un episodio de exhumación acelerada entre los 22-16 Ma al pie del frente topográfico y extendiéndose hasta el Mioceno Tardío hacia el este. La exhumación acelerada a 22-16 Ma en esta área se correlaciona con la inversión de la cuenca extensional de Abanico, desarrollada entre el Eoceno y el Oligoceno al sur de 32°S.

Antes del Mioceno Temprano, una extensa pediplanicie cercana al nivel del mar dominaba el paisaje de la actual Cordillera de la Costa. Al norte de los 31°S, esta superficie se desarrolló al pie de un relieve Eoceno reconocido por la termocronología, mientras que al sur de los 31°S lo hizo al oeste del cordón magmático Eoceno. El desarrollo de esta pediplanicie es consistente con la escasa exhumación sufrida por la Cordillera de la Costa durante el Eoceno-Oligoceno Tardío como indican los datos termocronológicos. La pediplanicie fue dislocada durante el Mioceno Temprano generando el alzamiento de ~ 1,1 km de la Cordillera de la Costa oriental respecto de la Cordillera de la Costa occidental. Posteriormente, durante el Mioceno Tardío, tanto la Cordillera de la Costa oriental como la occidental fueron alzadas ~ 1,2 km. Una nueva superficie de bajo relieve formada por plataformas de abrasión marina a lo largo de la costa y por *strath terraces* y pedimentos al interior de los valles principales se desarrolló entre el Pleistoceno Temprano y Medio en la Cordillera de la Costa occidental y finalmente se alzó ~ 150 m post-500 ka.

Los principales eventos de alzamiento y/o exhumación acelerada identificados para el Mioceno Temprano, el Mioceno Tardío y el Pleistoceno Medio se correlacionan con episodios de incremento de la deformación contraccional reconocidos ampliamente a lo largo de los Andes Centrales, que habrían comenzado después del quiebre de la placa de Farallón en las placas de Nazca y Cocos a los 25 Ma.

A los que luchan

Agradecimientos

Y a pesar que este proceso se ha prolongado bastante más de lo que “debería”, me di cuenta al final que me daba hasta un poco de pena terminar. Por un lado está la incertidumbre de encontrar efectivamente un espacio (que me acomode) dentro del mundo científico-académico. Pero sobretodo me pasa que voy a extrañar la vida del postgrado y a las personas con las que por alguna razón u otra he compartido durante estos años y a quienes agradezco a continuación.

A mis profesores Reynaldo y Sébastien por su apoyo constante y por estar siempre dispuestos a discutir y a escucharme “pelar el cable” de los pedimentos, la termo, el Incaico, el Cretácico, etc y tratar de orientarme en el mar de información que estaba tratando de ordenar en mi cabeza y que muchas veces me tenía a medio ahogar. Me sorprendí al descubrir que aparte de científicos excepcionales eran personas excepcionales. Reynaldo con toda su experiencia, pero con una amplitud mental que se la quisieran muchos veinteañeros! y Seb el loco optimista que te hace creer que es posible escribir un artículo en una semana. De verdad aprecio muchísimo el tiempo y las experiencias compartidas con Uds. También me gustaría agradecer al resto de los académicos y geólogos que me ayudaron a realizar este trabajo: Steph, Vincent, Joseph, Luisa, Marcelo, Felipe Tapia, Germán y Chala.

A mis amigos que son o fueron del postgrado. A mis viejas amigas Juice y Kiti por el cariño y el apoyo de siempre. A mis grandes amigos que tal vez no serían tan amigos si no hubiésemos confluido en este doctorado: la Viole, el Feli, la Pame y el Sergio, por las discusiones de política, las confidencias, los carretes, los consejos y por la geo-poesía.

Y finalmente agradezco a mis padres, Patricio y Pía, y a mis hermanitos Bicho, Patito y Tomi por TODO. Esta tesis está dedicada a Uds. (y a los que luchan!!!).

INDEX OF CONTENTS

TABLE INDEX

CHAPTER 1

CHAPTER 2

CHAPTER 3

CHAPTER 4

CHAPTER 5

FIGURE INDEX

CHAPTER 1

CHAPTER 2

Article: Cenozoic erosion in the Andean forearc in Central Chile (33°–34°S): Sediment provenance inferred by heavy mineral studies.

CHAPTER 3

Article: Thermochronometric contraints on the development of the Andean topographic front in north central Chile (28.5-32ºS).

CHAPTER 4

Article: Geochronology of pediments and marine terraces in north-central Chile and their implications for Quaternary uplift in the Western Andes.

CHAPTER 5

Chapter 6

Chapter 1- INTRODUCTION

1.1 Preface

The morphology of active mountain belts results from the interplay between tectonic processes, which deform the lithosphere and result in uplifted regions of the Earth's surface; and erosional/ exhumational processes, which are mainly controlled by climate and rock type (Strecker et al., 2007). Thus, determining the timing of main uplift and related exhumational patterns is crucial to unravel the mechanisms by which orogens deform, rise and evolve.

The Central Andes (Fig.1.1a; 15-34°S) are characterized by along-strike variations of topography and the amount of shortening. Some authors have proposed that tectonic features like variations in subduction angle (Isacks, 1988; Jordan et al., 1983), slab age (Ramos et al., 2004); upper-plate initial thickness, composition and structure (Ramos et al., 1996; Lamb et al., 1997; Tassara and Yáñez, 2003; Giambiagi et al., 2012) or the subduction of oceanic ridges (Yáñez et al., 2001; Cembrano et al., 2003; Spikings et al., 2008) would be the dominant factors controlling north-to-south variations in Andean evolution. On the contrary, other authors have privileged climatic/erosional factors as latitudinal variations of erosion type and magnitude (Montgomery et al., 2001) or the climatically-driven variations of the amount of available sediment within the trench (e.g. Lamb and Davis, 2003), as responsible for such changes in the present-day Andean topography and shortening.

In particular, the Andes of north-central Chile between 28 and 32°S are a key area for understanding of geodynamics along the Central Andes as they correspond to a region of main transition of the present-day seismotectonic and climatic conditions. Moreover, it is believed that this region would record major latitudinal changes in the pre-Neogene geological evolution along the Central Andes.

The seismotectonic setting in north-central Chile is characterized by the nearly flat subduction (~ 10°) of the Nazca under the South American plate, contrary to the rest of the Central Andes where the subduction angle is ~ 30° (Fig. 1.1a). Slab-shallowing started after ~ 13 Ma, when magmatism markedly decreased throughout the studied region (Bissig et al., 2001; Kay and Mpodozis, 2002) and reached its peak around 9 Ma, when andesitic magmatism essentially ended in north-central Chile (Kay and Mpodozis, 2002). It is thought that flat subduction may be the consequence of subduction of the Juan Fernández oceanic ridge (Fig. 1a; Yáñez et al., 2001) or may be related to the combine effects of the trenchward motion of the Río de la Plata craton and slab retreat (Manea et al., 2012). With respect to its climatic conditions, the Andes of north-central Chile between 28 and 32°S show a semiarid climate. This climate is transitional between the hyperarid conditions of the Atacama Desert, to the north of 27°S; and the more humid conditions of Central Chile, to the south of 33°S (Fig. 1.1b). This transitional climate is reflected in a strong latitudinal precipitation gradient that would have been acquired after the Middle Miocene through the combination of several events including glaciations in West Antartica, formation of the Humboldt Current and Andean uplift itself (Le Roux, 2012). Finally, with respect to the pre-Neogene geological evolution, it is believed that during the Eocene to Oligocene contractional deformation led to the development of the Incaic Range to the north of 31°S (Pineda and Emparán, 2006; Pineda and Calderón, 2008; Bissig and Riquelme, 2010; Arriagada et al., in press), while an extensional volcano-sedimentary basin, known as the Abanico Basin (Charrier et al., 2002), developed south of 32°S.

The particular tectonic and climatic conditions prevailing in north-central Chile would have induced variations in landscape development with respect to the areas to the north of 27°S and to the south of 33°S, as no Central Depression is recognized to the east of the Coastal Cordillera in this region (Fig.1.1a and c). Some authors indicated that the highly compressive regime related to flat-subduction may be responsible for the absence of Central Depression in north-central Chile (Jordan et al., 1983). Other authors concluded that the Central Depression would be mostly an erosional feature south of 33°S (Farías et al., 2008). The same authors suggested that in north-central Chile its absence would be the consequence of larger uplift and dryer conditions than south of 33°S, together with the abundance of erosion resistant lithologies (Farías, 2007). However, determining the main tectonic and/ or climatic factors controlling landscape evolution in this region has been hampered by the scarcity of available geochronological/ thermochronological constrains on uplift/ exhumation timing.

The timing for main uplift events in north-central Chile has been studied mostly in the area of the Frontal Cordillera along the international border between Chile and Argentina at 29-30°S (Bissig et al., 2002). There, the age of a series of uplifted paleosurfaces is constrained by geochronological dating of overlying tuffs. Three pulses of tectonic uplift were recognized for the Early to Middle Miocene, the Middle Miocene and the Late Miocene (Bissig et al., 2002). This is in good agreement with structural data from Cenozoic volcano-sedimentary units exposed along the international border between Chile and Argentina that indicate that this area suffered contractional deformation throughout the entire Miocene (Winocur, 2010). Similarly, geochemical data of these units points to a transition to a more compressive tectonic regime during the Early to Middle Miocene, followed by Late Miocene re-equilibration of magmas with higher-pressure assemblages (Kay and Mpodozis, 2002; Litvak et al., 2007). However, it is unclear if the areas to the west, namely, the rest of the Frontal Cordillera and/ or the Coastal Cordillera, were also uplifted progressively during the Miocene or during a Late Miocene pulse as proposed for the forearc of southern Perú (Schildgen et al. 2007), northern Chile (Hoke et al. 2007; Jordan et al., 2010) and central Chile (Farías et al., 2008). Moreover, the possibility exists that significant Pliocene to Pleistocene uplift would have affected the Coastal Cordillera as Miocene to Pliocene marine deposits and Pleistocene wave-cut marine terraces are emerged along the coast of north-central Chile (Le Roux et al., 2005, 2006; Saillard et al., 2009; Regard et al., 2010). With respect to exhumation patterns, only preliminary apatite fission track (AFT) thermochronological data exists for the region of north-central Chile (Cembrano et al., 2003). According to these authors, tectonic-related exhumation within the Frontal

Cordillera mostly occurred between the Early and Middle Miocene and it would be the consequence of the north-to-south migration of the Juan Fernández ridge from 16 to 12 Ma throughout north-central Chile (Cembrano et al., 2003). However, the same authors also recognized periods of accelerated exhumation during the Late Eocene and the Late Miocene, which cannot be related to the Middle to Late Miocene migration of the Juan Fernández ridge throughout north-central Chile. Thus, other tectonic and/ or climatic factors would have influence exhumation patterns and landscape development during the Cenozoic in this area.

The present doctoral thesis intends to combine medium to large scale geomorphic analysis of paleosurfaces with geochronologic and thermochronometric data to constrain the timing of uplift and related exhumation within the Coastal and Frontal Cordilleras. The main goal is to reconstruct the short to long-term landscape evolution in north-central Chile (28- 32°S). The questions I propose to address are: When did the Andes rise in north-central Chile? Is the Late Miocene flattening of the slab responsible for this uplift? Did precipitation gradients influence landscape development? And are pre-Neogene variations in uplift and exhumation important in determining north-to-south differences in the subsequent landscape evolution throughout north-central Chile?

The thesis is organized as follows.

Chapter 1 corresponds to a general overview regarding the available theoretical framework for analyzing landscape evolution processes and the methodologies used here for determining uplift timing and the exhumational response of the orogen, including geomorphic analysis, cosmogenic isotope techniques and low temperature thermochronology.

Chapter 2 corresponds to the geotectonic and geological framework of the study region. This chapter includes an article entitled “Cenozoic erosion in the Andean forearc of Central Chile 33-34°S: Sediment provenance inferred by heavy mineral studies” included in the Geological Society of America Special Publication n° 487, Mineralogical and Geochemical Approaches to Provenance. In this article, the heavy minerals analysis of Cenozoic sediments exposed along the coastal area of central Chile is used to reconstruct erosional paths and determining which faults were active during the different time periods defined by changes in provenance. This study concerns the area of central Chile, which is located immediately to the south of the geographic region analyzed in the present thesis. This region displays present-day seismotectonic and climatic conditions that are contrasting with the ones observed in the studied region. The subduction angle is 30°S and a humid climate prevails (Fig. 1a and b). Moreover, the Central Depression is observed to the east of the Coastal Cordillera (Fig. 1a and c). Thus, the analysis of Cenozoic erosion in this area gives valuable information to be considered in the evaluation of the tectonic/ climatic factors controlling landscape evolution in north-central Chile.

Chapter 3 analyses Late Mesozoic and Cenozoic tectonic-related exhumational patterns in north-central Chile. It introduces us to the big picture of Andean evolution in this area at the scale of hundreds of kilometers and tens of millions of years. It includes a manuscript entitled “Thermochronometric contraints on the development of the Andean topographic front in north central Chile (28.5-32ºS)” which was submitted to *Tectonics* in October 2013. In this article, the timing of tectonic-related exhumation throughout the Frontal and Coastal Cordilleras is determined using U-Pb zircon geochronology and low temperature thermochronology of Apatite Fission Track (AFT) and U-Th/He in apatite (AHe) of intrusive and metamorphic rocks.

Chapter 4 analyses Quaternary uplift along the Coastal Cordillera in north-central Chile. The timing of uplift during the Quaternary is determined through the study of an extensive planation surface exposed within the main river valleys and the coastal area and now uplifted ca.150-100 m above the present-day thalwegs and sea-level. Chapter 4 includes an article published in January 2013 in *Geomorphology* entitled “Geochronology of pediments and marine terraces in north-central Chile and their implications for Quaternary uplift in the Western Andes”. In this article, geomorphic mapping and ^{10}Be/ ^{26}Al cosmogenic dating are used to constrain the development and the timing of uplift of the mentioned planation surface. This surface corresponds to the lowest and the youngest of an assemblage of five paleosurfaces that dominates the landscape of the present-day Coastal Cordillera and the western Frontal Cordillera in north-central Chile. The geomorphic mapping and dating results obtained in this article are taken again in chapter 5 in order to constrain the evolution of entire paleosurface assemblage.

Chapter 5 analyses the Neogene to Quaternary history of uplift and incision of paleosurfaces from the Coastal Cordillera and the western Frontal Cordillera in north-central Chile. It includes an article accepted for publication in the *Geological Society Special Publication*: *Geodynamic Processes in the Andes of central Chile and Argentina*. The article is entitled “Neogene to Quaternary landscape evolution to the west of the topographic front in north-central Chile (28- 32°S): Interplay between tectonic and erosional processes”. In this work, the geomorphic analysis of uplifted paleosurfaces is combined with U-Pb zircon geochronology of overlying tuffs to reconstruct the Neogene landscape evolution in north-central Chile (28-32°S) to the west of the main topographic front. The obtained results are discussed considering the cosmogenic ages presented in chapter 4 for the youngest of the paleosurfaces exposed within the Coastal Cordillera and available geochronologic data for paleosurfaces described near the international border between Chile and Argentina (Bissig et al., 2002; Nalpas et al., 2009). Finally, the roles that tectonic and erosional processes may have played on the development of the present-day topography in north-central Chile are suggested. Chapter 5 also includes the results and a brief discussion regarding ^{21}Ne analysis of one of the paleosurfaces described in the mentioned article.

Finally, chapter 6 corresponds to a final discussion and conclusions of the present thesis.

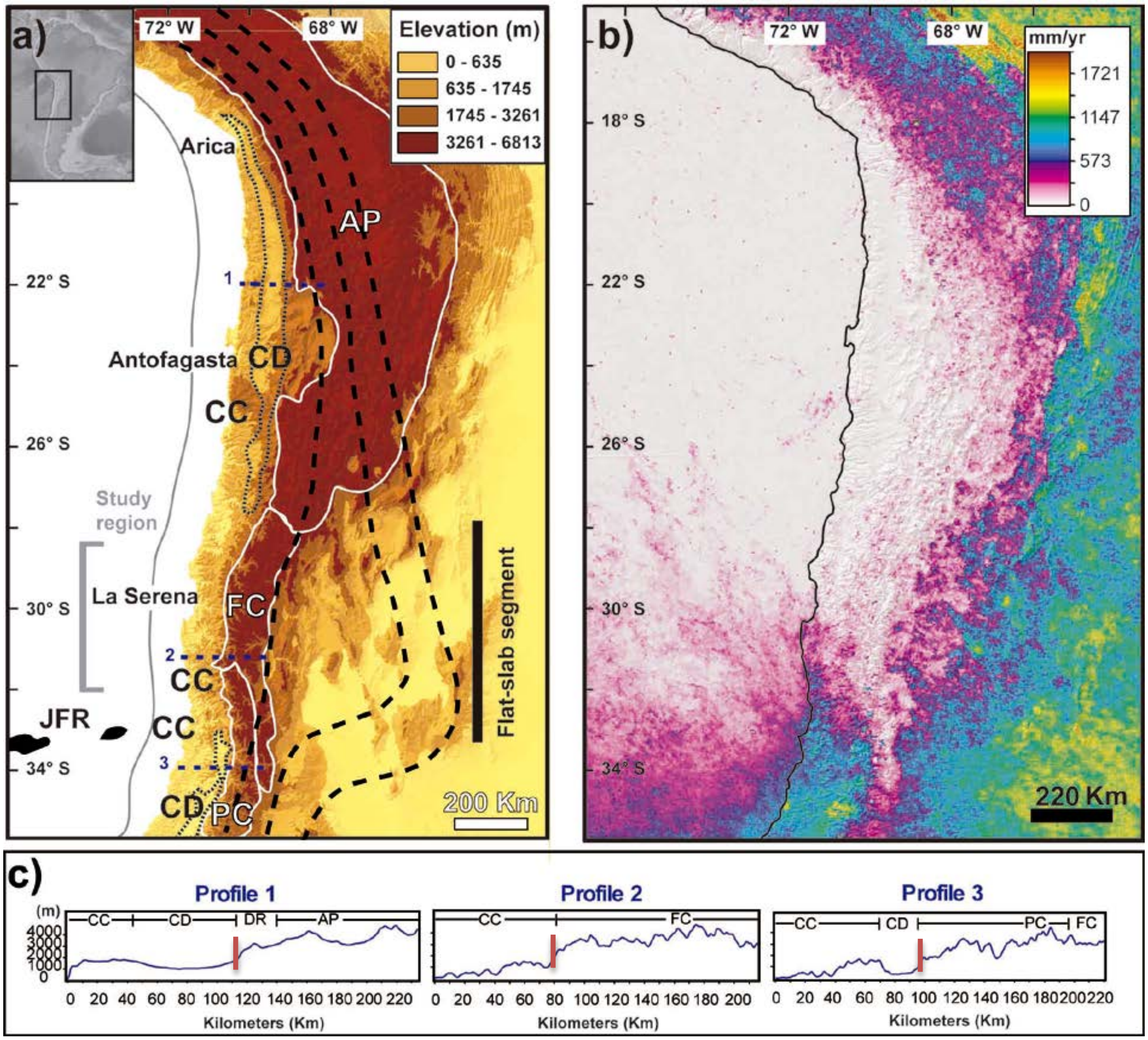

Fig. 1.1. a) Main morphostructural units and tectonic setting of the western Central Andes (15-34°S). Dashed black lines mark the contours of depth of the Nazca Plate underneath the South America Plate at 100, 150 and 200 km (Cahill and Isacks, 1992). Grey solid line marks the position of the trench. b) Shaded relief image map color-coded for mean annual precipitation from Kenji Matsuura and Cort J. Willmott (2011) world database available at http://climate.geog.udel.edu/~climate/html_pages/download.html. c) Topographic profiles showing the absence of Central Depression in the studied region. Trace in Fig 1.1a. CC= Coastal Cordillera, CD= Central Depression, AP=Altiplano-Puna (including the Western and Eastern Cordilleras), FC= Frontal Cordillera, PC= Principal Cordillera and DR= Domeyko Range. Red lines mark the position of the topographic front.

1.2 Theoretical Framework

1.2.1 What controls landscape evolution?

As previously stated, the morphology of active mountain ranges results from the interplay between tectonics, which deforms and uplifts regions of the Earth's surface, and climate that together with rock type modulates the efficiency of erosion (Fig. 1.2).

Tectonics in subduction margins could uplift regions of the Earth's surface mainly through crustal thickening by shortening (e.g. Mc Quarrie, 2002), delamination at the base of the crust and/or the upper mantle (e.g. Garzione et al., 2006), lower crustal flow (e.g. Isacks 1998) and/or underthrusting of crustal material along terrane boundaries (Isacks 1998, Farías et al., 2010; Muñoz et al., 20013). The tectonic uplift generated by these mechanisms can directly influence erosion as it elevates areas of the Earth's surface with respect to regional base level, increasing river gradients (Fig. 1.2A) and, consequently, enhancing fluvial incision and transport rates (Burbank, 2002). Higher incision rates along main channels would destabilize the entire drainage basin, increasing slope across valley walls (Fig. 1.2A) and leading to a rise in mass wasting and sediment supply into rivers (e.g. Burbank and Anderson, 2001). In shorter time scales, earthquakes are able to trigger landslides within unconsolidated or highly fractured rocks (Fig. 1.2B), increasing sediment load and erosion rates at a month to year scale (e.g. Hovius et al., 2011). Tectonic uplift can also indirectly affect erosion through changes in climate. On a regional scale, it has been proposed that when tectonics elevates large areas of the Earth's surface (e.g. Tibetan Plateau) to altitudes where temperatures are markedly lower (Fig. 1.2C), changes on hemispheric-scale atmospheric circulation may occur (e.g. Ruddiman et al., 1997). These changes could have a profound impact on erosional patterns. Locally, a higher topography reached by tectonic uplift can lead to orographically-induced precipitation windward and to rain-shadow effects leeward (Fig. 1.2C, Willet, 1999; Roe, 2005). Consequently, fluvial incision rates would increase windward and diminish leeward due to the higher/lower discharge (Fig. 1.2D). In high elevation mountains, tectonic uplift can control the dominant erosion type, as alpine glaciation (Fig. 1.2E) would only occur once topography reaches certain elevation threshold (Fig. 1.2C, Whipple et al., 1999).

Besides the already mentioned orographic controlled precipitation, rain-shadow and glaciation effects, climate strongly influences erosion as it controls vegetation, which is thought to stabilize soil, leading to lower runoff and base flows (Fig.1.2 F, Iroumé et al., 2005). In turn, erosion influences climate on a global scale through the carbon cycle (Fig.1.2 G). Weathering of silicate rocks is one of the mechanisms balancing the entering of CO_2 into the atmosphere and the capture of CO_2 in carbonate rocks (Raymo and Ruddiman, 1992). Erosion causes exposure of fresh rock that would be later available for chemical erosion and allows burial of biomass within sedimentary basins reducing the amount of carbon participating in the cycle.

Feedbacks between erosion and tectonics are expected as erosion may strongly influence deep earth processes as it redistributes mass across Earth's surface, affecting the state of stress and strain rates within the crust. A change on lithostatic stresses within the crust triggered by erosion (Fig. 1.2H) would lead to isostatic uplift as the crust has to re-equilibrate within the surrounding mantle in response to the new loading conditions (e.g. Molnar and England, 1990). However, if erosional fluxes outpace crustal thickening rate, mean elevation and orogenic area are expected to be progressively reduced (Fig. 1.2I), leading to a progressive decrease in sediment and erosional fluxes (Fig. 1.2I). In tectonic settings as a foreland basin, erosion is actually able to control the locus of deformation. This is because a rise in loading conditions due to enhanced deposition (Fig. 1.2H) would promote shifting of deformation fronts towards areas where lithostatic stress is lower (Willett, 1999). For the particular case of the Andes, it has been proposed that erosion, and ultimately climate, would control the amount of deformation as shear stresses at the plates interface are influenced by the amount of sediment in the trench available to be subducted that finally acts as a lubricant for interplate slip (Lamb and Davis, 2003).

Key factors controlling the efficiency of erosional processes that are usually underestimated correspond to the lithology and the internal structure of rocks. Soft or highly fractured lithological units and lithological or structural discontinuities are easier to erode than homogeneous and/or hard rocks. As the spatial distribution of rocks exposed at surface change through time, erosion rates could also vary temporarily and spatially throughout the orogen (Fig. 1.2J), eventually affecting the locus of deformation. For example, through time deep crystalline rocks are likely to be exhumed and crop out in an orogen where erosion rates are largely due to high precipitation (Willet, 1999; Beaumont et al., 2001). Because crystalline rocks are highly resistant to erosion, lithostatic stresses would increase, promoting deformation to migrate towards the external portion of the orogen (Fig. 1.2H; Hilley et al., 2004). As the rheology of the crust relates deformation and/ or deformation rates to loading conditions, the pre-existing rheological state of the crust likely influences the deformation history during orogenesis (Hilley and Coutand, 2010). For example, it has been shown that previous geology can largely influence structural styles as reactivation of preexisting normal faults in crystalline basement has resulted in hybrid thick-and thin-skinned deformation in some areas of the Andes (Fig. 1.2K; Ramos et al., 1996; Giambiagi et al., 2003).

Finally, it is possible to conclude that the interaction between tectonics and climate is complex as feedbacks may occur between both types of processes and because this interaction is strongly controlled by the geological setting in which they evolve. Therefore, in order to understand the geomorphic features of landscape it is necessary to identify and discriminate the climatic from the tectonic signal of the processes that took place in both the short-term and the long term, but also to have a deep knowledge of the geological scenario in which these interactions have taken place. However, it is also important to consider that if both processes are coupled, it would be mostly impossible to discriminate among their respective signals.

1.2.2 How to study landscape evolution?

Tectonic Geomorphology corresponds to the study of the interplay between tectonic and surface processes that shape landscape in regions of active deformation at time scales ranging from days to millions of years (Burbank and Anderson, 2001). Initially, the lack of adequate methods for establishing chronological constrains on landscape evolution and quantification of geomorphic processes prevented from major development in this subject. However, over the last decades several advances have been made in this field and new analytical methods have emerged allowing the dating of landform formation and constraining of its subsequent evolution. Among them some of the most widely used are cosmogenic dating and low temperature thermochronology. Finally, geomorphic and morphometric analysis has consolidated as an effective tool in the study of the interplay between surface/ rock uplift and climate-driven erosional patterns (e.g. Montgomery et al, 2001; Clark et al., 2004, 2006; Hoke et al., 2007; Farías et al., 2008; Hoke and Garzione, 2008)

As concluded in the previous section, in order to study landscape evolution it is necessary to identify the climatic and the tectonic signals of the processes that took place in both the short and the long term. However, it is difficult to identify and differentiate between both signals as feedbacks may exist in the interplay between tectonic and climatic processes. Therefore, the study of their outcomes, namely uplift and erosion/ exhumation, is therefore crucial to understand how mountain building and topographic rise occur.

1.2.3 How to constrain uplift timing and magnitude?

1.2.3.1 Geomorphic analysis

From the perspective of tectonic geomorphology, the first thing to search for in the field in order to determine the timing and amount of uplift corresponds to features of the landscape that have been displaced from their original position due to tectonics. In order to obtain a reliable measure of the amount of displacement it is first necessary to establish the pre-deformational geometry of such features. Uplifted geomorphic markers correspond to identifiable geomorphic features or surfaces which provide a reference frame against which to gauge differential or absolute deformation (Burbank and Anderson, 2001). The best geomorphic markers are readily recognizable landforms, surfaces or linear trends of known original geometry and age and high preservation potential with respect to the time scale of the tectonic processes involved (Burbank and Anderson, 2001). As it very frequently occurs that these conditions are not fully accomplished, significant effort must be put in determining the age and the original geometry of the marker. Examples of uplifted geomorphic markers have been described for tectonic processes spanning different time and spatial scales. For example, regionally extended (~ tens of Kms) subplanar continental erosion surfaces formed during the Miocene have been widely described for the Central Andes of southern Perú (Tosdal et al., 1984; Quang et al., 2005) (Fig. 1.3a). As in order to inhibit incision these surfaces necessarily formed next to a lower base level and are now located hundreds of meters above present-day thalwegs, they have been generally interpreted as uplifted features due to forearc regional surface uplift. In a much shorter spatial scale (~ meters to tens of meters) and in a different tectonic setting, alluvial terraces in the Gobi-Altay Mountains in Mongolia are directly offset by reverse-oblique faults at the scale of the Pleistocene (Fig. 1.3b).

The medium-scale geomorphology of north-central Chile is characterized by the ubiquitous presence of low relief surfaces at high elevations (see chapter 4; Paskoff, 1970; Bissig et al., 2002; Garrido, 2009; Urresty, 2009) whose morphology resembles the subplanar paleosurfaces described for southern Perú. This type of surfaces have been described throughout the Central Andes forearc not only in southern Peru, but also in northernmost Chile, the southern Atacama desert and central Chile (e.g Mortimer, 1973; Tosdal et al., 1984; Dunai et al., 2005; Nisshizumi et al., 2005; Riquelme et al., 2007; Evenstar et al., 2009; Hoke et al., 2007; Quang et al., 2005; Farías et al., 2005; 2008). They are characterized by their low relief and slope, indicating that they once formed near its base level; but are presently located at high elevations and strongly incised due to base level fall. However, it has been shown that these type of surfaces can also be formed at high elevations (above sea-level) if downstream aggradation occurs, allowing the establishment of a new and higher base level (Babault et al., 2005). Thus, their present-day location at high elevations does not necessarily implicate that they were uplifted. However, if is possible to demonstrate that the fall in base level pointed out by incision is due to surface uplift, these surfaces can be used to establish geochonological constrains on uplift timing. In turn, this would depend on whether the substrate of these surfaces is suitable for cosmogenic age determinations (e.g. Hall et al., 2008) and/ or if datable material is found covering them (Clark et al., 1967; Mortimer, 1973; Tosdal et al., 1984; Bissig et al., 2002; Quang et al., 2005).

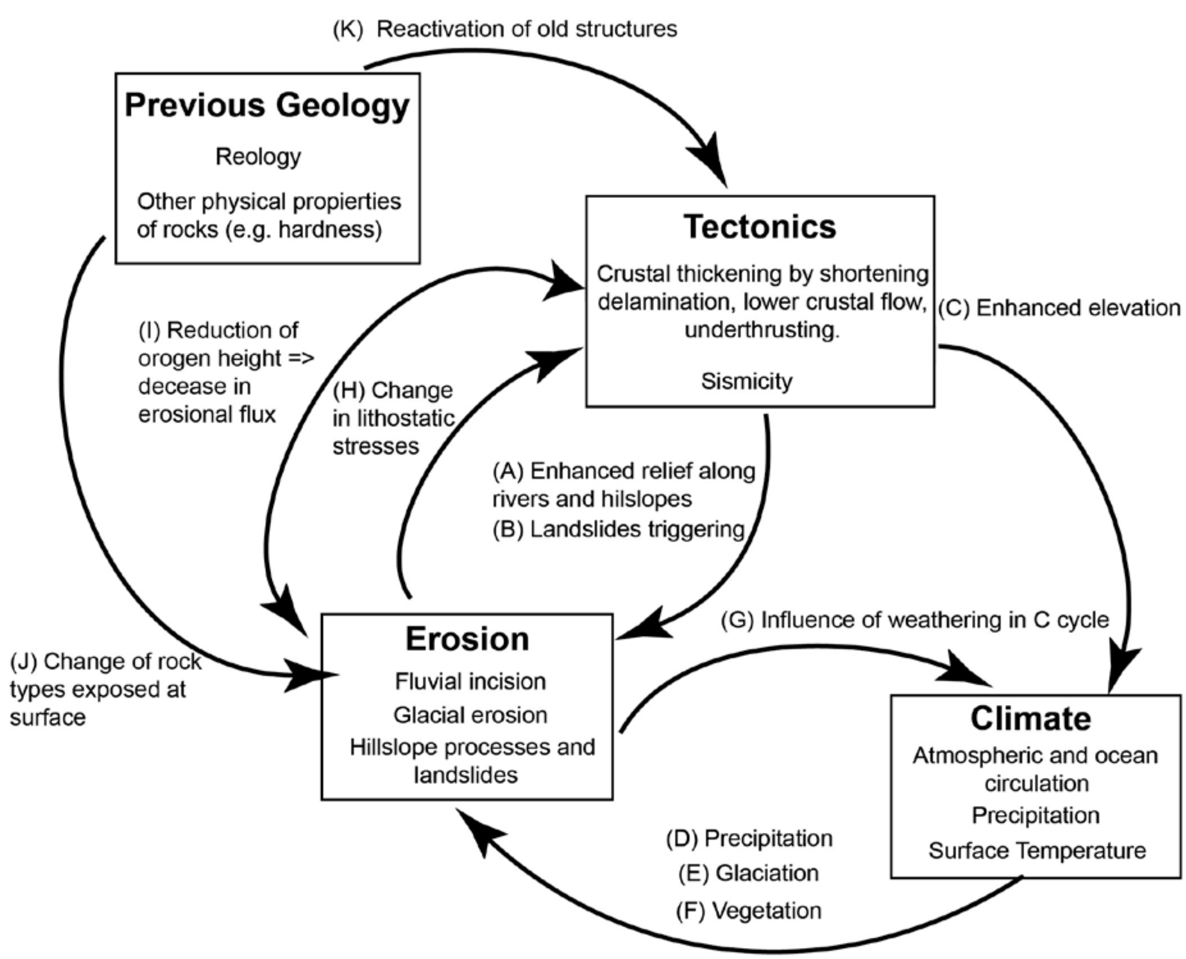

Fig. 1.2. Feedbacks and interactions between tectonics, climate, erosion and geological processes. Modified from Willet et al. (2006).

In the present thesis, five levels of low relief/slope surfaces have been recognized throughout the Coastal Cordillera and some areas of the Frontal Cordillera in north-central Chile. In this study, these surfaces are used as uplifted geomorphic markers to determine the age of main uplift throughout the studied region. The methodology applied for the identification and the geomorphic analysis of these surfaces is explained in detail in the article included in chapter 5. Among the five levels, two levels were dated indirectly through U-Pb zircon geochronology on tuffs overlying these surfaces. The results, discussion and conclusions regarding the obtained ages are included in the mentioned article. Another low relief/slope level was dated using cosmogenic ^{21}Ne. A brief discussion and conclusion with respect to the significance of the results obtained through ^{21}Ne dating are included in chapter 5. Finally, the lowest and younger uplifted geomorphic marker throughout the study region was dated using ^{10}Be/ ^{26}Al cosmogenic isotopes. The results and interpretations of the cosmogenic dating are presented in the article included in chapter 4. In the following paragraphs, the principles of the use of cosmogenic isotopes for obtaining surface exposure ages and erosion rates are explained.

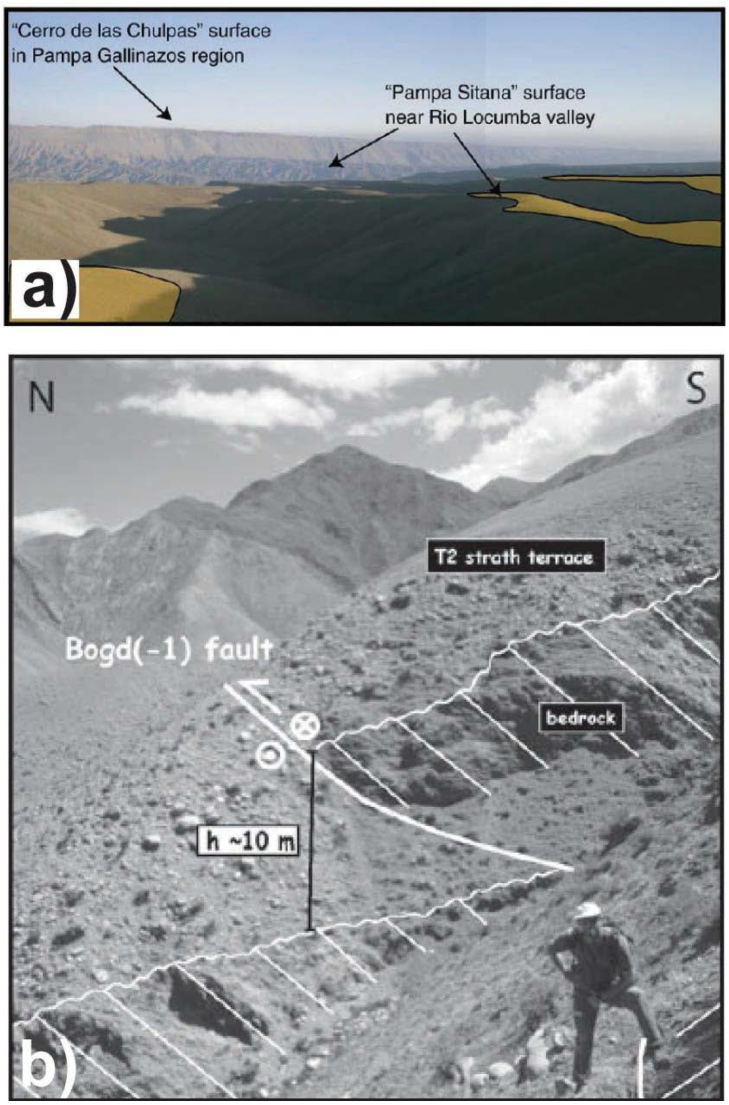

Fig.1.3. Examples of uplifted geomorphic markers. a) Low relief continental planation surfaces from southern Perú (Hall et al. 2008). b) Strath/alluvial terraces offset by faults in the Gobi-Altay Mountains in Mongolia (Vasallo, et al, 2007).

1.2.3.2 Cosmogenic nuclides

One of the most widely used techniques for determining surface exposure ages correspond to cosmogenic isotopes. Cosmogenic isotopes are produced by the interaction of cosmic rays with the nucleus of atoms within extraterrestrial material, such as meteorites; and within terrestrial material, such as the particles of the atmosphere or minerals within rocks at the Earth's surface. Primary cosmic radiation correspond to high-energy particles (0.1 – 10 GeV nucleon^{-1}), primarily protons (83%), a small fraction of alpha particles (13%), minor heavier nuclei (1%) and electrons (3%) (Smart and Shea, 1985). They are produced outside the Solar System and are thought to mainly originate within our galaxy. In order to reach our atmosphere primary cosmic rays need to pass through the Earth's magnetic field (Fig. 1.4a). The magnetic field is shaped by electric currents in the Earth's core and the solar wind (Fig. 1.4a). Primary cosmic radiation will undergo complicated trajectories in the magnetic field and may even be prevented from getting access to our atmosphere, if their energy is too low. The particles that manage to reach the Earth's atmosphere interact with the nucleus of atoms in the air, generating a cascade of ionized particles and electromagnetic radiation known as secondary cosmic rays (Fig 1.4b). Secondary cosmic rays that reach the Earth's surface interact with nucleus of atoms of elements within rocks, being strongly attenuated in flux and energy due to nuclear interactions and ionization losses (Fig 1.4b and 1.5). As a result of these nuclear interactions, new isotopes are generated with a production rate that decreases exponentially with depth, being mainly produced between 0-3 meters below the Earth's surface (Fig 1.4b and 1.5). This corresponds to the main principle supporting the use of *in situ* cosmogenic isotopes for the study of surface processes, in particular, for determining surface exposure ages.

The production of cosmogenic isotopes is highly dependent on the intensity of the cosmic- ray flux impinging on top of the surface to be dated. The intensity of cosmic- ray flux is mainly influenced by the effects of the geomagnetic field and the atmospheric pressure. As previously stated the geomagnetic field is the main obstacle for primary cosmic-rays to enter the Earth's atmosphere. The direction and sense of the geomagnetic field change with latitude (Fig. 1.4a). Therefore, the intensity of cosmic-ray flux depends also on the geographic latitude. The Earth's magnetic field inhibits low energy primary cosmic-rays to penetrate the atmosphere near the equator and deflects most of the radiation out towards high latitudes, which receive radiation presenting a wider energy spectrum. Once cosmic-rays reach the Earth's atmosphere, the highest the atmospheric pressure they encounter, the highest are the probabilities for nuclear interactions between them and the atoms in the atmosphere. Thus, the intensity of cosmic-ray flux reaching rocks at the Earth´s surface is lower if atmospheric pressure is high. Atmospheric pressure is high near sea-level and it is relatively lower at high elevations. Therefore, at the same latitude, the intensity of cosmic- ray flux would be lower near the sea and higher on top of mountains like the Andes. Empirical production rates for a given isotope on a given mineral (e.g. ^{10}Be in quartz) have been generally measured on a natural surface of known age and simple exposure history at sea level and high latitudes. These empirical measurements have been calibrated to finally generate scaling factors to account for variations in latitude and elevation.

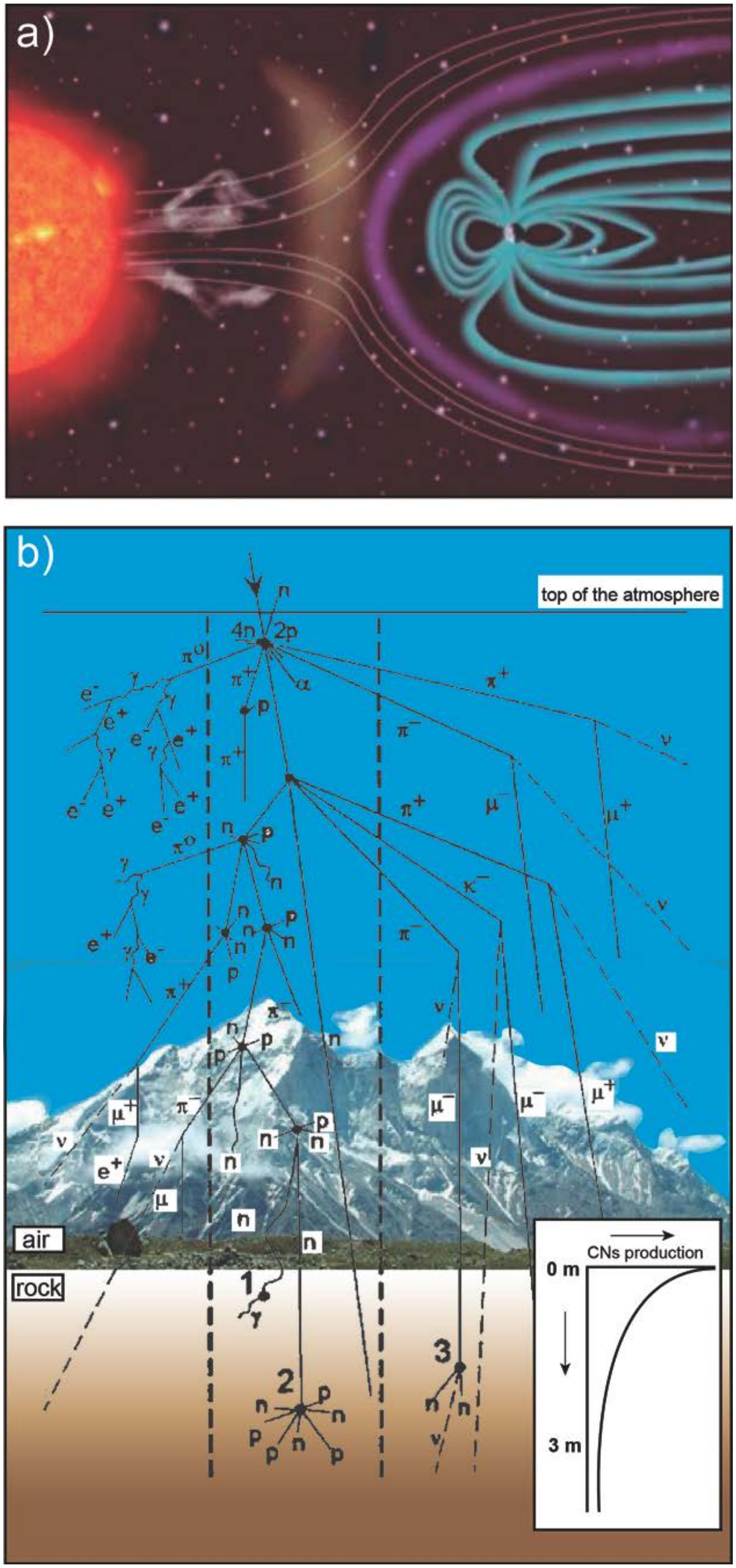

Fig. 1.4. a) Image showing the control of solar wind and electric currents in the Earth's core in shaping the Earth's magnetic field. Pale blue lines indicate the shape of the magnetic field. b) Major components of cosmic-ray cascade, showing secondary particle production in the atmosphere and below the first meters below the Earth's surface. ***n**:* neutron; ***p**:* proton, ***α**:* alpha particle, ***γ**:* gamma ray or photon, $\boldsymbol{e^+}$*:* positron, $\boldsymbol{e^-}$*:* electron, **μ**: muon, **v**: neutrino, $\boldsymbol{\kappa^{\pm}}$ and $\boldsymbol{\pi^{\pm}}$ are mesons. **CNs**: Cosmogenic nucleids.

The scaling factor of Lal (1991) for ^{10}Be in quartz follows the form of the polynomial:

$$P_0\ (\mathrm{L}, \mathrm{z}) = \mathrm{a(L)} + \mathrm{b(L)}z + \mathrm{c(L)}z^2 + \mathrm{d(L)}\ z^3\ (1)$$

where P_0 (at/gr/yr) corresponds to the production rate at surface, L corresponds to the geomagnetic latitude and *z* corresponds to the elevation at which the sample was collected. The coefficients a, b, c and d would depend on the geomagnetic latitude and they are summarized in Table 1.1.

Importantly, the direction and sense of geomagnetic field and, therefore, the intensity of cosmic- ray flux, also depends on time. Other scaling factors which account for temporal variations of the geomagnetic field are Dunai (2001), Lifton et al. (2005) and Desilets et al. (2006).

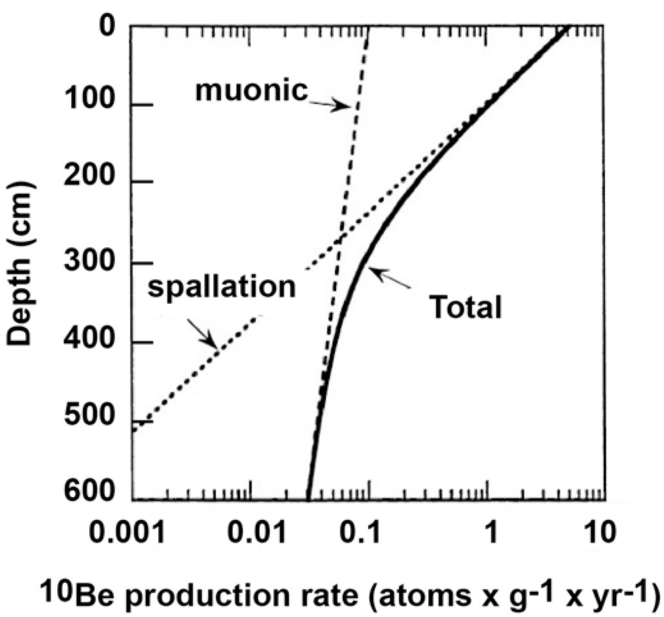

Fig. 1. 5. Production rate of ^{10}Be in quartz at high latitude at sea-level as a function of depth. ^{10}Be in quartz arenite is produced by spallation and muon capture reactions. Spallation occurs after a high energy particle as a neutron collides with a silicon nucleus, resulting in the production of neutrons and protons. Muon capture is the capture of a negative muon by a proton from a silicon nucleus, usually resulting in production of a neutron and a neutrino and sometimes a gamma photon. Note that ^{10}Be production rate strongly decreases below 300 cm (3m). Modified from Gosse and Phillips (2001).

According to the different energy of the secondary cosmic rays, different types of reactions and ionization losses are produced, such as spallation, muon capture, etc (further explanation in Fig 1.5). Depending on whether the isotope is radiogenic or stable it would or would not decay after its cosmogenic generation. In the case of ^{10}Be, once it is produced in quartz due to spallation and muon capture reactions between secondary cosmic rays and silicon atoms (Fig. 1.5), the ^{10}Be isotopes are likely to disintegrate into ^{9}Be. Similarly, in quartz ^{26}Al is formed by spallation reactions with ^{26}Al and silicon atoms to finally decay into ^{26}Mg. On the contrary, in quartz ^{21}Ne only accumulate due to the spallation reactions affecting silicon atoms because it corresponds to a stable cosmogenic isotope. According to this, radiogenic isotopes as ^{10}Be or ^{26}Al are used to date Pliocene to Holocene surfaces depending on their respective half-life, whereas the stable ^{21}Ne can be used to date surfaces as old as several millions years. Importantly, in both cases cosmogenic concentration would also depend on the erosion rate affecting the dated landform. The influence of erosion rate on cosmogenic isotope concentration $N\,(\mathrm{x},\,\mathrm{t})$ (atom/g) is implicit in expression (2) that corresponds to the simplest case in which a radiogenic isotope is solely produced by spallation, there is no initial concentration of the isotope in the analyzed mineral and erosion rate is constant.

$$N\,(\mathrm{x},\mathrm{t}) = P(0)\; e^{-\frac{\rho x}{\Lambda}} \left(\lambda + \frac{\epsilon\rho}{\Lambda}\right)^{-1} \left(1 - e^{-(\lambda+\epsilon\rho/\Lambda)t}\right) \quad (2)$$

where x corresponds to depth (cm), t is the exposure time (yr), $P(0)$ is the production rate of the isotope for the analyzed mineral on surface (at/gr/yr), ρ is the rock's density (gr/cm^3), ϵ is the erosion rate (cm/yr) and λ is the disintegration constant (yr $^{-1}$). Λ is the attenuation length (gr/cm^2), which corresponds to the thickness of a slab of the sampled rock required to attenuate the intensity of the cosmic-ray flux by a factor of e^{-1}. The unknown quantities in equation (2) are ϵ and t.

Geomagnetic latitude	a	b	c	d
0	0.5790	0.4482	0.1723	0.0359
10	0.5917	0.4415	0.1944	0.0363
20	0.6691	0.4764	0.2320	0.0435
30	0.8217	0.6910	0.1712	0.0822
40	0.9204	0.8849	0.2487	0.1031
50	0.9865	1.0298	0.2992	0.1333
60-90	1.0000	1.0889	0.3105	0.1382

Table 1.1. Coefficients in equation (1) used to calculate ^{10}Be production rate in quartz depending on geomagnetic latitude according to Lal (1991).

In principle, it is possible to determine both the age and the erosion rate of a geomorphic surface by analyzing two (or more) different nuclides (Lal, 1991) using equation (2). The results of this approach are commonly illustrated in two-nuclide diagrams, with the concentration of one nuclide on the x-axis and the ratio of the two nuclides on the y-axis (Fig. 1.6). In Fig. 1.6 the concentrations of ^{26}Al and ^{10}Be in a surface that has been continuously exposed to cosmic radiation since its formation at a constant erosion rate can only be projected within the "steady-state erosion island" and its position within it is determined by its age and erosion rate.

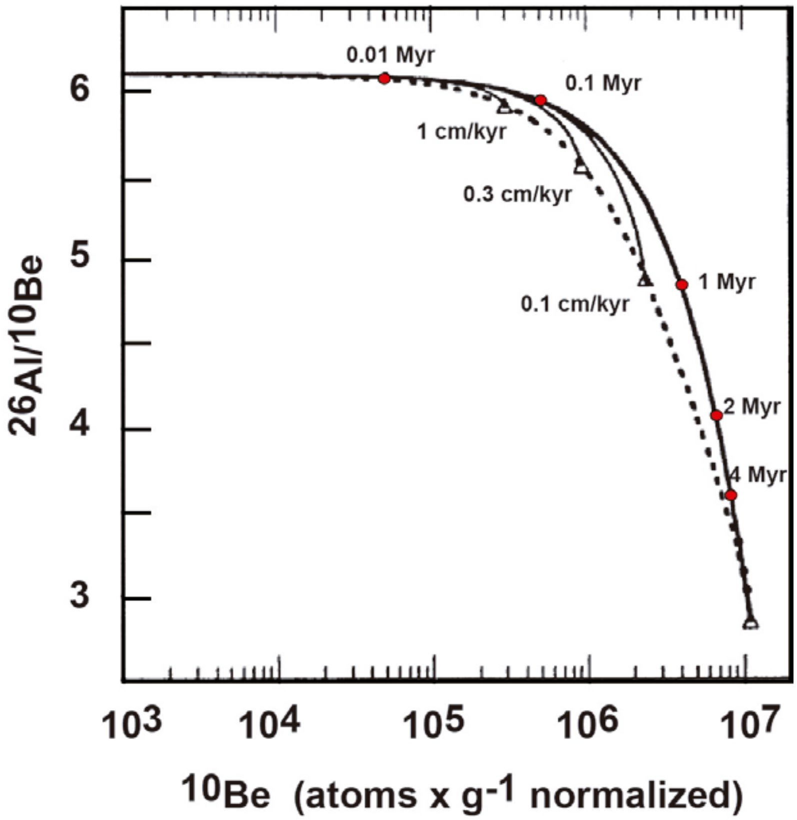

Fig. 1.6. Two nuclides diagram showing $^{26}Al/ ^{10}Be$ ratios for erosion rates of 0 cm/kyr (thick black line) and for 0.1, 0.3 and 1 cm/kyr cm/kyr (thin black lines) plotted against log ^{10} Be concentration normalized for production at sea level and high latitude. Red dots in upper line show the $^{26}Al/ ^{10}Be$ and ^{10}Be values at 0.01, 0.1, 1, 2 and 4 Myr. The steady state erosion island is formed by the upper curve (thick black line) representing $^{26}Al/ ^{10}Be$ and ^{10} Be values for an erosion of 0 cm/kyr and the envelope (dashed line) formed by $^{26}Al/^{10}Be$ and ^{10} Be values for erosion rates > 0 cm/kyr. Modified from Gosse and Phillips (2001).

1.2.4 How to constrain erosion/ exhumational patterns?

The geomorphic analyses and dating of uplifted geomorphic markers can be used to determine the time and magnitude of surface uplift. However, in order to constrain the development and/or later evolution of these landforms is necessary to quantify the magnitude of the erosional processes affecting them. One way to decipher erosional patters at the scale of millions of years is through the study of the exhumational paths of rocks on their way towards the Earth's surface. Low temperature thermochronology corresponds to a widely used technique in the study of the exhumational response of orogens to uplift. It is based on the accumulation of the radioactive decay products of certain isotopes and the temperature-dependence of these products retention. The temperatures in which the radioactive decay products of thermochronometric systems are retained range from ~ 60 (U-Th/ He in apatite) to ~ 550°C (^{40}Ar-^{39}Ar in hornblende), making them sensitive to exhumation through crustal depths of about one to tens of kilometers. Thus, low temperature thermochronology can constrain exhumation rates and their spatial-temporal variations on time-scales of ~10^5-10^7 years (Reiners and Brandon, 2006). Such time-scales commensurate with orogenic growth and possible erosion-tectonic feedbacks response times. Moreover, as low temperature thermochronology permits to quantify the thermal histories of rocks, several other tectonic and surface processes in active convergent margins can be investigated using this technique including tectonic exhumation by normal faults, thermal histories of sedimentary basins, sediment provenance, paleotopography of a landscape, etc. In the present thesis, low temperature thermochronology of Apatite Fission Tracks (AFT) and (U-Th)/He in apatite (AHe) are used to constrain tectonic -related exhumation along the Frontal and Coastal Cordilleras in north-central Chile.

1.2.4.1 Apatite fission-track thermochronology (AFT)

Apatite fission-track thermochronology (AFT) is based on the thermally sensitive retention of narrow radiation damage trails (i.e. fission tracks), generated as a result of the spontaneous nuclear fission decay of ^{238}U in those minerals. ^{238}U particles represent the father isotope, the fission-tracks (FTs) correspond to the daughter products and the length of the tracks give additional information about the rock's thermal history. The most widely accepted theory of track formation corresponds to the "ion explosion spike" (Fig. 1.7; Fleischer et al., 1975). According to this theory, tracks form as positively-charged particle strips lattice electrons along its trajectory, leaving an array of positively-charged atoms (Fig.1.7a). These atoms would be later displaced from their original lattice sites due to Coulomb repulsion forces (Fig.1.7b). As a result, a series of interstitials and vacancies are generated. Finally, the stressed area expands, deforms the surrounding crystal lattice and finally forms the tracks (Fig. 1.7c).

Fresh FTs have a total length of ~16 µm in apatite. The defects in crystal lattice that form the tracks tend to migrate by diffusion, reducing progressively the track length. This process is known as *annealing*. The annealing process strongly depends on temperature. Higher temperatures lead to enhanced annealing. Thus, temperatures must remain low for FTs to be retained in a geological time scale. The temperatures in which tracks are annealed, known as the Partial Anneling Zone (PAZ), ranges between ~ 120 and 60°C (Fig. 1.8).

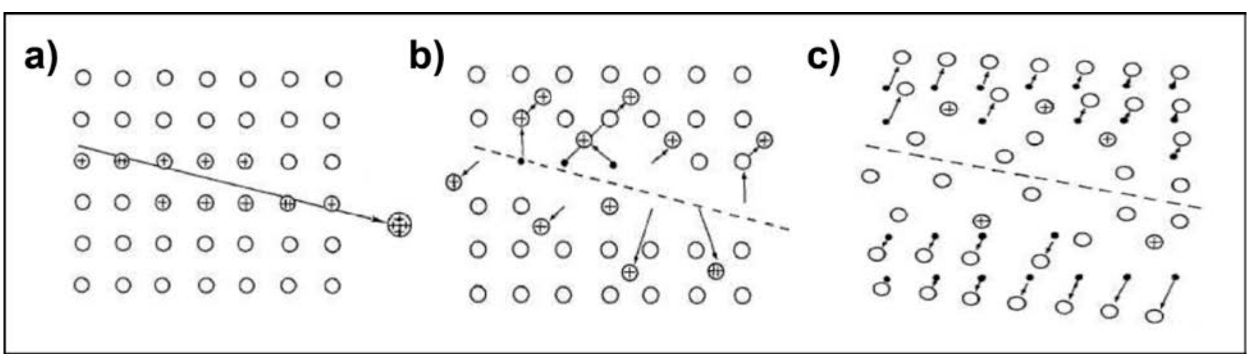

Fig. 1.7. Ion explosion spike theory for fission track formation. See explanation in the text. Modified from Fleischer et al. (1975).

Assuming a geothermal gradient of 30°C/ km, which is normal for a subduction zone, the PAZ can be translated into depths of ~ 4 and 2 km into the crust (Fig. 1.8). If rocks in their way towards the surface stay stationary within the PAZ, the tracks would be anneal and the mean track length (MTL) of the sample would display values < 14 µm together with relatively large standard deviation values > 1.2 µm for MTL (Gleadow et al., 1986; Green et al., 1986). In such case, the AFT age does not necessarily have a geological meaning. On the contrary, if rocks are relatively rapidly exhumed through the PAZ the MTL of the sample would present values > 14 µm together with relatively small standard deviation values < 1.2 µm (Gleadow et al., 1986; Green et al., 1986). In this case, the AFT age indicates the time since the rock was accelerated exhumed through the PAZ. For the AFT data further presented in this thesis, it is important to consider that the annealing behavior of fission tracks in apatite are highly dependent on the chlorine content (Green et al., 1986; Carlson et al., 1999; Barbarand et al., 2003). Chlorine-rich apatites present more resistance to anneal than fluorine-rich apatites (Green et al., 1986). This is because they are annealed at higher temperatures than fluorine-rich apatites. This implicates that chlorine-rich and fluorine-rich apatites from the same sample could present diverging AFT ages, despite having undergone the same thermal history. The relevance that compositional factors can have in apparent AFT ages is represented in Fig. 1.9a. In this figure, the AFT ages of individual grains of the same sandstone sample collected at the same depth in a core from the Otway Basin are plotted against their respective chlorine content. Age differences of more than ~ 100 Ma are observed between apatites presenting the highest and the lowest chlorine contents (Fig. 1.9a). Moreover, apatites presenting the highest chlorine contents have not been reset and their AFT age equals the age of the deposit (Fig. 1.9 a). Thus, incorporation of compositional effects is essential in extracting accurate thermal history information from AFT data (e.g. Argent et al. 2002; Crowhurst et al. 2002). Compositional effects in AFT data are generally incorporated using the Dpar parameter, which corresponds to the arithmetic mean fission-track etch figure parallel to the crystallographic c-axis (Burtner et al., 1994; Donelick, 1993, 1995). The Dpar is a measure of apatite solubility that positively correlates with chlorine content (Fig. 1.9b, Carlson et al., 1999; Barbarand et al., 2003). At present it is the most widely used parameter to account for apatite behavior in AFT analysis as it would provide roughly the same predictive capability as chlorine content (Ketcham et al., 1999). However, as it would be shown in chapter 3, Dpar could sometimes fail as a predictor for apatite behavior. Finally, further information concerning the analytical procedure in AFT measurements is available in the article “Thermochronometric contraints on the development of the Andean topographic front in north central Chile (28.5-32ºS)” included in chapter 3.

1.2.4.2 Apatite (U-Th)/He thermochronology (AHe)

Apatite (U–Th)/He (AHe) thermochronology is based on the thermally sensitive retention of ^{4}He (alpha particles) produced by the decay of ^{238}U, ^{235}U, ^{232}Th and ^{147}Sm in apatite crystals. The amount of ^{4}He accumulated in time t follows the equation:

$$^{4}He = 8^{238}U\left(e^{\lambda 238t} - 1\right) + \frac{7^{238}U}{137.88}\left(e^{\lambda 235t} - 1\right) + 6\,Th\left(e^{\lambda 232t} - 1\right) \quad (3)$$

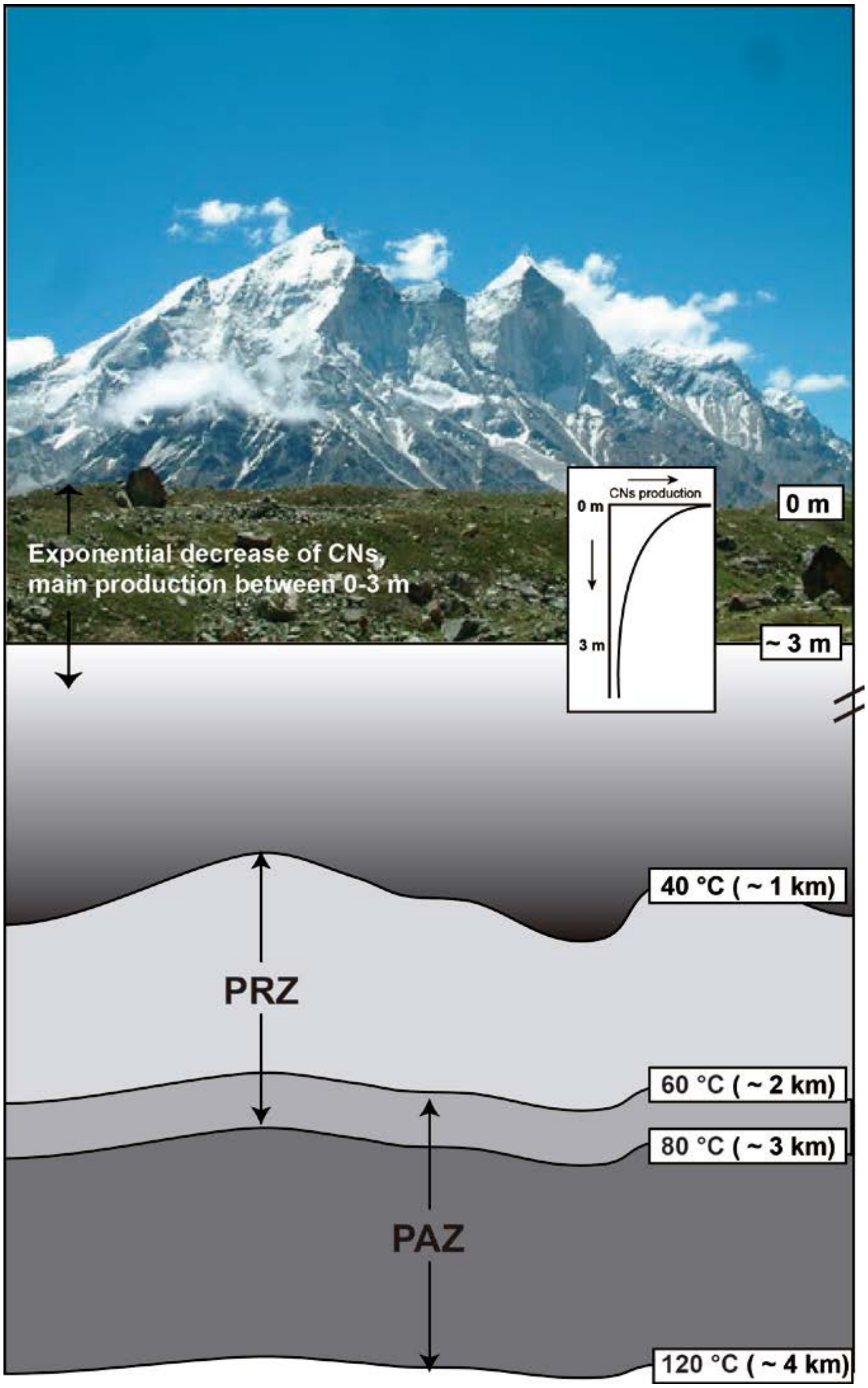

Fig. 1.8. Scheme showing the temperatures ranges for the Partial Anneling Zone (PAZ) of the AFT system and the Partial Retention Zone (PRZ) of AHe system. Depths corresponding to these temperature ranges were calculated assuming a normal geothermal gradient of 30 °C/ km. Note that the PAZ and the PRZ overlap. Note that low temperature isotherms mimics landscape topography. CNs= Cosmogenic nucleids.

Assuming that He is solely produced by the decay of ^{238}U, ^{235}U, ^{232}Th and ^{147}Sm, measurements of daughter and parents isotopes allow us to determine the time since the apatite was subjected to temperatures in the range of the Partial Retention Zone (PRZ, see Fig. 1.8) . Importantly, for this to be a good assumption it is necessary to rule out the possibility of mineral inclusions that modified the concentration of parent and daughter. Thus, apatites are conspicuously examined in search of U-rich inclusions under binocular microscope (Fig. 1. 10), to finally exclude inclusion-bearing apatites from He measurements. The analytical procedure is explained in the article "Thermochronometric contraints on the development of the Andean topographic front in north central Chile (28.5-32ºS)" included in chapter 3.

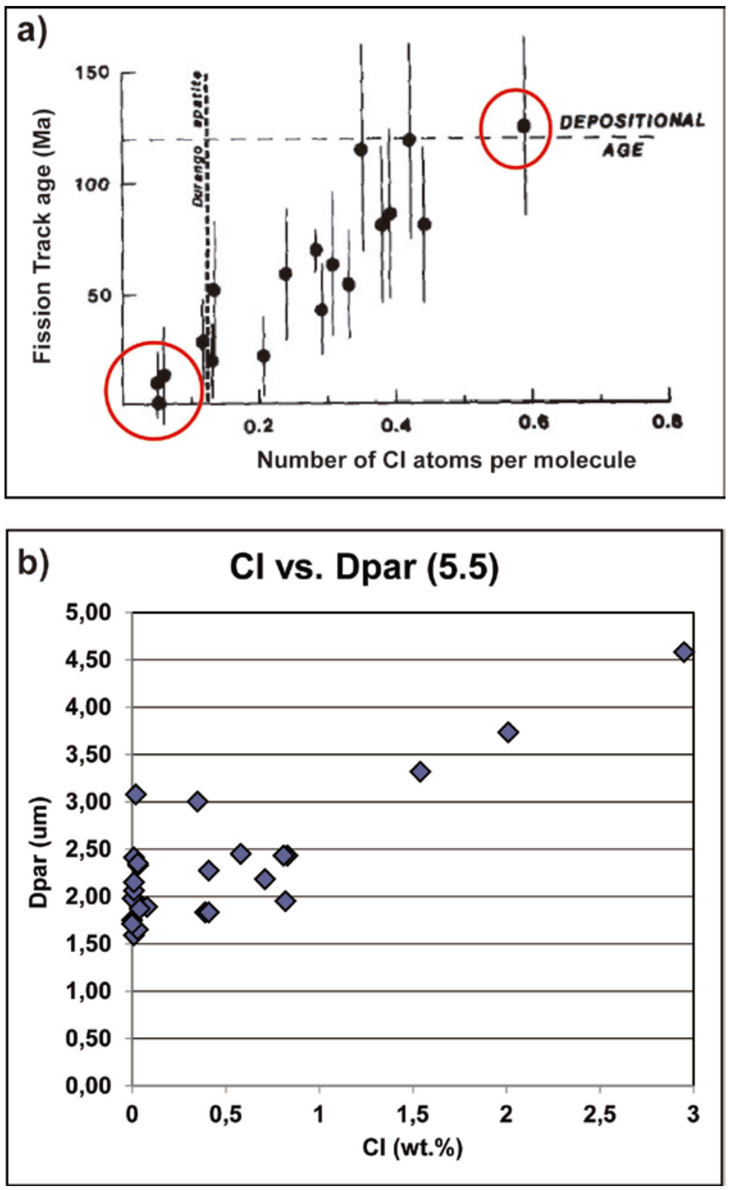

Fig.1.9. a) Relationship between apparent fission-track age and chlorine content in individual apatites grains from a sample collected from a depth of 2585 m within the Otway Basin. Red circles mark apatites presenting extreme chlorine compositions and divergent apparent fission-track ages. Taken from Green et al. (1986). b) Relationship between chlorine content and chlorine content in individual apatites grains from the database of Carlson et al (1999) and Barbarand et al. (2003).

Similar to tracks in the AFT system, ^{4}He would accumulate in geological time scales only if temperatures remain low. The temperatures at which ^{4}He is only partially retained (Partial Retention Zone, PRZ) ranges between ~ 80 and 40°C, overlapping with the PAZ (Fig. 1.8). As explained in the case of the AFT system, depending on whether rocks were accelerated cooled through the PRZ or remained stationary within it, the AHe age presents or not a geological meaning, respectively.

Assuming a geothermal gradient of 30°C/ km, the highest and lowest temperatures within the PRZ can be translated into depths of ~ 3 (2.6) and 1 (1.3) km into the crust (Fig. 1.8). Contrary to what is observed in the AFT system, there is no-known dependence of ^{4}He diffusion behavior on apatite chemistry. However, it has been shown that diffusion kinetics of ^{4}He is influenced by the damage inflected to crystal lattice by the nuclear interactions involved in radiation decay (Shuster et al., 2006; Flowers et al., 2009). Damaged areas within the crystal lattice in apatite grains act as traps for ^{4}He (Shuster et al., 2006; Flowers et al., 2009). Thus, the higher the radiation damage accumulated in the apatite, the lower the He diffusivity (Flowers et al., 2009). Consequently, the effective closure temperature of the AHe system increases and older AHe ages are expected (Flowers et al., 2009). Such effect is mostly expected in very old rocks (> 1000 Ma), where radiation damage could have significantly affected He diffusivity (Flowers et al., 2009). Therefore, such effect it is not expected in rocks from the Chilean flank of the Central Andes, which are all younger than Precambian (SERNAGEOMIN, 2003)

Importantly, some precautions must be taken with respect to the dimensions of the apatite grains to be dated with the AHe method. Alpha particles produced by U and Th travel ~ 20 µm through the apatite grain. Thus, they may be ejected from crystal edges. In order to account for the effect of alpha particle ejection a correction must be applied to raw AHe ages or ^{4}He measurements, known as the F_t factor (Farley et al., 1996). The F_t factor is calculated based on the values of width and length of individual apatite crystals measured under the binocular microscope (Fig. 1. 10).

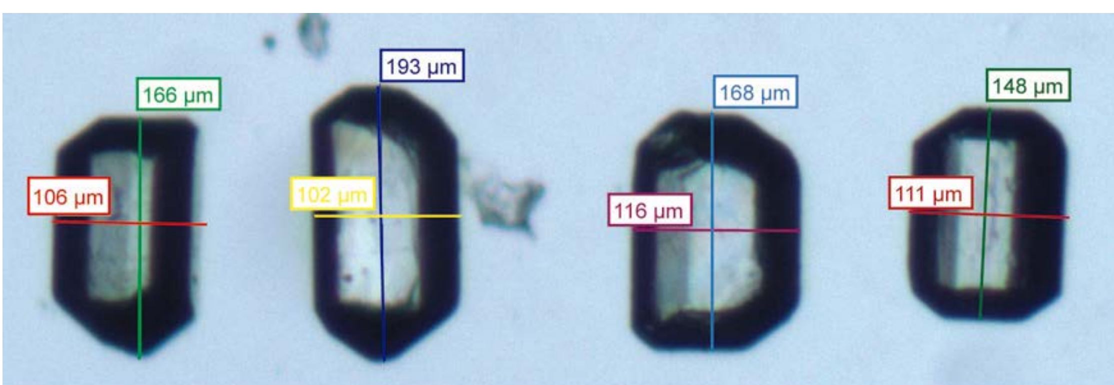

Fig. 1.10. Microphotographs of inclusion-free euhedral apatites picked for (U-Th)/He thermochronology (sample LL02).

1.2.4.3. Thermal modeling of thermochronometry data

In order to obtain time-temperature paths, themochronometric data is usually model using computer programs as HeFTy (Ketcham, 2005), the program used in chapter 3 to model AFT and AHe data together. HeFTy is based in two types of modeling that are complementary. Forward models predict how the thermochronometric systems would evolve under known initial conditions and time-temperature history. They are based in laboratory experiments that are later extrapolated to geological time-scales. Once a forward model has been created and verified, it then becomes possible to apply it in the inverse sense. An inverse model finds the intervening time-temperature history given a measured ending condition and an assumed starting one. In general, more than one history is consistent with a given ending condition. As a result, an inverse model solution usually consists of a set of thermal histories that are consistent with the measured data, as judged by some statistical criterion (Fig. 1.11).

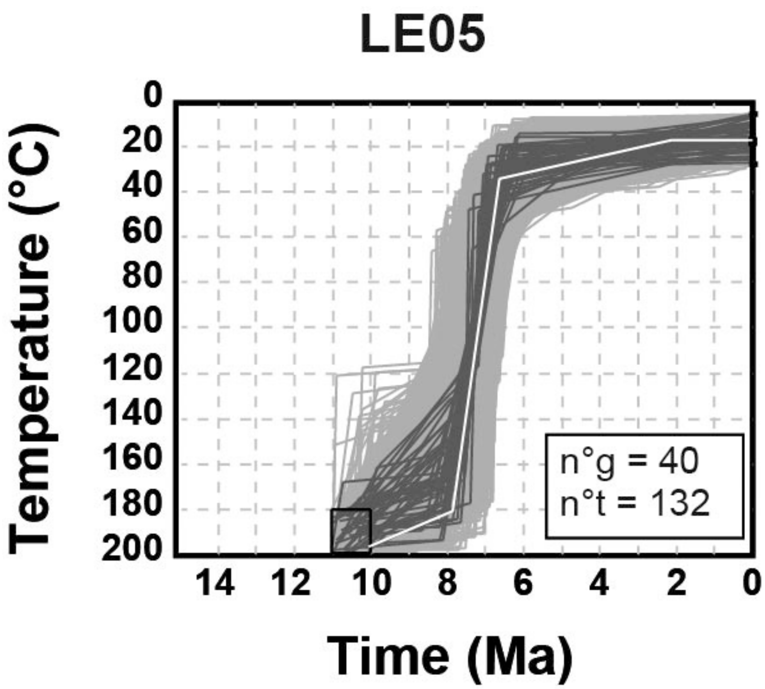

Fig. 1.11. Time-temperature paths obtained through thermal modeling of AFT and AHe data of sample LE05 using HeFTy (Ketcham, 2005). Grey lines correspond to acceptable fit paths (probability of fitting of lengths and age> 0.05), black lines correspond to good fit paths (probability of fitting of lengths and age > 0.5) and white lines represent best-fit paths, n° g= number of grains counted for AFT age determinations, n° t= number of tracks lengths measured

2.1. Tectonic and climatic setting

The present-day tectonic configuration in the Central Andes (15º-34ºS, Fig. 2.1a) was acquired after the breakup of the Farallon Plate into the Nazca and the Cocos Plates at about 25 Ma (Fig. 2.1a, 2.2, Pardo-Casas y Molnar, 1987; Somoza, 1998; Sdrolias and Muller, 2006). As a result of this major tectonic plate reorganization, between ~ 30 and 20 Ma the convergence rate of the Farallon (Nazca) Plate relative to the South American Plate raised from 50 or 60 to a maximum of 150 mm/yr (Fig. 2.2; Pardo-Casas y Molnar, 1987) and the convergence changed from oblique (~ 40º S) to almost orthogonal (~ 10º S) (Somoza, 1998). According to Somoza (1998), the convergence rate has diminished continuously since ~ 20 Ma (Fig. 2.2). On the contrary, Sdrolias and Muller (2006) and Pardo-Casas and Molnar (1987) indicate that convergence velocity decreased since ~ 15 Ma and 10 Ma, respectively (Fig. 2.2). Regardless of the differences between the mentioned authors, they all recognized a strong decreased in convergence velocity around ~ 10 Ma (Fig. 2.2). Finally, the present-day absolute velocities (relative to the mantle) correspond to 3.2 cm/yr and 4.7 cm/yr for the Nazca and South American Plates respectively (Fig. 2.1a; HS2-Nuvel1, Gripp y Gordon, 1990).

Before 25 Ma plate tectonic reconstructions indicate that convergence velocity of the Farallon Plate relative to the South American Plate suffered previous periods of acceleration between ~ 60 and 40 Ma (Fig. 2.2; Pardo-Casas and Molnar, 1987; Sdrolias and Muller, 2006). With respect to the South American Plate, its westward velocity was accelerated around ~ 100 Ma related to the opening of the South Atlantic Ocean and around ~ 40 Ma (Fig. 2.2; Soler and Bonhomme, 1990). According to Silver et al. (1998), the westward velocity of the South American Plate has been also accelerated since ~ 25 Ma as a consequence of the deceleration of the African Plate and the concomitant diversion of mantle flow westward.

The periods of accelerated convergence have been related to supposedly discrete events of shortening throughout the Central Andes, namely, the Peruvian (~ 110-90 Ma, Steinmann, 1929), the K-T (~ 65 Ma, Cornejo et al., 2003; Charrier et al., 2007), the Incaic (~ 45-35 Ma Steinmann 1929; Charrier & Vicente 1972; Coira et al. 1982; Cornejo et al. 2003; Charrier et al., 2007; 2013) and the Quechua (~ 20-0 Ma) or Pehuenche (20-10 Ma, Charrier et al., 2013) tectonic phases (Fig. 2.2). According to the concept of tectonic phases, the Andes would have been constructed during discrete pulses of shortening since the Early-Late Cretaceous followed by periods of tectonic quiescence, with pulses of shortening coinciding with major changes in the convergence parameters between the (Farallon) Nazca and South American plates. However, in the last years two main opposing models for the timing of Andean uplift and deformation have emerged, which challenge the tectonic phases theory. One indicates that uplift and deformation has been slow and continuous since ~ 60 or 40 Ma (McQuarrie et al., 2005; Barnes and Ehlers, 2009) or continuous at least since ~ 40 Ma but with punctuated episodes of accelerated uplift and deformation during the Late Oligocene-Early Miocene and the Late Miocene (Charrier et al., 2013). Accelerated deformation during the Eocene to Oligocene would coincide with the Incaic phase, whereas accelerated deformation since the Late Oligocene coincides with the Quechua or Pehuenche phases. Finally, the other end-member model for Andean evolution proposes a main rapid uplift during the Late Miocene after ~ 10 Ma (Garzione et al., 2006; Hoke et al., 2007; Farías et al., 2008).

The studied region of north-central Chile between 28 and 32ºS is located above the Chilean (Pampean) flat-slab segment (Fig. 2.1a). This segment is characterized by a strong interplate coupling between both tectonic plates, a highly compressed continental crust and the absence of Quaternary volcanism (Pardo et al., 2002). Based on the study of marine magnetic surveys, Yáñez et al. (2001) suggested that flat subduction in this region is related to the subduction of the buoyant Juan Fernández aseismic ridge at 33° S (Fig. 2.1b). The collision point of the Juan Fernández ridge migrated rapidly (~ 20 cm/yr^{-1}) from the northern to the southern part of the studied region between ~ 16 and 11 Ma (Yáñez et al., 2001), when it started to move at a much slower rate (3.5 cm/ yr^{-1}). Since ~ 10 Ma it has been subducting at the same piercing point at 33°S (Fig. 2.1b). The greater buoyancy of the Juan Fernández ridge with respect to the rest of the slab together with its quasi-stationary position would have favored the shallowing of the slab since ~ 10 Ma (Yáñez et al., 2001). At the present-day, the Juan Fernández ridge separates a sediment starved trench where subduction erosion may dominate to the north of 33°S, from a sediment filled trench where recent sediment accretion dominates to the south of 33°S (von Huene et al., 1999; Yáñez et al., 2001). Recently, numerical experiments suggest that the Chilean flat slab would be rather related to the combined effects of the trenchward motion of the Río de la Plata craton (see Fig. 2.3) and slab retreat (Fig. 2.1c, Manea et al., 2012). According to these experiments, as a thick cratonic crust approaches to the trench and the wedge closes, two opposite forces control slab geometry. On one hand, the suction between the ocean (i.e. slab) and the continental margin increases, favoring slab flattening. On the other hand, the mantle confined within the closing wedge pushes the slab backward, increasing the subduction angle. However, if trench roll-back is an active process, as it has been shown to occur in the Chilean flat slab segment since ~ 25 Ma (Schellart et al., 2007), the pushing effect of the confined mantle tends to be small relative to the suction forces that would finally generate slab flattening (Fig. 2.1.c).

The climate of north-central Chile between 28 and 32°S is semiarid and transitional between the hyperarid Atacama Desert north of 27°S, and the more humid conditions of central Chile south of 33°S. The semiarid climate is due to the year-round influence of the southeast Pacific anticyclone (SEP), with the northward penetration of the southern hemisphere westerlies only possible when the SEP is weakened or displaced northwards (Veit, 1996). Most rainfall occurs during the austral winter when the SEP is weakened with annual mean values of 80 mm at 30°S and 180 mm at 32°S. Colder conditions prevail at the coastal area due to the presence of sub-antarctic waters brought to these latitudes by the Humboldt Current System and also related to coastal upwelling processes which strengthen the high atmospheric stability associated with the SEP (Rutllant et al., 1998).

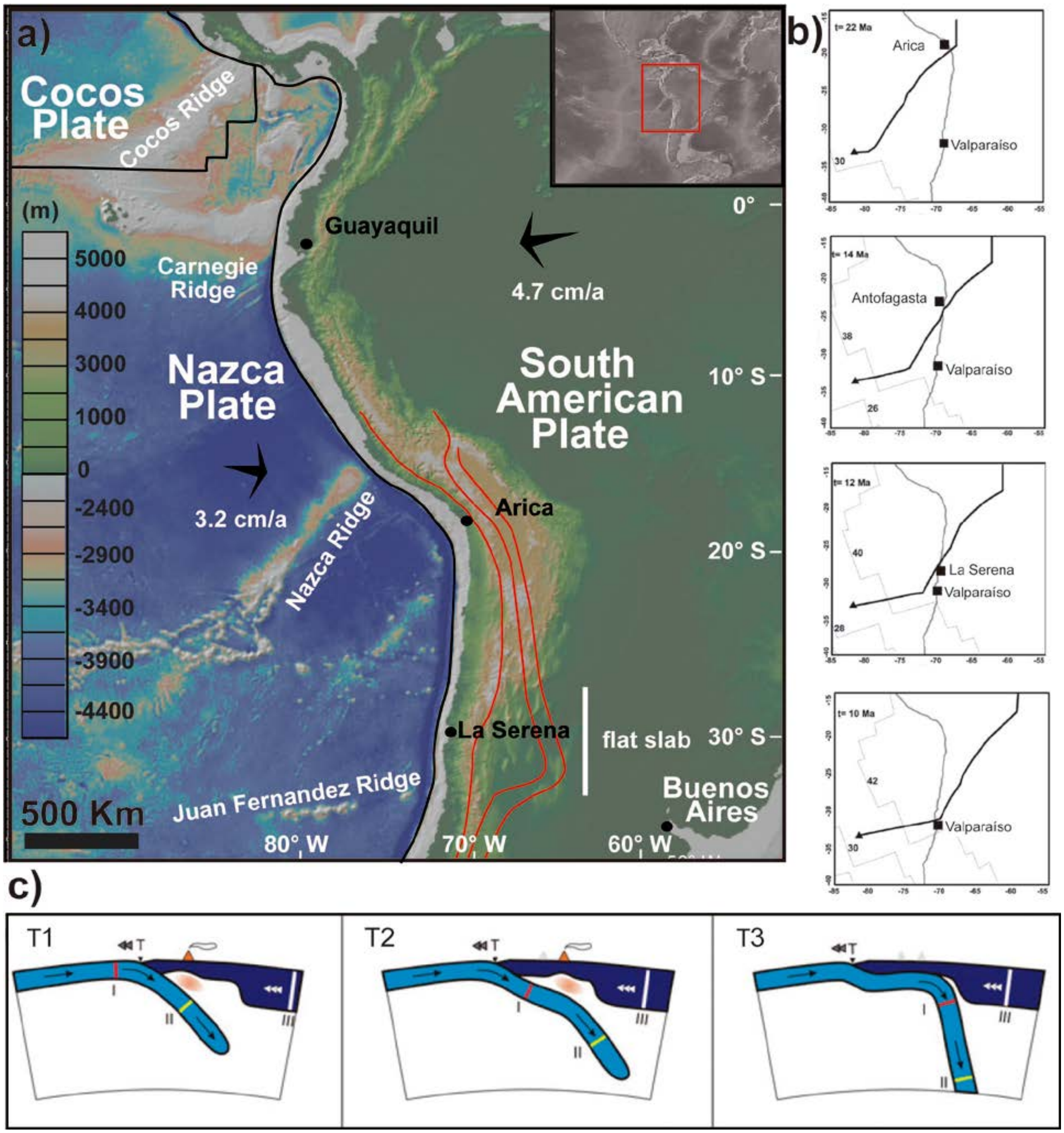

Fig.2.1. a) Present-day tectonic setting in the Central Andes (15-34°S). Red solid lines mark the contours of depth of the Nazca Plate underneath the South America Plate at 100, 150 and 200 km (Cahill and Isacks, 1992) b) North-to-south migration of the Juan Fernández ridge from the Early to the Late Miocene (from Yáñez et al., 2011) c) Cartoon showing the combine effects of the trenchward motion of a thick cratonic crust and slab retreat (from Manea et al., 2012).

Despite the blockage exerted by the Andean range to the income of the southern hemisphere easterlies, it has been suggested that air masses brought by these winds would have favoured the occurrence of periods of greater humidity during the late Pleistocene and Holocene throughout the Semiarid Andes (Zech et al., 2006). Finally, the occurrence of anomalous rainy years in central to northern Chile has commonly been associated with the development of El Niño conditions in austral winter–spring (e.g. Ortega et al., 2012). Such conditions would arise in part from a weakened SEP and from a higher frequency/persistence of blocking anticyclones west of the Antarctic Peninsula. These anomalies result in an equatorward shift of stormtracks, allowing for cyclogenesis and frontal incursions off and along the central and north-central coast of Chile (Rutllant and Fuenzalida, 1991; Montecinos and Aceituno, 2003).

During the Paleogene, the climate in north-central Chile was warmer and more humid than at present as indicated by the woody components of paleoflora from fossiliferous localities just south of La Serena (Villagrán et al., 2004). Since ~ 21 to 15 Ma subtropical vegetation was replaced by sclerophytic shrubs indicating a warm, seasonal climate receiving scarce rainfall from both the east and the west (Villagrán et al., 2004). The transition between a hyperarid climate to the north of 27°S and a humid climate south of 33°S occurred after the Middle Miocene (Le Roux, 2012). During this period, the combination of a series of events including glaciations in West Antartica, formation of the Humboldt Current and uplift of the Andes are thought to have been responsible for the development of a strong latitudinal precipitation gradient throughout the study area (Le Roux, 2012).

2.2. Morphostructural units

The morphostructural units in north-central Chile correspond, from west to east, to the Coastal Cordillera and the Frontal Cordillera (Fig. 2.3a and c). Further east, out of the study region and in Argentina, the Precordillera and the Sierras Pampeanas are recognized (Fig. 2.3a and b). The border between the Frontal Cordillera and the Coastal Cordillera corresponds to a topographic front that defines a marked rise in mean elevations throughout west to east transects. The scarp related to the topographic front is generally around 1700-1400 m high and, contrary to what may have been expected, it is not necessarily aligned with main faults (see section 2.3). Moreover, previous geomorphic analyses indicate that the topographic front is an ancient mountain front, which probably evolved as a degradational feature during the Neogene (Aguilar et al., 2013).

The Coastal Cordillera presents a mean elevation of ~ 2000 m a.m.s.l (Fig. 2.3b). It is mostly formed by an east-dipping homoclinal block of Mesozoic volcano-sedimentary rocks covering a Paleozoic and Mesozoic metamorphic and intrusive basement (Fig. 2.3b). The mentioned rocks are covered by Cenozoic sedimentary rocks of marine and continental origin along the coast and throughout the main valleys, respectively (Fig. 2.3b). The Frontal Cordillera reaches elevations of ~ 6800 m a.m.s.l, (Fig. 2.3b). It is mostly composed by a basement block of Paleozoic to early Mesozoic intrusive and volcanic rocks covered to the east by Cenozoic volcanic and volcanoclastic units (Fig. 2.3b). Together they present a thick-skinned structural style (Allmendinger et al., 1990; Winocur et al., in press). Towards the border with the Coastal Cordillera the Paleozoic basement is covered by a succession of folded Mesozoic volcano-sedimentary rocks (Fig 2.3 b). As shown in Fig 2.3b, the summits of the Frontal Cordillera form a plateau morphology presenting a width ~ 80 km (Allmendinger et al. 1990).

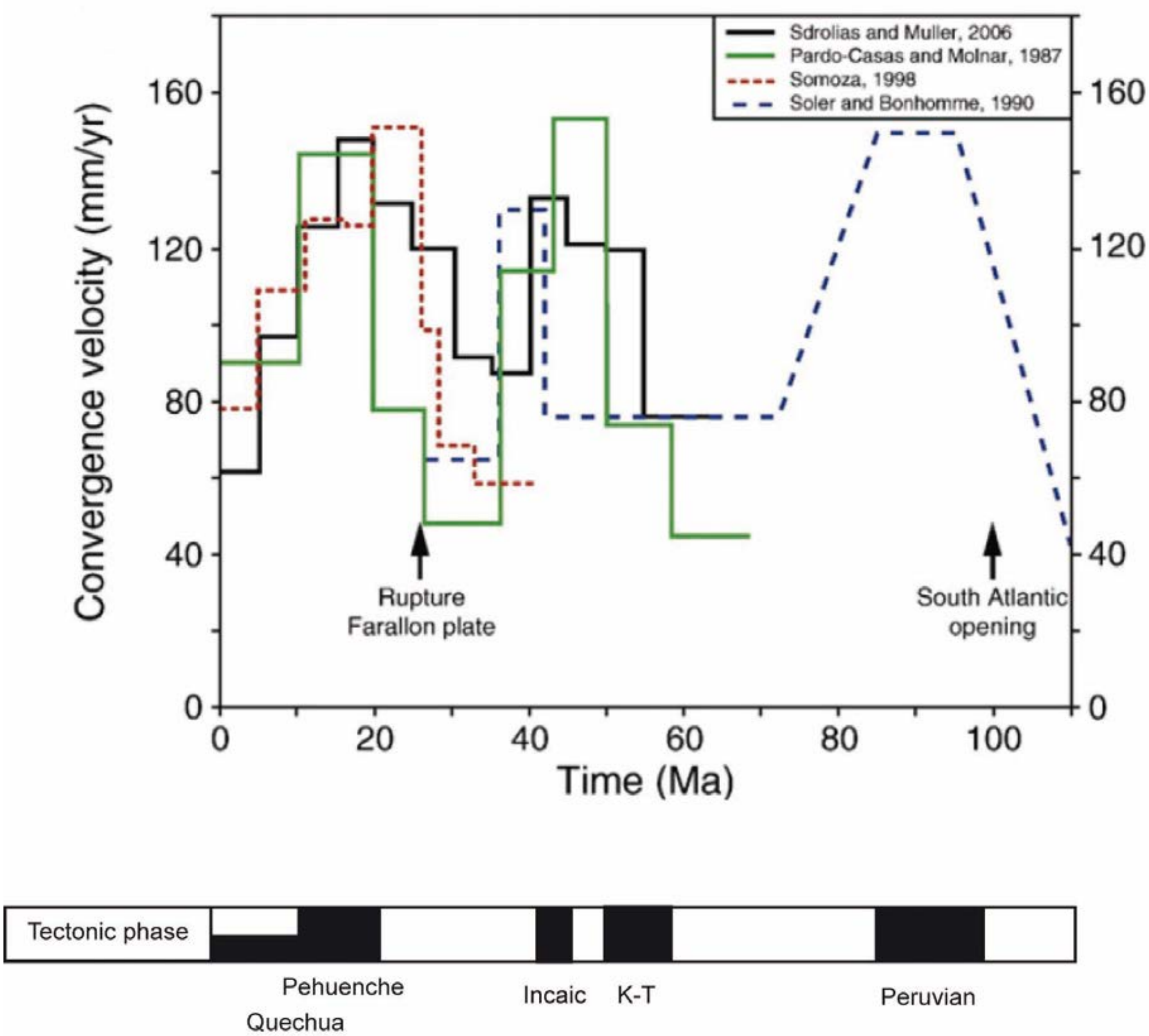

Fig. 2.2. Convergence velocity (mm/yr) between the Farallon-Nazca and the South American plates since the Early Cretaceous. Modified from Martinod et al. (2010).

In Argentina, the Precordillera reaches maximum elevations around ~ 4000 m a.m.s.l. and is mostly formed by Paleozoic sedimentary rocks forming a thin-skinned fault and thrust belt plus Cenozoic synorogenic deposits (Fig 2.3b). Further east, the Sierras Pampeanas present generally lower elevations between 2000-1000 m a.s.l., although locally they can reach elevations as high as 5900 m. a.s.l near 28°S (Sierra de Famatina). They are mostly composed by Proterozoic to lower Paleozoic blocks of metamorphic and granitic rocks presenting thick-skinned deformation and related Cenozoic synorogenic deposits. Between the Frontal Cordillera and the Precordillera, the Iglesia basin corresponds to a piggy-back basin filled with Cenozoic sedimentary and volcanoclastic deposits (Fig. 2.3b).

Contrary to the rest of the Central Andes, no Central Depression is observed separating the Coastal Cordillera and the Frontal Cordillera in north-central Chile (Fig 2.3a and b). On one hand, it has been suggested that the highly compressive regime related to flat-subduction would be responsible for the absence of the Central Depression in this region (Jordan et al., 1983). On the other hand, the studied region has been compared with the region of central Chile southwards of 33°S, where the Central Depression has been interpreted as an erosional feature (Farías, 2007). According to these authors, a combination of larger uplift and much dryer climatic conditions than south of 33°S together with the abundance of erosion resistance lithologies would be responsible for the absence of a Central Depression in north-central Chile.

2.3. Previous geological evolution

It has been widely recognized that the previous geological history has strongly determined the structure and rheologic characteristics of the Andean basement (Mpodozis & Ramos, 1989; Tassara, 2005; Charrier et al., 2007; Hilley and Coutand, 2009), conditioning the orogen response to varying tectonic and erosional conditions. Therefore, knowledge of the pre-Cenozoic evolution of the South American margin is crucial for understanding its more recent landscape evolution.

The continental margin of South America has been an active margin during most of its evolution starting in the late Proterozoic, presenting only a brief period of no or very slow subduction during the late Paleozoic-early Mesozoic (Coira et al., 1982; Mpodozis and Ramos, 1989; Charrier et al., 2007). The evolution of the active margin can be subdivided in two main periods separated from each other by the episode of no or very slow subduction: a “collisional” and an “erosional” period. The collisional period is characterized by the accretion of a series of terranes and related westward arc migration. The “erosional” period is mostly characterized by the eastward retreat of the continental margin and the arc probably due to subduction erosion, with only minor terrane accretion (Table 2.1; Charrier et al., 2007). These three main periods are subdivided into tectonic cycles, stages and substages based on the presence of regional unconformities or evidence of major paleogeographic changes (Table 2.1; Mpodozis and Ramos, 1989; Charrier et al., 2007).

2.3.1. The collisional period: anatomy of the Andean crust

The terrane accretions that occurred during the collisional period would have largely influenced the subsequent development of the Andean orogeny, as they have determined the composition and rheology of the Andean crust (Ramos et al., 1986; Ramos, 2009; Charrier et al., 2007). Such control it is evidenced by the tendency of terrane’s sutures to spatially correlate with the boundaries between present-day morphotectonic units of the Andes (Fig. 2.3b). The collisional period is subdivided into the Pampean, Famatinian and Gondwanan tectonic cycles (Table 2.1).

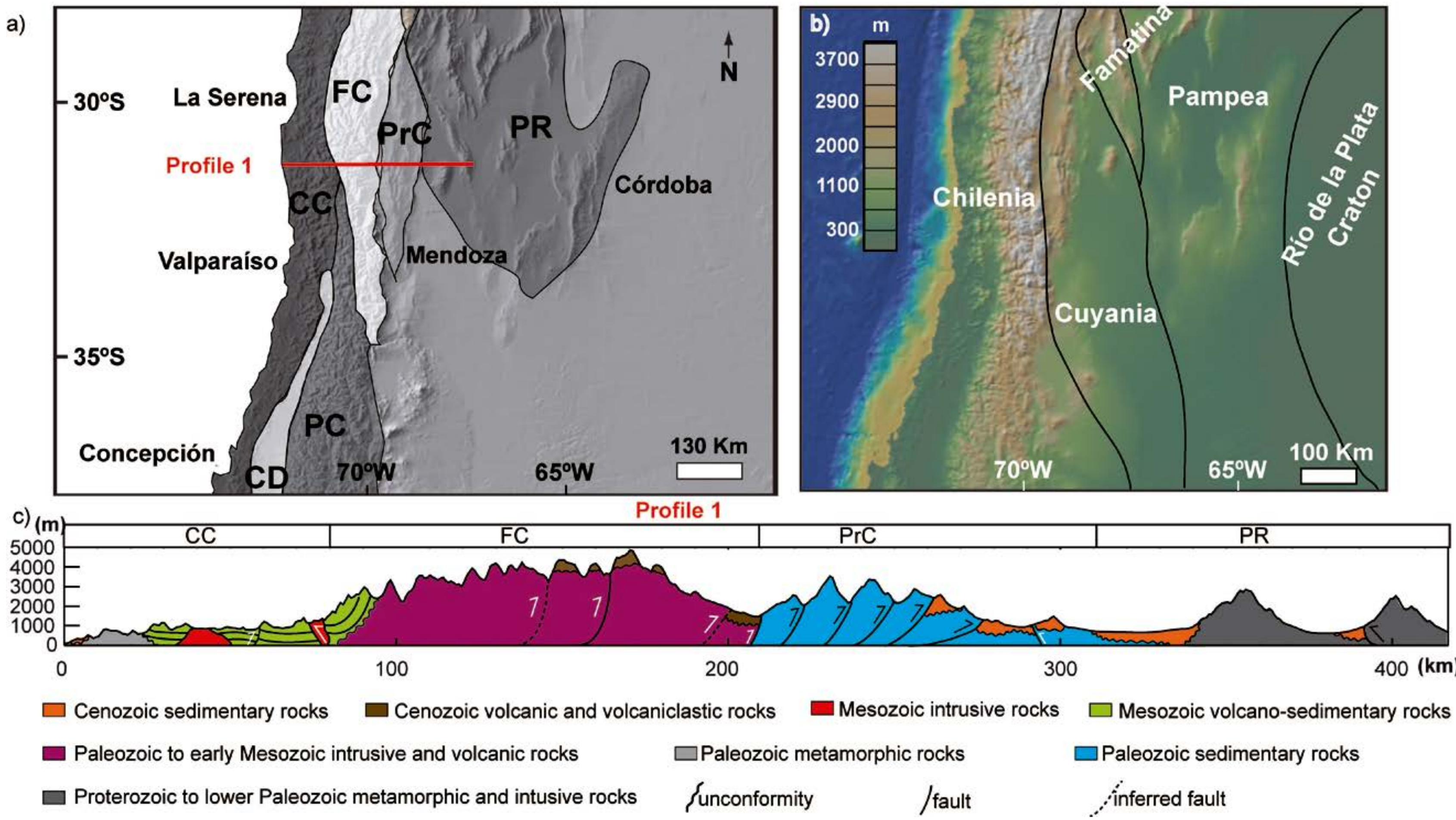

Fig 2.3. a) Main morphostructural units in the studied region. CC= Coastal Cordillera, CD= Central Depression, PC= Principal cordillera, FC= Frontal Cordillera, PrC= Precordillera, PR= Pampean Ranges. b) Probable sutures (black solid lines) between terranes accreted to western Gondwana between the Late Proterozoic and the Middle Paleozoic (based on Ramos et al., 2000; Astini and Dávila, 2004; Porcher et al., 2004; Abre et al., 2001) c) Schematic west to east structural profiles crossing the morphostructural units of the Andes at 30.5°S. Based on Ramos et al. (2002) and Vergés et al. (2007)

During the Pampean and Famatinian cycles a series of terranes were successively accreted to the western margin of Gondwana, corresponding to the present-day western South America. At the latitude of north-central Chile (28-32°S) these terranes correspond to Pampia, Famatina, Cuyania and Chilenia (Fig. 2.3b). Some of these terranes correspond to parautochthonous blocks generated by rifting of the western Gondwana margin that were later drifted back against Gondwana. Others would correspond to allochthonous blocks detached from the present-day western North America, known as Laurentia, during Paleozoic times. According to several authors (Thomas and Astini, 2003; Ramos, 2004) Gondwana and Laurentia would have interacted successively during the Pampean and Famatinian tectonic cycles. The first terrane amalgamated to the western margin of Gondwana corresponds to Pampia, that was accreted to the stable Rio de La Plata craton during the Late Proterozoic (Ramos, 1994). This terrane would correspond to an allochthonous terrane (Rapela et al., 1998), detached during the Rodinia break-up. There are no exposures of this terrane in north-central Chile. Rock exposures of Pampia include the Sierras Pampeanas to the east of the Sierra de Famatina and the Precordillera in the Argentinean foreland (Fig. 2.3b). The westward drift and accretion of this terrane is associated with the development of an associated magmatic arc and an orogenic belt in the eastern Sierras Pampeanas (e.g. Ramos, 2009). The Famatina terrane corresponds to a parautochthonous block with Gondwanan signature (e.g. Ramos, 2009); whereas the Cuyania terrane corresponds to a Laurentian-derived allochthonous terrane (Thomas and Astini, 2003; Ramos, 2004). The Famatina terrane is spatially correlated with the Sierras de Famatina in the northern part of the present-day Sierras Pampeanas, whereas Cuyania correspond to the present-day Precordillera and Sierra Pie de Palo (Fig. 2.3b). The accretion of the Famatina and the Cuyania terranes resulted in significant deformation by middle to late Ordovician times associated to the so-called Famatinian orogeny (e.g. Astini et al., 1995, 1996). During the Devonian, the last terrane that was supposedly accreted to western Gondwana corresponds to the hypothetical Chilenia Terrane (Ramos et al., 1984, 1986). It is thought that Chilenia was detached from Laurentia in Paleozoic times (e.g. Ramos, 2009). However, geological evidence about the nature of this terrane remain elusive as inferences about its existence are largely indirect. These evidences include the geochemical signatures used to interpret the petrogenesis of part of the Paleozoic to Early Mesozoic basement of the Frontal Cordillera. This data points out to a significant contribution from melts derived from a radiogenic continental basement, which probably corresponds to Chilenia (Mpodozis and Kay, 1990). The only rocks that were initially interpreted as Chilenia's basement in Chile correspond to La Pampa gneisses, which crop out in the northern part of the studied region in the Huasco valley at ~ 29ºS. However, recent works indicate a maximum age of igneous emplacement of ~ 307 Ma for these rocks (Álvarez et al., 2013), younger than age of docking of Chilenia (ca. 395 Ma; Davis et al., 2000) and already during the younger Gondwanan tectonic cycle.

Exposures of rocks formed during the Gondwanan tectonic cycle are abundant within the region under study. During this tectonic cycle, a magmatic arc would have developed along the present-day Frontal Cordillera (Table 2.1), flanked to the west by a forearc basin and an accretionary subduction complex. The intrusive rocks representing the magmatic arc correspond to Carboniferous to Permian granitoids from the Elqui superunit in the Elqui-Limarí batholith, exposed along the Frontal Cordillera (Fig. 2.4). These rocks record a change from I to S type magmatism related to crustal thickening on an active continental margin (Mpodozis and Kay, 1990). The volcanics related to this magmatic arc are possibly the Guanaco Sonso member of the Pastos Blancos Group (Thiele, 1964; Martin et al., 1999) and the Matahuaico Formation (Dedios, 1967). The accretionary subduction complex developed during this tectonic cycle is represented by the Paleozoic basement exposed along the coast within the Coastal Cordillera. These rocks correspond to Devonian to Permian phyllites, schists and intense to gently folded turbiditic sandstones and calcareous marine deposits of the Choapa Metamorphic Complex (Table 2.1; Fig. 2.4) (Hervé., 1988; Rebolledo and Charrier, 1994; Rivano and Sepúlveda, 1991). The rocks interpreted to have been deposited in a forearc basin during the Gondwanan tectonic cycle are exposed along the coast within the Coastal Cordillera and throughout the Frontal Cordillera. The ones exposed along the coast correspond to the turbiditic deposits of the Arrayán Formation and the Unidad Sedimentaria Agua Dulce (Rebolledo and Charrier, 1994; Rivano and Sepúlveda, 1991). In turn, the rocks exposed throughout the Frontal Cordillera (Fig. 2.4) correspond to contact metamorphosed plataformal marine deposits of the Las Placetas Beds (Reutter, 1974), Hurtado Formation and El Cepo Metamorphic Complex (Mpodozis and Cornejo, 1988). The metamorphic rocks and turbiditic marine deposits of the Coastal Cordillera are unconformably overlain by coarse to fine marine deposits (Huentelauquén Formation and Quebrada Mal Paso Beds) that were deposited in the forearc basin by the Permian (Rivano and Sepúlveda, 1991). The unconformity between the metamorphic rocks/ turbiditic deposits and the coarse to fine marine deposits evidences that major paleogeographic changes affected the forearc basin by the early Permian (Charrier et al., 2007). They have been related to the San Rafael tectonic phase described for western Argentina (Rapalini et al. 1989). Deformation during this tectonic phase has been associated to the accretion of a new terrane to western Gondwana, known as the “Terrane X” (Mpodozis and Kay, 1990). According to Charrier et al. (2007), the San Rafael tectonic phase may have been caused by amalgamation or accretion of the Devonian to Permian subduction complex during the Gondwanan tectonic cycle.

2.3.2. The Pre Andean cycle

The paleogeography during the Pre Andean cycle (latest Permian to Early Jurassic) was characterized by the presence of a series of NNW-SSE extensional basins. It is thought that these basins developed during a period of no or very slow subduction, probably related to crustal warping during a stationary period for the continental drifting of Gondwana (e.g. Charrier 1979; Mpodozis & Ramos 1989; Mpodozis & Kay 1990). The distribution of the extensional basins would be related to NW-trending weakness zones represented by the sutures that bound the allochthonous terranes accreted in Proterozoic and Paleozoic times (Ramos et al., 1994). Widely distributed exposures of Late Paleozoic to Triassic volcanic and intrusive rocks associated to this tectonic cycle are recognized in Chile and Argentina and are generally referred as the Choiyoi Magmatic Province (Kay et al., 1989). Within the studied region the magmatic rocks assigned to this tectonic cycle correspond to Permo-Triassic calc-alkaline to transitional A-type granites exposed along the Frontal Cordillera and interpreted as result of extensive crustal melting (Fig. 2.4; Inguagás superunit; Mpodozis & Kay 1990). The magmatic activity would be related to silicic volcanic rocks and volcanoclastic deposits exposed as part of the Mesozoic succession of the Coastal Cordillera (Rivano and

Sepúlveda, 1991) and along the Frontal Cordillera (Mpodozis and Cornejo, 1986; Nasi et al., 1990) (Fig. 2.4, Table 2.1). The silicic volcanic rocks are intercalated between Middle Triassic and Upper Triassic to Lower Jurassic transitional to marine deposits (Rivano and Sepúlveda, 1991; Mpodozis and Cornejo, 1986; Nasi et al., 1990) corresponding to the basins sedimentary infill (see Table 2.1). These sedimentary rocks define two rift phases, which are separated by Middle to Upper Triassic silicic volcanic and volcanoclastic rocks, generally referred as the La Totora-Pichidangui volcanic pulse, which is part of the Choiyoi Magmatic Province (Table 2.1). No unconformity is observed separating the Upper Triassic to Lower Jurassic deposits from the rest of the Mesozoic volcano-sedimentary succession throughout the studied region.

2.3.3. The Andean cycle

The Andean cycle (late Early Jurassic to Present) is characterized by renewed subduction activity related to Andean arc magmatism that continued almost uninterrupted right to the present-day (Coira et al., 1982; Mpodozis and Ramos, 1989; Charrier et al., 2007). The Andean Cycle was divided by Charrier et al. (2007) in three stages (Table 2.1) based on the presence of two regional unconformities related to the Peruvian (110-90 Ma) and the K-T (65 Ma) "tectonic phases", respectively (see section 2.1).

2.3.3.1. First stage

The first stage of the Andean cycle (late Early Jurassic–late Early Cretaceous) is characterized by the development of an arc and an extensional back-arc basin to the east presenting two transgression-regression cycles, defining two substages (Table 2.1). Within the studied region the rocks assigned to the first stage are mostly exposed as part of the Mesozoic volcano-sedimentary succession of the Coastal Cordillera and throughout the western Frontal Cordillera (Fig. 2.4). The rocks exposed in the Coastal Cordillera consist of Lower to Upper Jurassic marine to continental deposits and intermediate to acid volcanic and volcanoclastic rocks corresponding from north to south to the Agua Salada Volcanic Complex, the Ajial and the Horqueta formations (Vergara et al., 1995; Emparán and Pineda, 2006) for the first substage and the Bandurrias, Arqueros and the Quebrada Marquesa formations for the second substage (Segerstrom 1960; Aguirre and Egert, 1965; Arévalo 2005). These rocks present arc affinities (Vergara et al., 1995; Morata and Aguirre, 2003) and are interpreted as deposits of a north-south oriented arc established once subduction was resumed along the South American margin (Vergara et al., 1995). In turn, along the Coastal and Frontal Cordilleras a series of Jurassic to Lower Cretaceous marine calcareous rocks with evaporitic intercalations (see Table 2.1, Fig. 2.4) are interpreted as the backarc basin fill (Nasi et al. 1990; Mpodozis & Cornejo 1988; Pineda & Emparan 2006, Arévalo et al., 2009). These rocks are intercalated with thick successions of andesitic and dacitic lavas and conglomerates (Nasi et al., 1990; Mpodozis and Cornejo, 1988), that would represent rift phase sediments and volcanism related to backarc extension (see Table

Cycle			Tectonic conditions and/or paleogeography	Main Geological Units
"Erosional"	Andean		**late Early Jurassic – Present** renewed subduction activity related to Andean arc magmatism and continued almost uninterrupted right through to the present day	
		3d stage Late Palaeogene-Recent	inversion of extensional basin	Escabroso Group, C° de Las Tórtolas Fm. (FC) and Farellones Fms, Miocene magmatic belt
			development of an intra-arc volcano-sedimentary extensional basin	Tilito Fm and Abanico Fm, Oligocene magmatic belt
			arc-retroarc system in a thin crust	Eocene to Oligocene magmatic belt (FC)
			deformation during the Incaic tectonic phase	
		2d stage late Early Cretaceous-Early Palaeogene	magmatic arc related to the development of great calderas	Quebrada Yungay and Los Elquinos Fms., late Cretaceous to Paleocene belt (CC)
			deformation during the K-T tectonic phase	
			volcanoclastic deposits to the east of the inverted basins	Cerrillos Fm; La Totora Beds, Viñita (Salamanca) and Las Chilcas Fms (CC)
			inversion of backarc basins during the Peruvian phase	
		1st stage late Early Jurassic-late Early Cretaceous	development of an arc and an extensional backarc basin in which two trangression regresions cycles are observed, defining two substages:	
			Second substage (Kimmeridgian to Aptian–Albian)	**Second substage** Arc => Bandurrias, Arqueros, Quebrada Marquesa Fm; early to middle Cretaceous magmatic belt (CC) Backarc=> Chanarcillo Group (CC), Pucalume and Río Tascadero Fms (FC) Forearc S La Serena=> Lo Prado and Veta Negra Fm (CC)
			First substage (late Early Jurassic to Kimmeridgian)	**First substage** Arc =>Agua Salada Volcanic Complex, Ajial and Horqueta Fms., Jurassic magmatic belt (CC) Backarc => Lautaro, upper Tres Cruces Fms. (FC) and Cerro La Calera Fm. (CC) Algarrobal and Mostazal Fms (backarc volcanism and rift phase sediments, FC)
"No subduction"	Pre Andean		**latest Permian - earliest Jurassic** developing of NNW-SSE extensional basins during a period of no or very slow subduction probably related to crustal warping during a stationary period for continental drifting of Gondwana two rift phases define two stages an are related widespread plutonic activity related to volcanism throughout the complete cycle	Ingaguás Superunit (FC) and Talinay Complex (CC)
		2d stage Late Middle Triassic to Early Late Triassic	marine and continental deposition throughout NNW-SSE basins	Los Molles (CC), Lautaro, Las Breas and lower Tres Cruces Fms (FC)
		1st stage Late Permian to late Anisian	silicic volcanic and volcanoclastic deposits (*La Totora - Pichidangui* volcanic pulse)	Pichidangui and La Ligua Fms (CC) and La Totora and Pastos Blancos (Los Tilos menber) in FC
			marine deposition throughout NNW-SSE	Canto del Agua and El Quereo Fms (CC) and San Félix Fms (western border FC)
"Collisional"	Gondwanan		**Late Devonian - earliest Permian** development of a magmatic arc along the present-day FC flanked to the west by a forearc basin in present.day FC and CC and an accretionary complex further west along the present-day CC	
		3d stage Early Permian to Middle– Late? Permian	deposition of coarse to fine marine deposits in a shallowing forearc basin in CC	Huentelauquen Fm and Quebrada Mal Paso Beds/ CC
			deformation related to San Raphael phase	
		2d stage Late Carboniferous to earliest Permian	major develoment of the arc	Elqui Superunit, Pastos Blancos Fm (Guanaco sonso member), Matahuaico Fm and upper Choiyoi Group/ FC (Chile and Argentina)
		1st stage Middle/Late Devonian to Early Carboniferous	development of a subduction complex represented by metamorphic in the CC and a forearc basin represented by turbiditic deposits in the CC and plataformal deposits in the FC	Choapa Metamorphic Complex, Arrayán Fm, Unidad Sedimentaria Agua Dulce/ CC Las Placetas Beds, Hurtado Fm, El Cepo Metamorphic Complex/ FC
	Famatinian		**latest Cambrian - Early Devonian** Terrane accretions related to Laurentia- Gondwana interactions	La Pampa Gneisses/ FC-Huasco river
	Pampean		**Late Proterozoic - Early Cambrian** Two interpretations for this period: Interaction of Laurentia (present-day western North America) with western margin of Gondwana (present-day western South America) resulting in deformation and terrane accretion or active continental margin in northern Chile and Argentina and terrane accretion further south	no geological units in the study region

Table 2.1. Chronostratigraphic chart showing tectonic cycles and main geological events and units throughout north-central Chile. CC= Coastal Cordillera, FC= Frontal Cordillera.

2.1; e.g. Charrier et al., 2007).

Importantly, for the second substage another group of rock units are recognized throughout the Coastal Cordillera west from the arc-related deposits. These rocks correspond to the Lo Prado and Veta Negra formations. The first one mainly consists of marine sandstones, limestones and a bimodal succession of ignimbrites and basalts; whereas the second one corresponds mainly to basaltic to andesitic volcanic succession with minor sedimentary intercalations (Thomas, 1956; Piracés, 1976; Vergara et al., 1995). These formations have been interpreted as deposited in a forearc basin exposed southwards from 30°S (Lo Prado forearc basin, Charrier et al., 2007; modified by Jara and Charrier, in press).

Although plutonic activity was rather continuous during the first and second substages (Charrier et al., 2007), two north-south elongated intrusive belts present well differentiated exposures in the Coastal Cordillera of the studied region (Fig. 2.4): the Middle Jurassic to Early Cretaceous Mincha Superunit (Parada et al., 1988) and the late Early Cretaceous Illapel Plutonic Complex (the Illapel Super-unity of Rivano et al., 1985; amended by Parada et al., 1999). The former one consists of mainly monzogranites, sienogranites, tonalites and granodiorites, whereas the second one consists of tonalites and granodiorites, with minor diorites and trondhjemitic differentiates. The Illapel Plutonic Complex is thought to have developed under strong crustal extensional conditions of P= 1.8 ± 0.6 kbar and T= 723.4 ± 75°C (Varas, 2011).

During the Peruvian (Steinmann, 1929) and the K-T (Cornejo et al., 2003) phases the marine basins developed during the second substage of the first stage of the Andean cycle would have been inverted along north-to-south faults located at the western and eastern borders of the Coastal Cordillera (Fig. 2.4). These faults correspond to La Silla del Gobernador Fault (Arancibia, 2004) along the western border and the Agua de Los Burros Fault (Arévalo et al., 2009) and the El Chape Fault (Pineda and Emparán, 2006) along the eastern border of the Coastal Cordillera (Fig. 2.4).

2.3.3.2. Second stage

The second stage of the Andean cycle (late Early Cretaceous–Early Palaeogene) took place in between the periods of accelerated contractional deformation represented by the Peruvian and the Incaic tectonic phases. This stage is characterized by the development of a series of fault controlled extensional basins located along the magmatic arc and frequently associated with formation of great calderas (Charrier et al., 2007). The rock units assigned to this stage are exposed along the eastern border of the Coastal Cordillera and the western border of the Frontal Cordillera. Two main groups can be recognized. In some areas, the two groups of stratified units are separated from each other by an unconformity, probably formed after the K-T tectonic phase around ~ 65 Ma (Arévalo et al., 2009; Pineda and Calderón, 2009; Martínez et al., 2013). The older units correspond to Lower Cretaceous to Lower Paleogene continental basic to intermediate volcanic rocks and coarse to fine sedimentary deposits, interpreted as developed in continental extensional basins to the east of the inverted marine basins of the first stage (Charrier et al., 2007). They correspond to the Cerrillos Formation (Nasi et al., 1990), the Quebrada La Totora Beds (Pineda and Calderón, 2008) and the Viñita (Aguirre and Egert, 1965; amended by Emparán & Pineda, 1999) and Salamanca formations (Rivano et al., 1993). It has been suggested that these deposits would have developed in continental extensional basins (Charrier et al., 2007; Pineda and Calderón, 2008; Martínez et al., 2013). However, coarse conglomeratic facies within these deposits suggests that they may correspond, at least in part, to syntectonic deposits generated during the Peruvian phase. The younger stratified units of the second stage correspond to caldera-related pyroclastic deposits and basic to intermediate volcanic successions. They correspond to the Quebrada Yungay Beds (Pineda and Emparán, 2006) and Los Elquinos (Dedios, 1967) and Estero Cenicero (Rivano and Sepúlveda, 1991) formations. Arc-related plutonic activity of the second stage of the Andean Cycle is represented in the study region by intrusive units exposed at the border between the Coastal Cordillera and the Frontal Cordillera and along the Frontal Cordillera. Two main plutonic belts, one from the Late Cretaceous to Paleocene and another of Eocene to Oligocene ages are recognized (Fig. 2.4; SERNAGEOMIN, 2003). At the end of this stage, tectonic inversion related to the Incaic tectonic phase occurred along east and west vergent NNE-SSW to N-S trending faults within the Frontal Cordillera (Emparán and Pineda, 1999; Pineda and Emparán, 2006; Pineda and Calderón, 2008; Salazar, 2012). In particular, in the area of La Serena the Vicuña and Rivadavia faults (Fig. 2.4) would have formed a pop-up system around ~ 40- 34 Ma throughout the western border of the Frontal Cordillera (Emparán and Pineda, 1999; Pineda and Emparán, 2006; Pineda and Calderón, 2008).

2.3.3.3. Third stage

The third stage of the Andean Cycle is characterized by the development of north-to-south oriented magmatic arcs and their associated foreland basins, which are successively shifted eastward after deformational events. At the beginning of this stage the main morphologic feature corresponds to the Incaic Range. The Incaic range formed at the end of the second stage by the inversion and associated uplift of NNE-SSW to N-S trending faults with east and west vergency along the Frontal Cordillera.

The stratified units developed during the third stage are mainly exposed along the western border of the Coastal Cordillera and the Frontal Cordillera (Fig. 2.4).

Along the Coastal Cordillera, the stratified units of the second stage correspond to sedimentary deposits. They include the marine to transitional sandstones and limestones of the Early Miocene to Pleistocene Coquimbo Formation (Le Roux et al., 2005) (Fig. 2.4). South of 30°S, the mentioned deposits interfinger towards the east with unconsolidated fluvial gravels and alluvial breccias of the Miocene to Pleistocene Confluencia Formation (Rivano and Sepúlveda, 1991) (Fig. 2.4). North of 30°S, the Early Miocene Domeyko Gravels correspond to fluvial and alluvial gravels that were

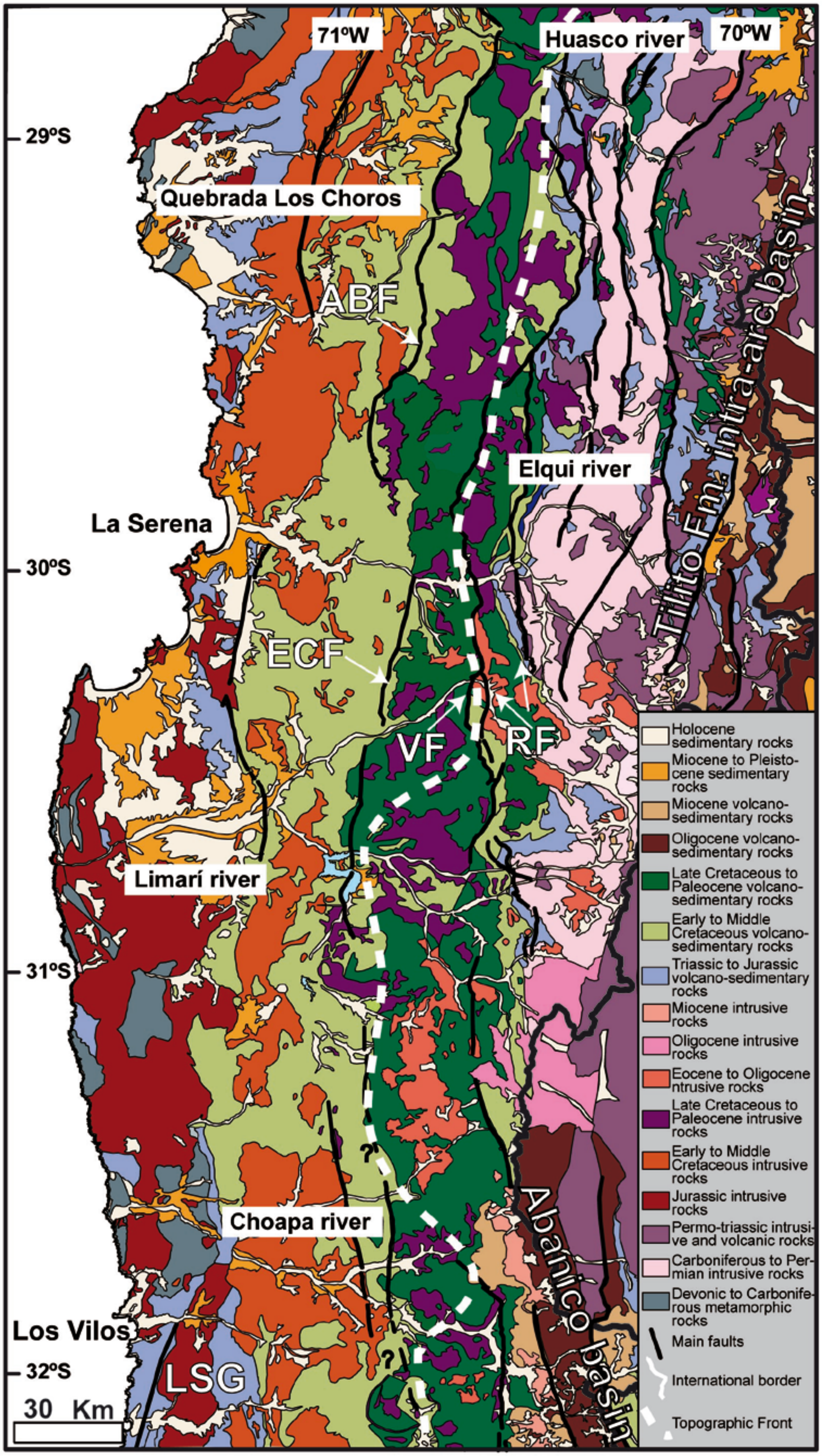

Fig 2.4. Geological map of north-central Chile, modified from Sernageomin (2003). ABF: Agua de los Burros Fault, ECF= El Chape Fault, VF= Vicuña Fault, RF= Rivadavia Fault, LSG= LA Silla del Gobernador Fault.

deposited within a topographic depression in the present-day Coastal Cordillera (Arévalo et al., 2009). The sedimentary units exposed along the Coastal Cordillera would represent the erosional material associated to uplift affecting both the Coastal and Frontal Cordilleras during the Miocene (Valdés, 2009).

Along the Frontal Cordillera the stratified units of the second stage are exposed along the international border between Chile and Argentina. They correspond mostly to Oligocene to Late Miocene volcanic and volcanoclastic rocks presenting interbedded Lower to Upper Miocene sedimentary deposits (Fig. 2.4). The sedimentary deposits are associated with pedimentation surfaces (Bissig et al., 2001). The stratified units in the Frontal Cordillera were first recognized as the Doña Ana Formation (Thiele, 1964; Maksaev et al., 1984). Later, the Tilito and Escabroso members of the original Doña Ana Formation were redefined and elevated to the status of Tilito and Escabroso formations. Consequently, the Doña Ana Formation was elevated to the status of Doña Ana Group (Martin et al. 1995). Recently, based on more detailed geological mapping in the Frontal Cordillera of La Serena area, the Escabroso Formation was subdivided and elevated to group status (Heather and Diaz, 2000), leaving the Doña Ana Group nomenclature obsolete. However, Doña Ana Group is still the most widely used nomenclature to refer to these units (e.g. Litvak et al., 2007; Winocur et al., in press). The Late Oligocene to earliest Miocene Tilito Formation consists mainly of rhyolites, dacitic tuffs and volcanic breccias; whereas the Early Miocene Escabroso Group consists of andesites flows, breccias and volcanoclastic sediments. The Escabroso Group is unconformably overlain by the andesitic lavas and tuffs of the Early to Middle Miocene Cerro de las Tótolas Formation (Maksaev et al., 1984). The Tilito Formation would be related to the development of an Oligocene intra-arc extensional basin (Table 2.1; Kay and Mpodozis, 2002; Litvak et al., 2007; Winocur, 2010; Winocur et al., accepted). It is correlated to the Abanico Formation exposed south of 32°S that also developed within a volcano-sedimentary extensional basin (the Abanico Extensional Basin, Charrier et al., 2002). The Tilito Formation intra-arc basin would have been tectonically inverted in successive pulses from the Early to the Late Miocene (Winocur, 2010). Although magmatism markedly decreased after 13 Ma throughout north-central Chile, minor volcanism continued until the Late Pliocene (Bissig et al., 2001; Kay and Mpodozis, 2002; Litvak et al., 2007). The Middle Miocene to Late Pliocene units correspond to the essentially dacitic to rhyolitic volcanics of the Vacas Heladas Formation (Martin et al., 1995; Bissig et al. 2001; Cerro de las Tórtolas II according to Kay et al., 1999 and Tambo Formation in Martin et al., 1997), the Vallecito Formation (Thiele, 1964; Maksaev et al., 1984, Bissig et al., 2001) and the Cerro de Vidrio dome (Bissig et al., 2001). The sedimentary deposits interbedded between the volcanic rocks and their related pedimentation surfaces have been related to uplift pulses affecting the area along the international border between Chile and Argentina during the Miocene and the Pliocene (Bissig et al., 2001; Nalpas et al., 2009).

Arc-related magmatic activity for this stage is represented by three main intrusive units of the Eocene to Oligocene, the Oligocene and the Early to Middle Miocene (Fig. 2.4). The Eocene to Oligocene belt consists of granodiorites and tonalites with subordinated diorites (Nasi et al., 1990; Rivano and Sepúlveda, 1991; Martin et al., 1995), whereas the Oligocene belt is formed by monzogranites and granodiorites with minor monzodiorites and diorites (Rivano and Sepúlveda, 1991). The Early to Middle Miocene belt is mostly exposed southwards from 31.5°S (Fig. 2.4). It is composed of andesitic and dioritic porphyries and granodioritic and tonalitic stocks (Maksaev et al., 1984, Rivano and Sepúlveda 1991).

2.4. Cenozoic erosion in the Andean forearc of Central Chile 33-34°S

2.4.1. Introduction

The following article reconstructs the possible erosional paths and identified the morphostructural units subjected to erosion during the Cenozoic across the Andean forearc of central Chile between 33 and 34°S. Central Chile is located just to the south of the Andean region analyzed in the present thesis. The present-day tectonic and climatic conditions in central Chile are markedly different to the ones described earlier in this chapter for north-central Chile. The subduction angle is normal ~ 30°S at least since ~ 10 Ma (Charrier et al., 2012) and the climate is more humid than north of 33°S since the Middle Miocene (Le Roux, 2012). Moreover, south of 33°S the Central Depression develops to the east of the Coastal Cordillera, contrary to what is observed in north-central Chile. Thus, comparison of the results obtained in this article and the ones obtained in the present thesis give us insights on how variability of tectonic/climatic conditions define differences in the present-day morphology of the Andes.

Importantly, the main obstacle on determining the erosional paths in central Chile corresponds to the uncertainty in the age of the sediments whose provenance is analyzed. These deposits correspond to the marine to transitional Navidad, Lincacheo, Rapel and La Cueva formations, which were deposited within the Navidad Basin, exposed now along the coast of central Chile. That obstacle initially preclude us to be more conclusive with respect to where were located the main topographic features subjected to erosion during the Cenozoic in Central Chile. However, over the last year new sedimentological and geochronological studies focused in these deposits have been published and a generally consensus exists now (Le Roux et al., 2013; Finger et al., 2013) that sedimentation within the Navidad Basin would have started in the Early Miocene (Gutiérrez et al., 2013) rather than in the Late Miocene (Finger et al., 2007; Encinas et al., 2008). This has important implication on the interpretation of the provenance results that are discussed at the end of this chapter.

2.4.2. Article: “Cenozoic erosion in the Andean forearc of Central Chile 33-34°S: Sediment provenance inferred by heavy mineral studies”.

Geological Society of America Special Papers

Cenozoic erosion in the Andean forearc in Central Chile (33°–34°S): Sediment provenance inferred by heavy mineral studies

María Pía Rodríguez, Luisa Pinto Lincoñir and Alfonso Encinas

Geological Society of America Special Papers 2012;487;141-162
doi: 10.1130/2012.2487(09)

The Geological Society of America
Special Paper 487
2012

Cenozoic erosion in the Andean forearc in Central Chile (33°–34°S): Sediment provenance inferred by heavy mineral studies

María Pía Rodríguez
Luisa Pinto Lincoñir
Departamento de Geología, Facultad de Ciencias Físicas y Matemáticas, Universidad de Chile, Casilla 13518, Correo 21, Santiago, Chile

Alfonso Encinas
Departamento de Ciencias de la Tierra, Facultad de Ciencias Químicas, Universidad de Concepción, Edmundo Larenas 129, Casilla 160-C, Concepción, Chile

ABSTRACT

The forearc of Central Chile (33°–34°S) is formed by three N-S–trending morphostructural units, including, from west to east, the Coastal Cordillera, the Central Depression, and the Principal Cordillera. The Cenozoic sedimentary rocks that could represent the erosional material generated throughout the morphotectonic evolution of these units accumulated in the marine Navidad Basin. The age of the marine deposits is controversial, as foraminifer biostratigraphy indicates that marine deposition started during the late Miocene, whereas $^{87}Sr/^{86}Sr$ data indicate that deposition started during the early Miocene. We carried out single heavy mineral microprobe analysis and standard heavy mineral analysis of these deposits in order to qualitatively identify the geological units subjected to erosion in the central Chilean forearc during Cenozoic times. Our analysis focused mainly on unweathered and unaltered detrital garnet, pyroxene, and amphibole. The textural characteristics and geochemical signature of these minerals were used to determine their original rock type; their magmatic affinity, in the case of pyroxenes of volcanic origin; and their metamorphic grade, in the case of amphiboles of metamorphic origin. We have also compared the composition of detrital garnet, pyroxene, and amphibole with preexisting chemical data of these minerals in the possible source rocks, which, along with the analysis of the detrital heavy mineral suite in each sample, allows us to determine the specific geological unit from which they were generated. Three erosional-depositional stages are recorded by our analysis. Whereas the chemistry of pyroxene and amphibole characterized volcanic-subvolcanic sources within the present-day Central Depression for the first stage, the Central Depression and the Principal Cordillera for the second stage, and the Principal Cordillera for the third stage; the composition of garnet is indicative of metamorphic and plutonic sources within the Coastal Cordillera during all three stages. If marine deposition inside the Navidad Basin started during

Rodríguez, M.P., Pinto Lincoñir, L., and Encinas, A., 2012, Cenozoic erosion in the Andean forearc in Central Chile (33°–34°S): Sediment provenance inferred by heavy mineral studies, *in* Rasbury, E.T., Hemming, S.R., and Riggs, N.R., eds., Mineralogical and Geochemical Approaches to Provenance: Geological Society of America Special Paper 487, p. 141–162, doi:10.1130/2012.2487(09). For permission to copy, contact editing@geosociety.org.

the early Miocene, the provenance results would record erosion and deposition contemporary with volcanic activity. On the other hand, if marine deposition started during the late Miocene, the provenance results show a retrograde erosive response to landscape for a regional uplift event proposed for that period in the study area. Also, assuming that provenance results are directly related to the action of faults, our data indicate that the main relief-generating fault during the early stages of Andean uplift corresponds to the Los Ángeles–Infiernillo Fault, rather than the San Ramón Fault, as stated by the proposed morphotectonic models for the study area. In addition, the ubiquitous provenance from the Coastal Cordillera is more likely to represent the erosion of nearshore basement rocks affected by faulting along the eastern border of the Navidad Basin, rather than uplift and erosion of the Coastal Cordillera, as previously considered. Single-mineral geochemical analysis of detrital pyroxene and amphibole can be used in other sedimentary basins related to arc-magmatic systems with short transport distances, like the ones in the western Andean border, where these minerals tend to be largely unweathered. In particular, our work represents an advance in this field, as the chemistry of detrital amphibole has not been used before to discriminate source rocks presenting different geochemical signatures.

INTRODUCTION

The morphostructural units that constitute the Andean forearc in Central Chile are the Coastal Cordillera, the Central Depression, and the Principal Cordillera. Each of these units can be subdivided into subunits on the basis of their morphological and lithological characteristics, which will be described in detail in the next section (see also Fig. 1). Two main morphotectonic models have been proposed for the study region, which differ in the interpretation for uplift timing and for the main vergence assigned to the first-order structure controlling morphotectonic evolution. The morphotectonic model of Farías et al. (2008) proposes a main regional uplift event that affected the entire forearc during the late Miocene with an east-vergent, crustal-scale décollement underneath the Andean orogen as the first-order structure and an associated second-order fault, the San Ramón Fault, controlling forearc uplift. In this model the main deformation event corresponds to the tectonic inversion of an extensional basin filled with volcanic deposits, which took place somewhat earlier during the late Oligocene to early Miocene (Charrier et al., 2002, 2005; Fock, 2005). On the other hand, the morphotectonic model of Armijo et al. (2010) states that the main uplift and deformation were coeval, and started during the late Oligocene to early Miocene, associated with westward fault propagation and related folding along the San Ramón Fault, which steps down eastward, constituting the first-order structure. A debate similar to the one concerning uplift timing involves the age of the deposits generated through Andean uplift. The sedimentary rocks that could represent the erosional material related to uplift and exhumation in Central Chile accumulated in the marine Navidad Basin, and now crop out in the western Coastal Cordillera (Fig. 1; Navidad, Lincancheo, Rapel, and La Cueva Formations; Encinas et al., 2006a, 2008). Whereas foraminifer biostratigraphy indicates that deposition started during the late Miocene (Finger et al., 2007; Encinas et al., 2008), $^{87}Sr/^{86}Sr$ determinations from macrofossils indicate that initiation of marine deposition started earlier during early Miocene times (Encinas, 2006; Nielsen and Glodny, 2009; Gutiérrez et al., 2009; Hinojosa and Gutiérrez, 2009). In this study we present the results of standard heavy mineral analysis (with a density greater than 2.89 g/cm^3) and single-grain microprobe analysis of heavy mineral grains from marine deposits of the Navidad Basin with the purpose of identifying source rocks for the sedimentary units in the basin (see Morton, 1985; Pettijohn et al., 1987; Weltje and von Eynatten, 2004). We have applied a single-mineral geochemical approach, because in a continental volcanic arc like the Andes, where the majority of rocks are arc-related, this type of analysis can give us detailed information about source rocks usually unavailable from conventional heavy mineral analysis (Mange and Morton, 2007). Our work is focused on the most common heavy minerals in Andean-type igneous rocks, pyroxene and amphibole, in order to find geochemical signatures in these detrital minerals that could be diagnostic of the particular geological units in which they were generated. As metamorphic sources for the Cenozoic deposits possibly also exist, we analyzed the chemistry of detrital garnet, because garnet is a ubiquitous mineral in the metamorphic outcrops in Central Chile. In general, our results show that in sedimentary basins related to arc-magmatic systems with short transport distances, such as the ones in the western Andean border, detrital pyroxene and amphibole are largely unweathered. This implies that the geochemical data obtained from them reflect the chemistry of these minerals in their original source rocks and are useful in qualitatively determining the geological units in which they were generated. Our results allow us to develop a provenance-based erosional model, which is compared with the morphotectonic models proposed for the study region in order to determine which models are consistent with the erosional paths recorded in the Cenozoic deposits.

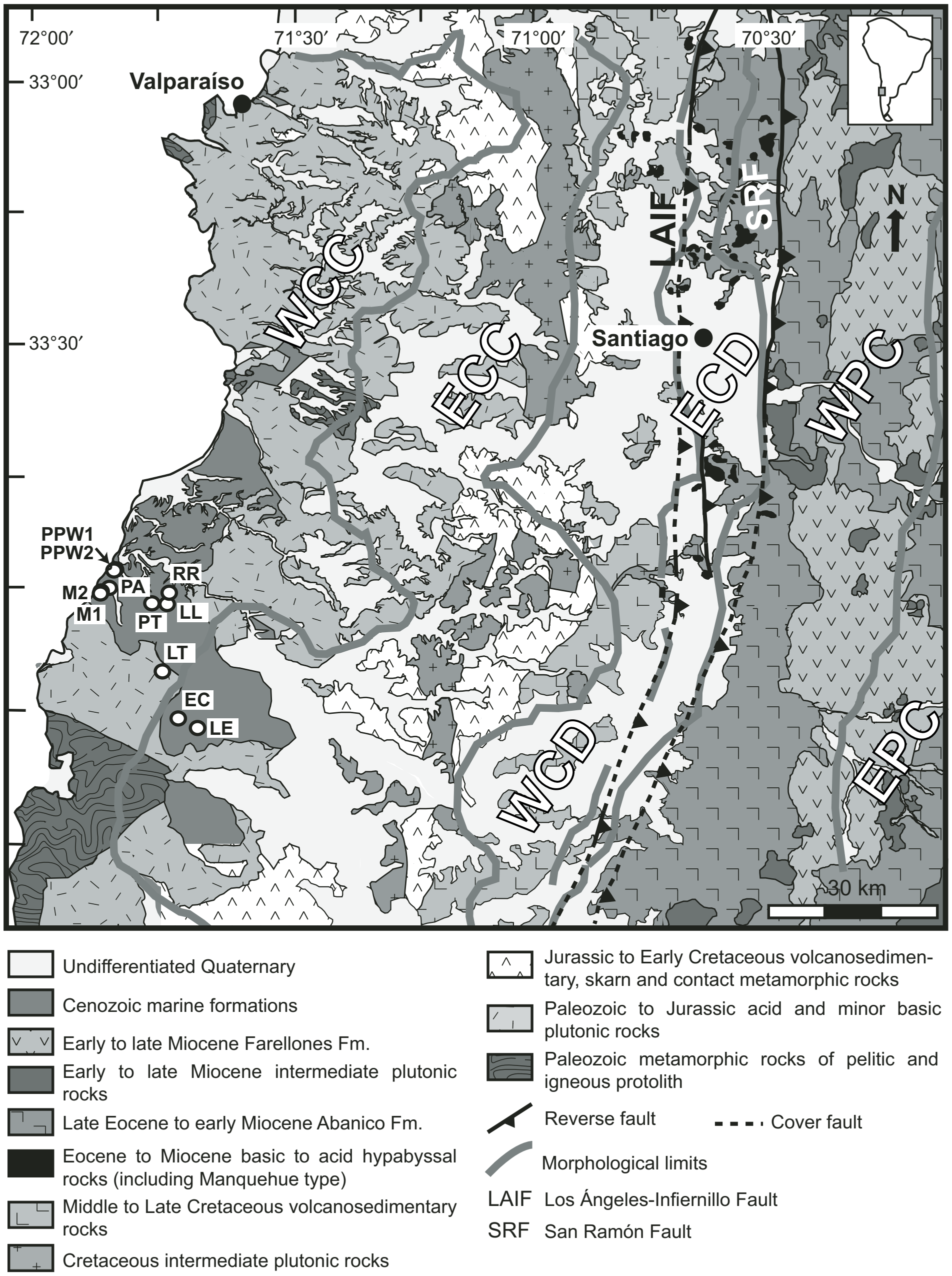

Figure 1. Geological map of the study region (modified from Thiele, 1980; Gana et al., 1996; Wall et al., 1996; Sellés and Gana, 2001; SERNAGEOMIN, 2003). Morphostructural units in the study region are indicated as follows: WCC—western Coastal Cordillera; ECC—eastern Coastal Cordillera; WCD—western Central Depression; ECD—eastern Central Depression; WPC—western Principal Cordillera; EPC—eastern Principal Cordillera. White circles indicate stratigraphic columns where heavy minerals used in this study were extracted.

GEOLOGICAL SETTING

The Coastal Cordillera reaches 2150 m above sea level (a.s.l.) in the study region and can be subdivided into a western and an eastern domain (Fig. 1). The western Coastal Cordillera reaches ~500 m a.s.l. and is composed mainly of a series of erosional surfaces of marine origin, probably constructed during the late Pliocene–Pleistocene (Gana et al., 1996; Rodríguez, 2008) (Fig. 1). The rocks in the western Coastal Cordillera comprise a Paleozoic to Jurassic metamorphic and intrusive basement covered by Cenozoic marine deposits, the provenance of which is studied in this chapter. The Paleozoic metamorphic basement consists mainly of Barrovian-type metapelitic rocks (Western Series of the Paired Metamorphic Belt, Hervé, 1988; Willner, 2005) and migmatitic gneisses (Valparaíso Metamorphic Complex, Gana et al., 1996; Creixell, 2007). The Paleozoic plutonic rocks are granitoids of intermediate to acid composition, whereas the Triassic and Jurassic plutonic rocks present a characteristic bimodal composition (Gana et al., 1996; Wall et al., 1996). The Cenozoic marine deposits (Navidad, Lincancheo, Rapel, and La Cueva Formations) are described in detail in the next section. In contrast, the eastern Coastal Cordillera (Fig. 1) reaches

~2000 m a.s.l. and presents low relief surfaces at its summit, which have been interpreted as remnants of an ancient peneplain (Brüggen, 1950; Borde, 1966; Farías et al., 2006, 2008). The rocks in the eastern Coastal Cordillera consist of a thick Jurassic–Cretaceous volcano-sedimentary succession of bimodal composition and Cretaceous plutonic rocks of intermediate composition. The lower part of the stratified succession is affected by contact metamorphism on pelitic and calcareous sediments (Núñez, 1991; Gana et al., 1996).

The Central Depression separates the Coastal Cordillera from the Principal Cordillera (Fig. 1). Morphologically it consists of a Quaternary sedimentary and ignimbritic cover with some isolated hills and junction ridges between the Coastal Cordillera and the Principal Cordillera. The junction ridges represent the highest elevations within the Central Depression, reaching 1600 m a.s.l. The isolated hills and junction ridges have been interpreted as inselbergs related to more resistant lithologies (Farías et al., 2008). The Central Depression is also divided into two domains, one to the west, the western Central Depression, and one to the east, the eastern Central Depression (Fig. 1). The western Central Depression is mostly made up of Late Cretaceous volcano-sedimentary rocks (Thomas, 1958), and the eastern Central Depression is composed of volcanic rocks of the Abanico West Formation and related hypabyssal intrusives rocks (López-Escobar and Vergara, 1997; Wall et al., 1999; Vergara et al., 1999, 2004; Nyström et al., 2003; Fuentes, 2004) (Fig. 1). North of 35°S, the Abanico West Formation outcrops contain rocks of basic to intermediate compositions, whereas south of 35°S they contain rocks of intermediate to acid compositions (López-Escobar and Vergara, 1997). Reported $^{40}Ar/^{39}Ar$ plagioclase and K/Ar whole-rock ages for the Abanico West Formation in the study region are between 34.3 ± 2.2 Ma and 19.3 ± 1.4 Ma (Gana and Wall, 1997). The hypabyssal intrusives in the eastern Central Depression have been related to three subvolcanic episodes. The first (Oligocene, $^{40}Ar/^{39}Ar$ plagioclase ages between 30.9 ± 1.9 Ma and 25.2 ± 0.6 Ma) presents basaltic to rhyolitic compositions. The second (early Miocene, K/Ar whole-rock ages between 22.3 ± 1.8 Ma and 20.3 ± 1.9 Ma) reflects mainly basaltic compositions. The third (Miocene, $^{40}Ar/^{39}Ar$ plagioclase and amphibole and K/Ar whole-rock ages between 20.3 ± 5.4 Ma and 16.7 ± 0.9 Ma) reflects dacitic compositions, and its products are usually known as Manquehue-type porphyries (Sellés, 1999; Fuentes, 2004; Vergara et al., 2004). According to Vergara et al. (2004), these porphyries correspond to the feeder system of stratovolcanoes, which are now completely eroded.

The Principal Cordillera reaches its highest elevations near 6000 m a.s.l. near 33°S. It is subdivided into the western Principal Cordillera, consisting of Cenozoic rocks strongly deformed at its westernmost side. The central Principal Cordillera also consists of Cenozoic rocks, and the eastern Principal Cordillera consists of Mesozoic rocks (Farías, 2007). Along the eastern border of the central Principal Cordillera the Cenozoic deposits are intensely deformed, and in the eastern Principal Cordillera the Aconcagua fold and thrust belt is developed mainly in the Argentinean foreland at the latitude of Santiago. The rocks in the western Principal Cordillera correspond mainly to volcanic rocks with basic to acid compositions (Farellones Formation) and intermediate to acid Miocene plutonic rocks and volcanic rocks (Abanico East Formation) (Fig. 1). Reported ages for the Farellones Formation in the Santiago region are between 21.6 ± 0.2 ($^{40}Ar/^{39}Ar$ plagioclase) and 16.6 ± 0.7 Ma (K/Ar whole-rock ages) (Beccar et al., 1986; Aguirre et al., 2000), whereas rocks related to the Farellones Formation in the Rancagua region present somewhat younger ages, between 14.4 ± 0.9 Ma and 7.8 ± 0.4 Ma (K/Ar whole-rock, hornblende, and biotite ages; Kay et al., 2005). In the Principal Cordillera, Pliocene volcanic outcrops are scarce, and only the andesitic to dacitic "Coladas de Valle" (K/Ar whole-rock ages between 1.8 ± 0.2 Ma and 2.3 ± 0.4 Ma; Charrier and Munizaga, 1979) have been studied in any detail.

The principal fault zones recognized in the forearc of Central Chile that could be related to deformation and surface uplift are the Los Ángeles–Infiernillo Fault (Aguirre, 1957, 1960; Fock, 2005) and the San Ramón Fault (Brüggen, 1950; Rauld, 2002; Rauld et al., 2006) (Fig. 1). The Los Ángeles–Infiernillo Fault corresponds to a N-S–trending vertical structure that separates the western Central Depression from the eastern Central Depression, and has been described as a normal fault inverted during one or more deformation events during the late Oligocene–early Miocene (Fock, 2005). However, superficial seismic activity has been recognized at this fault within Santiago city (Pardo et al., 2008). The N-S–trending San Ramón Fault lies along the western border of the western Principal Cordillera, separating this morphostructural unit from the Central Depression to the west. Along this fault, tectonic activity affecting alluvial and fluvial deposits has been recognized, allowing this structure to be interpreted as a west-vergent reverse fault that could have controlled the uplift of the Principal Cordillera (Rauld, 2002; Rauld et al., 2006).

CENOZOIC SEDIMENTS

In the forearc of Central Chile, the Navidad, Lincancheo, Rapel, and La Cueva Formations (Darwin, 1846; Brüggen, 1950; Tavera, 1979; Gana et al., 1996; Encinas et al., 2006a, 2006b, 2008) represent the only Cenozoic deposits that could contain material related to uplift and subsequent erosion in the Central Chilean Andes (Borde, 1966). These units were accumulated in the Navidad Basin, and at present they crop out in the western Coastal Cordillera between Valparaíso and Punta Topocalma (Fig. 1).

The Navidad Formation (Encinas et al., 2006a, 2008) is ~100–200 m thick. It overlies Upper Cretaceous marine strata of the Punta Topocalma Formation (Cecioni, 1978) or Paleozoic granitic basement, and it underlies the Licancheo Formation (Encinas et al., 2006a) (Fig. 2). The Navidad Formation comprises a basal conglomerate, interpreted as deposited in a coastal environment (Encinas et al., 2006a), overlain by a succession of interbedded siltstone and sandstone with minor conglomerate, interpreted as deep-marine (~2000 m) deposits (Encinas, 2006;

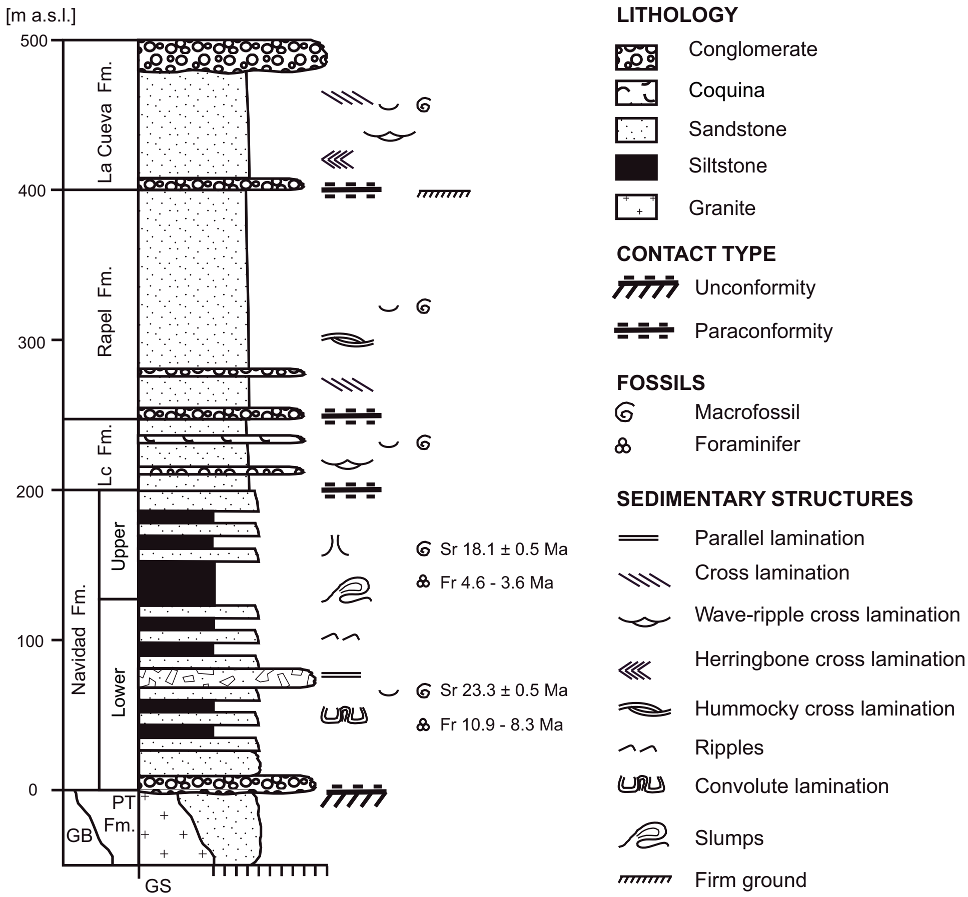

Figure 2. Schematic stratigraphic column for Navidad Basin sediments. GB—granitic basement; PT Fm.—Punta Topocalma Formation; Lc Fm.—Lincancheo Formation; GS—grain size of sediments. Sr refers to $^{87}Sr/^{86}Sr$ age determinations, and Fr refers to foraminifer ages.

Finger et al., 2007; Encinas et al., 2008). Analysis of planktonic foraminifers has established the ages of two siltstone beds in the Navidad Formation. One siltstone bed near the base has an age of 10.9–8.3 Ma (late Miocene), whereas the other at a higher stratigraphic level has an age of 4.6–3.6 Ma (early Pliocene) (Finger et al., 2007; Encinas et al., 2008). On the contrary, $^{87}Sr/^{86}Sr$ determinations in macrofossils indicate ages of 23.3 ± 0.5 Ma (late Oligocene–early Miocene) and 18.1 ± 0.5 Ma (early Miocene) for the same stratigraphic levels, respectively (Encinas, 2006; Nielsen and Glodny, 2009; Gutiérrez et al., 2009; Hinojosa and Gutiérrez, 2009). Although the molluscan fauna of the Navidad Formation is remarkably similar to macrofossils documented in the late Oligocene to early Miocene of Peru, it has been interpreted as having been reworked from older units (Encinas, 2006; Finger et al., 2007; Nielsen and Glodny, 2009). From now on, we refer to the stratigraphic levels between the base and the level representing ca. 10.9 Ma (foraminifers) or ca. 23.3 Ma (strontium) as *lower Navidad Formation,* and to the stratigraphic levels between the ca. 4.6 Ma (foraminifers) or ca. 18.1 Ma (strontium) level and the top as *upper Navidad Formation* (Fig. 2).

The Lincancheo Formation (Encinas et al., 2006a) has a maximum thickness of 40 m. It overlies marine strata of the Navidad Formation or the Paleozoic granitic basement, and underlies the Rapel Formation (Encinas et al., 2006a). It comprises mainly fine-grained, massive sandstones and minor siltstones, conglomerates, and coquinas of centimeter thickness, and it has been interpreted as high-energy, shallow-marine deposits (Encinas et al., 2006a). Based on planktonic foraminifers, age determinations for the Navidad Formation, and the stratigraphic relationships with the Navidad and Rapel Formations, an imprecise Pliocene age has been assigned to the Lincancheo Formation (Encinas et al., 2006a). On the other hand, $^{87}Sr/^{86}Sr$ ages of 18.0 ± 0.5 Ma and 12.9 ± 0.7 Ma (early to middle Miocene) were also obtained for the Lincancheo Formation (Encinas, 2006) (Fig. 2).

The Rapel Formation (Encinas et al., 2006a), which has a maximum thickness of 154 m, overlies the marine Lincancheo Formation and Paleozoic granitic basement, and underlies the La Cueva Formation (Encinas et al., 2006a). It comprises fine-grained sandstones with scarce conglomerates and siltstones (Fig. 2). The lower part of the Rapel Formation has been interpreted as deltaic deposits, whereas the upper part was deposited in a high-energy, shallow-marine environment (Encinas et al., 2006a). By means of its stratigraphic relationship with the La Cueva Formation, an imprecise Pliocene age has been assigned to the Rapel Formation (Encinas et al., 2006b). However, considering $^{87}Sr/^{86}Sr$ ages determined for the Lincancheo

Formation (Encinas, 2006), a late Miocene to Pliocene age could also be assigned to the Rapel Formation.

The La Cueva Formation (Encinas et al., 2006a, 2006b) has a maximum thickness of 100 m. It overlies the Rapel Formation or the Paleozoic intrusive basement, and it unconformably underlies Pleistocene continental deposits (Encinas et al., 2006a). The widespread facies of the La Cueva Formation consists of medium- and coarse-grained sandstone with planar, trough, and herringbone cross-bedding. Toward the top a matrix- to clast-supported conglomerate, formed mainly by volcanic clasts, caps the section (Encinas et al., 2006b) (Fig. 2). The La Cueva Formation has been interpreted as high-energy, shallow-marine deposits (Lavenu and Encinas, 2005; Encinas et al., 2006a), and the conglomerate at the top of the section has been interpreted as a lahar deposit (Encinas et al., 2006b). The age of the La Cueva Formation is not well defined, but a maximum early Pliocene age was ascribed on the basis of a whole-rock K/Ar age of 4.6 ± 0.4 Ma from a scoria clast interbedded within the deposit (Encinas et al., 2006b). This age should be taken with caution, as it was obtained from a volcanic clast, which is more likely to represent the age of the source rocks for the deposit rather than the age of the deposit. For this reason we prefer a late Pliocene age for the La Cueva deposition on the basis of macrofossils (Brüggen, 1950; Herm, 1969).

ANALYTICAL METHODS

For this study, 22 samples were collected from the Navidad, Lincancheo, Rapel, and La Cueva Formations. Samples mainly comprise medium-grained and fine-grained sandstones with subordinate coarse-grained sandstones and fine-grained conglomerates, representing the main lithologies found in the studied basin. The collected samples consist of semi-consolidated material, which was easily disaggregated by hand, and are characterized as well-sorted sediments. We collected 7 kg of each sample, as our experience in other sedimentary basins of the western Andean forearc indicates this to be sufficient for obtaining enough heavy minerals for analysis (Pinto et al., 2004, 2007; Rodríguez, 2008; Valdés, 2009). The heavy mineral fraction was obtained according to a standard laboratory technique described by Parfenoff et al. (1970). The process involved the following steps for each disaggregated sample: (1) washing and decanting, using a wash pan and drying at room temperature (20°–30 °C); (2) obtaining the 0.25–0.50 mm fraction by sieving; and (3) separation of the heavy mineral fraction by gravity settling in heavy liquids (LST, d = 2.85 g/cm^3)[1]. According to Parfenoff et al. (1970), the separation using heavy liquids upon the 0.25–0.50 mm fraction makes it possible to obtain monomineral grains, which we later corroborated when observing the samples under a binocular magnifying glass. It is important to mention that the clay fraction and the mica minerals tend to be removed during washing. However, both the clay fraction and the mica are difficult to analyze by microprobe, because the small grain size of the clays and the flat shape of the micas make it almost impossible to obtain a well-polished thin section. Once the heavy mineral fraction was obtained, a mineralogical analysis was carried out using a binocular microscope to recognize the different mineral species within each sample. Special attention was paid in identifying color variations of pyroxene, amphibole, and garnet, which represent compositional variations of these minerals (Krawinkel et al., 1999; Pinto et al., 2007). The heavy mineral distributions for each sample were obtained by visual approximation under the binocular microscope (Table 1). It is important to mention here that our study is qualitative. We report the heavy mineral distribution only to show the relative abundances of the minerals rather than to quantify the relative contributions from different sources.

For microprobe analysis the heavy mineral grains were hand picked, mounted in epoxy, polished, and carbon coated. Analyses were carried out at the Laboratoire de Mécanismes de Transferts en Géologie, LMTG (CNRS-IRD-Université Paul Sabatier, Toulouse, France), using an electron microprobe CAMECA SX50 and at the Laboratorio de Microscopía Electrónica (Departamento de Geología, Universidad de Chile, Santiago, Chile) by a scanning electron microscope with probe analytical abilities (SEM-PROBE), using the wavelength dispersive method, 15 kV acceleration potential, and a beam current of 10 nA. The following oxides were analyzed: SiO_2, TiO_2, Al_2O_3, FeO, MnO, MgO, CaO, Na_2O, Cr_2O_3, K_2O, and NiO. Cr_2O_3 and NiO contents could not be obtained by all analyses. Fe_2O_3 and H_2O were calculated assuming mineral stoichiometry.

Microprobe analyses were carried out on each of the mineral species recognized in the heavy mineral association of each sample. Only Ti-Fe oxides were not analyzed. At least five grains for each mineral species (or color variation where present) were analyzed in each sample where possible.

RESULTS

In order to recognize the lithological units that could have supplied material to the Navidad sedimentary basin, we performed single-grain microprobe analysis for each detrital heavy mineral species recognized in the Navidad, Lincancheo, Rapel, and La Cueva Formations. We compared our results with regional information and published mineral chemistry data for potential source rocks in Central Chile. Here we present the geochemical results for detrital garnet, as the garnet composition gives us insight into sources of metamorphic rock, and also for detrital pyroxene and amphibole, as their composition helps us to determine sources of volcanic and plutonic rocks.

Garnet

Optical and Geochemical Characteristics of Garnet

The distribution of garnet changes between the different levels and formations: In the lower Navidad Formation, garnet

[1]LST—lithium/sodium alpha-tungstosilicate; d—density.

TABLE 1. DETRITAL HEAVY MINERAL SUITE AND RELATIVE ABUNDANCE IN SAMPLES FROM CENOZOIC MARINE FORMATIONS OF CENTRAL CHILE

Sample	Formation (level)	Locality/Stratigraphic column	Grt	St	Ol	Zrn	Ttn	And	Cpx	Opx	Am	Bt	Ep	Rt	Py	Ap
nav 6	La Cueva Fm.	El Cajon (EC)							60	30	10					
nav 1	La Cueva Fm.	La Estrella (LE)	10			1		10	4		15		60			
nav 2	La Cueva Fm.	La Estrella (LE)	8					11	14	9	39		20			
nav 4	La Cueva Fm.	La Estrella (LE)	7					3	28	35	12		15			
nav 5	La Cueva Fm.	Litueche (LT), El Cajon (EC)	6	0.5		0.5		tr	28	32	15		18			
nav 7	La Cueva Fm.	Litueche (LT), El Cajon (EC)	1						25	32	17		25			
nav 9	La Cueva Fm.	Cuesta Los Leones (LL)	7			45			5	3	10		30	tr		
nav 11	Rapel Fm.	Rio Rapel (RR)	6	2		3		4	28	15	15		27			
nav 13	Lincancheo Fm.	Rio Rapel (RR)						10	40	30			20		tr	
nav 33	Lincancheo Fm.	Pataguilla (P)							15	3	30		52			
nav 32	Navidad Fm. (upper levels)	Matanzas (M1, M2)	1			1			13	22	20	1	22			20
nav 31	Navidad Fm. (upper levels)	Matanzas (M1, M2)							16	24	30		30			
nav 27	Navidad Fm. (upper levels)	Punta Alta (PA)	1			tr			3		90		6			
nav 26	Navidad Fm. (upper levels)	Punta Alta (PA)	3			1			1		90		5			
nav 19	Navidad Fm. (upper levels)	Punta Perro (PPW1, PPW2)	10			10			2	3	35		40			
nav 29	Navidad Fm. (lower levels)	Matanzas (M1, M2)	tr			5			15	57	8		15		tr	
nav 23	Navidad Fm. (lower levels)	Punta Alta (PA)	20	1		8	4	tr	7	1	29		30			
nav 22	Navidad Fm. (lower levels)	Punta Alta (PA)	2	tr			5	tr	10		40		43			
nav 21	Navidad Fm. (lower levels)	Punta Perro (PPW1, PPW2)	tr			1.5			30	40	23	0.5	5			
nav 17	Navidad Fm. (lower levels)	Punta Perro (PPW1, PPW2)	10	1		15			15	40	8		10	1	tr	
nav 16	Navidad Fm. (lower levels)	Punta Perro (PPW1, PPW2)	5	1					10	59	10		15			
nav 14	Navidad Fm. (lower levels)	Punta Perro (PPW1, PPW2)	5	2		25		tr	20	40	tr		7	1		

Abbreviations: tr—mineral in trace quantity (<0.5% of heavy mineral site of sample); Am—amphibole group; And—andalusite; Ap—apatite; Bt—biotite; Cpx—clinopyroxene; Ep—epidote; Grt—garnet group; Ol—olivine; Opx—orthopyroxene; Py—pyrite; Rt—rutile; St—staurolite; Ttn—titanite; Zrn—zircon. Abbreviations according to Kretz (1983) and Siivola and Schmid (2007).

is present in almost every sample, generally forming ≤5% of the heavy mineral fraction (Table 1). The abundance of garnet reduces to ≤1% in the majority of samples from the upper Navidad Formation, and is completely absent from the Lincancheo Formation. Garnet appears again in the Rapel and La Cueva Formations, where it reaches 10% of the heavy mineral fraction (Table 1). With respect to the garnet composition, Cenozoic marine formations yield detrital garnets belonging to the aluminous series (pyrope-almandine-spessartine) and the calcic series (andradite-grossularite). The compositional diagram for the aluminous series uses Fe^{2+}, Mg, and Mn^{2+} as poles, defining three different fields for garnets where the almandine (Alm), pyrope (Pyr), or spessartine (Sps) molecules predominate (Fig. 3). Calcic series garnets are classified as andradite or grossular, based on their Fe^{3+} and Al^{VI} quantities (Table DR1[2]).Within the aluminous series, two types of garnets can be recognized on the basis of their Mn^{2+} content: (1) almandines with very low Mn^{2+} contents, whose compositions plot very close to the Fe^{2+}-Mg axis, and (2) almandines with slightly higher Mn^{2+}, which deviate from the former trend (Fig. 3). Higher contents of the Mn^{2+} molecule are related to changes in the color of garnet: Almandines poor in Mn^{2+} are pale pink, whereas almandines slightly richer in Mn^{2+} are dark pink. The very low Mn^{2+} almandine is present in the Navidad Formation ($Alm_{80-72}Py_{15-18}Sps_{3-4}$), the Rapel Formation ($Alm_{79}Py_{16}Sps_{2}$), and the La Cueva Formation ($Alm_{83-56}Py_{13-35}Sps_{2-2}$). The slightly richer Mn^{2+} almandine is present in the Navidad Formation ($Alm_{81-77}Py_{2-15}Sps_{16-5}$) and the La Cueva Formation ($Alm_{65-71}Py_{2-1}Sps_{31-27}$). In addition, one virtually pure spessartine grain was recognized in the La Cueva Formation (Fig. 3). Garnets of the calcic series, comprising very pure andradites (And_{100}) and grossular ($And_{65}Gro_{18}$), were recognized only in the La Cueva Formation (Table DR1).

[2]GSA Data Repository Item 2012141—Table DR1: Chemical analysis of calcic series garnets from La Cueva Formation, and Table DR2: Chemical analysis of clinopyroxenes from Navidad Basin deposits—is available at www.geosociety.org/pubs/ft2012.htm, or on request from editing@geosociety.org or Documents Secretary, GSA, P.O. Box 9140, Boulder, CO 80301-9140, USA.

Possible Source Rocks for Garnet

Garnet is a characteristic mineral of metamorphic rocks, although it can also be found in some acid igneous rocks (Deer et al., 1992). In particular, almandine is a common mineral found in Barrovian-type mica schists like those from the Western Series of the Paired Metamorphic Belt from the western Coastal Cordillera (Willner, 2005). In the Navidad, Rapel, and La Cueva Formations, the composition of detrital almandines with very low Mn^{2+} resembles the composition of garnet from the Western Series metapelites (Fig. 3). Moreover, in the Navidad, Rapel, and La Cueva Formations the very low Mn^{2+} garnet occurs with andalusite and staurolite (Table 1), representing a typical metamorphic assemblage from the Western Series metapelites (Willner, 2005). With respect to the other types of aluminous series garnets from the Cenozoic formations, the detrital almandines with slightly higher Mn^{2+} contents that occur in the Navidad and La Cueva Formations are similar to garnets of migmatitic gneiss from the Valparaíso Metamorphic Complex, which also crops out at the western Coastal Cordillera (Fig. 3). In this case, larger amounts of Mn^{2+} in detrital garnet are in good agreement with provenance from a metamorphosed igneous protolith (Deer et al., 1997a). Furthermore, rounded and ovoid detrital zircon in the Navidad Formation (Table 1) may also be related to a metamorphic source (Hoskin and Schaltegger, 2003). The pure spessartine recognized in the La Cueva Formation suggests a new metamorphic source composed of skarn, as garnets with such composition are characteristic of such rocks (Deer et al., 1997a). The presence of andradite and grossularite in the La Cueva Formation indicates a source composed of contact or thermally metamorphosed calcareous sediments (Deer et al., 1997a). In the study area, outcrops of thermally metamorphosed calcareous sediments and related skarn deposits are common at the base of the Jurassic–Cretaceous succession in the eastern Coastal Cordillera. Other calcic minerals found in the La Cueva Formation, like epidote and actinolite, support a source formed by contact-metamorphosed calcareous sediments. The presence of rutile, which is also typical of these types of metamorphic rocks (Deer et al., 1992), further supports derivation from contact-metamorphosed calcareous sediments.

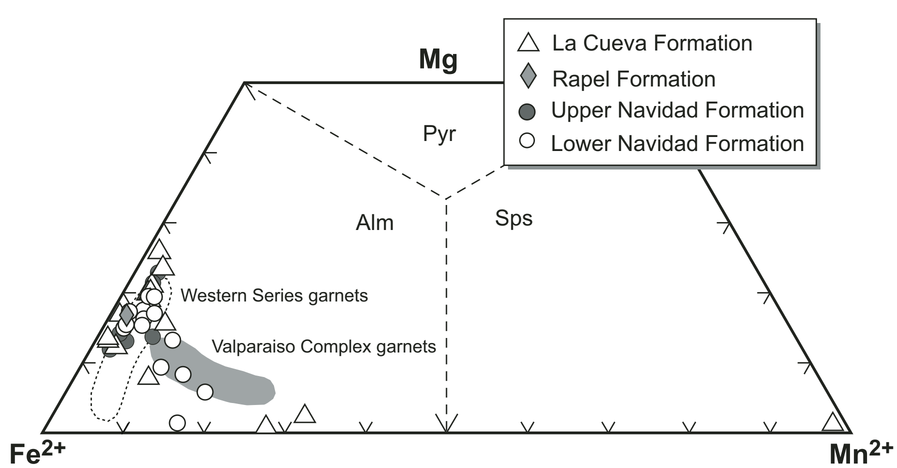

Figure 3. Compositional diagram of detrital aluminous-series garnets from Cenozoic marine formations of Central Chile. Pyr—pyrope; Alm—almandine; Sps—spessartine.

Pyroxene

Optical and Geochemical Characteristics of Pyroxene

There are marked changes in stratigraphic abundance of orthopyroxene (OPx) and clinopyroxene (CPx) in the Navidad Formation: In general, pyroxenes are the most abundant heavy minerals in its lower levels, whereas they are scarce in the majority of the samples from the upper part (Table 1). In the lower Navidad Formation, OPx predominates over CPx, reaching 59% and 32%, respectively. The abundance of pyroxenes rises again in the Lincancheo and Rapel Formations compared with the upper levels of the Navidad Formation, reaching 40% for CPx and 30% for OPx. Instead of OPx, pigeonite (Pg) was recognized in low percentages (3%, Table 1) in the lower Lincancheo Formation. In the La Cueva Formation, CPx and OPx abundances are variable: They are scarce at the base, variable in the middle part, and in the upper (lahar) level pyroxenes are by far the most abundant minerals in the heavy mineral fraction, with CPx (60%) predominant over OPx (30%) (Table 1).

In general, both types of pyroxenes are well preserved and unweathered in the Navidad, Lincancheo, Rapel, and La Cueva Formations. Their characteristic euhedral to subhedral prismatic crystal habit is interpreted to be related to a porphyritic rock source of volcanic or subvolcanic origin.

The compositions of CPx and OPx in each sedimentary formation are in good agreement with the coexistence of both types of pyroxenes in the same rock source, as tie lines can be drawn between their compositions on a Morimoto diagram (Fig. 4). In general, CPx corresponds to augite, and minor diopside and OPx correspond mainly to enstatite (Fig. 4). Differences in pyroxene compositions between different levels and formations are related to their Fe contents. Some of the augites and enstatites from the lower Navidad Formation have significantly higher Fe contents than pyroxenes from the upper Navidad Formation and from the Lincancheo, Rapel, and La Cueva Formations (Fig. 4). In studying the lower Navidad Formation it was even possible to identify CPx and OPx crystals with ferroaugite and ferrosilite compositions, respectively (Fig. 4). The higher Fe content of OPx and CPx in the lower Navidad Formation could be related to the magmatic affinity of their source rocks. Tholeiitic magmas are characterized by a strong Fe enrichment during the first stages of differentiation, related to late crystallization of Fe and Ti oxides.

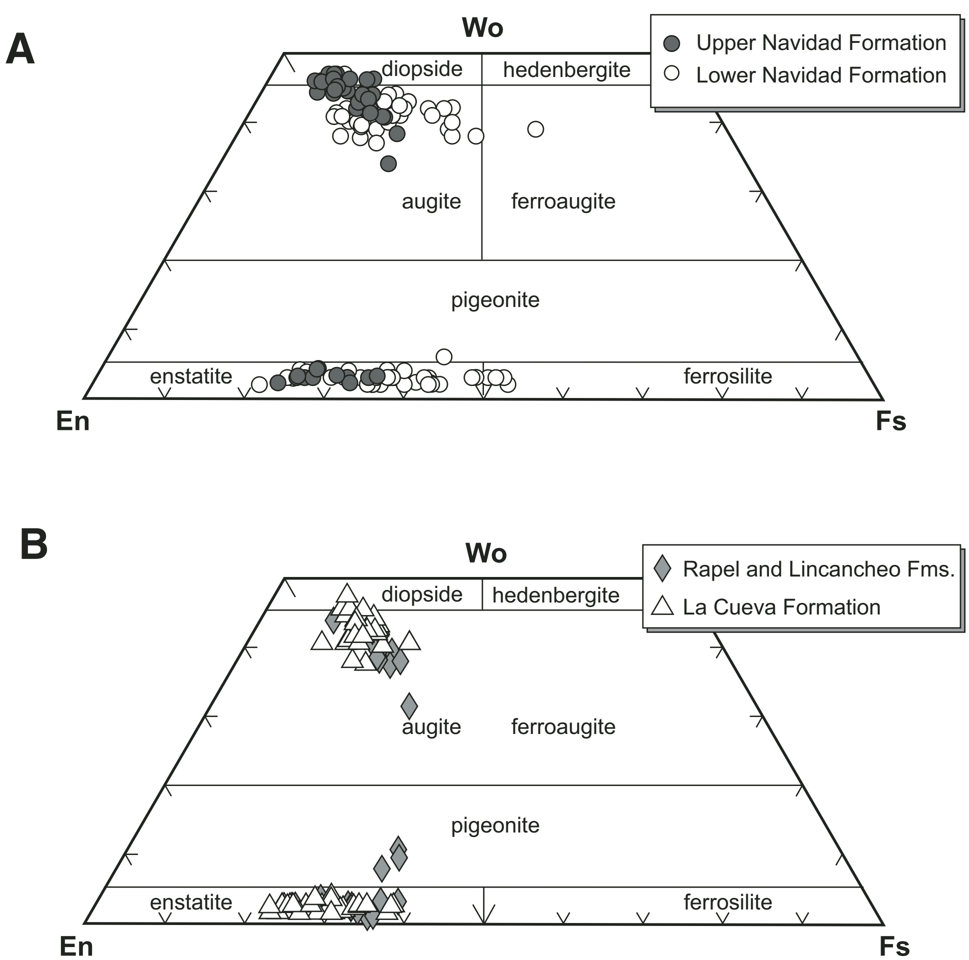

Figure 4. Classification diagram from Morimoto (1988) for detrital pyroxenes from (A) Navidad Formation, and (B) Lincancheo, Rapel, and La Cueva Formations. Wo—wollastonite; En—enstatite; Fs—ferrosilite.

On the contrary, Fe enrichment is prevented in calc-alkaline magmas by the early crystallization of Fe and Ti oxides (Best and Christiansen, 2000). Because of this, Fe-enriched pyroxenes would crystallize from tholeiitic magmas through the process of fractional crystallization (Deer et al., 1997b). Hence, the high-Fe OPx and CPx from the lower Navidad Formation are interpreted as being derived from tholeiitic source rocks.

We also used the diagrams of Leterrier et al. (1982) to recognize magmatic affinities of source rocks for detrital CPx. These diagrams consider the Na, Ca, Al, Ti, and Cr concentrations of CPx phenocrysts to discriminate the geodynamic setting of intermediate to basic volcanic rocks. Leterrier et al. (1982) diagrams also can be used on detrital CPx of volcanic origin if the minerals are well preserved (Krawinkel et al., 1999; Pinto et al., 2004). As the use of Leterrier diagrams is restricted to CPx from intermediate to basic rocks, it is necessary to recognize if any of the detrital CPx found in the Cenozoic deposits is derived from volcanic rocks of intermediate to acid composition. For this purpose the Al content in CPx was examined. It is well known that low rates of silica activity favor the replacement of Si by Al^{IV} (Le Bas, 1962; Carmicheal et al., 1970; Simonetti et al., 1996). This means that Al^{IV} contents are higher in CPx from intermediate to basic volcanic rocks than in CPx from intermediate to acid volcanic rocks. In the Navidad Formation the Al^{IV} content of CPx from the lower levels spans a wide range between 0.01 and 0.14 a.p.f.u. (atoms per formula unit) (Table DR2 [see footnote 2] and Fig. 5), but it presents a narrower range and higher values, from 0.05 to 0.16 a.p.f.u., in the upper levels (Table DR2 and Fig. 5). The Al^{IV} contents of CPx from the Lincancheo and Rapel Formations are similar to those of CPx from the upper levels of the Navidad Formation, presenting values from 0.05 to 0.14 a.p.f.u., whereas in the La Cueva Formation the Al^{IV} range

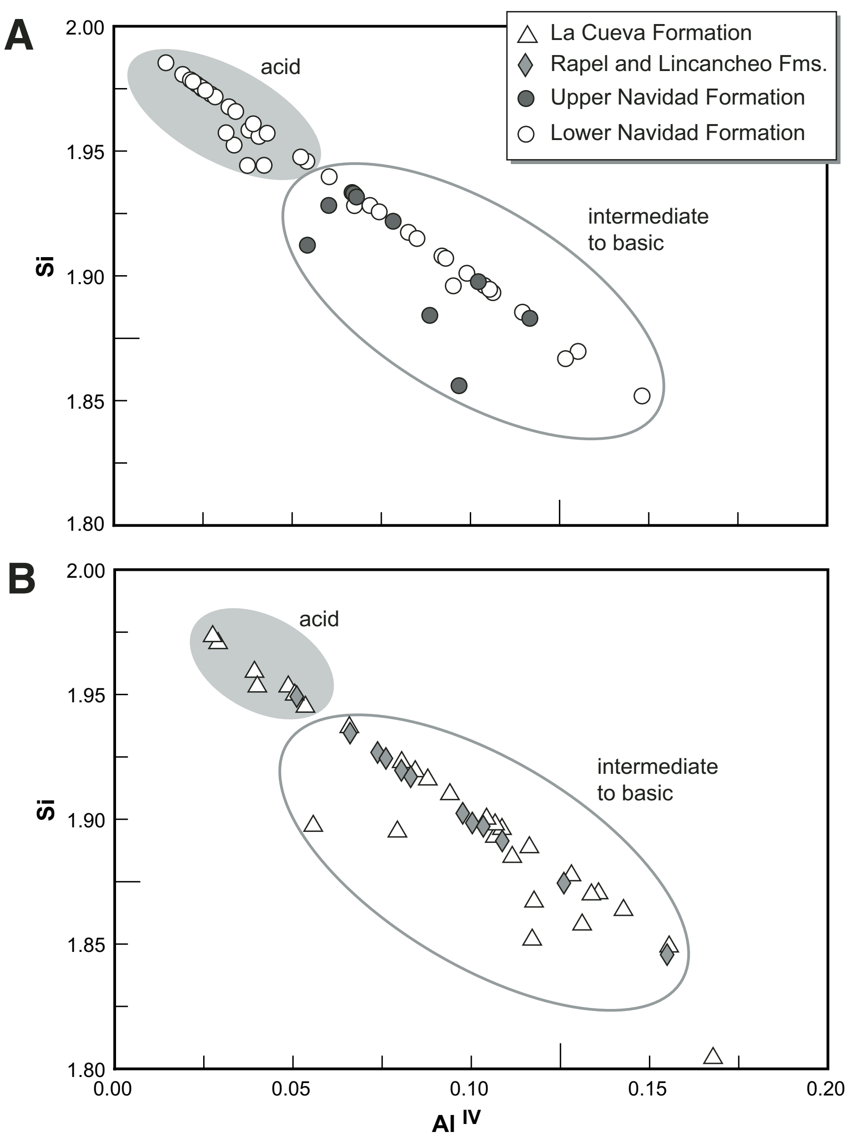

Figure 5. Si versus Al^{IV} diagram for detrital clinopyroxenes of volcanic origin from (A) Navidad Formation, and (B) Lincancheo, Rapel, and La Cueva Formations.

of CPx increases again, from 0.02 to 0.17 a.p.f.u. (Table DR2 and Fig. 5). These features suggest that CPx in the lower Navidad Formation and the La Cueva Formation were derived from volcanic rocks with a wider compositional range compared with the upper Navidad Formation and the Lincancheo and Rapel Formations. However, although the relationship between the high Al^{IV} and relatively low Si content in CPx is clear, to apply the Leterrier et al. (1982) diagrams it is necessary to establish a minimum Al^{IV} content to discriminate between detrital CPx derived from intermediate to basic volcanic rocks, and detrital CPx related to intermediate to acid volcanic sources. To establish this minimum value, we checked the microprobe analysis of CPx phenocrysts published by Deer et al. (1997b): Intermediate to acid rocks including a dacite, a rhyolite, and a trachite have Al^{IV} contents ranging from 0.03 to 0.05 a.p.f.u. Considering these values, we applied Leterrier et al. (1982) diagrams only to detrital CPx that yields an Al^{IV} content of >0.05 a.p.f.u. The results indicate that intermediate to basic CPx from the lower Navidad Formation is related to volcanic rocks with tholeiitic, calc-alkaline, and mid-oceanic-ridge basalt (MORB) affinities, whereas the CPx from the upper Navidad Formation and the Lincancheo, Rapel, and La Cueva Formations comes mainly from a calc-alkaline volcanic source (Fig. 6). It was also possible to identify a few CPx grains related to alkaline volcanic sources in the La Cueva Formation.

As the Leterrier et al. (1982) diagrams were applied to CPx with an Al^{IV} content >0.05 a.p.f.u., there remains uncertainty about the magmatic affinities of source rocks for CPx with an Al^{IV} content ≤0.05 a.p.f.u., which are abundant mainly in the lower Navidad Formation. Figure 7 shows that CPx with Al^{IV} contents ≤0.05 a.p.f.u have the highest Fe^{2+} contents. As stated above, CPx with high Fe^{2+} contents must have crystallized from tholeiitic magmas, indicating that detrital CPx from the lower Navidad Formation was derived from volcanic rocks of tholeiitic composition.

Possible Source Rocks for Pyroxenes

Pyroxenes occur as stable phases in almost every type of igneous rock and also occur in rocks formed under conditions of both regional and contact metamorphism (Deer et al., 1992).

In the Cenozoic marine sediments, we have recognized that euhedral to subhedral prismatic crystals of detrital CPx and OPx represent a volcanic or subvolcanic origin. On the Morimoto diagrams, CPx and OPx compositions indicate that both types of pyroxenes are related to the same source rock. Based on the Al^{IV} and Fe contents of CPx and by the use of the Leterrier et al. (1982) diagrams, our results suggest that in the lower Navidad Formation, source rocks for CPx are intermediate to basic volcanics of mainly tholeiitic and calc-alkaline and minor MORB affinities, together with intermediate to acid volcanic rocks with tholeiitic affinities. In the upper Navidad Formation and Lincancheo, Rapel, and La Cueva Formations, source rocks for CPx correspond mainly to intermediate to basic volcanics with calc-alkaline affinities. In the La Cueva Formation, some CPx yields an Al^{IV} content ≤0.05 a.p.f.u, which would indicate the presence

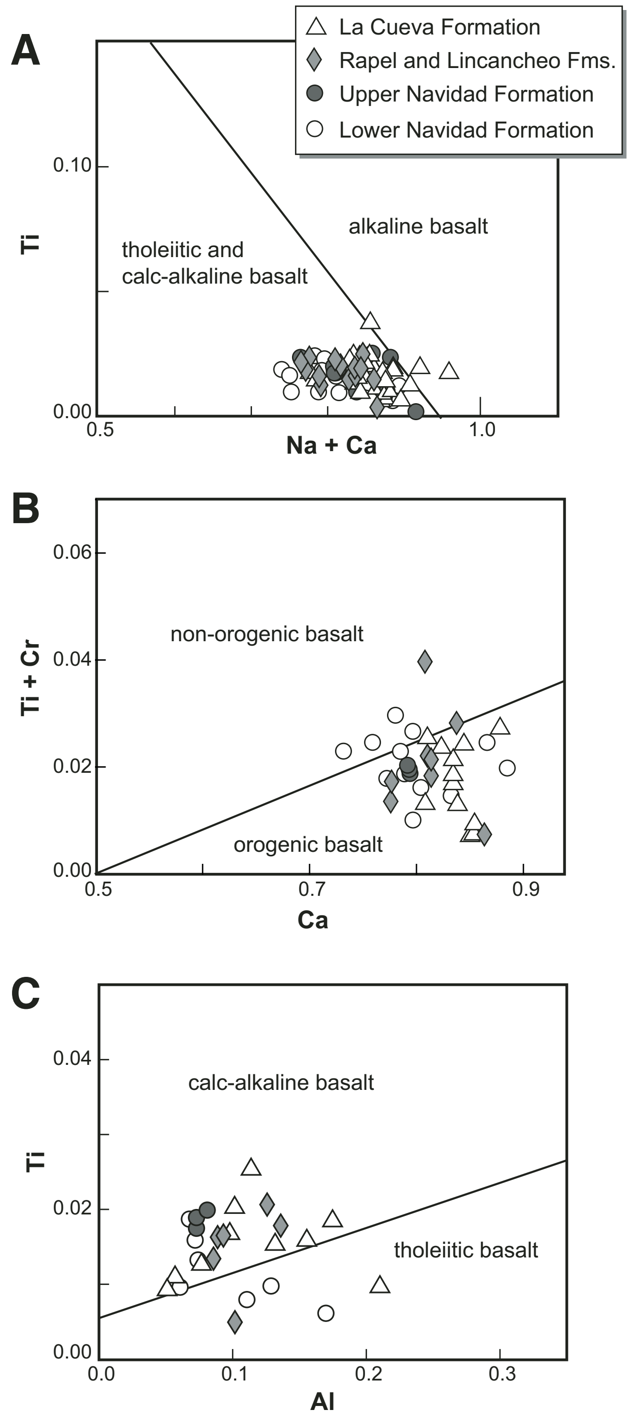

Figure 6. Discrimination diagrams of Leterrier et al. (1982) for detrital clinopyroxenes of volcanic origin in the Navidad, Lincancheo, Rapel, and La Cueva Formations. (A) Ti versus Na + Ca. (B) Ti + Cr versus Ca. (C) Ti versus Al.

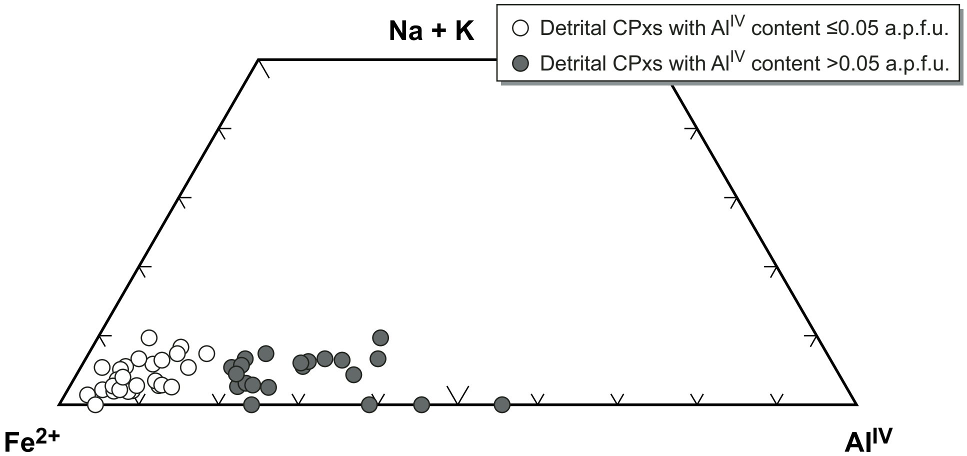

Figure 7. Composition of detrital clinopyroxenes from lower levels of the Navidad Formation for the alkalis (Al^{IV}–Fe^{2+} ternary diagram); a.p.f.u.—atoms per formula unit.

of another source of intermediate to acid volcanic composition, but it was not possible to identify its magmatic affinity. From the Leterrier et al. (1982) diagrams we also identified a minor amount of detrital CPx in the La Cueva Formation related to intermediate to basic source rocks with alkaline affinities.

To recognize the specific source rocks for pyroxenes from the Cenozoic deposits, it is necessary to compare the mineralogical and geochemical characteristics of volcanic formations from Central Chile with our results. In Central Chile the co-occurrence of OPx and CPx has been recognized mainly in the Eocene–Miocene Abanico West Formation in the eastern Central Depression and in the Miocene Farellones Formation at the western Principal Cordillera. On the other hand, CPx is the main heavy mineral described in Mesozoic volcanic formations from the eastern Coastal Cordillera and western Central Depression. These features indicate that possible source rocks for detrital pyroxenes in Cenozoic deposits correspond to the Abanico West and Farellones Formations. Outcrops of the Abanico West and Farellones Formations are difficult to differentiate in the field, but they present characteristic magmatic affinities: Rocks from the Abanico West Formation represent tholeiitic, MORB, and calc-alkaline affinities, whereas rocks from the Farellones Formation have a calc-alkaline affinity. Thus, the geochemical characteristics of the detrital CPx from the lower Navidad Formation indicates provenance from the Abanico West Formation in the eastern Central Depression or a mixture between the Abanico West Formation and Farellones Formation in the western Principal Cordillera. By contrast, detrital pyroxenes from the upper Navidad Formation and the Lincancheo, Rapel, and La Cueva Formations are related mainly to the Farellones Formation source in the western Principal Cordillera. With respect to CPx from the La Cueva Formation, which is related to alkaline volcanic rocks, such magmatic affinity has been recognized only in volcanic rocks of Mesozoic formations from the eastern Coastal Cordillera, which we consider to have been their potential source.

Amphibole

Optical and Geochemical Characteristics of Amphibole

Although amphibole is an abundant heavy mineral in the lower Navidad Formation (Table 1), the highest abundances occur in the upper Navidad Formation, reaching 90% of the heavy mineral fraction in some samples. In the Lincancheo, Rapel, and La Cueva Formations, amphibole is abundant but generally subordinate to pyroxenes (Table 1).

Two types of detrital amphibole are recognized in the Cenozoic deposits: Type 1 consists of short anhedral to subhedral crystals, whereas type 2 consists of elongate euhedral to subhedral prismatic crystals. These characteristics suggest that type 1 amphiboles are related to intrusive plutonic or metamorphic rocks, whereas type 2 amphiboles are related to porphyritic volcanic or subvolcanic source rocks.

All detrital amphiboles analyzed are calcic. Type 1 amphiboles are classified as magnesiohornblendes and actinolite with minor tschermakite, magnesiohastingsite, and ferrohornblende. Type 2 is classified as magnesiohastingsite and magnesiohornblende, with minor pargasite, edenite, and tschermakite (Fig. 8). In the lower Navidad Formation, detrital amphiboles correspond to type 1, with very few exceptions of type 2, but in the upper Navidad Formation, type 2 amphiboles largely predominate over type 1. In the Lincancheo, Rapel, and La Cueva Formations, both types were recognized in similar quantities (Fig. 8).

For type 1 amphiboles, we used the Al^{VI} versus Al^{IV} diagram (Fig. 9) to identify amphiboles related to metamorphic or igneous plutonic source rocks (Leake, 1965). Type 1 amphiboles related to metamorphic sources are mainly actinolites and minor magnesiohornblendes with high Si a.p.f.u., plotting close to the actinolite compositional field, whereas type 1 amphiboles related to igneous plutonic sources are mainly magnesiohornblendes with medium to low Si values and minor ferrohornblende and tschermakite (Fig. 8). In the Navidad Formation, type 1 amphiboles are related mainly to both metamorphic and igneous plutonic rock

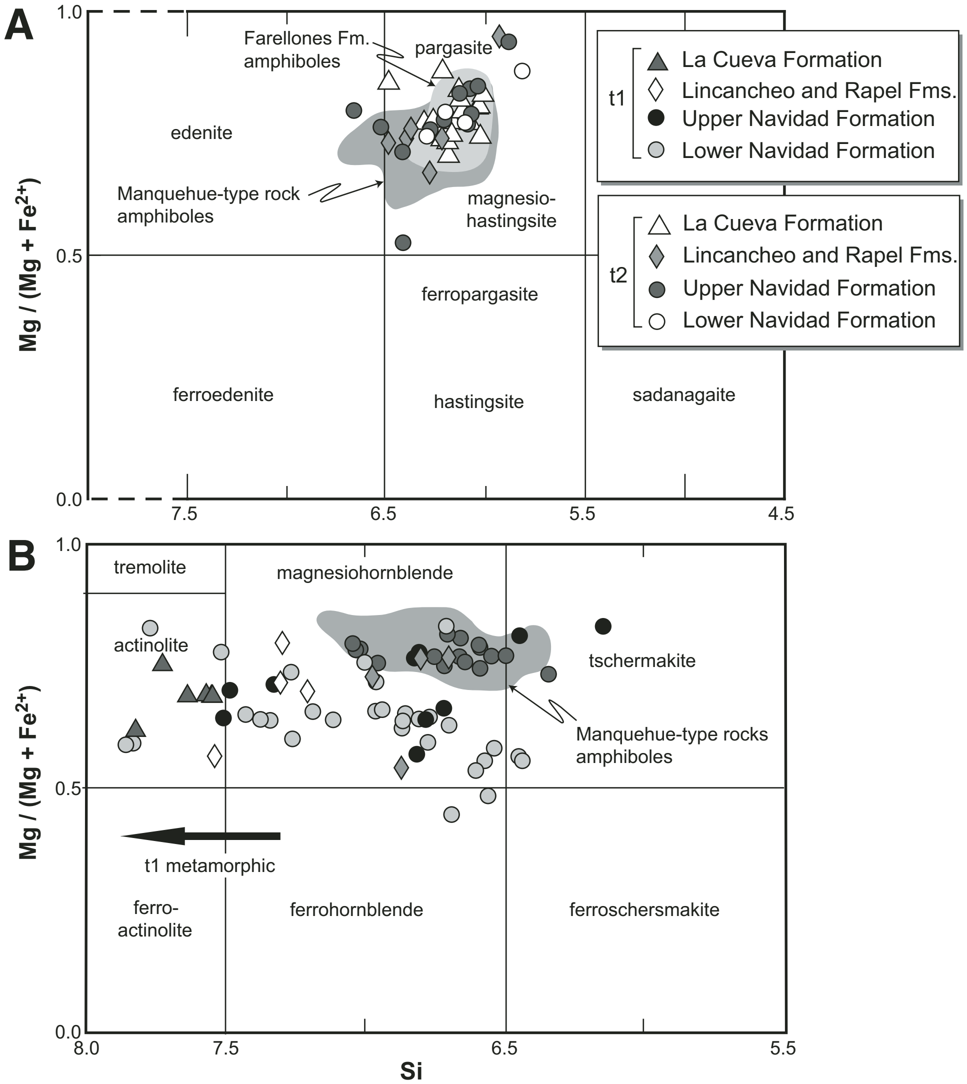

Figure 8. Composition of detrital amphiboles from the Navidad, Lincancheo, Rapel, and La Cueva Formations on the classification diagram of Leake et al. (1997): (A) $(Na^+K)_A \geq 0.5$. (B) $(Na^+K)_A < 0.5$.

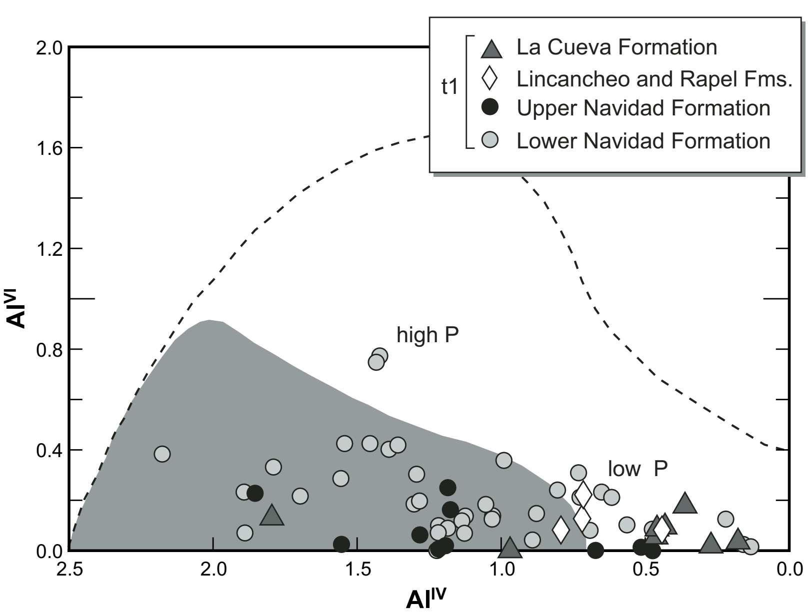

Figure 9. Composition of type 1 (t1) detrital amphiboles from Navidad, Lincancheo, Rapel, and La Cueva Formations on Al^{VI} versus Al^{IV} discrimination diagram of Leake (1965). Gray: compositional field for amphiboles in plutonic rocks. White: compositional field for amphiboles in metamorphic rocks.

sources, whereas in the Lincancheo, Rapel, and La Cueva Formations, type 1 amphiboles are related mainly to metamorphic source rocks (Fig. 9). With respect to metamorphic amphiboles, higher Al^{VI} contents have been related to higher pressure (P) crystallization conditions (Leake, 1965). According to this, type 1 amphiboles related to metamorphic sources in the lower Navidad Formation crystallized from both low P and higher P metamorphic source rocks, whereas in the upper Navidad Formation and the Lincacheo, Rapel, and La Cueva Formations, metamorphic amphiboles were formed only at low P conditions (Fig. 9). With respect to plutonic amphiboles, low X_{Mg} ($X_{Mg} = Mg/[Mg + Fe^{2+}]$) values in these minerals are usually related to rocks with an acid composition (Deer et al., 1997c). In the lower Navidad Formation, the presence of type 1 amphiboles with compositions of ferrohornblende and low X_{Mg} magnesiohornblende indicates acid plutonic source rocks for these levels (Fig. 8).

For type 2 amphiboles, we used the alkalis versus Al^{IV} diagram to discriminate between different volcanic source rocks (Fig. 10). Type 2 amphiboles in upper levels of the Navidad Formation and the Lincancheo and Rapel Formations show a positive correlation between their alkali and Al^{IV} contents, whereas type 2 amphiboles in the La Cueva Formation contain only high alkali and Al^{IV} contents. The compositional field of amphiboles from Manquehue-type rocks and the Farellones Formation is also shown on the alkalis versus Al^{IV} diagram. The type 2 amphibole composition in the upper levels of the Navidad Formation and the Lincancheo and Rapel Formations on the alkalis versus Al^{IV} diagram mimics the composition of amphiboles from Manquehue-type rocks (Fig. 10). In the La Cueva Formation the alkali and Al^{IV} contents of type 2 amphiboles are remarkably similar to amphiboles from the Farellones Formation (Fig. 9).

Possible Source Rocks for Amphibole

Calcic amphibole is a common mineral phase of both igneous and metamorphic rocks. Among igneous rocks, calcic amphibole is a particularly common constituent of the intermediate members of the calc-alkaline series. Among metamorphic rocks, calcic amphibole appears in regionally metamorphosed basic rocks formed under greenschist to amphibolite series conditions and is also present in contact-metamorphosed limestones (Deer et al., 1992).

In the Cenozoic deposits we have recognized detrital amphiboles representing a metamorphic, igneous plutonic, and volcanic or subvolcanic origin. Detrital amphiboles of metamorphic origin are related mainly to low and relatively high P formation conditions in the lower Navidad Formation and to low P formation conditions in the Lincancheo, Rapel, and La Cueva Formations. The only possible sources for high P metamorphic amphiboles in Central Chile are Jurassic amphibolites from the western Coastal Cordillera. Low P metamorphic amphiboles could be derived from contact-metamorphosed sedimentary rocks from the eastern Coastal Cordillera and regionally metamorphosed rocks from the entire forearc. For this reason it is not possible to determine the source of the low P amphiboles based only on their mineral chemistry. It is therefore necessary to consider other detrital heavy minerals of low P metamorphic parentage to finally establish the provenance of the amphibole. The presence of epidote and titanite supports a regionally metamorphosed source rock for the lower Navidad Formation, and the presence of spessartine, andradite, grossularite, and epidote (Table 1) indicates a calcareous contact-metamorphic source for the La Cueva Formation. As regionally metamorphosed volcanic rocks are present throughout the entire forearc of Central Chile, it is not possible to

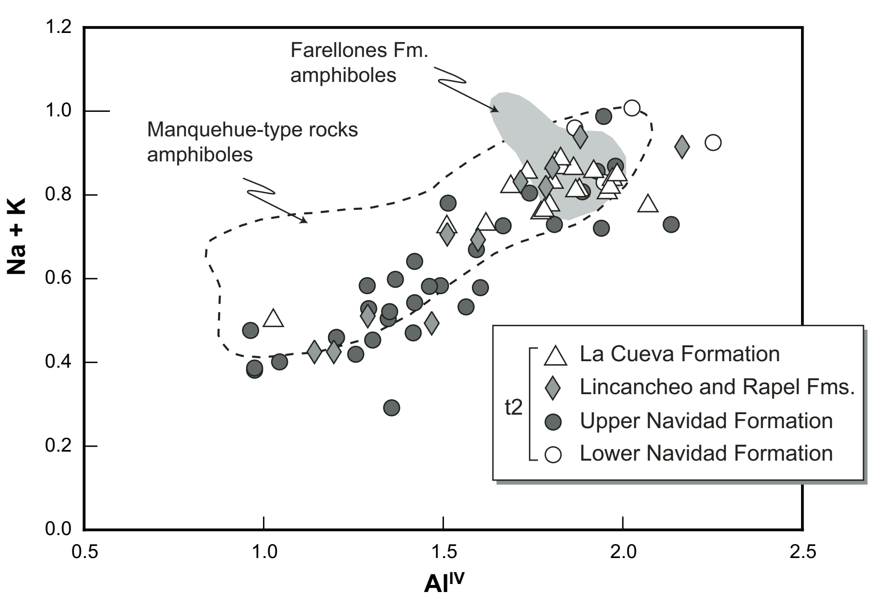

Figure 10. Composition of type 2 detrital amphiboles from the Navidad, Lincancheo, Rapel, and La Cueva Formations on the alkalis versus Al^{IV} discrimination diagram. Compositional fields of amphiboles in Manquehue-type rocks and in the Farellones Formation are shown.

determine a source area for the low P heavy mineral assemblage in the lower Navidad Formation. On the contrary, as the contact-metamorphosed calcareous deposits crop out mainly in the eastern Coastal Cordillera, the low P heavy mineral assemblage in the La Cueva Formation must be related to this source.

Detrital amphiboles of plutonic origin from the lower Navidad Formation have X_{Mg} values indicative of acidic compositions. This is in good agreement with the presence in these levels of zircon with low width/length ratios (Table 1) (Deer et al., 1992). Among the plutonic rocks from Central Chile, those with the most distinctive acidic character occur in the Paleozoic, Triassic, and Jurassic intrusive belts in the western Coastal Cordillera. Therefore, we consider these rocks to have been the possible sources for type 1 plutonic amphiboles.

With respect to detrital amphiboles of volcanic or subvolcanic origin, the possible source rocks in Central Chile correspond to Manquehue-type hypabyssal rocks or their related volcanics, which crop out in the eastern Central Depression and the Farellones Formation in the western Principal Cordillera. Amphibole has rarely been recognized in the Mesozoic volcanic units of the western Central Depression, amphibole crystals in these units having been altered and transferred to hematite (thin section collection, Servicio Nacional de Geología y Minería). This precludes their preservation within sedimentary rocks. The compositional similarity of detrital amphiboles from the upper Navidad, Lincancheo, and Rapel Formations with amphiboles from Manquehue-type rocks indicates that these porphyries or associated volcanic rocks in the eastern Central Depression were potential source rocks. On the other hand, the compositional similarity between detrital amphiboles from the La Cueva Formation and amphiboles from the Farellones Formation indicate derivation from volcanic rocks of the Farellones Formation in the western Principal Cordillera.

SOURCE ROCKS FOR THE CENOZOIC DEPOSITS

Based on the textural and geochemical features of detrital garnet, pyroxene, and amphibole, together with their accompanying heavy mineral assemblages in Cenozoic sedimentary formations, we have recognized some lithological units that could represent the source rocks for the mentioned deposits. In this section we will discuss which of these lithological units are the main and more likely sources at each stratigraphic level, comparing our results with geochronological and geological data from the Cenozoic sedimentary formations and their possible sources.

Lower Navidad Formation

Within the heavy mineral suite of the lower Navidad Formation the volcanic (subvolcanic) assemblage formed by **enstatite + augite (diopside)** has been recognized. Geochemical characteristics of detrital clinopyroxene and orthopyroxene indicate a provenance from the Abanico West Formation or a mixture between the Abanico West Formation and the Farellones Formation. As reported ages for the Abanico West Formation in the studied region range from 34.3 ± 2.2 Ma to 19.3 ± 1.4 Ma (Gana and Wall, 1997), and volcanic clasts from the lower Navidad Formation represent $^{40}Ar/^{39}Ar$ and K/Ar ages between 26.1 ± 1.7 Ma and 20.75 ± 0.34 Ma (Encinas, 2006), it is possible to establish the Abanico West Formation as the main source rock for the lower Navidad Formation. An Abanico West Formation provenance means that material deposited in the lower levels of the Navidad Formation was supplied mainly from the eastern Central Depression.

The plutonic heavy mineral assemblage formed by **ferrohornblende ± magnesiohornblende ± zircon** corresponds to another component of the lower Navidad Formation heavy mineral suite. X_{Mg} values of detrital ferrohornblende and magnesiohornblende, and the presence of zircon, indicate an acidic plutonic source. As acid plutonic rocks are mainly present in the Paleozoic, Triassic, and Jurassic intrusive belts, the mentioned plutonic heavy mineral assemblage indicates that the lower Navidad Formation is also the result of erosion from the western Coastal Cordillera. Moreover, metamorphic heavy mineral assemblages in the lower Navidad Formation, represented by **almandine ± staurolite ± andalusite** and **zircon ± slightly high Mn^{2+} almandine,** indicate a provenance from metapelites of the Western Series of the Paired Metamorphic Belt and migmatitic gneisses of the Valparaíso Metamorphic Complex, also indicating the western Coastal Cordillera as the source area for sedimentary rocks of the lower Navidad Formation.

Upper Navidad Formation

The **magnesiohornblende + magnesiohastingsite** volcanic (subvolcanic) assemblage is present within the upper Navidad Formation heavy mineral suite (Table 1). A Manquehue type of source rock is suggested by the compositional similarity of the detrital amphiboles and the Manquehue type of amphiboles (Sellés, 1999).

Augite (diopside) + enstatite represents another heavy mineral volcanic (subvolcanic) assemblage in the upper Navidad Formation heavy mineral suite (Table 1, Nav 31 and Nav 32). The geochemical characteristics of the detrital clinopyroxene indicate a provenance from the Farellones Formation. This is supported by the presence of zircon, which has also been widely recognized in this lithological unit. A mixture of Manquehue-type rocks and the Farellones Formation provenance indicates that the source areas for material deposited in the upper Navidad Formation were in the eastern Central Depression and western Principal Cordillera.

Finally, the heavy mineral assemblage formed by **almandine ± zircon** (Table 1) is problematic, because although almandine composition resembles the composition of garnets from the metapelites of the Western Series of the Paired Metamorphic Belt, we have not recognized andalusite and staurolite in the heavy mineral suite from the upper Navidad Formation. The absence of staurolite and andalusite in upper Navidad Formation samples could not be explained by size density sorting effects

(Garzanti et al., 2008, 2009), because the analyzed size window (0.25–0.5 mm) is suitable for the sample grain size (mostly medium-grained sandstones), and almandine garnet (3.86 g/cm^3) tends to be denser than staurolite (3.73 g/cm^3) and andalusite (3.16–3.20 g/cm^3). Therefore, in this case, the heavy mineral assemblage formed by **almandine ± zircon** is more likely to represent an acid intrusive source rock, such as those from the Paleozoic, Triassic, and Jurassic intrusive belts.

Lincancheo and Rapel Formations

The heavy mineral suite in the Lincancheo and Rapel Formations is dominated by the volcanic (subvolcanic) heavy mineral assemblage **augite + enstatite (pigeonite) + magnesiohastingsite ± pargasite ± magnesiohornblende.** Geochemical characteristics of detrital clinopyroxene indicate provenance from the Farellones Formation, but detrital amphibole compositions indicate a Manquehue-type source rock. This means that the main source areas for the Lincancheo and Rapel Formations were the western Principal Cordillera and eastern Central Depression.

It was also possible to identify a secondary supply from metamorphic sources in the Lincancheo and Rapel Formations heavy mineral suite. The metamorphic heavy mineral assemblages recognized in the Lincancheo and Rapel Formations correspond to **epidote ± actinolite** and **almandine ± andalusite ± staurolite.** As stated before, the **epidote ± actinolite** heavy mineral assemblage can be related to the regional metamorphism that affected volcanic rocks throughout the entire forearc, and it is not possible to establish a specific source area. In contrast, the **almandine ± andalusite ± staurolite** heavy mineral assemblage indicates a provenance from the Western Series of the Paired Metamorphic Belt and a source area in the western Coastal Cordillera.

La Cueva Formation

In the La Cueva Formation the volcanic (subvolcanic) heavy mineral assemblage **augite + enstatite + magnesiohastingsite ± pargasite** dominates the heavy mineral suite. The geochemical characteristics of detrital clinopyroxene and amphibole mimic the compositions of clinopyroxene and amphibole from the Farellones Formation in the western Principal Cordillera. Based on preliminary provenance studies, the lahar that caps the La Cueva Formation was previously related to volcanic rocks from the western Principal Cordillera, most probably the Farellones Formation (Encinas et al., 2006b), which is consistent with our results. However, the same authors also obtained ages of 4.6 ± 0.4 Ma and 7.7 ± 1 Ma for volcanic clasts collected in the lahar deposits. These ages are younger than the ages reported from the Farellones Formation, and therefore are inconsistent with a Farellones Formation source. However, these ages were obtained from biotite and amphibole crystals in pumice clasts and a scoria clast, corresponding to lithologies that differ from those found in the heavy mineral assemblage from the matrix of the lahar deposit. The volcanic heavy mineral assemblage found in the lahar deposit includes clinopyroxene, amphibole, and orthopyroxene. This is a common assemblage in the Farellones Formation, but it also occurs in the rare outcrops of Pliocene lavas from the western Principal Cordillera (Charrier and Munizaga, 1979). However, the lack of geochemical and mineralogical studies of these rocks prevents us from comparing them with the heavy minerals from the marine deposits. Nevertheless, an overall provenance from the Farellones Formation and the late Pliocene volcanics from the western Principal Cordillera is proposed for the La Cueva Formation.

In the La Cueva Formation a minor contribution of **clinopyroxene** with alkaline affinities indicates a source formed by Mesozoic volcanic rocks from the eastern Coastal Cordillera. We also recognized a metamorphic heavy mineral assemblage in the La Cueva Formation, which includes **spessartine ± andradite ± grossularite ± epidote ± actinolite ± rutile**. This assemblage indicates a source rock formed by contact-metamorphosed calcareous rocks, whereas the presence of **zircon ± almandine**, as observed in the upper Navidad Formation, implies acid intrusive rock as an additional source. As thermally metamorphosed calcareous sediments are present mainly at the base of the Mesozoic succession in the western Coastal Cordillera–eastern Coastal Cordillera border, and acid plutonic rocks are present mainly in the Paleozoic to Jurassic intrusive belts in the western Coastal Cordillera, an overall provenance from the western Central Cordillera and the eastern Central Cordillera can be proposed for the La Cueva Formation.

DISCUSSION

The similarities in the source rocks among the different stratigraphic levels of the marine units allow us to recognize three erosional stages in the Navidad Basin. Stage 1 corresponds to deposition of the lower Navidad Formation. Stage 2 corresponds to deposition of the upper Navidad, Lincancheo, and Rapel Formations. Stage 3 corresponds to deposition of the La Cueva Formation. We have recognized sources from the present-day Central Depression and Principal Cordillera, more specifically from the eastern Central Depression and the western Principal Cordillera (Fig. 1), which supplied minerals from Cenozoic volcanic and/or subvolcanic rocks; and sources from the Coastal Cordillera, more specifically from the western Coastal Cordillera, the western Coastal Cordillera–eastern Coastal Cordillera border, and the eastern Coastal Cordillera (Fig. 1), which supplied minerals from Paleozoic to Mesozoic metamorphic, plutonic, and volcanic rocks. Sources from the Central Depression and Principal Cordillera are located successively to the east and correspond to the Abanico West Formation for stage 1, Manquehue-type rocks and the Farellones Formation for stage 2, and finally to the Farellones Formation and Pliocene volcanics for stage 3. Sources from the Coastal Cordillera correspond to the Paleozoic to Jurassic intrusive belts, the Western Series, and the Valparaíso Metamorphic Complex for stage 1, the Western Series for stage 2, and contact metamorphosed calcareous sediments and Mesozoic volcanics for stage 3. In this case, an eastward shift of the locus of erosion is also recorded, but from stage 2 to stage 3.

Provenance Model

Considering the two main source areas recognized for the marine deposits, we discuss in the following paragraphs the morphotectonic implications for each source separately. In order to develop our provenance model, we consider fault-controlled topographic uplift as the main control on provenance changes for the Navidad Basin.

Central Depression and Principal Cordillera

In the forearc of Central Chile the principal fault zones that could be related to surface uplift are the Los Ángeles–Infiernillo Fault (Aguirre, 1957, 1960; Fock, 2005) and the San Ramón Fault (Rauld, 2002; Rauld et al., 2006). For stage 1 we have recognized erosion of the Abanico West Formation, now in the present-day eastern Central Depression. Uplift of a region containing rocks from the eastern Central Depression would have to have been controlled by the Los Ángeles–Infiernillo Fault, which separates the Abanico West Formation rocks to the east from Mesozoic units to the west (Figs. 1 and 11). During stage 2 the main sources were the Manquehue-type rocks of the eastern Central Depression and the Farellones Formation of the western Principal Cordillera. In this case it is necessary to invoke the action of the San Ramón Fault, at the border between the Central Depression and the Principal Cordillera, in order to uplift a region containing rocks of the western Principal Cordillera. The absence of an Abanico West Formation provenance during stage 2 would

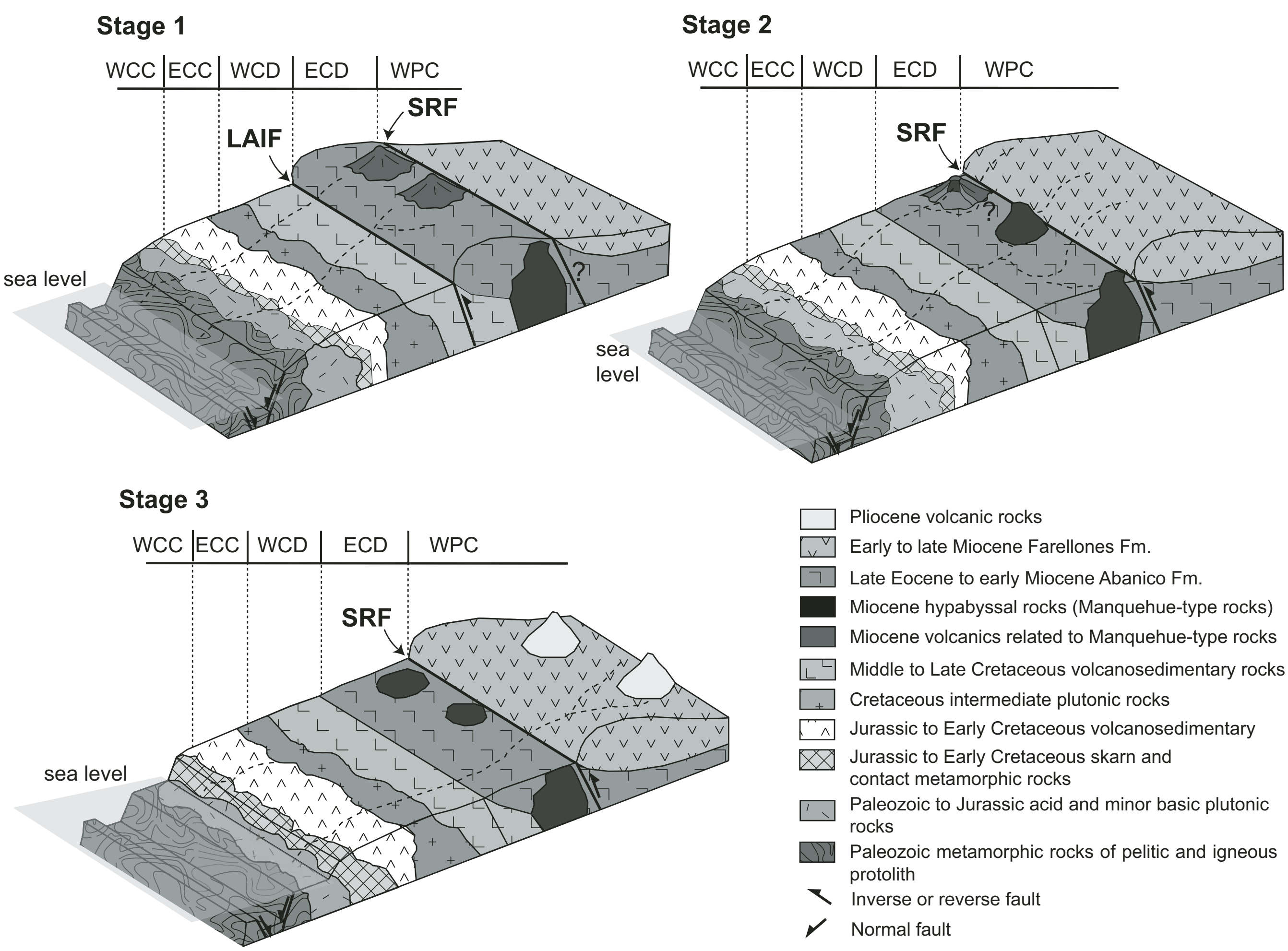

Figure 11. Provenance-based erosional model for the Central Chilean forearc. LAIF—Los Ángeles–Infiernillo Fault; SRF—San Ramón Fault. Question marks represent uncertainties in our model of evolution. In stage 1 the question mark indicates that we have no assurance that the San Ramón Fault has acted simultaneously with the Los Ángeles–Infiernillo Fault. In stage 2 the question mark indicates that we have no assurance that part of the eroded rocks corresponds to the Manquehue-type hypabyssal rocks or to their associated volcanics. See text for details. WCC—western Coastal Cordillera; ECC—eastern Coastal Cordillera; WCD—western Central Depression; ECD—eastern Central Depression; WPC—western Principal Cordillera.

indicate that once these rocks were almost completely removed during stage 1, the locus of erosion shifted eastward during stage 2 and affected the Manquehue-type rocks and/or their related volcanics that formed part of the block uplifted during stage 1. For stage 3, the sedimentary provenance in general indicates that the Farellones Formation was still being eroded. In particular, for the lahar deposit in the La Cueva Formation, a local contribution from both the Farellones Formation and a Pliocene volcanic unit cropping out in the western Principal Cordillera is recognized. This indicates the permanence of the topographic relief generated during stage 2, probably through continuous activity of the San Ramón Fault (Fig. 11).

Coastal Cordillera

For stages 1 and 2 we have recognized a Coastal Cordillera provenance corresponding to the intrusive belts and the metapelites from the western Coastal Cordillera, whereas for stage 3 the Coastal Cordillera provenance comes from the calcareous metamorphic rocks cropping out at the western Coastal Cordillera–eastern Coastal Cordillera border, together with alkaline volcanics in the eastern Coastal Cordillera. According to sedimentological data for the beginning of stages 1 and 2 (Encinas et al., 2006a), the paleocoastline was very close to the present coastline and within the western Coastal Cordillera, whereas during stage 3 the coastline moved eastward to the western Coastal Cordillera–eastern Coastal Cordillera border (Fig. 1), implying that the recognized Coastal Cordillera sources correspond to nearshore rock outcrops. This indicates that topographic highs next to the respective paleocoasts were supplying material to the marine deposit. Several lines of evidence—including the presence of shallow-marine deposits overlain by deep-marine deposits, the development of interformational erosional surfaces, and numeric analysis of microfaults—indicate that tectonic subsidence and uplift occurred along the Cenozoic margin of Central Chile (Encinas et al., 2006a; Buatois and Encinas, 2006; Lavenu and Encinas, 2005; Melnick and Echtler, 2006). Therefore, it is possible that tectonic processes within the Navidad Basin controlled the sediment provenance (Lavenu and Encinas, 2005; Melnick and Echtler, 2006). This basin was developed in an overall extensional tectonic regime, with a series of normal faults that affected the marine deposits and the adjacent basement rocks (Lavenu and Encinas, 2005). For these reasons, we propose that normal faulting of the nearshore basement exposed local topographic highs that were eroded, supplying erosional material to the Navidad Basin (Fig. 11).

Comparison with Morphotectonic Models Proposed for the Study Region

As stated earlier, the morphotectonic models proposed for the study region by Farías et al. (2008) and Armijo et al. (2010) assign different timings to the main uplift event, corresponding to the late Miocene and the late Oligocene to early Miocene, respectively. Similarly, foraminifer biostratigraphy indicates that deposition started during the late Miocene, whereas $^{87}Sr/^{86}Sr$ ages from macrofossils indicate that marine deposition started during the early Miocene. Further radiometric and paleontologic studies are necessary to elucidate this problem, and determining the real age of the Navidad Basin is beyond the scope of this study. However, a late Miocene age for the onset of deposition in this basin is in good agreement with the uplift age proposed by Farías et al. (2008), and, in turn, an early Miocene age is in good agreement with the uplift event proposed by Armijo et al. (2010). In the following paragraphs we use this concordance to constrain the age of erosional stages and compare each morphotectonic model with the provenance model in order to determine how consistent the models of Farías et al. (2008) and Armijo et al. (2010) are with the erosional paths recorded by sediments inside the Navidad Basin.

Comparison with the Tectonic Model of Farías et al. (2008)

According to the foraminifer biostratigraphy ages assigned to the lower and upper levels of the Navidad Formation, and assuming a late Pliocene age for the La Cueva Formation (Brüggen, 1950; Herm, 1969), the erosional stages defined by the provenance results would correspond to the following time spans: stage 1 from late Miocene to early Pliocene (10.9–4.6 Ma), stage 2 from early Pliocene to late Pliocene (4.6 Ma to an indeterminate late Pliocene age), and stage 3 during the late Pliocene. The provenance model indicates that the locus of erosion in the area of the Central Depression and the Principal Cordillera has moved successively to the east, which is in part consistent with the interpretation of Farías et al. (2008) that a wave of retrograde erosion affected the forearc of Central Chile following late Miocene regional uplift. Provenance data for stages 2 and 3 are in good agreement with a locus of erosion at the Central Depression–Principal Cordillera border at ca. 4 Ma, and within the Principal Cordillera at ca. 3.85–2.3 Ma (see figure 10b *in* Farías et al., 2008), as indicated by dating of incision markers carried out by Farías et al. (2008). Nevertheless, important aspects in the interpretation made by Farías et al. (2008) differ from our provenance model. In stage 1, Farías et al. (2008) consider that the main topographic relief in the Chilean forearc during this time corresponds to the Principal Cordillera, uplifted during the late Miocene by the San Ramón Fault (Fig. 1). Uplift of the Principal Cordillera is ascribed to movement on the San Ramón Fault, because low-relief surfaces interpreted as remnants of an ancient low-elevation peneplain would have been offset by the San Ramón Fault. The low-relief surfaces are at the summits of the present-day Coastal Cordillera, Principal Cordillera, and hills inside the Central Depression; correlation between them is problematic, as it is based only on their morphological resemblance in the absence of geochronological data for the surfaces. These surfaces could have been formed during consecutive cycles of high tectonic activity followed by intense erosion, and therefore they do not necessarily correspond to the same original surfaces. In this case, there would be no reason to consider the San Ramón Fault rather than the Los Ángeles–Infiernillo Fault as having been responsible for generation of the topographic relief eroded during stage 1. If foraminifer ages are correct, the role of the Los Ángeles–Infiernillo Fault in Andean uplift has been widely underestimated by the model of Farías et al. (2008). Another aspect that disagrees with our provenance assessment is that according to Farías et al. (2008) the late Miocene uplift event also affected a tectonic block made up of the eastern Coastal Cordillera, western Central Depression, and eastern Central Depression. In this context the fault responsible for uplift was at the tip of the uplifted surface, namely the western Coastal Cordillera–eastern Coastal Cordillera border. However, this fault is not recognized in geological maps or in previous works regarding the surface geology of the Coastal Cordillera in the study area. Moreover, Farías et al. (2008) do not present field evidence supporting the existence of a fault at the western Coastal Cordillera–eastern Coastal Cordillera border. As low-relief surfaces at the summits of the eastern Coastal Cordillera are interpreted by these authors as part of a low elevation peneplain extending throughout the entire forearc and regionally uplifted only during the late Miocene, they use a fault at the western Coastal Cordillera–eastern Coastal Cordillera border to explain the present-day elevation of ~2000 m a.s.l. of the eastern Coastal Cordillera. We suggest that the main differences between the Farías et al. (2008) model and the interpretation of our provenance data are mostly related to the incorrect correlation of geomorphic markers from the Coastal Cordillera, Central Depression, and Principal Cordillera.

Comparison with the Tectonic Model of Armijo et al. (2010)

According to the $^{87}Sr/^{86}Sr$ data for the lower and upper Navidad Formation, and taking into account a late Pliocene age for the La Cueva Formation (Brüggen, 1950; Herm, 1969), we can constrain the provenance-based erosional stages as follows: stage 1 during the early Miocene (23–18 Ma); stage 2 from the early Miocene to late Pliocene (18 Ma to an undetermined late Pliocene age); and stage 3 during the late Pliocene (undetermined late Pliocene age). As sources of the Central Depression–Principal Cordillera area correspond to the Abanico West Formation for stage 1, the Manquehue-type rocks and the Farellones Formation for stage 2, and the Farellones Formation and Pliocene volcanics for stage 3, overlapping ages are observed between the marine deposits and their sources for all three stages. This would indicate that these deposits are the result of erosion of volcanic edifices, and deposition owing to volcanic activity. For stage 2, the overlapping ages between the marine deposits and the present-day outcrops of the Miocene Manquehue-type rocks is problematic, as these rocks are hypabyssal intrusives and therefore could not have been eroded at the same time in which they were emplaced. Nevertheless, Manquehue-type rocks are interpreted as remnants of deeply eroded stratovolcanoes that used to be within the present-day Central Depression (Vergara et al., 2004). Therefore, it is possible that the volcanic rocks that formed these stratovolcanoes could represent a source for the stage 2 deposits (Fig. 11). The Armijo et al. (2010) model proposes that the Farellones Formation was deposited in a "piggyback" basin behind (to the east of) the San Ramón Fault. This idea is in good agreement with the absence of the Farellones Formation during stage 1, as this piggyback basin was separated from the drainage system flowing to the west (Armijo et al., 2010), where Navidad Basin sediments were deposited. However, the model of Armijo et al. (2010) does not explain the Abanico West provenance recognized in sediments deposited during stage 1, as they do not recognize the Los Ángeles–Infiernillo Fault. Moreover, these authors have not included this fault in their model, even when previous works have recognized deformation along the Los Ángeles–Infiernillo Fault during the late Oligocene to early Miocene (Sellés, 1999; Fuentes, 2004; Fock, 2005). The Armijo et al. (2010) model states that erosion of the Principal Cordillera could have not started earlier than 16 Ma (Armijo et al., 2010). This disagrees with our model, which indicates that the western Principal Cordillera was already being eroded at the beginning of stage 2 (18 Ma). With respect to the Coastal Cordillera, Armijo et al. (2010) consider that part of its uplift is related to alternating cycles of subduction erosion and accretion at the continental margin, which may swing the Coastal Cordillera gently like a seesaw over ~10^6 periods of time. This observation is in good agreement with a strong influence of the tectonic processes that affected the continental margin during deposition in the Navidad Basin, as shown by the provenance model for erosional stages 1, 2, and 3.

Finally, the main difference between our provenance model and previous morphotectonic models for the study region is the recognition in our model of the Los Ángeles–Infiernillo Fault as an important relief-generating structure during stage 1 (Fig. 11). However, as erosion of rocks would depend on the degree of development of the drainage system, it is not possible to say that the San Ramón Fault did not uplift the western Principal Cordillera block during this stage. If the Los Ángeles–Infiernillo and San Ramón Faults uplifted simultaneously the blocks formed by the eastern Central Depression and western Principal Cordillera during stage 1, the drainage network that supplied material to the Navidad Basin was propagated to the east by retrograde erosion, affecting, first, the eastern Central Depression block, which was in a westernmost position with respect to the western Principal Cordillera block (Fig. 11).

CONCLUSIONS

The heavy mineral analysis of the marine units in the Navidad Basin allows us to identify three stages of erosion of the Central Chilean forearc. Variations in the chemistry of detrital pyroxene and amphibole indicate that a volcanic origin source area was first in the present-day eastern Central Depression, later at the eastern Central Depression–western Principal Cordillera border, and finally in the western Principal Cordillera. Metamorphic and intrusive sources from the Coastal Cordillera are identified through compositional changes of detrital garnet, correlating well with the position of the paleocoast during the different stages. Therefore, these sources are interpreted as representing the erosion of nearshore basement rocks, which were affected by faulting along the eastern border of the Navidad Basin. Our work highlights the role of the Los Ángeles–Infiernillo Fault on Andean uplift, a fault that was previously underestimated by the morphotectonic models proposed for the study region. Uplift along this fault during the early or late Miocene would have created an important relief to the east, including part of the present-day Central Depression and Principal Cordillera.

ACKNOWLEDGMENTS

We acknowledge funding by the Departamento de Investigación y Desarrollo (DI), Universidad de Chile (Project 2004 DI, I2 04/02-2) to Luisa Pinto Lincoñir. Financial support for travel and stay in France for conducting geochemical analysis was given by the Bourse Amérique Latine at the Université Paul Sabatier (Toulouse III, France) and the French Institute of Research Collaboration (IRD). This research was also supported by the Fondecyt Project Nº 1030965 and the Proyecto Anillo ACT N° 18 (Bicentenario-CONICYT) both to Reynaldo Charrier, and Project Fondecyt N° 1090165 to Luisa Pinto. The authors are grateful to Philippe de Parseval and François Fontan (Université de Toulouse, France), Mauricio Belmar (SGS, Chile), and Juan Vargas (Facultad de Ciencias Físicas y Matemáticas, Universidad de Chile) for valuable help in preparation and analysis of heavy mineral samples and assembling the data file. Careful reviews by Reynaldo Charrier and Jacobus Le Roux (Facultad de Ciencias Físicas y Matemáticas, Universidad de Chile), Andrew Morton (HM Research, UK), Robert Rainbird (Geological Survey of Canada), and Sergio Andò (Department of Geology of Milano-Bicocca, Italy) helped greatly to improve the manuscript. Discussions with Luis Felipe Hinojosa and Néstor Gutiérrez (Facultad de Ciencias, Universidad de Chile) contributed significantly to the improvement of this chapter.

REFERENCES CITED

Aguirre, L., 1957, Perfil geológico entre la Cuesta de Chacabuco y el límite con la República Argentina [M.S. thesis]: Santiago, Universidad de Chile, 406 p.

Aguirre, L., 1960, Geología de los Andes de Chile Central, provincia de Aconcagua: Instituto de Investigaciones Geológicas Boletín, v. 9, 70 p.

Aguirre, L., Feraud, G., Vergara, M., Carrasco, J., and Morata, D., 2000, $^{40}Ar/^{39}Ar$ ages of basic flows from the Valle Nevado stratifies sequence (Farellones Formation), Andes of Central Chile: Puerto Varas, Chile, Sociedad Geológica de Chile, Congreso Geológico Chileno, 9th, v. 1, p. 583–585.

Armijo, R., Rauld, R., Thiele, R., Vargas, G., Campos, J., Lacassin, R., and Kausel, E., 2010, The West Andean Thrust, the San Ramón Fault, and the seismic hazard for Santiago, Chile: Tectonics, v. 29, TC2007, doi:10.1029/2008TC002427.

Beccar, I., Vergara, M., and Munizaga, F., 1986, Edades K-Ar de la Formación Farellones, en el cordón del cerro La Parva, Cordillera de los Andes de Santiago, Chile: Revista Geológica de Chile, v. 28, p. 109–113.

Best, M.G., and Christiansen, E.H., 2000, Igneous Petrology: Boston, Blackwell Science, 516 p.

Borde, J., 1966, Les Andes de Santiago et leur Avant-Pays: Étude de Géomorphologie: Bordeaux, France, Union française d'Impression, 559 p.

Brüggen, J., 1950, Fundamentos de la Geología de Chile: Santiago, Chile, Instituto Geográfico Militar, 374 p.

Buatois, L.A., and Encinas, A., 2006, The Clossifungites ichnofacies at the boundary between the Navidad (Rapel Member) and La Cueva formations, Pliocene of the Coastal Cordillera, Chile: Its sequence stratigraphic significance: Ameghiniana, v. 43, p. 3–9.

Carmicheal, I.S.E., Nicholls, J., and Smith, L., 1970, Silica activity in igneous rocks: American Mineralogist, v. 55, p. 246–263.

Cecioni, G., 1978, Petroleum possibilities of the Darwin's Navidad Formation near Santiago, Chile: Publicación Ocasional del Museo Nacional de Historia Natural de Chile, v. 25, p. 3–28.

Charrier, R., and Munizaga, F., 1979, Edades K–Ar de volcanitas cenozoicas del sector cordillerano del río Cachapoal, Chile (34°15′ Lat. S): Revista Geológica de Chile, v. 7, p. 41–51.

Charrier, R., Baeza, O., Elgueta, S., Flynn, J.J., Gans, P., Kay, S.M., Muñoz, N., Wyss, A.R., and Zurita, E., 2002, Evidence for Cenozoic extensional basin development and tectonic inversion south of the flat-slab segment, southern Central Andes, Chile (33°–36°S.L.): Journal of South American Earth Sciences, v. 15, p. 117–139, doi:10.1016/S0895-9811(02)00009-3.

Charrier, R., Bustamante, M., Comte, D., Elgueta, S., Flynn, J.J., Iturra, N., Muñoz, N., Pardo, M., Thiele, R., and Wyss, A.R., 2005, The Abanico extensional basin: Regional extension, chronology of tectonic inversion and relation to shallow seismic activity and Andean uplift: Neues Jahrbuch für Geologie und Paläontologie Abhandlungen, v. 236, p. 43–77.

Creixell, C., 2007, Emplazamiento y petrogénesis de enjambres de diques máficos Mesozoicos de Chile central (30°–33°45′ S): Implicancias tectónicas en el desarrollo del arco Jurásico-Cretácico Inferior [Ph.D. thesis]: Santiago, Universidad de Chile, 275 p.

Darwin, C., 1846, Geological Observations on South America, The Geology of the Voyage of the Beagle, Volume Part III: London, Smith Elder and Co., 279 p.

Deer, W.A., Howie, R.A., and Zussman, J., 1992, An Introduction to the Rock-Forming Minerals: London, Longman Group, 696 p.

Deer, W.A., Howie, R.A., and Zussman, J., 1997a, Orthosilicates, Rock-Forming Minerals: Geological Society [London], v. 1A, 919 p.

Deer, W.A., Howie, R.A., and Zussman, J., 1997b, Double-Chain Silicates, Rock-Forming Minerals: Geological Society [London], v. 2B, 764 p.

Deer, W.A., Howie, R.A., and Zussman, J., 1997c, Single-Chain Silicates, Rock-Forming Minerals (2nd edition): Geological Society [London], v. 1A, 668 p.

Encinas, A., 2006, Estratigrafía y sedimentología de los depósitos marinos mio-pliocenos del área de Navidad (33°–34°S), Chile Central: Implicaciones con respecto a la tectónica del antearco [Ph.D. thesis]: Santiago, Universidad de Chile, 177 p.

Encinas, A., Le Roux, J.P., Buatois, L.A., Nielsen, S.N., Finger, K.L., Fourtanier, E., and Lavenu, A., 2006a, New stratigraphic scheme for the Mio-Pliocene marine deposits of the Navidad area (33°00′–34°30′S), central Chile: Revista Geologica de Chile, v. 33, p. 221–246.

Encinas, A., Maksaev, V., Pinto, L., Le Roux, J.P., Munizaga, F., and Zentilli, M., 2006b, Pliocene lahar deposits in the Coastal Cordillera of central Chile: Implications for uplift, avalanche deposits, and porphyry copper systems in the Main Andean Cordillera: Journal of South American Earth Sciences, v. 20, p. 369–381, doi:10.1016/j.jsames.2005.08.007.

Encinas, A., Finger, K.L., Nielsen, S.N., Lavenu, A., Buatois, L.A., Peterson, D.E., and Le Roux, J.P., 2008, Rapid and major coastal subsidence during the late Miocene in south-central Chile: Journal of South American Earth Sciences, v. 25, p. 157–175, doi:10.1016/j.jsames.2007.07.001.

Farías, M., 2007, Tectónica y erosión en la evolución del relieve de los Andes de Chile central durante el Neógeno [Ph.D. thesis]: Santiago, Universidad de Chile, 194 p.

Farías, M., Charrier, R., Carretier, S., Martinod, J., and Comte, D., 2006, Erosión versus tectónica en el origen de la Depresión Central de Chile Central: Antofagasta, Chile, Congreso Geológico Chileno, 11th, p. 201–204.

Farías, M., Charrier, R., Carretier, S., Martinod, J., Fock, A., Campbell, D., Cáceres, J., and Comte, D., 2008, Late Miocene high and rapid surface uplift and its erosional response in the Andes of Central Chile (33°–35°S): Tectonics, v. 27, TC1005, doi:10.1029/2006TC002046.

Finger, K.L., Nielsen, S.N., Devries, T.J., Encinas, A., and Peterson, D.E., 2007, Paleontologic evidence for sedimentary displacement in Neogene forearc basins of central Chile: Palaios, v. 22, p. 3–16, doi:10.2110/palo.2005.p05-081r.

Fock, A., 2005, Cronología y tectónica de la exhumación en el Neógeno de los Andes de Chile Central entre los 33° y los 34°S [M.S. thesis]: Santiago, Universidad de Chile, 179 p.

Fuentes, F., 2004, Petrología y metamorfismo de muy bajo grado de unidades volcánicas oligoceno-miocenas en la ladera occidental de Los Andes de Chile Central (33°S) [Ph.D. thesis]: Santiago, Universidad de Chile, 398 p.

Gana, P., and Wall, R., 1997, Evidencias geocronológicas $^{40}Ar/^{39}Ar$ y K–Ar de un hiatus Cretácico Superior-Eoceno en Chile Central (33°–33°30′S): Revista Geológica de Chile, v. 24, p. 145–163.

Gana, P., Wall, R., and Gutiérrez, A., 1996, Mapa geológico del área Valparaíso-Curacaví, regiones de Valparaso y Metropolitana: Servicio Nacional de Geología y Minería, map scale 1:100,000, 1 sheet, 20 p. text.

Garzanti, E., Ando, S., and Vezzoli, G., 2008, Settling equivalence of detrital minerals and grain-size dependence of sediment composition: Earth and Planetary Science Letters, v. 273, p. 138–151, doi:10.1016/j.epsl.2008.06.020.

Garzanti, E., Ando, S., and Vezzoli, G., 2009, Grain-size dependence of sediment composition and environmental bias in provenance studies: Earth and Planetary Science Letters, v. 277, p. 422–432, doi:10.1016/j.epsl.2008.11.007.

Gutiérrez, N., Pedroza, V., and Hinojosa, L.F., 2009, Edad de la Formación Navidad: Nuevos antecedentes para un viejo problema: Santiago, Sociedad Geológica de Chile, Congreso Geológico Chileno, 12th, 4 p.

Herm, D., 1969, Marines Pliozän und Pleistozän in Nord und Mittel-Chile unter besonderer Berücksichtigung der Entwicklung der Mollusken-Faunen: Zitteliana, v. 2, p. 159.

Hervé, F., 1988, Late Paleozoic subduction and accretion in Southern Chile: Episodes, v. 11, p. 183–188.

Hinojosa, L.F., and Gutiérrez, N., 2009, Cambio Climático y Diversidad: El caso de La Formación Navidad, Mioceno de Chile central: Santiago, Sociedad Geológica de Chile, Congreso Geológico Chileno, 12th, 4 p.

Hoskin, P., and Schaltegger, U., 2003, The composition of zircon and igneous and metamorphic petrogenesis: Reviews in Mineralogy and Geochemistry, v. 53, p. 27–62, doi:10.2113/0530027.

Kay, S.M., Godoy, E., and Kurtz, A., 2005, Episodic arc migration, crustal thickening, subduction erosion, and magmatism in the south-central Andes: Geological Society of America Bulletin, v. 117, p. 67–88, doi:10.1130/B25431.1.

Krawinkel, H., Wozazek, S., Krawinkel, J., and Hellmann, W., 1999, Heavy-mineral analysis and clinopyroxene geochemistry applied to provenance analysis of lithic sandstones from the Azuero–Soná Complex (NW Panama): Sedimentary Geology, v. 124, p. 149–168, doi:10.1016/S0037-0738(98)00125-0.

Kretz, R., 1983, Symbols for rock-forming minerals: American Mineralogist, v. 68, p. 277–279.

Lavenu, A., and Encinas, A., 2005, Deformación frágil de los depósitos neógenos de la cuenca de Navidad (Cordillera de la Costa–34°S–Chile central): Revista Geológica de Chile, v. 32, p. 229–248.

Leake, B.E., 1965, The relationship between tetrahedral aluminum and the maximum possible octohedral aluminum in natural calciferous and subcalciferous amphiboles: American Mineralogist, v. 50, p. 843–851.

Leake, B.E., and 21 others, 1997, Nomenclature of amphiboles: Report of the Subcommitee on Amphiboles of the International Mineralogical Association, Commission on New Minerals and Mineral Names: American Mineralogist, v. 82, p. 1019–1037.

Le Bas, M., 1962, The role of aluminum in igneous clinopyroxenes with relation to their parentage: American Journal of Science, v. 260, p. 267–288, doi:10.2475/ajs.260.4.267.

Leterrier, J., Maury, R., Thonon, P., Girard, D., and Marchal, M., 1982, Clinopyroxene composition as a method of identification of the magmatic affinities of paleo-volcanic series: Earth and Planetary Science Letters, v. 59, p. 139–154, doi:10.1016/0012-821X(82)90122-4.

López-Escobar, L., and Vergara, M., 1997, Eocene-Miocene Longitudinal Depression and Quaternary volcanism in the Southern Andes, Chile (33–42.5°S): A geochemical comparison: Revista Geológica de Chile, v. 24, p. 227–244.

Mange, M.A., and Morton, A.C., 2007, Geochemistry of heavy minerals, *in* Mange, M.A., and Wright, D.K., eds., Heavy Minerals in Use: Developments in Sedimentology, v. 58, p. 345–391.

Melnick, D., and Echtler, H.P., 2006, Inversion of forearc basins in south-central Chile caused by rapid glacial age trench fill: Geology, v. 34, p. 709–712, doi:10.1130/G22440.1.

Morimoto, N., 1988, Nomenclature of pyroxenes: Mineralogical Magazine, v. 52, p. 535–550, doi:10.1180/minmag.1988.052.367.15.

Morton, A., 1985, Heavy minerals in provenance studies, *in* Zuffa, G.G., ed., Provenance of Arenites: Boston, Reidel Publishing, p. 249–277.

Nielsen, S.N., and Glodny, J., 2009, Early Miocene subtropical water temperatures in the southeast Pacific: Palaeogeography, Palaeoclimatology, Palaeoecology, v. 280, p. 480–488, doi:10.1016/j.palaeo.2009.06.035.

Núñez, R., 1991, Antecedentes geológicos y petrográficos del área de la Mina El Sauce: Un skarn cálcico de cobre, Cabildo, región de Aconcagua, Chile [M.S. thesis]: Santiago, Universidad de Chile, 56 p.

Nyström, J.O., Vergara, M., Morata, D., and Levi, B., 2003, Tertiary volcanism during extension in the Andean foothills of central Chile (33°15′–33°45′S): Geological Society of America Bulletin, v. 115, p. 1523–1537, doi:10.1130/B25099.1.

Pardo, M., Vera, E., Monfret, T., and Yáñez, G., 2008, Crustal seismicity and 3D seismic wave velocity models in the Andes cordillera of Central Chile (33°–34.5°S) from local earthquakes: Nice, France, International Symposium on Andean Geodynamics (ISAG), 6th, p. 377–380.

Parfenoff, A., Pomerol, Ch., and Tourenq, J., 1970, Les Minéraux Lourds en Grains: Méthodes d'Étude et Détermination, 578 p.

Pettijohn, F.J., Potter, P.E., and Siever, R., 1987, Sand and Sandstone: New York, Springer, 553 p.

Pinto, L., Herail, G., Moine, B., Fontan, F., Charrier, R., and Dupre, B., 2004, Using geochemistry to establish the igneous provenances of the Neogene continental sedimentary rocks in the Central Depression and Altiplano, Central Andes: Sedimentary Geology, v. 166, p. 157–183, doi:10.1016/j.sedgeo.2003.12.002.

Pinto, L., Herail, G., Fontan, F., and de Parseval, P., 2007, Neogene erosion and uplift of the western edge of the Andean Plateau as determined by detrital heavy mineral analysis: Sedimentary Geology, v. 195, p. 217–237, doi:10.1016/j.sedgeo.2006.08.001.

Rauld, R., 2002, Análisis Morfoestructural del Frente Cordillerano Santiago Oriente entre el Río Mapocho y la Quebrada de Macul [Undergraduate thesis]: Santiago, Universidad de Chile, 57 p.

Rauld, R., Vargas, G., Armijo, R., Ormeño, A., Valderas, C., and Campos, J., 2006, Cuantificación de escarpes de falla y deformación reciente en el frente cordillerano de Santiago: Antogafasta, Chile, Congreso Geológico Chileno, 11th, p. 447–450.

Rodríguez, M.P., 2008, Evolución de la erosión y del relieve del antearco de Chile Central (33°–34°S) durante el Neógeno mediante el análisis de Minerales Pesados detríticos y la Geomorfología [M.S. thesis]: Santiago, Universidad de Chile, 158 p.

Sellés, D., 1999, La Formación Abanico en el Cuadrángulo Santiago (33°15′–33°30′S; 70°30′–70°45′O), Chile Central, Estratigrafía y Geoquímica [M.S. thesis]: Santiago, Universidad de Chile, 154 p.

Sellés, D., and Gana, P., 2001, Geología del área Talagante-San Francisco de Mostazal. Santiago: Servicio Nacional de Geología y Minería, Serie Geología Básica, v. 74, 99 p., map scale 1:100,000, 1 sheet.

SERNAGEOMIN, 2003, Mapa Geológico de Chile, escala 1:1000.000. Servicio Nacional de Geología y Minería, map scale 1:1,000,000, 1 sheet, 23 p. text.

Siivola, J., and Schmid, R., 2007, Recommendations by the IUGS Subcommission on the Systematics of Metamorphic Rocks: List of mineral abbreviations: Web version 01.02.07 (http://www.bgs.ac.uk/scmr/docs/papers/paper_12.pdf), IUGS Commission on the Systematics in Petrology.

Simonetti, A., Shore, M., and Bell, K., 1996, Diopside phenocrysts from nephelinite lavas, Napak volcano, eastern Uganda: Evidence for magma mixing: Canadian Mineralogist, v. 34, p. 411–421.

Tavera, J., 1979, Estratigrafía y paleontología de la Formación Navidad, Provincia de Colchagua, Chile (30°50′–34°S): Boletín del Museo Nacional de Historia Natural, v. 36, p. 176.

Thiele, R., 1980, Hoja Santiago, Región Metropolitana: Servicio Nacional de Geología y Minería, Carta Geológica de Chile, v. 29.

Thomas, H., 1958, Geología de la Cordillera de la Costa entre el Valle de La Ligua y la Cuesta de Barriga: Instituto de Investigaciones Geológicas: Boletin, Instituto de Estudios de Poblacion y Desarrollo (Dominican Republic), v. 2, p. 1–86.

Valdés, C., 2009, Erosión Neógena de la Cordillera de los Andes en el segmento del flat-slab [M.S. thesis]: Concepción, Universidad de Concepción, 196 p.

Vergara, M., Morata, D., Hickey-Vargas, R., Lopez-Escobar, L., and Beccar, I., 1999, Cenozoic tholeiitic volcanism in the Colbun area, Linares Precordillera, central Chile (35°35′–36°S): Revista Geologica de Chile, v. 26, p. 23–41.

Vergara, M., López-Escobar, L., Palma, J.L., Hickey-Vargas, R., and Roeschmann, C., 2004, Late Tertiary episodes in the area of the city of Santiago de Chile: New geochronological and geochemical data: Journal of South American Earth Sciences, v. 17, p. 227–238, doi:10.1016/j.jsames.2004.06.003.

Wall, R., Gana, P., and Gutiérrez, A., 1996, Geología de la Hoja Santiago, área de San Antonio–Melipilla, regiones de Valparaíso, Metropolitana y del Libertador General Bernardo O'Higgins: Servicio Nacional de Geología y Minería, Mapas Geológicos, v. 2, map scale 1:100,000, 1 sheet, 20 p. text.

Wall, R., Sellés, D., and Gana, P., 1999, Geología de la Hoja Santiago, área de Tiltil-Santiago, Región Metropolitana Servicio Nacional de Geología y Minería, Mapa Geológico, v. 11, map scale 1:100,000, 1 sheet.

Weltje, G.A., and von Eynatten, H., 2004, Quantitative provenance analysis of sediments: Review and outlook: Sedimentary Geology, v. 171, p. 1–11, doi:10.1016/j.sedgeo.2004.05.007.

Willner, A.P., 2005, Pressure-temperature evolution of a late Paleozoic paired metamorphic belt in North-Central Chile (34°–35°30′S): Journal of Petrology, v. 46, p. 1805–1833, doi:10.1093/petrology/egi035.

Manuscript Accepted by the Society 29 November 2011

Printed in the USA

2.4.3. Final considerations considering an Early to Middle Miocene age for the Navidad Formation.

The final consensus reached over the last year with respect to the age of the Navidad Basin deposits allows to better constrain landscape evolution in central Chile. According to the $^{87}Sr/^{86}Sr$ and $^{40}Ar/^{39}Ar$ determinations made by Gutiérrez et al. (2013), the erosional stages indicated by provenance results can be assigned as it follows: stage 1 to the Early Miocene (23- 18 Ma), stage 2 to the Early to Late Miocene (18-12 Ma) and stage 3 to after the Late Miocene. The main conclusion that can be extracted from this information is that in central Chile the main topographic feature subjected to erosion of river systems draining towards the west during the Early Miocene was located in the present-day eastern Central Depression (see Fig. 11 in “Cenozoic erosion in the Andean forearc of Central Chile 33-34°S: Sediment provenance inferred by heavy mineral studies”). This is consistent with structural and geochronological studies indicating that the Los Ángeles- Infiernillo Fault corresponds to the western border of the Abanico Basin, whose inversion began during the Late Oligocene-Early Miocene (Fock, 2005).

Chapter 3- THERMOCHRONOMETRIC CONSTRAINS IN LATE MESOZOIC AND CENOZOIC EXHUMATION ALONG THE COASTAL AND FRONTAL CORDILLERAS IN NORTH-CENTRAL CHILE

3.1 Introduction

The content of this chapter includes the results, the analysis and the implications in terms of tectonic-related exhumation of the apatite fission tracks (AFT) and the apatite (U-Th)/ He low temperature thermochronology on rocks from the Coastal and Frontal Cordilleras in north-central Chile. Two scientific contributions are here in presented:

1) An abstract and the corresponding poster presentation included on the Thermo 2012 (13th International Congress on Thermochronology) in Guilin, China. This work is entitled “High chlorine content variations in apatite: consequences on thermochronology interpretation of data from Central Andes, Chile”. This work deals with the possible compositional effects that may affect AFT ages of the samples collected in this thesis (see section 3.2).

2) A manuscript entitled “Thermochronometric contraints on the development of the Andean topographic front in north central Chile (28.5-32ºS)” which was submitted to Tectonics in October 2013. In this article, the timing of tectonic-related exhumation throughout the Frontal and Coastal Cordilleras is determined using U-Pb zircon geochronology and low temperature thermochronology of Apatite Fission Track (AFT) and U-Th/He in apatite (AHe) of intrusive and metamorphic rocks (see section 3.3).

Finally, the chapter ends with the final conclusions regarding the timing of tectonic-related exhumation throughout the studied region.

3.2 High chlorine content variations in apatite: Consequences on thermochronology interpretation of data from Central Andes, Chile. (Poster presentation in Thermo 2013 - 13th International Congress on Thermochronology, Guilin, China).

M.P. Rodríguez[1*], S. Brichau**[2]**, P. de Parseval[2], S. Carretier[2], M. Farías[1], R. Charrier[1, 3] and R. A. Ketcham[4]

1Departamento de Geología, Universidad de Chile, Plaza Ercilla 803, Santiago, Chile
2 Université Paul Sabatier, OMP/ IRD/ CNRS, GET, 14 Av. E. Belin, F-31400 Toulouse, France
3 Universidad Andrés Bello, Sazie 2315, Santiago, Chile
4 Jackson School of Geosciences, University of Texas, Austin, Texas, U.S.A.
* Corresponding author: maria.p.rodriguez@gmail.com

Uplift ages and related exhumation in the Central Andes is a highly debated topic. In order to better constrain tectonomorphic evolution within the Central Andes we collected 28 samples for zircon U-Pb, apatite fission-track and (U-Th)/He (AFT and AHe) dating from the Coastal and the Frontal/Principal Cordilleras in Chile between 30 and 33°S. Samples from the Coastal Cordillera give U-Pb ages from ~ 120 to 100 Ma, while AFT ages range between ~ 65 Ma and 50 Ma. In the Frontal/Principal Cordillera, the U-Pb method displays ages from ~ 60 Ma to 40 Ma, and AFT ages range between ~ 40 Ma and 30 Ma. These data are in agreement with previously published studies indicating that deformation and related exhumation is younger in the Frontal/Principal Cordillera than in the Coastal. However, results reveal serious inconsistencies between the AFT and AHe data sets. AHe ages are around ~ 30 Ma in the Coastal Cordillera and range between ~ 20 and 10 Ma in the Frontal/Principal Cordillera. Large differences between AFT and AHe ages of about ~ 35-25 Ma in Coastal Cordillera and ~30-10 Ma in Frontal/Principal Cordillera suggest very slow exhumation rates with a period of long residence within the AFT partial annealling zone (PAZ). However, most of samples display high mean track lengths (>14.1 µm) and measured Dpar ranging from ~1.6 to ~3 µm. The highest Dpar values suggest that some apatites are chlorine-rich, implying a greater resistance to annealing. To confirm this hypothesis, apatite composition has been defined by microprobe. Consistently, most of the analyzed apatites show high chlorine contents (>1%) for the sample in which the highest Dpar was measured. In certain samples this concentration can reach as much as 2.3 wt% of chlorine. For such extreme compositions, calculations indicate that the closure temperature for fission tracks in apatite could be ~ 20°C higher than average. In this study the inconsistencies observed in our data set between AFT and AHe method seem to be due to specific composition of the apatites and therefore explain the huge gap between AFT and AHe ages. Furthermore, we find that the AFT closure temperatures for a 10°C/Km cooling rate predicted by Dpar values are generally more than 5°C lower than the ones predicted by the chlorine content. This study demonstrates the importance of carrying out microprobe analyses for an accurate interpretation of thermochronological data set.

HIGH CHLORINE CONTENT VARIATIONS IN APATITE: CONSEQUENCES ON THERMOCHRONOLOGY INTERPRETATION OF DATA FROM CENTRAL ANDES, CHILE

Institut de recherche pour le developpement

Introduction

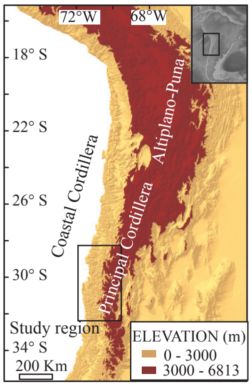

Uplift ages and related exhumation in the Central Andes is a highly debated topic.

In order to better constrain tectonomorphic evolution within the Central Andes we collected 28 samples for zircon U-Pb, apatite fission-track (AFT) and apatite (U-Th)/He (AHe) dating from the Coastal to the Principal Cordilleras in Chile between 29 and 33°S.

U-Pb , AFT and AHe data

U-Pb ages were determined in zircon by LA-ICPMS. Etching procedure for AFT used was 5.5 M HNO_3 for 20 s at 21 °C. Spontaneous tracks were measured using unpolarized light at 2000x magnification and ^{238}U concentrations in apatite were determined using LA-ICPMS. AHe ages are mean ages among 4 to 3 hand picked individual grains. He was extracted in vacuo by heating with a laser in a noble gas spectrometer and U and Th determinations made by ICP-MS.

Samples from the Coastal Cordillera give U-Pb ages from ~ 120 to 100 Ma, while AFT ages range between ~ 65 Ma and 50 Ma. In the Principal Cordillera, the U-Pb method displays ages from ~ 60 Ma to 40 Ma, and AFT ages range between ~ 40 Ma and 30 Ma.

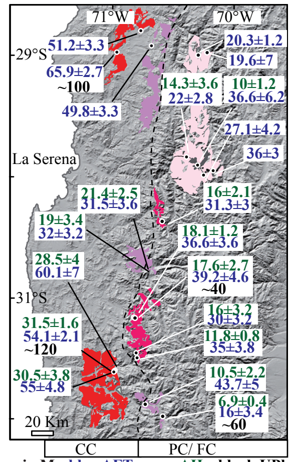

Ages in Ma blue AFT green AHe black UPb

AHe ages are around ~ 30 Ma in the Coastal Cordillera and range between ~ 20 and 10 Ma in the Frontal/ Principal Cordillera

These data are in agreement with previously published studies indicating that deformation and related exhumation is younger in the Principal Cordillera than in the Coastal Cordillera.

However, results reveal major, but potentially informative inconsistencies between the AFT and AHe data sets

Inconsistencies between AFT and AHe data sets

We obtained AFT and AHe for 21 samples. Most samples show large differences between AFT and AHe ages of about ~ 45-25 Ma in Coastal Cordillera and ~30 – 10 Ma in Principal Cordillera

The large difference between AFT and AHe ages suggest very slow exhumation rates with a period of long residence within the AFT partial annealling zone (PAZ)

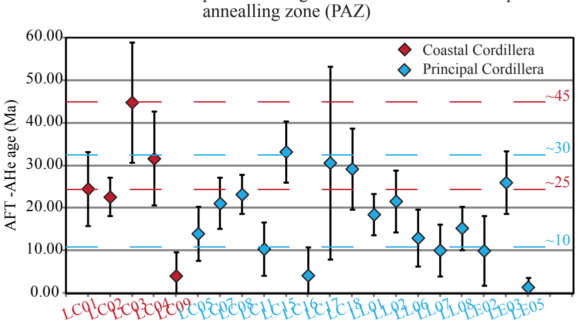

However, most of samples feature high mean track lengths (>14.1 µm) that are generally inconsistent with a long residence within the PAZ

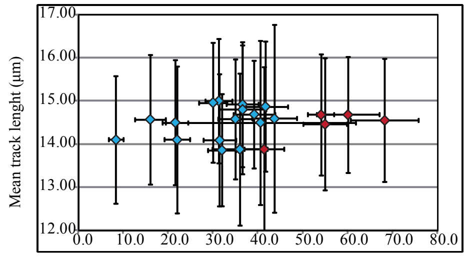

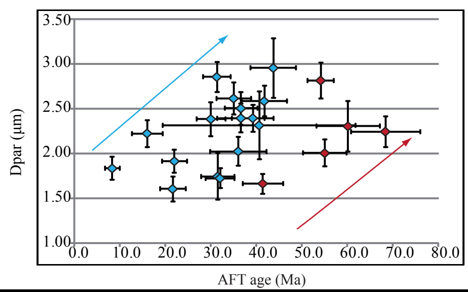

Maximum long etch pit diameter (Dpar) values in both the Coastal and the Principal Cordilleras tend to rise with AFT age, suggesting some kind of compositional influence on AFT age

Most samples have Dpar values higher than 1.75 µm, suggesting that apatites are chlorine-rich, implying a greater resistance to annealing.

To confirm if apatites from the study region are chlorine rich, apatite composition was determinated by microprobe

Chlorine content on apatite

We perfomed ~ 30 microprobe analysis per sample in order to obtain apatite composition. 5 grains in each sample were analyzed at its core and rim and no significant intracristalline variation was identified

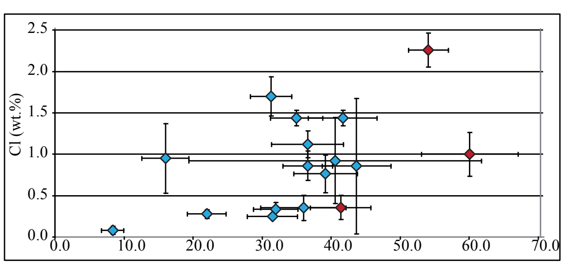

Consistent with our hyphothesis, most of the analyzed apatites show high chlorine contents (>1%) within error (error=standard deviation among replicates)

Dpar vs. Cl

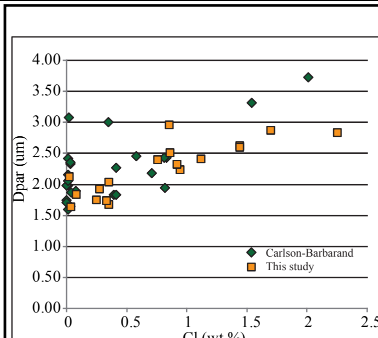

We compare the Dpar values and chlorine content in our samples with the values obtained by Carlson et al. (1999) and Barbarand et al. (2003)

The relationship between Dpar and chroline in our samples is different than the same relationship in the data of Carlson-Barbarand. In general, in our samples the Dpar values for chlorine content higher than 1% are significantly lower than Dpar values predicted by the Carlson-Barbarand calibration

The observed differences of the Dpar-chlorine relationship between our data and the data of Carlson-Barbarand may be due to a difference on how Dpar was measured or differences in other sample properties that affect etching and, therefore, Dpar size.

Finally, the inconsistencies between AFT and AHe method are probably due to specific composition of the apatites and could explain the huge gap between AFT and AHe ages.

3.3. Thermochronometric contraints on the development of the Andean topographic front in north central Chile (28.5-32ºS) (manuscript submitted to Tectonics in October 2013)

María Pía Rodríguez[1,2*] Reynaldo Charrier[1,2,3] Stephanie Brichau[4], Sébastien Carretier[1,4] Philippe de Parseval[4]; Marcelo Farías[1] and Richard A. Ketcham[5]

[1] Departamento de Geología, Facultad de Ciencias Físicas y Matemáticas, Universidad de Chile, Casilla 13518, Correo 21, Santiago, Chile.

[2] Advance Mining Technology Center (AMTC), Facultad de Ciencias Físicas y Matemáticas, Universidad de Chile, Santiago, Chile.

[3] Escuela de Ciencias de la Tierra, Universidad Andres Bello, Santiago.

[4] Université de Toulouse, UPS, IRD, CNRS, GET, 14 Av. Edouard Belin, 31400, Toulouse, France.

[5] The University of Texas at Austin, Department of Geological Sciences, University Station C1100 Austin, TX 78712, USA.

* corresponding author e-mail: maria.p.rodriguez@gmail.com

Keywords: Andean topographic front, north-central Chile, thermochronology, tectonic-related exhumation.

Abstract

We combine U-Pb zircon geochronology and low temperature thermochronology to constrain the tectonic-related exhumation controlling the development of the Andean topographic front in north central Chile. While Paleozoic and Cenozoic rocks in the Frontal Cordillera show AFT and AHe ages between ~ 40 and 8 Ma and ~ 20 to 6 Ma, respectively; Mesozoic rocks from the Coastal Cordillera show AFT ages between ~ 60 and 40 Ma and AHe ages around 30 Ma. Thermal models indicate the Coastal Cordillera was accelerated exhumed ~ 65 -50 Ma and suffered little exhumation since ~ 45 Ma. Thermal models for the Frontal Cordillera north of 31°S indicate that exhumation started ~ 30 and 35 Ma along the western and eastern Frontal Cordillera, respectively. In the former area exhumation was continuous until shortly after 20 Ma, whereas episodes of accelerated exhumation at ~ 22 -18 Ma and around 7 Ma affected the central and eastern Frontal Cordillera, respectively. South of 31°S accelerated exhumation at the foot of the front occurred around 22 -16 Ma, while in the areas to the east exhumation

occurred until the Late Miocene. Our data suggests a progressive construction of the Andean topographic front since the Early Oligocene north of 31°S and the Early Miocene south of 31°S. Accelerated exhumation in the Early and Late Miocene correlates with periods of increased contractional deformation starting after the Early Oligocene break-up of the Farallon Plate, rather than to the Late Miocene onset of flat subduction throughout the studied region.

1. Introduction

The large scale geomorphology of the western flank of the Central Andes (15-34° S) is dominated by a steep rise in elevation throughout west to east transects (Fig. 1a). This first-order geomorphologic feature represents a topographic front flanking the highly elevated areas to the east corresponding to the Altiplano - Puna, the Frontal Cordillera and the Principal Cordillera from north to south (Fig. 1a). Despite north - south variations in subduction regime and climatic conditions (Fig. 1 a and b) this topographic front is observed uninterruptedly from southern Peru to central Chile; suggesting that its evolution was coeval throughout the Central Andes. However, it is unclear if the uplift related to development of the front has been slow and steady since ~ 60 or 40 Ma (e.g. Barnes and Ehlers, 2009); continuous at least since ~ 40 Ma but punctuated with later episodes of accelerated uplift (Charrier et al., 2013) or rapid after ~ 10 Ma (Garzione et al., 2006; Hoke et al., 2007; Farías et al., 2008). Furthermore, and possibly due to its spectacular landscape, most studies have focused in understanding the forearc tectonomorphic evolution at the latitude of the Altiplano-Puna plateau (Fig. 1a; Charrier and Muñoz, 1996; Victor et al., 2004; Farías et al. 2005; García and Hérail, 2005; Hoke et al., 2007; Hoke and Garzione, 2008; Jordan et al., 2010; García et al., 2011; Schildgen et al., 2007; Charrier et al., 2013); while areas to the south have been comparatively less studied (Fig. 1a; Mortimer et al., 1973; Riquelme et al., 2007; Farías et al., 2008; Armijo et al., 2010; Bissig and Riquelme, 2010). Here, we present the case of the western flank of the Andes between 28.5 and 32ºS. This region corresponds to a key area to understand Andean geodynamics as it is located above the Pampean or Chilean flat-slab segment (Fig. 1a). In this segment, the subduction angle is ~ 10°; contrary to the rest of the Central Andes where this angle is ~ 30° (e.g. Cahill and Isacks, 1992). Two main theories exist for the origin of this flat-slab segment. One indicates that slab flattening is related to the subduction of the Juan Fernández ridge at the same piercing point since ~ 10 Ma (Fig. 1a; Yañez et al., 2001). The other one points to trenchward motion of a thick upper plate and trench roll-back (Manea et al., 2012) as the main causes for Late Miocene flat subduction. Despite the debate regarding its origin, a highly compressive tectonic regime is thought to be related to flat-subduction (Pardo et al., 2002; Yañez et al., 2001). However, the effects, if any, of flat subduction in the tectonomorphic evolution within the Chilean flank are unclear. Analogue modeling indicates that shortening related to horizontal subduction would occur at large distances from the trench (Martinod et al., 2010). This is consistent with structural data indicating Late Miocene high shortening rates (e.g. Ramos et al., 2002; Dávila et al., 2010) and active upper crustal seismicity in the Argentinean foreland (e.g. Alvarado and Beck, 2006). Moreover, preliminary thermochronological data indicates that uplift-related exhumation within the Frontal Cordillera mostly occurred between the

Early and Middle Miocene (Cembrano et al., 2003), before the Late Miocene onset of flat subduction. Similarly, geochemical data of Cenozoic volcanic units points to a transition to a more compressive tectonic regime during the same period, followed by Late Miocene re-equilibration of magmas with higher-pressure assemblages (Kay and Mpodozis, 2002; Litvak et al., 2007; Winocur et al., accepted). The scarce structural data available for the Frontal Cordillera contains evidence for Eocene to Oligocene deformation mostly next to the topographic front (Mpodozis and Cornejo, 1988; Pineda and Emparán, 2006; Pineda and Calderón, 2008) and Miocene deformation along the international border between Chile and Argentina (Maksaev et al., 1984; Mpodozis et al., 2009; Jara and Charrier, accepted; Winocur et al., accepted).

In this study, we applied U-Pb zircon geochronology combined with low-temperature thermochronology, including apatite fission track (AFT) and apatite (U-Th)/He (AHe), in order to recognize tectonic-related exhumation at both sides of the topographic front. As available structural geology for this region is sparse, this study does not aim to document the precise exhumation pattern related with faults potentially involved in uplift. Our study is instead focused on recognizing the first-order regional differences in tectonic-related exhumation at both sides of the topographic front and probable west-to-east variations in exhumation timing throughout the Frontal Cordillera. The questions we propose to address are: when did the Andean topographic front developed in this region, and is the flattening of the slab and the onset of the present seismotectonic setting responsible for its development?

2. Regional Setting

The present-day plate tectonic configuration in the Central Andes (15º-34ºS) was acquired after the breakup of the Farallon Plate into the Nazca and the Cocos Plates at about 25 Ma ago (Pardo-Casas y Molnar, 1987; Somoza, 1998). As a result of this major tectonic plate reorganization, between ~30 and 20 Ma the convergence rate of the Farallon (Nazca) Plate relative to the South American Plate rose from 50 or 60 to a maximum of 150 mm/yr (Pardo-Casas y Molnar, 1987; Somoza, 1998). The current convergence between the Nazca and South American plates is characterized by along strike variations of the subduction angle from flat (~ 10º) to normal (~ 30º) (Fig. 1a) (Cahill and Isacks, 1992; Jordan et al., 1983; Pardo et al., 2002). The area examined by this study is located between 28 and 32ºS, above the Pampean or Chilean flat-slab segment (27-33°S; Fig. 1a). Contrary to what is observed in the areas to the north of 27°S and to the south of 33°S, no Quaternary volcanic arc is developed within the studied region. Moreover, magmatism would have markedly decreased after 13 Ma following the initiation of slab flattening (Bissig et al., 2001; Kay and Mpodozis, 2002; Litvak et al., 2007). The morphotectonic units above the flat-slab region correspond to the north-south oriented Coastal Cordillera, Frontal Cordillera, Principal Cordillera, Precordillera and Sierras Pampeanas (Fig. 1a). Within the studied region the Coastal Cordillera and Frontal Cordillera are included (Fig. 1a), with the Principal Cordillera only observed at the southern limit of the studied region, to the south of 31.5°S (Fig. 1a). Contrary to regions to the north of 27°S and to the south of 33°S, no Central Depression is developed to the east of the Coastal Cordillera within this area (Fig.1a).

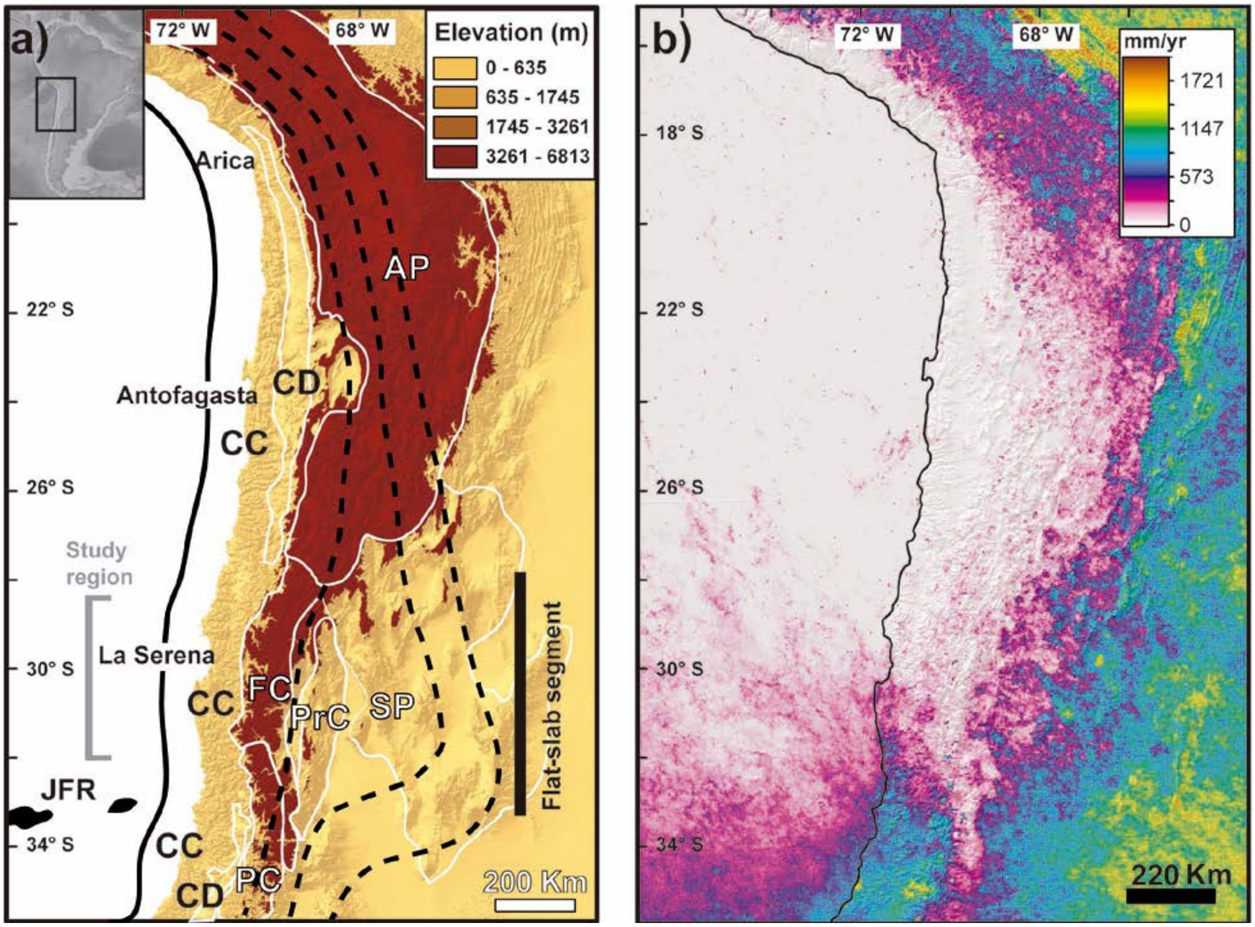

Fig. 1. a) Shaded relief image of the SRTM (90 m x pixel) digital elevation model throughout the Central Andes showing the topographic front and main morphostructural units. Dash lines marked the isobaths at 50, 100 and 150 km of the Nazca below the South American plate according to Cahill and Isacks (1990). White lines show the borders between main morphostructural units. Solid blak line marks the position of the trench. CC= Coastal Cordillera, CD= Central Depression, AP=Altiplano-Puna, FC= Frontal Cordillera. . SP= Sierras Pampeanas and PC= Principal Cordillera. JFR= Juan Fernández ridge. b) Shaded relief image throughout the Central Andes map color-coded for mean annual precipitation from Kenji Matsuura and Cort J. Willmott (2011) world database available at http://climate.geog.udel.edu/~climate/html_pages/download.html

The Coastal Cordillera is separated from the Frontal Cordillera by a topographic front (Fig. 2a and b). The topographic front corresponds to a marked rise in mean elevation along a north to south strip between the 71.7º and 71.9ºW (Fig. 2a and b). Whereas the mean elevation in the Coastal Cordillera is around ~1000 m a.s.l. with maximum values of ~ 3200 m a.s.l.; mean elevation in the Frontal Cordillera is ~ 3700 m a.s.l. with maximum values ~ 6800 m a.s.l. The scarp that forms the topographic front is around ~ 1000 m (Fig. 2b). The topographic front is generally aligned with exposures of Late Cretaceous volcanoclastic rocks and is not directly related to the traces of major faults (Fig. 3a).

The Coastal Cordillera presents a Devonian to Carboniferous metamorphic and metasedimentary basement along the coast, which is unconformably overlain by an east-dipping homoclinal block of middle Triassic to Late Cretaceous volcano-sedimentary rocks (Fig. 3a). Both the Paleozoic basement and the Mesozoic volcano-sedimentary rocks are intruded by three north south-oriented Mesozoic plutonic belts with ages ranging from the Middle Triassic to Jurassic, the Early to Middle Cretaceous and the Late Cretaceous to Paleocene (Fig. 3 a and b). Near the coast and within the main valleys some of the Paleozoic and Mesozoic rocks are unconformably covered by subhorizontal Early Miocene to Pleistocene marine to continental deposits (Fig. 3a; Rivano and Sepúlveda, 1991; Emparán and Pineda, 2006; Pineda and Calderón, 2008; Arévalo et al., 2009).

In Chile and in Argentina the Frontal Cordillera corresponds to a morphostructural unit defined by the presence of uplifted blocks of Paleozoic basement (Fig. 3a and b). In the studied region the Frontal Cordillera is in turn divided in three north-south trending subunits: the western, central and eastern Frontal Cordilleras (Fig. 3b). The central Frontal Cordillera is predominantly formed by Carboniferous to Permian magmatic and minor metamorphic units (Mpodozis and Cornejo, 1988; Nasi et al., 1990; Pineda and Calderón, 2009; Bissig et al., 2001) (Fig. 3a and b). The western Frontal Cordillera corresponds to a stratified succession of Triassic to Late Cretaceous volcano-sedimentary rocks intruded by a Late Cretaceous to Paleocene belt of plutonic units (Fig. 3a and b). The stratified succession changes gradually from subvertical folded strata next to the Carboniferous to Permian core of the central Frontal Cordillera to subhorizontal strata away from it. (Fig. 3b). To the east, the eastern Frontal Cordillera is formed by a block of Permo-Triassic volcanic and intrusive rocks unconformably overlain by folded Triassic to Late Cretaceous volcano-sedimentary rocks and Late Oligocene to Early Miocene volcano-sedimentary rocks (Fig. 3a and b). The Oligocene to Early Miocene rocks are in turn unconformably covered by subhorizontal to slightly folded Middle Miocene volcano-sedimentary rocks (Fig. 3a). A NNE-SSW trending plutonic belt of Eocene age intrudes the western, central and eastern Frontal Cordilleras (Fig. 3a). South of 31° S, the Carboniferous to Permian core of the central Frontal Cordillera is no longer recognized (Fig. 3a).

South of 31.5ºS, the Frontal Cordillera is no longer recognized along the Chilean flank (Fig. 3a and b). Instead, the Principal Cordillera is defined by the presence of a core of Cenozoic volcano-sedimentary rocks flanked to the east and to the west by Mesozoic sedimentary successions (Fig. 3a and b). Close to 32°S the core is composed by folded Early Oligocene to Early Miocene volcano-sedimentary rocks (Mpodozis et al., 2009; Jara and Charrier, accepted) intruded by an Early Miocene north-to-south belt of intrusive rocks (Fig. 3a and b). To the west a block of folded Late Cretaceous volcano-sedimentary rocks intruded by Late Cretaceous to Paleocene magmatic rocks is exposed. Both the Early Oligocene to Early Miocene core and the Late Cretaceous block are covered by subhorizontal to slightly deformed Late Oligocene to Early Miocene volcano-sedimentary rocks (Fig. 3a and b, Jara and Charrier, accepted).

The Andean evolution in north-central Chile is characterized by the alternation between contractional and extensional periods (Charrier et al., 2007). Orogenic processes began by the Late Cretaceous with the tectonic inversion of (Late Triassic?) Jurassic to Early Cretaceous extensional back-arc basins developed along the present-day Coastal Cordillera and Frontal Cordillera (Emparán and Pineda, 2000; Arancibia, 2004; Emparán

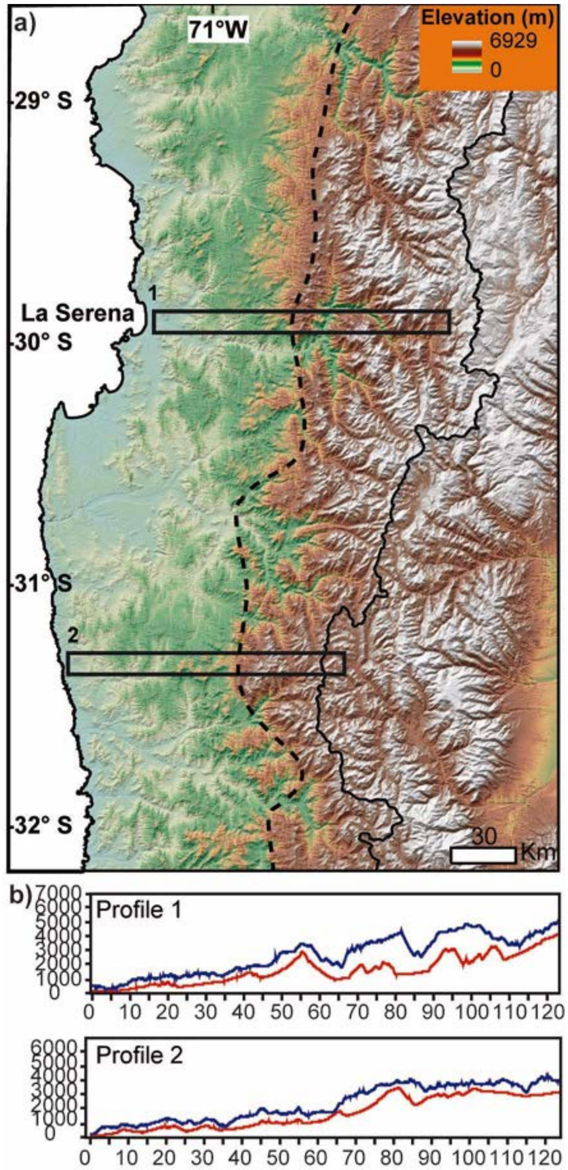

Fig. 2. a) Elevation map throughout north-central Chile based in the SRTM DEM. b) Maximum and minimum elevation profiles in a 5 km diameter swath across the Andean topographic front in north-central Chile.

and Pineda, 2006; Charrier et al., 2007). Contractional deformation started ~ 100 Ma, as evidenced by dating of mylonitic zones in faults along the coastal area (e.g. Arancibia, 2004) (Fig. 2). Renewal of extension occurred before ~ 90 Ma related to the development of continental back-arc basins along the present-day Coastal Cordillera and Frontal Cordillera (Pineda and Emparán, 2006; Charrier et al., 2007; Pineda and Calderón, 2008). These basins were inverted between the Late Cretaceous and the Early Paleocene (Pineda and Emparán, 2006; Charrier et al., 2007; Pineda and Calderón, 2008; Martínez et al., 2013), probably together with Jurassic to Early Cretaceous basins that were not inverted in the previous phase of deformation (Martínez et al., 2012). A new episode of contraction took place along the western Frontal Cordillera during the Middle Eocene to Early Oligocene in the area located northwards from 31°S (Cembrano et al., 2003; Pineda and Emparán, 2006; Pineda and Calderón, 2008; Salazar, 2012). During the same time period, an extensional volcano-sedimentary

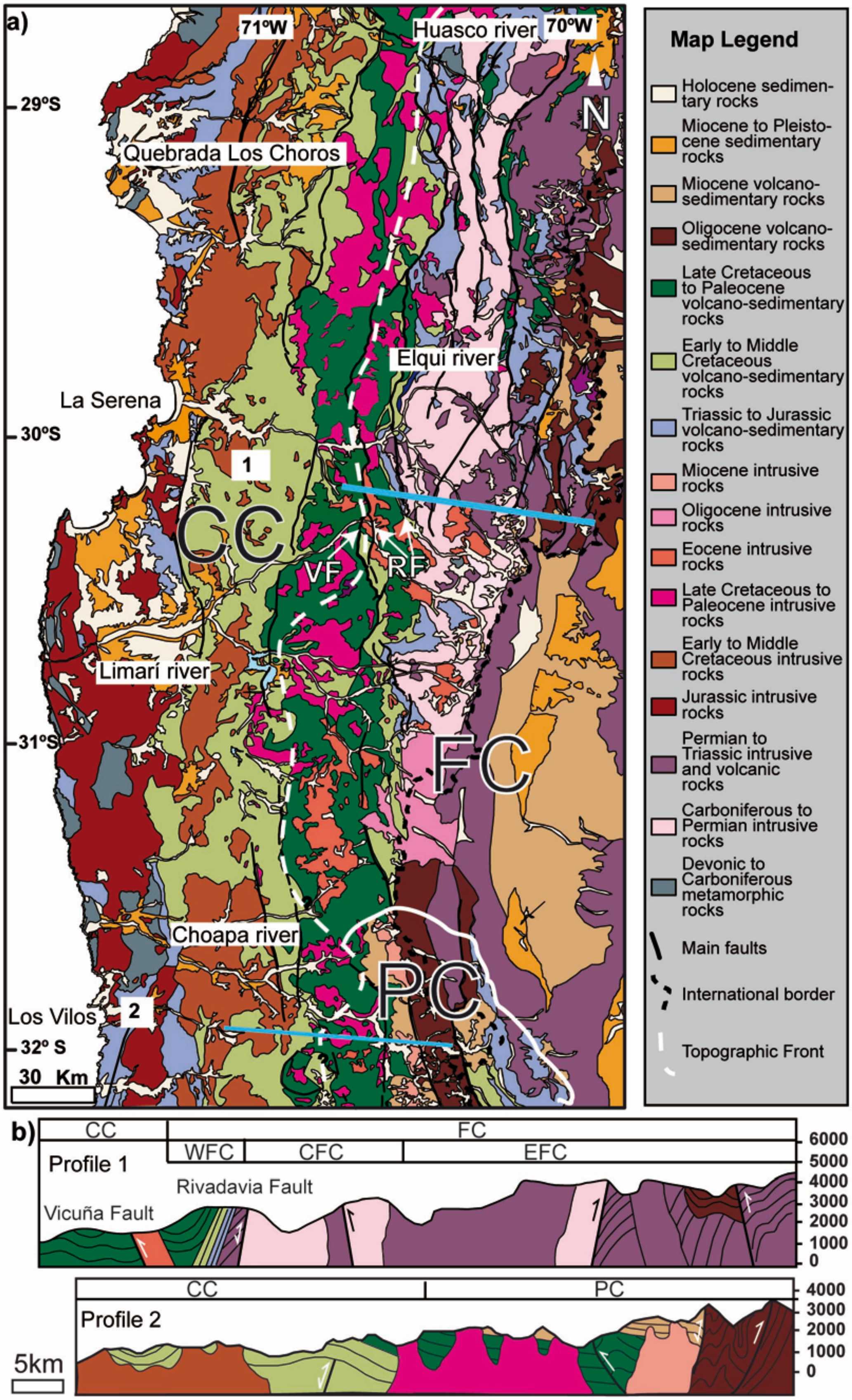

Fig. 3 a) Geological map of north-central Chile. Based in Sernageomin (2003). b) Simplified structural profiles across the Frontal Cordillera (profile 1) and the Principal Cordillera (profile 2). Trace of profiles in Fig.3a.. Modified from Mpodozis and Cornejo (1988) and Jara and Charrier (in press) basin, the Abanico Basin (Fig. 3), developed along the Principal Cordillera south of 32°S (Charrier et al., 2002; Jara and Charrier, accepted). New geochronological and structural data indicate that extensional conditions within the Frontal Cordillera to the north of 30°S would have started by the Late Oligocene, somewhat later than in the Principal Cordillera to the south of 32°S (Winocur et al., accepted). Late Oligocene extension focused within an intrarc basin developed along the eastern Frontal Cordillera (Fig. 3; Winocur et al., accepted). Tectonic inversion of the intra-arc basin started by the Early Miocene (Nasi et al., 1990; Bissig et al., 2001), roughly coinciding with the Late Oligocene to Early Miocene inversion of the Abanico basin to the south of 32°S (Charrier et al., 2002; Mpodozis et al., 2009; Jara and Charrier, accepted). Finally, according to structural and geomorphic analysis of paleosurfaces along the eastern Frontal Cordillera, contractional deformation and uplift related to the progressive inversion of the intra-arc basin also occurred during the Middle Miocene around 16-14 Ma (Bissig et al., 2002, Winocur, 2010) and during the Late Miocene after ~ 12-11 Ma (Bissig et al., 2002; Winocur, 2010) and around 6 Ma (Bissig et al., 2002).

3. Sampling strategy

Most samples collected correspond to granitoids excepting samples JA05 and JA07 which are gneisses (Table 1). Samples were collected from four different areas (Fig. 4) including three west to east transects across the topographic front. The Huasco-Choros transect is located in the northern part of the study region, whereas the northern Choapa and southern Choapa transects are located in the southern part of the studied region (Fig. 4). The idea underlying this sampling strategy was to identify eventual differences in exhumation timing between these two regions, as suggested by the absence of Carboniferous to Permian basement (central Frontal Cordillera) south of 31°S (Fig. 4). Samples from the Coastal Cordillera within the northern Choapa transect were collected from a near vertical profile in order to recognize elevation-related differences in thermochronological ages. The rest of the Coastal Cordillera samples were collected at the bottom or near the bottom (< 500 m) of their respective valleys. Besides the samples from the Coastal Cordillera, throughout the Huasco-Choros transect samples from the central Frontal Cordillera were collected at the bottom of the Huasco valley. The Elqui transect only includes samples collected at the bottom of the Elqui river Valley where the river is draining the central and eastern Frontal Cordillera (Fig. 4). Samples from the western Frontal Cordillera in the Elqui transect were collected, but no apatites were recovered. Throughout the Limarí river basin several samples were collected within the western and central Frontal Cordillera at the bottom or near the bottom (< 500 m) of the respective valleys. However, we only recovered apatites on samples collected from the western Frontal Cordillera (Fig. 4). Samples from the northern Choapa transect were collected at different elevations relative to the valley's thalwegs within the western Frontal Cordillera. Finally, samples from the southern Choapa transect were collected from the Principal Cordillera only at the bottom of the valley.

Table 1. U Pb, AFT and AHe data for the analyzed samples

Sample	Raw AHe Age ± 2σ (Ma)	FTs mean (dmnls)	AHe Age ± 2σ(Ma)	AFT Age ± 2σ (Ma)	Mean length ± 2σ / Nº tlm (μm ± 2σ) / Nº tlm	Dpar ± 2σ (μm)	%Cl ± 2σ (%Ox)	Tc range Dpar (ºC)	Tc range %Cl (ºC)	U-Pb Age ± 2σ or geochronologic ages from other studies (Ma)
Huasco-Choros Transect										
Coastal Cordillera										
G-2	-	-	-	49.8 ± 3.3	14.21 ± 1.7/ 200	2.53 ± 0.32	-			76 ± 2 K-Ar Bt (Arévalo et al., 2009)
G-3	-	-	-	***51.2 ± 3.3***	13.57 ± 2.11/ 201	2.17 ± 0.27	-			95 ± 2 K-Ar Bt (Arévalo et al., 2009)
G-4	-	-	-	65.9 ± 2.7	14.22 ± 1.55/ 204	1.88 ± 0.14	-			114.5 ± 1.2 Ma 40Ar-39Ar Amp (Arévalo et al., 2009)
Frontal Cordillera										
JA-05	-	-	-	***19.6 ± 0.7***	13.79 ± 1.52/ 203	**1.68 ± 0.21**	-			~307 Ma U-Pb zr (Álvarez et al., 2013a)
JA-07	-	-	-	20.3 ± 1.2	14.12 ± 1.38/162	**1.61 ± 0.19**	-			~485 U-Pb zr (Álvarez et al., 2013b)
Elqui transect										
Frontal Cordillera										
LE06	-	-	-	***36 ± 3.0***	13.28 ± 1.84/ 153	2.12 ± 0.16	0.03 ± 0.01	112-107	105-105	~ 242 Ma U-Pb zr (Martin et al., 1999)
LE04	-	-	-	27.1 ± 4.2	12.97 ± 1.86/ 135	**1.63 ± 0.16**	0.04 ± 0.12	104-101	107-104	285.7 ± 1.5 Ma U-Pb zr (Pankurst et al. 1996)
LE03	7.1 ± 0.9	0,70	10.0 ± 1.2	36 ± 6.2	13.88 ± 1.76/ 210	2.03 ± 0.16	0.35 ± 0.15	110-106	112-107	~221 K-Ar Bt (Nasi et al., 1990)
LE02	8.2 ± 3.9	0,68	12.0 ± 5.4	***22 ± 2.8***	14.1 ± 1.7/ 132	**1.92 ± 0.13**	0.28 ± 0.05	108-104	109-108	266 ± 7 Ma K-Ar Amp (Nasi et al 1990)
Limarí Valley										
LL08	11 ± 1.8	0,68	16 ± 2.1	31.3 ± 3.0	15 ± 1.44/ 210	2.86 ± 0.17	1.7 ± 0.24	122-118	132-125	42.6 ± 1 (this work)
LL07	16 ± 2.3	0,74	21.4 ± 2.5	31.5 ± 3.6	14.09 ± 1.53/ 179	**1.75 ± 0.26**	0.25 ± 0.03	108-101	109-108	~67 K-Ar Bt (Pineda and Calderón, 2008)
LL06	14.2 ± 2.6	0,74	19 ± 3.4	***32 ± 3.2***	13.86 ± 1.3/ 210	**1.73 ± 0.11**	*0.33 ± 0.08*	105-102	111-108	
LL01	13.4 ± 1.1	0,74	18.1 ± 1.2	**36.6 ± 3.6**	14.92 ± 1.45/ 210	2.51 ± 0.18	0.86 ± 0.17	117-112	119-114	
LL02	12.9 ± 1.9	0,73	17.6 ± 2.7	***39.2 ± 4.6***	14.69 ± 1.25/ 210	2.4 ± 0.15	0.76 ± 0.23	116-111	119-112	39.3 ± 1 (this work)
Northern Choapa Transect										
Frontal Cordillera										
LC05	11.2 ± 2	0,70	16 ± 3.2	***30 ± 3.2***	14.96 ± 1.39/ 210	2.39 ± 0.19	-	-	-	
LC07	12.2 ± 0.5	0,78	15.5 ± 0.8	***36.6 ± 5.2***	14.8 ± 1.49/ 190	2.4 ± 0.16	1.12 ± 1.12	116-111	123-118	46.6 ± 0.6 (this work)
LC17	7.1 ± 0.7	0,71	10 ± 1.4	40.6 ± 21.2	14.5 ± 1.9/ 15	2.32 ± 0.38	0.89 ± 0.52	118-107	125-110	
LC16	12.9 ± 2.2	0,75	17.4 ± 3.9	21.6 ± 2.8	14.5 ± 1.45/ 90	**1.61 ± 0.14**	-	-	-	
LC18	9.1 ± 3.1	0,73	12.5 ± 4.5	41.7 ± 5.0	14.87 ± 1.51/ 210	2.59 ± 0.17	1.44 ± 0.09	119-113	126-124	

LC08	8.4 ± 0.9	0,71	11.8 ± 0.8	35 ± 3.8	14.58 ± 1.39/ 210	2.62 ± 0.18	1.46 ± 0.09	119-114	126-124	
Coastal Cordillera										
LC01	23.9 ± 2.5	0,78	30.5 ± 3.8	55 ± 4.8	14.46 ± 1.53/ 210	2.01 ± 0.15	-	-	-	
LC02	25.8 ± 1.7	0,82	31.5 ± 1.6	54.1 ± 2.9	14.68 ± 1.4/ 210	2.82 ± 0.2	2.26 ± 0.21	122-117	140-133	118.8 ± 0.8 (this work)
LC03	17.2 ± 5.2	0,72	23.5 ± 6.5	***68.3 ± 7.6***	14.55 ± 1.43/ 210	2.25 ± 0.17	-	-	-	
LC04	21.9 ± 2.9	0,76	28.5 ± 4	60.1 ± 7	14.68 ± 1.34/ 156	2.31 ± 0.28	1.0 ± 0.26	116-108	122-115	
Southern Choapa Transect										
Coastal Cordillera										
LC09	-	-	-	***41.4 ± 4.4***	13.88 ± 1.9/ 184	**1.67 ± 0.11**	0.36 ± 0.15	104-101	112-107	75.8 ± 7.1 (this work)
Principal Cordillera										
LC11	4.9 ± 2.5	0,89	5.6 ± 2.8	16 ± 3.4	14.57 ± 1.5/ 125	2.23 ± 0.15	0.95 ± 0.42	113-109	124-112	61.6 ± 0.7 (this work)
LC15	7.5 ± 1.8	0,71	10.5 ± 2.2	***43.7 ± 5.0***	14.59 ± 2.17/ 210	2.96 ± 0.33	0.86 ± 0.82	126-117	128-105	

*AFT ages in bold italic do not pass the Chi-squared test, AFT samples in bold show Dpar values < 2µm .

4. Methodology

Low temperature thermochronology is based on the accumulation of the radioactive decay products of certain isotopes and the temperature-dependent retention of these products. In particular, the Apatite Fission Track (AFT) and the U-Th/He in apatite (AHe) methods used here are based on the accumulation of tracks caused by fission decay of ^{238}U; and on the ingrowth of ^{4}He produced by the U and Th series decay, respectively. Fission tracks in apatite are only partially retained and shorten between ~60-120°C; whereas ^{4}He is partially retained between ~40 and 80°C. The fact that tracks shorten (anneal) in a certain temperature range allow us to obtain important information about cooling paths, as rapidly cooled rocks would present mostly large tracks > 14 µm, contrary to slowly cooled rocks that would present shortened tracks < 14 µm (Green al., 1986). Importantly, it is widely known that apatites can present different annealing behaviors that are usually linked to compositional variations, with chlorine-rich apatites presenting more resistence to anneal than fluorine-rich apatites (e.g. Green et al., 1986). Therefore, the temperature in which AFT age is registered and the temperature range in which tracks anneal varies from chlorine-rich to fluorine-rich apatites. This has important implications in AFT data interpretations when both types of apatites are found within a single sample (e.g. Barnes et al., 2006). Variations in apatite annealing behavior are generally determined by measuring apatite solubility using the diameter of the etch figure (Dpar) (Donelick 1993), as it is thought that this method would provide the same predictivity capability as chlorine content (Ketcham et al., 1999).

Whole rock samples were mechanically crushed and sieved and heavy minerals were recovered using conventional heavy liquid and magnetic methods at the Laboratorio de Separación de Minerales at the Departamento de Geología, Universidad de Chile. U-Pb zircon dating was carried out by Apatite to Zircon Inc. using the LA-ICP-MS from the Geoanalytical Laboratory at Washington State University, following the procedure described in Chang et al. (2006). The AFT data was obtained at Apatite to Zircon Inc. using the laser ablation method (Donelick et al., 2005). Sample preparation for AFT analysis involves mounting of apatite grains in epoxy, polishing and etching in 5.5N HNO_3 for 20.0 s at 21 °C to reveal spontaneous fission tracks. Spontaneous fission tracks were counted in unpolarized light at 2000x magnification and LA-ICP-MS analysis to determine the ^{238}U were later made at the same grain areas where spontaneous tracks were counted. In order to increase the number of tracks available for length measurement, apatite grains were irradiated with ^{252}Cf (Donelick and Miller, 1991) and etched a second time following the protocol described above. The track lengths and the angle between the track and the c-axis were then measured. Additionally, for each grain age and track length measurement a Dpar value was obtained. AHe age determinations were made in the Caltech Noble Gas Lab. Individual apatite grains > 100 µm were screened for U-rich inclusions under a binocular microscope in polarized light at 120x magnification. Three to four single-grain analyses were used to calculate mean ages (see supplementary data). Euhedral to subhedral inclusion-free grains were then hand-picked and their dimensions (length and width) measured to calculate the FT factor, a correction made to AHe ages to account for the effect of α-particles that are eventually ejected out of the grain (Farley and Stockli, 2002). Single apatite grains were later placed in platinum foil tubes and heated in-vacuum with a laser to degas and measure

He by mass-spectrometry. After He analysis, apatite grains within platinum tubes were removed from the vacuum chamber, dissolved in acid and spiked for U-Th determinations to finally be analyzed by ICP-MS.

5. Results

6.1 Rock ages

Six new U-Pb zircon ages were obtained for samples collected from the Limarí Valley and the northern Choapa and southern Choapa transects (Fig. 4 and Table 1). Within the mentioned areas previous geochronological ages in the sampled rock units where our samples were collected are scarce and it was necessary to increase such information for our purposes. In particular, we collected several samples for geochronological determinations from the Eocene Fredes unit originally defined by Rivano and Sepúlveda (1991). For samples LC05, LC07, LC08, LC16, LC17 and LC18, collected from the Fredes unit in the northern Choapa transect, the U-Pb zircon age of 46.6 ± 0.6 Ma for LC07 is considered representative (Fig. 4). Similarly, for samples LL01 and LL02 collected from the Fredes unit within the Limarí Valley (Rivano and Sepúlveda, 1991) an age of 39.3 ± 1 Ma (LL02) was obtained. On the contrary, for sample LC11 previously assigned to the Fredes unit in the southern Choapa transect, a Late Cretaceous age of 61.6 ± 0.7 Ma was measured (Fig. 4). For samples LC01 to LC04 collected within a nearly vertical profile from the Early Cretaceous Illapel Plutonic Complex (Rivano and Sepúlveda, 1991; Parada et al., 1999), the U-Pb zircon age of 118.8 ± 0.8 Ma for LC02 is considered representative (Fig. 4). Within the southern Choapa transect, a Late Cretaceous U-Pb zircon age of 75.8 ± 7 Ma was obtained for sample LC09 collected from rocks previously assigned to the Early Cretaceous Illapel Plutonic Complex (Fig. 4). Finally, within the Limarí Valley an age of 42.6 ± 1 Ma was obtained for sample LL08 collected from the El Bosque unit (Pineda and Emparán, 2006). For the rest of the sampled units that were not dated in this work, previous U-Pb zircon ages (Álvarez et al., 2013a and b) and K-Ar and $^{40}Ar/^{39}Ar$ biotite and amphibole ages (Nasi et al., 1990; Rivano and Sepúlveda, 1991; Pankhurst et al., 1996; Martin et al., 1999; Arévalo et al., 2009) are herein considered as crystallization ages (Fig. 4 and Table 1). As a summary, considering the new U-Pb data given here and the geochronological constraints from previous works, the samples collected for thermochronologic analysis range from the Early to the Late Cretaceous throughout the Coastal Cordillera (Fig. 4), whereas samples from the Frontal Cordillera are Early Ordovician to Late Triassic in the Huasco-Choros and Elqui transects, latest Cretaceous to Eocene in the Limarí valley, Eocene in the northern Choapa transect and Paleocene in the southern Choapa transect (Fig. 4).

6.2. Thermochronology

AHe and AFT data are summarized in Table 1. All errors are displayed as ±2σ. A total of eighteen new AHe ages and twenty-eight new AFT ages are presented (Table 1).

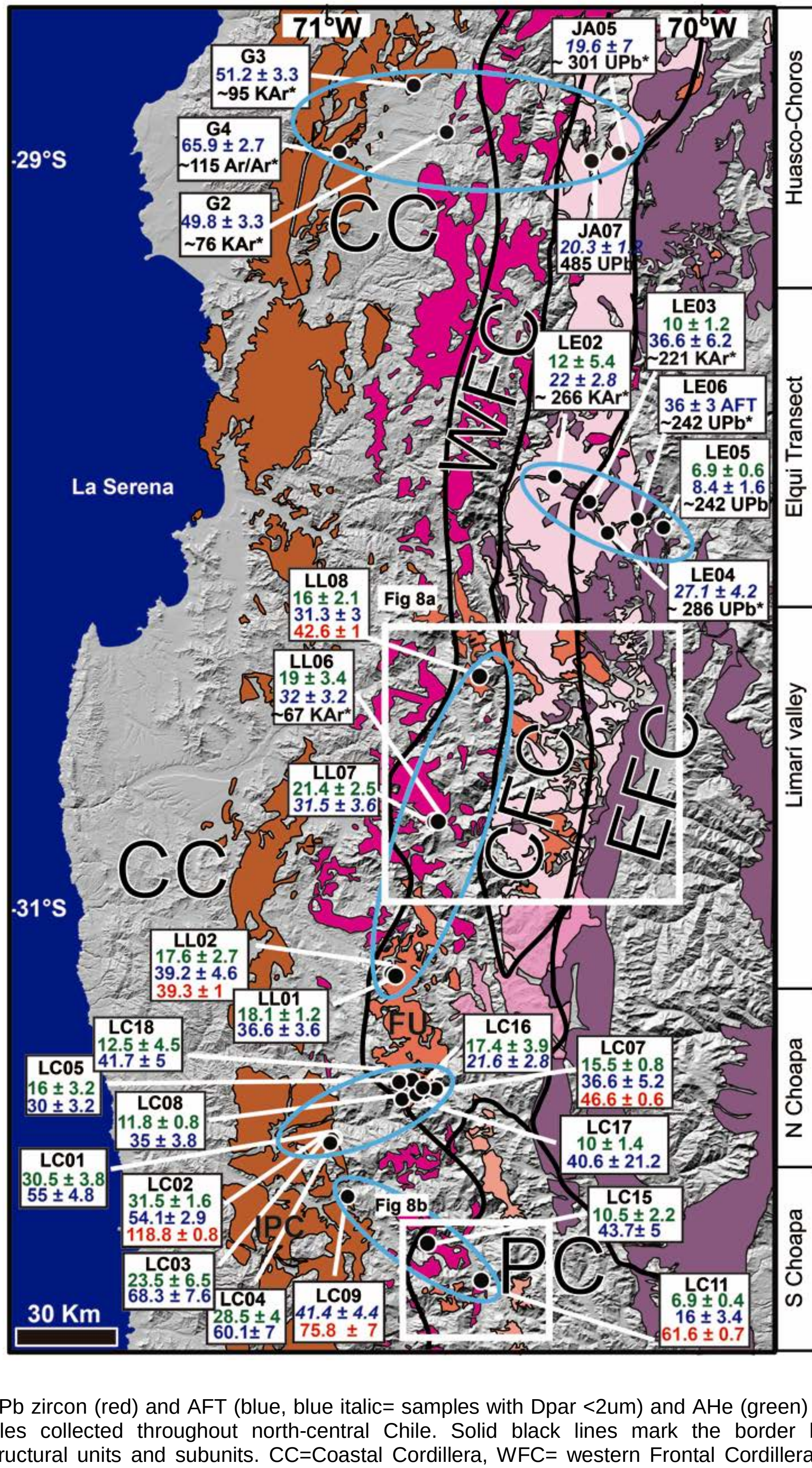

Fig. 4. U-Pb zircon (red) and AFT (blue, blue italic= samples with Dpar <2um) and AHe (green) ages obtained for samples collected throughout north-central Chile. Solid black lines mark the border between main morphostructural units and subunits. CC=Coastal Cordillera, WFC= western Frontal Cordillera, CFC=central Frontal Cordillera, EFC= eastern Frontal Cordillera, PC= Principal Cordillera. Pale blue ovals enclosed samples collected from different transects and areas. Map legend from Fig.3. IPC= Illapel Plutonic Complex, FU= Fredes Unit. Rock ages from previous works referenced in the text are in black and marked with an asterisk.

6.2.1 AFT ages

6.2.1.1 Coastal Cordillera

Within the Huasco-Choros transect AFT ages decrease from west to east between 65.9 ± 2.7 and 49.8 ± 3.3 (Fig. 5a, Table 1), with Mean Track Length (MTL) ranging from 14.22 ± 1.55 to 13.57 ± 2.11 µm. Similarly, in the northern and southern Choapa transects AFT ages are between 68.3 ± 7.6 and 41.4 ± 4.4 (Fig. 4); with MTL ranging from 14.68 ± 1.34 to 13.88 ± 1.9 µm (Table 1). Throughout the northern Choapa transect AFT ages of samples collected in a nearly vertical profile within the Early Cretaceous Illapel Plutonic Complex (LC01, LC02, LC03 and LC04) are the same within error (Fig. 5a). Dpar values from apatites collected from all transects within the Coastal Cordillera are generally high, ranging between 2.82 ± 0.2 and 1.88 ± 0.14 µm (Fig. 6), indicating that they probably correspond to high-T-annealing apatites (Donelick et al., 2005). Only one low Dpar value of 1.67 ± 0.11 µm (LC09, Fig. 6), most representative of a low-T-annealing apatite (Donelick et al., 2005), is observed among samples from the Coastal Cordillera. Importantly, sample LC09 presents the youngest AFT age among all Coastal Cordillera's samples (Fig. 6).

6.2.1.2 Frontal Cordillera

AFT ages obtained from the central Frontal Cordillera within the Huasco-Choros transect are 20.3 ± 1.2 Ma (JA07) and 19.6 ± 0.7 Ma (JA05) (Table 1 and Fig.4) with MTL of 14.12 ± 1.38 and 13.79 ± 1.52 µm (Table 1). Dpar values of JA07 and JA05 are 1.61 ± 0.19 and 1.68 ± 0.21 µm, respectively. Therefore, dated apatites from both samples are formed by low-T-annealing apatites (Donelick et al., 2005).

In the Elqui transect sample LE02 collected from the central Frontal Cordillera present an AFT age of 22 ± 2.8 with MTL of 14.10 ± 1.7 µm (Table 1, Fig. 4). AFT ages for samples LE03, LE04 and LE06 collected in the eastern Frontal Cordillera are the same within error; corresponding to 36 ± 6.2, 27.2 ± 4.2 and 36 ± 3 Ma (Table 1 and Fig. 4); respectively; with MTL ranging between 13.88 ± 1.76 and 12.94 ± 1.86 µm (Table 1). The easternmost and youngest sample collected from the eastern Frontal Cordillera throughout the Elqui transect presents an AFT age of 8.36 ± 0.81 Ma (Table 1, Fig. 5a) and MTL of 14.10 ± 1.48 µm (Table 1). In general, within the central and eastern Frontal Cordillera in the Elqui transect samples with Dpar values < 2 µm present the youngest AFT ages (LE04, LE02 and LE05); whereas samples with Dpar values > 2 µm present the oldest AFT ages (LE03 and LE06) (Fig. 4).

For the western Frontal Cordillera in the Limarí Valley AFT ages range between 39.2 ± 4.6 and 31.3 ± 3.0 Ma, with MTL between 15.00 ± 1.44 and 13.86 ± 1.30 µm and Dpar values between 2.86 ± 0.17 and 1.73 ± 0.11 µm representative of both high-T and low-T-annealing apatites (Table 1, Fig. 4). In the western Frontal Cordillera of the northern

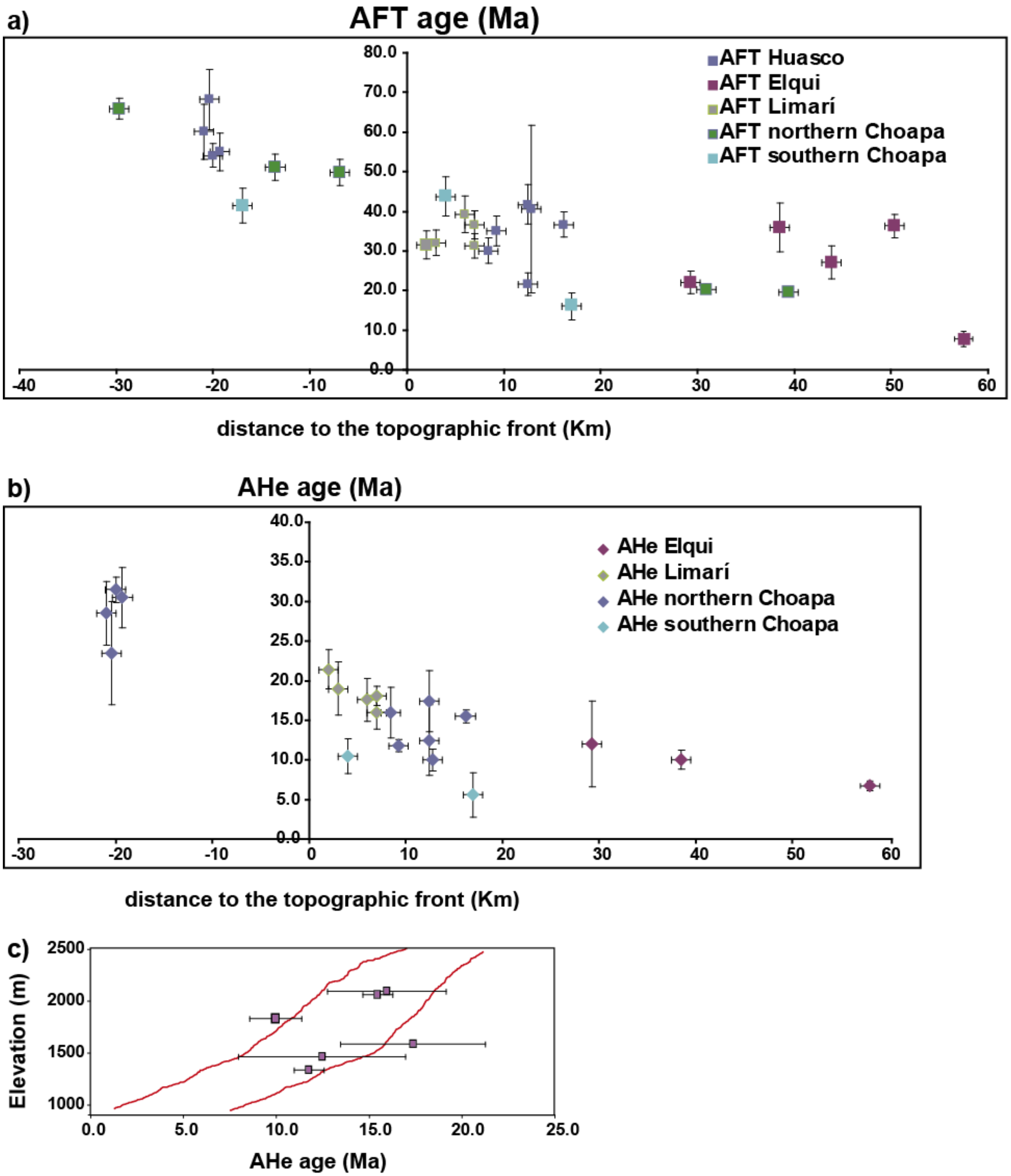

Fig. 5. a) AFT ages versus distance to the topographic front. b) AHe ages versus distance to the topographic front. c) Elevation of samples versus AHe ages plot above the thalwegs (red lines) of the respective tributaries where they were collected in the northern Choapa transect. Errors are 2σ± in all figures.

Choapa transect AFT ages are generally the same within error ranging between 41.7 ± 5 and 30 ± 3.2 Ma, except for sample LC16 that has a much younger age of 21.6 ± 2.8 Ma (Table 1, Fig. 4a). MTL for samples within the northern Choapa transect are between 14.96 ± 1.39 and 14.5 ± 1.9 µm; whereas Dpar values are generally between 2.62 ± 0.18 and 2.32 ± 0.38 µm and representative of high-T-annealing apatites (Donelick et al., 2005) (Table 1). The only exception corresponds to LC16, the youngest AFT age within the Frontal Cordillera in this transect, which presents a Dpar value of 1.61 ± 0.14 µm (Fig. 4) representative of low-T-annealing apatites (Donelick et al., 2005).

Finally, south of 31.5°, where the central Frontal Cordillera is no longer developed, the two AFT ages obtained in the Principal Cordillera of the southern Choapa transect (Fig. 4) are 43.7 ± 5.0 and 16.0 ± 3.4 Ma, with MTL of 14.59 ± 2.17 and 14.57 ± 1.5 µm, respectively and Dpar values representative of high-T-annealing apatites (Donelick et al., 2005).

Summarizing, samples from the Coastal Cordillera have AFT ages comprised between ~ 65 and 45 Ma (Fig. 4 and 5a; Table1). Most of these samples present generally long tracks >14 µm, except G3 and LC09 (Table 1). With the exception of LC09, Dpar values are indicative of high-T-annealing apatites (Fig. 4 and 6). AFT ages from the western Frontal Cordillera are mostly comprised between ~ 40 and 30 Ma and concentrate around ~ 20 Ma in the central Frontal Cordillera, they range mostly from ~ 36 to 27 Ma in the eastern Frontal Cordillera and from ~ 43 to 16 Ma in the Principal Cordillera further south (Fig. 4). There are two important exceptions in this age distribution. Sample LC16 collected from the western Frontal Cordillera in the northern Choapa transect presents an AFT age ~ 21 Ma, whereas sample LE05 from the eastern Frontal Cordillera in the Elqui transect presents an AFT age of ~ 8 Ma, the youngest age within the dataset (Fig. 4 and 5a). In general, MTLs of are both > 14 µm and < 14 µm are observed along the western, central and eastern Frontal Cordillera. Similarly, Dpar values along the Frontal Cordillera are representative of both fast- and slow-annealing apatites.

6.2.1.3. Possible compositional effects

From the information given above, it seems probable that Dpar values could be indicating variable annealing kinetics controlling AFT age as samples from the Frontal Cordillera with Dpar < 2 µm tend to present younger AFT ages, whereas samples with Dpar > 2 µm present older AFT ages (Table 1). Effectively, Figure 6 shows that a positive correlation between Dpar values and AFT age exists in samples from both the Coastal and the Frontal Cordilleras. Considering that chlorine content and Dpar value are positively correlated (Carlson et al., 1999; Barbarand et al., 2003), these features suggest that compositional effects might affect our AFT ages. In order to corroborate this hypothesis, microprobe analysis was carried out on 19 samples from the Coastal Cordillera and the Frontal Cordillera, with at least 30 analyses per sample in grains parallel to the **c**-axis (Table 1). Unfortunately, it was not possible to analyze chlorine content in exactly the same grains where AFT measurements were performed as those analyses were made afterward at the University of Toulouse. Effectively, most apatites presenting high Dpar values are chlorine-rich (> 1% within error), reaching chlorine contents as high as 2.3% (LC02, Table 1). Closure temperatures corresponding to the measured chlorine contents were calculated using HeFTy (Ketcham, 2005) assuming a cooling rate of 10ºC/ Ma. The closure temperatures obtained are as high as 137º C (LC02, Table 1), much higher than the nominal closure temperature of ~100º C usually

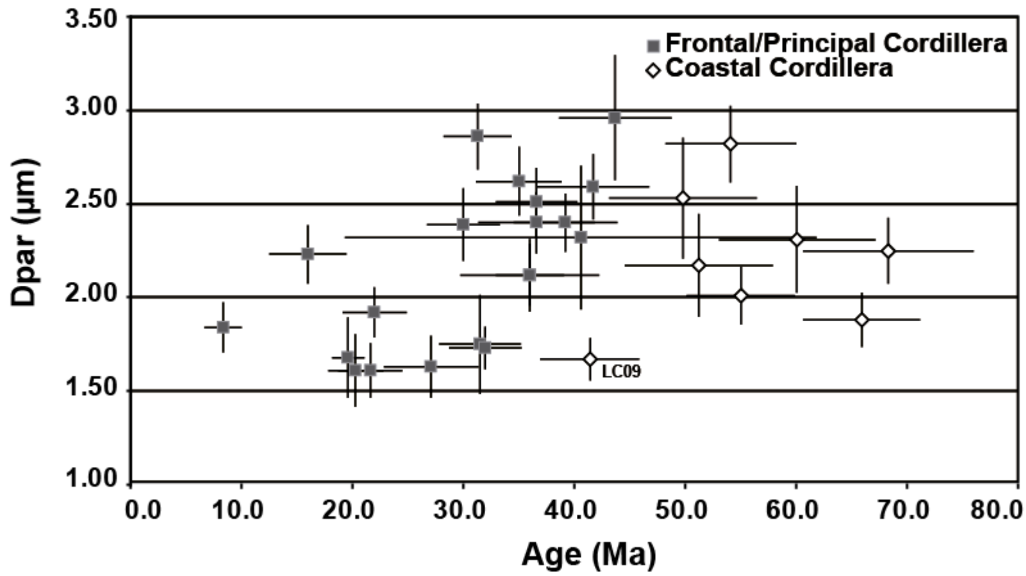

Fig. 6. Dpar versus AFT ages of samples collected throughout the Coastal and Frontal Cordillera.

considered for the AFT system. When comparing the closure temperatures predicted by the chlorine content with the ones predicted by the Dpar values in the same sample, differences as high as 18º C are observed (LC02, Table 1). Although on a few samples no important differences are observed (e.g. LC15, Table 1), the positive correlation between Dpar and AFT ages anyway suggests that differences in the thermal sensitivity of apatites are influencing these ages. Therefore, the possibility exists that some other compositional factors might control AFT ages. As will be explained later, the divergences in predicted closure temperature for the AFT system between the Dpar and % Cl kinetic parameters may be critical when attempting to explain AFT and AHe data simultaneously.

6.2.2. AHe ages

Four AHe ages from the Coastal Cordillera were obtained for the Early Cretaceous Illapel Plutonic Complex within the northern Choapa transect (Fig. 4). They range between 31.5 ± 1.6 and 23.5 ± 6.5 Ma, corresponding to the same age within error (Fig. 5b).

For the western Frontal Cordillera AHe ages vary between 21.4 ± 2.5 and 16 ± 2 in the Limarí valley, whereas AHe ages of samples collected from different elevations within the northern Choapa transect are somewhat younger and fall between 17.4 ± 3.9 and 10 ± 1.4 (Table 1, Fig. 4 and 5b).

In the Elqui transect, one AHe age of 12.0 ± 5.4 was obtained for sample LE02 of the central Frontal Cordillera, whereas samples from the eastern Frontal Cordillera present AHe ages of 10 ± 1.2 Ma and 6.9 ± 0.6 Ma from west to east (Fig. 4).

Finally, samples collected from the Principal Cordillera in the southern Choapa transect present AHe ages of 10.5 ± 2.2 and 5.6 ± 2.8 Ma from west to east.

As shown in Fig. 5b, within the Elqui transect and the southern Choapa transect, where samples from the central and eastern Frontal Cordillera and the Principal Cordillera were collected at the bottom of their respective valleys, the AHe ages are younger to the east. Within the northern Choapa transect samples, collected near the bottom of the two main tributaries valleys draining the western Frontal Cordillera have AHe ages between 10 ± 1.4 and 12.5 ± 4.5 Ma, whereas samples at the highest elevations within the valley present older ages ranging from 16 ± 2.3 to 15.5 ± 0.8 Ma (Fig. 5c).

Summarizing, AHe ages from the western Frontal Cordillera are between 20 and 16 Ma within the Limarí Valley and they range between ~17 and 10 Ma at different elevations within the northern Choapa transect, with younger ages at the bottom of the valleys. AHe ages at the bottom of the valleys in the central and eastern Frontal Cordillera range from ~ 12 to 6 Ma and from ~10 to 5 Ma in the Principal Cordillera from the Elqui and southern Choapa transects, respectively (Fig. 4).

6. Thermal modeling interpretation

We use the HeFTy program of Ketcham (2005) for thermal modeling of thermochronological data. No possible thermal histories for AHe and AFT data are found using Dpar as the kinetic parameter in samples LC01 to LC04 from the Early Cretaceous Illapel Plutonic Complex of the Coastal Cordillera (Fig. 4). Although Dpar values of these samples are higher than 2 µm (Fig. 4, Table 1), they are not high enough to predict thermal histories that also encompass the associated AHe data, because of the large difference between AFT and AHe ages and the generally long tracks > 14 µm observed. Since our measured chlorine contents generally imply closure temperatures that are higher than the ones predicted by the Dpar values, use of Cl as the kinetic variable may be more compatible with the large AFT- AHe age differences and the long tracks. However, because chlorine analyses were not performed exactly in the same grains on which fission tracks were counted and measured, an additionally layer of uncertainty is added by using this kinetic parameter for thermochronological modeling. Despite this limitation, some models were ran for sample LC02 using chlorine content as kinetic parameter to corroborate that Dpar may be incorrectly estimating the thermal sensitivity of these apatites. Inversions that could simultaneously encompass both AHe and AFT data were obtained for LC02, suggesting that Dpar could be failing to predict the thermal behavior of the chlorine-rich apatites in this sample (Fig. 7). These models suggest that rocks from the Early Cretaceous Illapel Plutonic Complex within the Coastal Cordillera suffered accelerated cooling ~ 65 - 50 Ma and finally cooled gradually since ~ 45 Ma (Fig. 7).

In the case of samples from the Frontal Cordillera, simultaneous thermal models encompassing AFT and AHe data are actually possible for samples with Dpar values < 2 µm which pass the chi-squared test. This is in good agreement with the fact that apatites with Dpar < 2 µm are considered fluorine-rich apatites, and no unusual compositional effects on AFT ages are expected (Ketcham et al., 1999). Therefore, in the following section thermal models are presented only for samples with Dpar values < 2 µm.

6.1. Western Frontal Cordillera

Sample LL07 was collected from granitic rocks assigned to the Late Cretaceous to Paleocene intrusive belt in the Limarí Valley (Pineda and Calderón, 2008). A K-Ar biotite age of ~ 67 Ma was obtained a few kilometers to the west of the sampling site (Pineda and Calderón, 2008). However, several Eocene stocks intrude the Late Cretaceous to Paleocene belt in this area (Fig. 4). Therefore, as sample LL07 may present an Eocene geochronological age, we prefer not to use the mentioned K-Ar age as a constrain for thermal modeling. Thus, the only constrain used to model sample LL07 is a present-day temperature 20 ± 10°C (Fig. 7). 179 Dpar values were measured on individual apatites grains from sample LL07. Most Dpar values are < 2 µm (176) with only three measurements > 2 µm. These three grains presenting Dpar values > 2 µm were excluded from the modeling as no thermal modeling solutions were found when they were considered (Fig. 7). Thermal modeling of AFT and AHe data from sample LL07 indicates these rocks from the western Frontal Cordillera in the Limarí Valley north of 31°S were continuously cooled starting before ~ 30 and ending shortly after 20 Ma (Fig. 7).

Sample LC16 collected from the Eocene Fredes unit along the northern Choapa transect was also modeled considering and a present-day temperature of 20 ± 10°C (Fig. 7). Thermal modeling of AFT and AHe data from sample LC16 is consistent with accelerated cooling from ~ 22 to 16 Ma throughout the western Frontal Cordillera along the northern Choapa transect south of 31°S (Fig. 7).

6.2. Central Frontal Cordillera

Sample JA07 was collected along the Huasco-Choros transect from rocks with a U-Pb age of ~ 485 Ma that is much older than its AFT age of ~ 20 Ma (Table 1). The available geological information is insufficient to constrain the thermal history of this sample before it acquired its AFT age. Therefore, the only constrain used to model sample JA07 is a present-day temperature of 20 ± 10°C (Fig. 7). Thermal modeling of sample JA07 is consistent with a thermal history in which rocks from the central Frontal Cordillera in the Huasco-Choros transect experienced accelerated cooling by ~ 22-18 Ma.

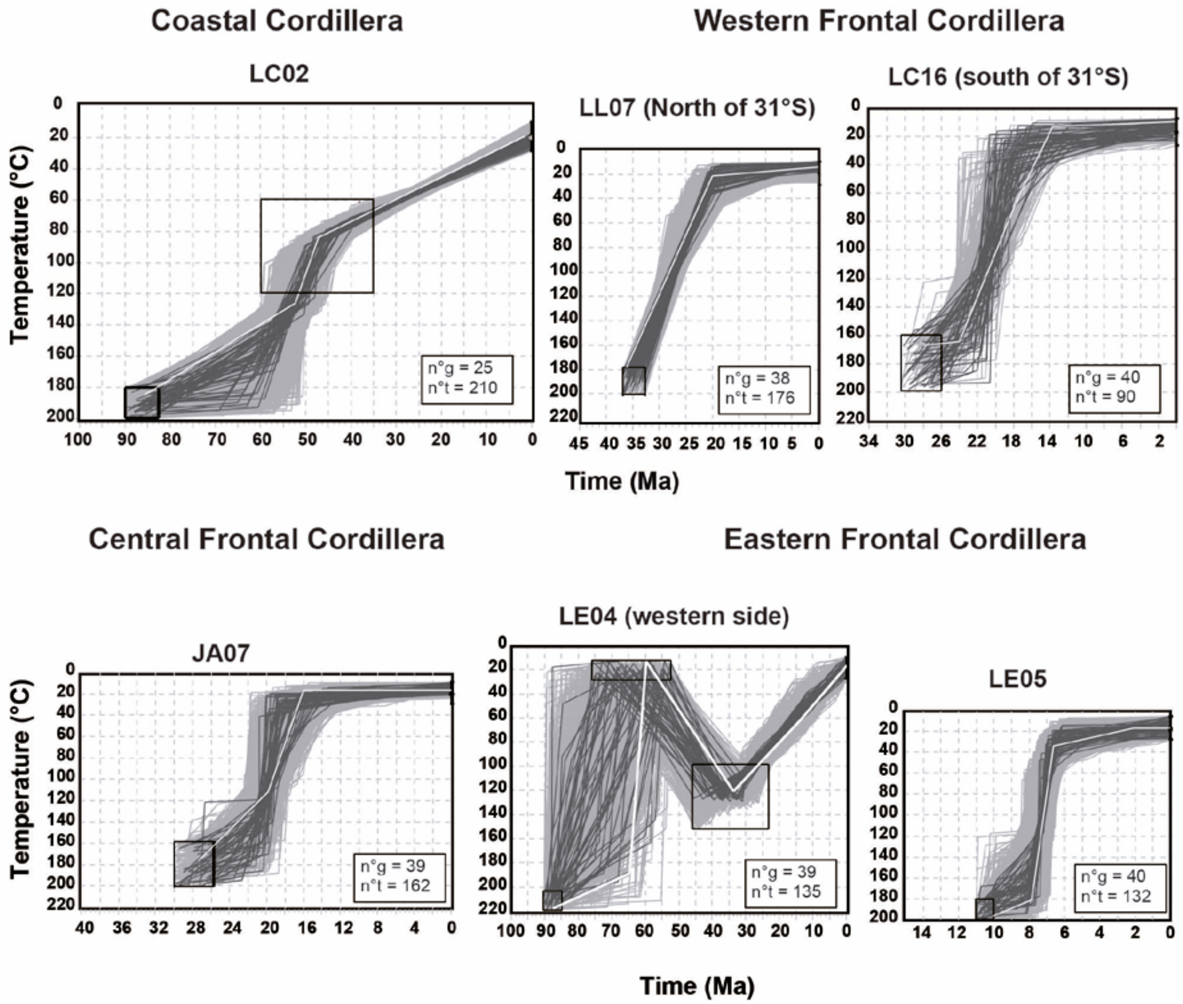

Fig. 7. Thermal models of thermochronological data obtained for samples LC02 from the Coastal Cordillera, samples LL07 and LC16 from the western Frontal Cordillera, sample JA07 from the central Frontal Cordillera and samples LE04 and LE05 from the eastern Frontal Cordillera. Grey lines correspond to acceptable fit paths (probability of fitting of lengths and age> 0.05), black lines correspond to good fit paths (probability of fitting of lengths and age > 0.5) and white lines represent best-fit paths, n° g= number of grains counted for AFT age determinations, n° t= number of tracks lengths measured.

6.3. Eastern Frontal Cordillera

Within the Elqui valley, samples LE04 and LE05 were collected from the eastern Frontal Cordillera. Both sample LE04 and sample LE05 were modeled only considering a finishing starting temperature/time ~ 20 ± 10°C at zero Ma (Fig. 7).

Although sample LE04 corresponds to an igneous sample, it present two distinct populations of apatites with diverging AFT ages, Dpar and track lenghts values. This might be related to compositional differences between the individual apatite grains analyzed in this sample. Thermal models of LE04 as a two-population sample are consistent with two periods of cooling (Fig. 7). The first one corresponds to a period of accelerated cooling starting at some moment during the Late Cretaceous or Early

Paleocene and the second one corresponds to a period of continuous cooling starting around ~ 35-30 and extending until the present-day (Fig. 7). Both cooling periods are separated from each other by a period of reheating starting during the Late Cretaceous or the Early Paleogene and ending by 35 Ma (Fig. 7).

Finally, thermal modeling of AFT and AHe data of sample LE05 that was collected from the eastern Frontal Cordillera but farther east than LE04, shows one episode of accelerated cooling from ~ 8 to 6 Ma (Fig. 7).

7. Discussion

7.1. Magmatic versus tectonic effects

North-to-south intrusive belts with increasing ages towards the east evidence continuous magmatic activity since the Early Jurassic to the Middle-Late Miocene, when magmatism would have markedly decreased in north-central Chile (Bissig et al., 2001; Kay and Mpodozis, 2002; Litvak et al., 2007; Fig. 3). Therefore, in order to interpret thermochronological data in terms of exhumation it is first necessary to exclude the possibility that the AFT and AHe ages only reflect the cooling of rocks after magmatic events.

Importantly, the relatively large difference between AFT and AHe ages throughout the Coastal Cordillera and the Frontal Cordillera already suggests that both thermochronological ages could not have been reset by the same magmatic event, otherwise both ages would be similar. However, there is still the possibility that AFT ages could reflect cooling after reheating or igneous cooling after emplacement at depths shallower than the AFT partial annealing zone (PAZ), but deeper than the AHe partial retention zone (PRZ). In such cases, AHe ages would correspond to subsequent exhumation throughout the last kilometers of depth.

7.1.1. Coastal Cordillera

Within the Huasco-Choros transect the AFT age measured on sample G4 (Fig. 4, Table 1) is the same within error than the available K-Ar and ^{40}Ar-^{39}Ar biotite and U-Pb zircon ages ranging between 76 ± 2 and 63.8 ± 0.7 Ma for the Late Cretaceous to Paleocene belt exposed to the east (Arévalo et al., 2009). However, rocks belonging to the Late Cretaceous to Paleocene belt do not intrude the exposures of the Early Cretaceous belt where the mentioned sample was collected and are located more than 30 km to the east of G4. Therefore, in this case a magmatic effect does not seem to be a probable explanation for the AFT ages of samples collected from the Early Cretaceous belt, and they probably reflect exhumation timing. South of La Serena a series of Late Cretaceous stocks, with K-Ar whole rock and biotite ages ranging between 83 ± 3 and 76 ± 3 Ma, intrude the exposures of the Early Cretaceous magmatic belt mostly on its eastern border (Fig. 4; Rivano and Sepúlveda, 1991; Emparán and Pineda, 2006). Sample LC09, which displays an U-Pb zircon age of 75.8 ± 7.1 Ma (Fig. 4; Table 1), is correlated with the mentioned Late Cretaceous stocks and intrudes the Early Cretaceous Illapel Plutonic Complex (Fig. 4). This age range overlaps within error with some of the AFT ages with MTL > 14 µm obtained for this unit (Fig. 4, Table 1) and with the episode of accelerated cooling shown by some of the thermal models with acceptable fitting for sample LC02 (Fig. 7). Thus, it is likely that the AFT data here may reflect cooling after emplacement of the Late Cretaceous stocks in the northern Choapa transect. However, from La Serena to the south the mentioned Late Cretaceous stocks have been interpreted to be syntectonic with episodes of tectonic inversion affecting the Mesozoic extensional basins from the Coastal Cordillera (Emparán and Pineda, 2006). Therefore, thermochronological data throughout the Coastal Cordillera within the studied region are probably reflecting the superimposed effects of both tectonic-related exhumation and syntectonic magmatism. In this case, tectonic-related exhumation and syntectonic magmatism are probably associated to increase contractional deformation during episodes of tectonic inversion of the Mesozoic extensional basins developed along the Coastal Cordillera.

7.1.2. Frontal Cordillera

7.1.2.1. Western Frontal Cordillera

Along the western Frontal Cordillera samples were collected from granitoids belonging to the Late Cretaceous to Paleocene and the Eocene magmatic belts (Fig. 4). In the Limarí river area, crystallization ages for the former are between ~ 69 and 67 Ma (Pineda and Calderón, 2008); whereas K-Ar and ^{40}Ar-^{39}Ar ages for the latter are between ~ 55 and 34 Ma (Pineda and Emparán, 2006; Pineda and Calderón, 2008). The Eocene magmatic rocks intrude the Late Cretaceous to Paleocene magmatic rocks in several places (Pineda and Calderón, 2008). At the southern part of the Limarí Valley (south of 31°S), samples LL01 and LL02 collected from the Eocene Fredes unit present AFT ages of 36.6 ± 3.6 and 39.2 ± 4.6 Ma, respectively; that are the same within error that the U-Pb ages of 39.3 ± 1 Ma obtained in this work for LL02 (Fig. 4). Thus, AFT ages of these samples could be reflecting the effects of igneous cooling. Similarly, within the Limarí Valley but towards the north of 31°S, the AFT ages of samples LL06, LL07, and LL08 are the same within error than K-Ar and ^{40}Ar-^{39}Ar biotite ages of intrusive units exposed a few kilometers to the east and K-Ar biotite age of dikes to the west (Pineda and Emparán, 2006; Pineda and Calderón, 2008; Fig. 8a). However, AHe ages of samples collected along the western Frontal Cordillera in both areas of the Limarí Valley are between 21 and 16 Ma, much younger than AFT and U-Pb ages. This indicates that these rocks cooled under the PRZ in the Miocene. Consistently, thermal modeling of the AFT and AHe data of sample LL07 indicates these rocks were cooled continuously starting shortly before ~ 30 and extending until shortly after 20 Ma (Fig. 7). Thus, cooling in the western Frontal Cordillera in the Limarí Valley north of 31°S started just after the emplacement of the Eocene intrusive bodies, which according to geochronological data took place between ~ 55 and 33 Ma. However, thermal relaxation of rocks occurs through advective heat transfer, whose thermochronologic signal corresponds to a pulse of accelerated cooling, rather than continuous cooling during tens of millions of years as observed here. Moreover, no Miocene magmatic or volcanic rocks are exposed in this area (Fig. 3). Thus, progressive cooling from ~ 30 to 20 Ma could not be reflecting magmatic cooling and it is interpreted to reflect exhumation timing throughout the western Frontal Cordillera in the Limarí Valley north of 31°S.

According to geochronological and structural data along the Vicuña and Rivadavia Faults (Fig. 3a and b), contractional deformation throughout the western Frontal Cordillera of the Elqui Valley and the Limarí Valley in the area north of 31°S would have taken place during the Middle Eocene to Early Oligocene, (Pineda and Emparán, 2006; Pineda and Calderón, 2008). Thus, AFT ages ranging between ~ 40 and 30 Ma north of 31°S are probably reflecting exhumation related to Eocene to Oligocene contractional deformation along these faults as previously interpreted for AFT data obtained along the western Frontal Codillera in the Elqui Valley (Cembrano et al., 2003). However, thermal models indicate that exhumation was continuous until shortly after ~ 20 Ma (Fig. 7). Thus, tectonic movements along the Vicuña and Rivadavia Faults would not be the only responsible for exhumation in this area and other processes should be invoked to account for Early Miocene cooling throughout the western Frontal Cordillera north of 31°S. Tectonic inversion of Late Oligocene extensional intra-arc basins at 30°S would have started during the Early Miocene along the eastern Frontal Cordillera (Winocur, 2010). Thus, one possibility is that contractional deformation during the Early Miocene was not only focalized along the eastern Frontal Cordillera, but also affected the western Frontal Cordillera to the west.

Within the northern Choapa Valley most samples, except LC16, present AFT ages that are generally between ~ 40 and 30 Ma (Table 1). These ages are younger within error than the U-Pb age of 46.6 ± 0.6 Ma obtained for the Eocene Fredes unit in this valley. However, most of these AFT ages overlap within error with the U-Pb age of the Fredes unit within the Limarí Valley further north (Table 1). Therefore AFT ages between ~ 40 and 30 from the northern Choapa Valley may probably reflect igneous cooling through the PAZ shortly after emplacement of this unit. The only important exception in this case corresponds to sample LC16 which has a much younger AFT age of 21.6 ± 2.8 Ma and the lowest Dpar value within the northern Choapa Valley (Table 1). This age is much closer to the AHe ages within the same valley ranging between ~16 - 10 Ma (Fig. 5c) and is the only sample for which a coherent thermal model was obtained (Fig. 7). According to these models, AFT and AHe data from sample LC16 are consistent with an episode of accelerated cooling ~ 22 - 16 Ma. As exposures of Miocene magmatic rocks are mostly constrained to the area south of 32°S (Fig. 4), accelerated cooling at 22-16 Ma identified in the western Frontal Cordillera of the northern Choapa transect south of 31°S would indicate exhumation of rocks. This period overlaps with a relatively longer period of continuous cooling between ~ 30 and 20 Ma indicated by thermal models in the western Frontal Cordillera to the north of 31°S within the Limarí Valley. It also correlates in age with the early stages of tectonic inversion of the Late Oligocene extensional intra-arc basins along the eastern Frontal Cordillera at 30°S (Winocur, 2010).

7.1.2.2. Central Frontal Cordillera

No Early Miocene magmatism has been recognized along the central Frontal Cordillera in the Huasco-Choros and Elqui transects (Fig. 4). Therefore, the period of accelerated cooling through the PAZ around ~ 22-18 Ma recognized for sample JA07 is more easily explained as being related to exhumation. Within the Elqui Valley sample LE02 was also collected from the central Frontal Cordillera and presents a Dpar < 2 µm. Similar to JA07, this sample presents an AFT age of ~ 22 Ma (Fig. 4) and long tracks >14 µm (Table 1) indicating that it cooled through the PAZ shortly after 22 Ma. Taking together the AFT age of 22 ± 2.8 Ma and the AHe age of 12 ± 5.4 Ma of sample LE02 (Fig. 4; Table 1) they are consistent with accelerated exhumation through both the PAZ and PRZ during the Early Miocene. Therefore, AFT and AHe data from this sample are consistent with the thermal modeling of AFT data of JA07. Finally, accelerated cooling of samples JA07 and LE02 around ~ 22 - 18 Ma is interpreted as reflecting tectonic-related exhumation. This time period overlaps with the period of continuous exhumation identified in samples from the western Frontal Cordillera north of 31°S and correlates well with the period of accelerated exhumation identified in samples from the western Frontal Cordillera south of 31°S. Again, Early Miocene accelerated exhumation correlates in age with the early stages of tectonic inversion of a Late Oligocene intra-arc basin developed along the eastern Frontal Cordillera at 30°S.

7.1.2.3. Eastern Frontal Cordillera

Throughout the eastern Frontal Cordillera thermal modeling of sample LE04 is consistent with a period of accelerated cooling starting at some moment during the Late Cretaceous or Early Paleocene, followed by reheating during the Early Paleocene which ended by 35 -30 Ma and a second period of continuous cooling since 35-30 until the present day (Fig. 7).

Along the eastern Frontal Cordillera of the Elqui Valley exposures of Late Triassic to Jurassic volcano-sedimentary rocks interpreted as developed within extensional basins are observed (Fig. 3). At 28°S, Late Triassic to Early Jurassic extensional basins are thought to have been tectonically inverted during the Late Cretaceous to Paleocene (Martínez et al., 2012). Thus, similar to the episode of accelerated cooling at ~ 65-50 Ma throughout the Coastal Cordillera, Late Cretaceous or Early Paleocene accelerated cooling along the eastern Frontal Cordillera probably corresponds to exhumation triggered by the tectonic inversion of Mesozoic extensional basins previously developed along both areas.

During the Eocene a magmatic arc developed along the border between the present-day central and eastern Frontal Cordilleras in the area of the Huasco, Elqui and Limarí Valleys (Fig. 4). In the Elqui area the intrusive bodies assigned to the Eocene Bocatoma unit (Martin et al., 1995) show K-Ar and ^{40}Ar-^{39}Ar ages between ~ 40 and 31 Ma (Martin et al., 1995; Bissig et al., 2001). Some exposures of intrusive bodies related to the late

Cretaceous to Paleocene magmatic arc are also exposed along the border between the central and eastern Frontal Cordilleras in the northern part of the Elqui river area (Fig. 4). Thus, reheating during the Early Paleocene and ending by 35 - 30 Ma is probably related to the development of the Late Cretaceous to Paleocene and Eocene magmatic arcs along the Frontal Cordillera of the studied area.

Following the cessation of Eocene arc magmatism, an extensional intra-arc basin developed related to the volcano-sedimentary Tilito Formation (Thiele, 1964; Maksaev et al., 1984; Martin et al., 1995) along the eastern Coastal Cordillera to the north of 30°S (Kay and Mpodozis, 2002; Winocur et al., accepted). Extension ended by the Early Miocene when the intra-arc basin was inverted (Maksaev et al., 1984; Mpodozis and Cornejo, 1988; Nasi et al., 1990; Winocur, 2010; Winocur et al., accepted). Not all faults were fully inverted by the Early Miocene (Winocur et al., accepted). Some were partially inverted, others preserved their original extensional geometry and some others were inverted later, throughout the entire Miocene and after ~ 11 Ma (Winocur, 2010). The last period of cooling throughout the eastern Frontal Cordillera starting around 35 - 30 Ma correlates in age with both the cessation of Eocene arc magmatism and the early stages of development of the Late Oligocene extensional intra-arc basin. Similar to what was explain for the case of the western Frontal Cordillera north of 31°S, the thermochronological signal of igneous cooling corresponds to a pulse of accelerated cooling, rather than continuous cooling during several tens of millions of years as observed here. Therefore, continuous cooling from 35 - 30 Ma until the present-day is more likely related to a progressive process of exhumation during which starts and stops are possibly, but that is beyond the resolving power of our dataset. Such progressive process of exhumation is probably the effect of extensional tectonics leading to the development of the intra-arc basin shortly before 27 Ma and the progressive tectonic inversion of the intra-arc basin starting in the Early Miocene and extending until after 11 Ma (Winocur, 2010) along the eastern Frontal Cordillera.

With respect to thermal modeling of sample LE05, as magmatism markedly decreased by the middle Miocene in the Elqui Valley area, the period of accelerated cooling through the PAZ and the PRZ around ~ 7 Ma recognized for this sample could not be related to cooling after cessation of magmatism. Therefore, accelerated cooling around ~ 7 Ma would be instead reflecting a main episode of tectonic-related exhumation throughout the eastern Central Cordillera. This main episode of tectonic-related exhumation could be correlated with contractional deformation recognized by Winocur (2010) after 11 Ma associated to tectonic inversion of a Late Oligocene extensional basin and the episode of surface uplift identified by Bissig et al. (2002) around 6 Ma along the eastern Frontal Cordillera of the Elqui river area.

7.1.2.4. Principal Cordillera

Within the Late Cretaceous to Paleocene belt from the southern Choapa Valley an AFT age of 16 ± 3.4 Ma is the same within error that a K-Ar biotite age (Rivano and Sepúlveda, 1991) obtained for rocks of the Early to Middle Miocene belt exposed just to the east, whereas to the west an AFT age of 43.7 ± 5 Ma is again similar to the available ages for Eocene magmatic rocks in that area (Fig. 8b). Thus, AFT ages of these samples are likely reflecting cooling after reheating of rocks due to the emplacement of Early to Middle Miocene and Eocene magmatic rocks, respectively. As observed elsewhere AHe ages of these samples are much younger (10-5 Ma) and cannot be related to magmatic reheating, as magmatism markedly decreased in this region after 13 Ma. Thus, AHe ages along the Principal Cordillera would reflect final exhumation of these rocks during the Late Miocene.

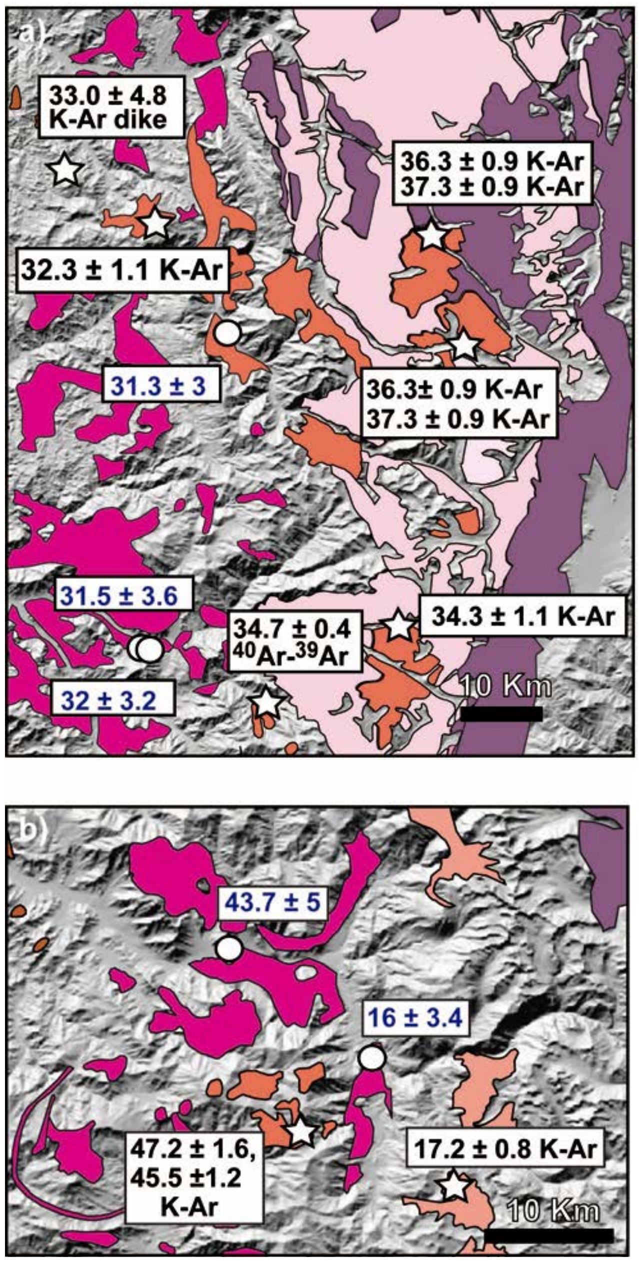

Fig. 8. a) Shaded relief image showing exposures of magmatic units within the Limarí Valley with AFT ages (in blue) and geochronological ages for Eocene and Oligocene magmatic units (in black) b) Shaded relief image showing exposures of magmatic units within the southern Choapa Valley with AFT ages (in blue) and geochronological ages for Eocene, Oligocene and Miocene magmatic units (in black).

7.2. Tectonic-related exhumation associated to the development of the Andean topographic front in north-central Chile

The very large difference among AFT and AHe ages and thermal modeling of AFT and AHe data indicates that the Coastal Cordillera was little exhumed during a great part of the Cenozoic. This is concordant with geomorphological, geological and structural data for the studied area. A series of subplanar bedrock surfaces form the summits of the Coastal Cordillera in this area (Paskoff, 1970; Aguilar et al., 2013; Rodríguez et al., accepted), which are interpreted as relicts of low relief/slope pediplains initially developed near sea level (Rodríguez et al., accepted). It is thought that a long-term inhibition of incision would favored the development of this type of surface (e.g. Phillips, 2002), which is consistent with the thermochronological data show here. The pediplains are carved into Early to Late Cretaceous rocks and covered by Early Miocene volcanic rocks (Rodríguez et al., accepted), which is in good agreement with negligible incision at least until ~ 30 Ma (early Oligocene) as indicated by AHe ages. Pediplains throughout the Coastal Cordillera in north-central Chile would have been uplifted ~1.1 km during the Early Miocene and ~1.2 km during the Late Miocene (Rodríguez et al., accepted). However, uplift since the Early Miocene would have been insufficient to exhume rocks throughout a new PAZ and PRZ as indicated by much older AFT and AHe ages. Finally, geological and structural data indicates that major deformation events took place throughout the Coastal Cordillera during the Late Cretaceous to Early Paleogene (e.g. Arancibia, 2004; Arévalo et al., 2009; Martínez et al., 2012); which is consistent with accelerated cooling during the Late Cretaceous -Early Paleogene as suggested by thermal modeling of AFT and AHe data from the Coastal Cordillera. A similar period of accelerated cooling is recognized along the eastern Frontal Cordillera, where Mesozoic extensional basins developed to the east of the Carboniferous to Permian basement core during the Late Triassic –Jurassic (Fig. 3).

According to our data, exhumation related to the development of the Andean topographic front has been progressive, with punctuated episodes of accelerated exhumation during the Early Miocene and the Late Miocene. Exhumation started during the Early Oligocene north of 31°S and during the Early Miocene south of 31°S. The difference in exhumation timing between both areas is consistent with structural and paleomagnetic data indicating that the western Frontal Cordillera in the area north of 31°S was affected by Eocene to Oligocene contractional deformation (Pineda and Calderón, 2008; Arriagada et al., in press), whereas the Principal Cordillera around 32°S was subjected to contractional deformation mostly during the Early Miocene (Mpodozis et al., 2009; Jara and Charrier, in press). Although Early Miocene accelerated exhumation is only observed in the central Frontal Cordillera to the north of 31°S and in the western Frontal Cordillera south of 31°S, thermal models indicate that the areas of the western and eastern Frontal Cordillera north of 31°S were also exhumed during this period. Thus, the Early Miocene exhumation signal is widespread throughout the Frontal Cordillera in the studied region. On the contrary, accelerated and progressive exhumation during the Late Miocene is focused in the eastern Frontal Cordillera.

Locally, Early Miocene accelerated exhumation correlates with the initial phases of tectonic inversion of the Late Oligocene intra-arc extensional basin developed along the eastern Frontal Cordillera at 30°S. Regionally, Early Miocene accelerated exhumation roughly correlates with a main period of Late Oligocene to Early Miocene increased uplift and deformation recognized throughout the entire Central Andes from the Altiplano-Puna plateau (e.g. Charrier et al., 2013) to the Principal Cordillera of central Chile at 32 - 36°S (Charrier et al., 2002; Farías et al., 2010). The Late Miocene episode of accelerated exhumation along the eastern Frontal Cordillera coincides with an episode of rapid forearc uplift at the latitude of the Altiplano-Puna plateau (Garzione et al., 2006; Hoke et al., 2007; Schildgen et al., 2007; Jordan et al., 2010) and central Chile at 33-34°S (Farías et al., 2008). It has been suggested that evidence pointing out to Late Miocene uplift in the Altiplano-Puna region; including geomorphic analysis, thermochronology and paleoelevation analysis, maybe reflecting accelerated incision due to climate change, rather than surface uplift (Barnes and Ehlers, 2009). However, given the strong precipitation gradient observed throughout the Central Andes, it seems difficult to imagine an along-strike coeval response of landscape to climate change. Moreover, the Late Miocene thermochronologic signal coincides with the final stages of inversion of the Late Oligocene intra-arc extensional basin (Winocur, 2010) and uplift of paleosurfaces along the eastern Frontal Cordillera (Bissig et al., 2002). Thus, Late Miocene accelerated exhumation may also be related to deformation and uplift. Our data is in good agreement with the proposal of Charrier et al. (2013) by which uplift and related exhumation throughout the Central Andes has occurred continuously since the Eocene-Oligocene, but with periods of increased contractional deformation by the Late Oligocene-Early Miocene and the Late Miocene. The Late Oligocene-Early Miocene episode of increased deformation is thought to be associated with a major change in the relative movement and a considerable increase in the convergence rate between the oceanic and continental plates that occurred after breakup of the Farallon into the Nazca and Cocos Plates (Charrier et al., 2013; Pardo-Casas and Molnar 1987). On the contrary, the Late Miocene episode of increased deformation correlates with a strong decreased of the convergence velocity of the Nazca plate around 10 Ma (Pilger 1983; Pardo-Casas and Molnar 1987). As deformation and uplift seems to have occurred during periods of both acceleration (Early Miocene) and deceleration (Late Miocene) of plate convergence, other factors must be taken into consideration. It has been proposed that Late Miocene uplift of the Andean forearc may be related to lower crustal flow due to the westward underthrusting of the Brazilian craton below the Altiplano-Puna (Isacks, 1988; Phillips et al., 2012) and of the Precordillera basement (Cuyania terrane) below the Principal-Frontal Cordilleras in central Chile (Farías et al., 2010; Muñoz et al., 2013). Lower crustal flow would have been favored by the presence of a major east-verging ramp detachment structure connecting the slab with the Bolivian/ Argentinean foreland where present-day shallow seismicity and active deformation is observed (Isacks, 1988; Farías et al., 2010; Muñoz et al., 2013). According to geophysical and structural data at 30-31°S, a similar structure is observed below the Precordillera (Cuyania terrane) in the Argentinean foreland and it is interpreted to have been active during the last 10 Ma (Alvarado et al., 2010 and references therein; Marot, 2013). It is believed that coupling along subduction zones would increase during periods of deceleration of plate convergence (Yañez and Cembrano, 2003). One possibility is that the Late Miocene deceleration of convergence may have favored coupling along the Frontal Cordillera (Chilenia terrane) and the Precordillera (Cuyania terrane), leading to the westward underthrusting of the Argentinean foreland. In turn, this would have triggered lower crustal deformation below the eastern Frontal Cordillera and uplift of this area. Finally, we hypothesize that during the Early Miocene, when the major east-verging ramp detachment structure was not developed; deformation, uplift and tectonic-related exhumation throughout the Frontal Cordillera was the consequence of the more intense stress transmission and widespread strain due to the considerable increase in the convergence rate after breakup of the Farallon into the Nazca and Cocos Plates (Charrier et al., 2013; Pardo-Casas and Molnar 1987). During the Late Miocene, once the east-verging ramp detachment structure was already established, tectonic-related exhumation and uplift along the eastern Frontal Cordillera may be the consequence of the decrease in convergence rate after ~10 Ma, the higher coupling along the Frontal Cordillera - Precordillera border and the concomitant westward underthrusting of the Precordillera basement.

8. Conclusions

Large differences among AFT and AHe ages and thermal modeling of thermochronological data indicate little exhumation in the Coastal Cordillera during most of the Cenozoic, probably after tectonic deformation during the Late Cretaceous- Early Paleocene.

AFT and AHe data points out to a progressive construction of the Andean topographic front since the Early Oligocene north of 31°S and the Early Miocene south of 31°S. The progressive construction of the front include episodes of accelerated exhumation in the Early and Late Miocene, which correlates with periods of increased contractional deformation widely recognized throughout the Central Andes.

The Early Miocene episode of tectonic-related exhumation is probably a consequence of a considerable increase in the convergence rate between the oceanic and continental plates that occurred after breakup of the Farallon into the Nazca and Cocos Plates 25 Ma ago. Finally, we hypothesize that Late Miocene tectonic-related exhumation and uplift along the eastern Frontal Cordillera may be a consequence of the decrease in convergence rate after ~10 Ma and concomitant westward underthrusting of the Precordillera basement.

9. Acknowledgements

This study was supported in part by the Chilean Government through the Comisión Nacional de Ciencia y Tecnología CONICYT (Anillo ACT-18 project, AMTC), the Advanced Mining Technology Center (AMTC) of the Facultad de Ciencias Físicas y Matemáticas-Universidad de Chile; FONDECYT Project 11085022 “Interacción Clima-Tectónica en el Alzamiento Andino de Chile Central durante el Neógeno”; FONDECYT Project 1120272 “Extension, inversion and propagation: key tectonic styles on the development of the Andean cordillera of central Chile-Argentina (32-36ºs)” and the Ecos

-Conicyt proyect C11U02 "Levantamiento de la costa pacífica de Sud América y acoplamiento interplaca en la zona de subducción". Additional support was obtained by IRD Project “Erosión en los Andes”. This study is part of the PhD thesis of M.P. Rodríguez, which was supported by a 4 year grant from CONICYT. We deeply thank Ken Farley for opening his laboratory for M. P. Rodríguez to perform AHe analysis and Lindsey Hedges for helping with AHe sample preparation. We thank Ray Donelick for acquiring the AFT data. We also thank David Shuster for valuable discussions on AHe data interpretation.

10. References

Aguilar, G., R. Riquelme, J. Martinod, and J. Darrozes (2013), Role of climate and tectonics in the geomorphologic evolution of the Semiarid Chilean Andes between 27-32 degrees S, *ANDEAN Geol.*, *40*(1), 79–101, doi:10.5027/andgeoV40n1-a04.

Alvarado, P., and S. Beck (2006), Source characterization of the San Juan (Argentina) crustal earthquakes of 15 January 1944 (M-w 7.0) and 11 June 1952 (M-w 6.8), *Earth Planet. Sci. Lett.*, *243*(3-4), 615–631, doi:10.1016/j.epsl.2006.01.015. [online] Available from: <Go to ISI>://WOS:000236600600025.

Alvarado, P., G. Sanchez, M. Saez, and B. de Machuca (2010), New evidence for the seismic activity of the Cuyania terrane in the flat slab subduction region of Argentina, *Rev. Mex. CIENCIAS Geol.*, *27*(2), 278–291.

Álvarez, J., C. Mpodozis, I. Blanco-Quintero, A. García-Casco, C. Arriagada, and D. Morata (2013a), U–Pb ages and metamorphic evolution of the La Pampa Gneisses: Implications for the evolution of the Chilenia Terrane and Permo-Triassic tectonics of north Central Chile, *J. South Am. Earth Sci.*, *47*(0), 100–115, doi:http://dx.doi.org/10.1016/j.jsames.2013.07.001. [online] Available from: http://www.sciencedirect.com/science/article/pii/S0895981113000898

Álvarez, J., I. Murillo, and C. Mpodozis (2013), U-Pb ages and metamorphic evolution of the La Pampa Gneisses and the Quebrada Seca Schists: implications for the evolution of the Chilenia Terrane and Permo-Triassic tectonics of North-Central Chile, in *Geosur2013*, p. -.

Arancibia, G. (2004), Mid-cretaceous crustal shortening: evidence from a regional-scale ductile shear zone in the Coastal Range of central Chile (32º S), *J. South Am. Earth Sci.*, *17*(3), 209–226, doi:10.1016/j.jsames.2004.06.001. [online] Available from: http://linkinghub.elsevier.com/retrieve/pii/S0895981104000537 (Accessed 28 January 2012)

Arévalo, C., F. Mourgues, Francisco and R. Chávez (2009), Geología del Área Vallenar-Domeyko, Región de Atacama, scale 1:100.000, Serv. Nac. de Geol. y Miner, Santiago.

Armijo, R., R. Rauld, R. Thiele, G. Vargas, J. Campos, R. Lacassin, and E. Kausel (2010), The West Andean Thrust, the San Ramon Fault, and the seismic hazard for Santiago, Chile, *Tectonics*, *29*, doi:Tc2007 10.1029/2008tc002427. [online] Available from: <Go to ISI>://000276029200001.

Arriagada, C; R. Ferrando, L. Córdova, D. Morata and P. Roperch (accepted), The Maipo Orocline: a first scale structural feature in the Miocene to Recent geodynamic evolution in the central Chilean Andes., *Andean* Geol.

Barbarand, J., A. Carter, I. Wood, and T. Hurford (2003), Compositional and structural control of fission-track annealing in apatite, *Am. Mineral.*, *198*, 107–137, doi:10.1016/S0009-2541(02)00424-2.

Barnes, J. B., T. A. Ehlers, N. McQuarrie, P. B. O. Sullivan, and J. D. Pelletier (2006), Eocene to recent variations in erosion across the central Andean fold- thrust belt , northern Bolivia : Implications for plateau evolution, *Earth Planet. Sci. Lett.*, *248*, 118–133, doi:10.1016/j.epsl.2006.05.018.

Barnes, J. B., and T. A. Ehlers (2009), End member models for Andean Plateau uplift, *Earth-Science Rev.*, *97*(1-4), 105–132, doi: 10.1016/ j.earscirev. 2009.08.003. [online] Available from: <Go to ISI>://WOS:00027314360005.

Bissig, T., J. K. W. Lee, A. H. Clark, and K. B. Heather (2001), The Cenozoic History of Volcanism and Hydrothermal Alteration in the Central Andean Flat-Slab Region: New 40 Ar- 39 Ar Constraints from the El Indio–Pascua Au (-Ag, Cu) Belt, 29°20′–30°30′ S, *Int. Geol. Rev.*, *43*(4), 312–340, doi:10.1080/00206810109465016. [online] Available from: http://www.tandfonline.com/doi/abs/10.1080/00206810109465016 (Accessed 30 August 2012).

Bissig, T., and R. Riquelme (2010), Andean uplift and climate evolution in the southern Atacama Desert deduced from geomorphology and supergene alunite-group minerals, *Earth Planet. Sci. Lett.*, *299*(3-4), 447–457, doi:DOI: 10.1016/j.epsl.2010.09.028. [online] Available from: http://www.sciencedirect.com/science/article/B6V61-518F0CS-3/2/bb88a23fa1f480e57b22ff13837997b7

Bissig, T., A. H. Clark, J. K. W. Lee, and C. J. Hodgson (2002), Miocene landscape evolution and geomorphologic controls on epithermal processes in the El Indio-Pascua Au-Ag-Cu belt, Chile and Argentina, *Econ. Geol.*, *97*(5), 971–996, doi:10.2113/97.5.971. [online] Available from: <Go to ISI>://WOS:000178050500003.

Brooks, B. a. (2003), Crustal motion in the Southern Andes (26°–36°S): Do the Andes behave like a microplate?, *Geochemistry Geophys. Geosystems*, *4*(10), 1–14, doi:10.1029/2003GC000505. [online] Available from: http://www.agu.org/pubs/crossref/2003/2003GC000505.shtml (Accessed 22 July 2012).

Cahill, T., and B. L. Isacks (1992), Seismicity and Shape of the Subducted Nazca Plate, *J. Geophys. Res. Earth*, *97*(B12), 17503–17529. [online] Available from: <Go to ISI>://A1992JY18900019

Carlson, W. D., R. A. Donelick, and R. A. Ketcham (1999), Variability of apatite fission-track annealing kinetics: I. Experimental results, *Am. Mineral.*, *84*(9), 1213–1223. [online] Available from: <Go to ISI>://WOS:000082349700001

Charrier, R. and N . Muñoz,. (1996), Uplift of the western border of the Altiplano on a west-vergent thrust system, Northern Chile, *J. South Am. Earth Sci.*, *9*(3-4), 171–181. [online] Available from: <Go to ISI>://A1996VU24500003

Charrier, R., O. Baeza, S. Elgueta, J. J. Flynn, P. Gans, S. M. Kay, N. Munoz, A. R. Wyss, and E. Zurita (2002), Evidence for Cenozoic extensional basin development and tectonic inversion south of the flat-slab segment, southern Central Andes, Chile (33 degrees-36 degrees SL), *J. South Am. Earth Sci.*, *15*(1), 117–139, doi:10.1016/s0895-9811(02)00009-3. [online] Available from: <Go to ISI>://WOS:000175725400009

Charrier, R., L. Pinto, and M. P. Rodríguez (2007), Tectonostratigraphic evolution of the Andean Orogen in Chile, in *The Geology of Chile*, edited by T. Moreno and W. Gibbons, pp. 21–114., The Geological Society, London.

Charrier, R., G. Hérail, L. Pinto, M. García, R. Riquelme, M. Farías, and N. Muñoz (2013), Cenozoic tectonic evolution in the Central Andes in northern Chile and west central Bolivia: implications for paleogeographic, magmatic and mountain building evolution, *Int. J. Earth Sci.*, doi:10.1007/s00531-012-0801-4. [online] Available from: http://www.springerlink.com/index/10.1007/s00531-012-0801-4 (Accessed 20 August 2012)

Clark, A. H., R. M. Tosdal, E. Farrar, and A. Plazolles (1990), Geomorphologic Environment and Age of Supergene Enrichment of the Cuajone, Quellaveco, and Toquepala Porphyry Copper-Deposits, Southeastern Peru, *Econ. Geol.*, *85*(7), 1604–1628. [online] Available from: <Go to ISI>://A1990EU00800016

Cembrano, J., M. Zentilli, A. Grist, G .Yáñez (2003), Nuevas edades de trazas de fisión para Chile Central (30-34°S): Implicancias en el alzamiento y exhumación en los Andes desde el Cretácico, paper presented at X Congr. Geol. Chileno, Universidad de Concepción, Concepción, Chile.

Davila, F. M., and A. Carter (2013), Exhumation history of the Andean broken foreland revisited, *Geology*, *41*(4), 443–446, doi:10.1130/G33960.1.

Donelick, R. a. (2005), Apatite Fission-Track Analysis, *Rev. Mineral. Geochemistry*, *58*(1), 49–94, doi:10.2138/rmg.2005.58.3. [online] Available from: http://rimg.geoscienceworld.org/cgi/doi/10.2138/rmg.2005.58.3 (Accessed 22 July 2012)

Donelick, R., and D. S. Miller (1991), Enhanced TINT fission track densities in low spontaneous track density apatites using 252Cf-derived fission fragment tracks. A model and experimental observations, *Nuclear Tracks Radiation Measurements*, *18*, 301 – 307, doi:10.1016/1359-0189(91)90022-A.

Donelick, R. A. (1993), A method of fission track analysis utilizing bulk chemical etching of apatite, Patent 5267274, *U.S. Patent and Trademark Off., Washington, D. C.*

Emparán, C., and G. Pineda (2006), Geología del Area Andacollo-Puerto Aldea, Región de Coquimbo, scale 1:100.000, Serv. Nac. de Geol. y Miner, Santiago.

Farías, M., R. Charrier, D. Comte, J. Martinod, and G. Herail (2005), Late Cenozoic deformation and uplift of the western flank of the Altiplano: Evidence from the depositional, tectonic, and geomorphologic evolution and shallow seismic activity (northern Chile at 19 degrees 30 ' S), *Tectonics*, *24*(4), doi:Tc4001 10.1029/2004tc001667. [online] Available from: <Go to ISI>://WOS:000230484000001.

Farías, M., R. Charrier, S. Carretier, J. Martinod, A. Fock, D. Campbell, J. Cáceres, and D. Comte (2008), Late Miocene high and rapid surface uplift and its erosional response in the Andes of central Chile (33°–35°S), *Tectonics*, *27*(1), doi:10.1029/2006TC002046. [online] Available from: http://www.agu.org/pubs/crossref/2008/2006TC002046.shtml (Accessed 22 August 2012).

Farías, M., D. Comte, R. Charrier, J. Martinod, C. David, A. Tassara, F. Tapia, and A. Fock (2010), Crustal-scale structural architecture in central Chile based on seismicity and surface geology: Implications for Andean mountain building, *Tectonics*, *29*, 22, doi:Tc3006 10.1029/2009tc002480. [online] Available from: <Go to ISI>://000278249500001.

Farley, K. a., and D. F. Stockli (2002), (U-Th)/He Dating of Phosphates: Apatite, Monazite, and Xenotime, *Rev. Mineral. Geochemistry*, *48*(1), 559–577, doi:10.2138/rmg.2002.48.15. [online] Available from: http://rimg.geoscienceworld.org/cgi/doi/10.2138/rmg.2002.48.15 (Accessed 30 August 2012).

Garcia, M., and G. Herail (2005), Fault-related folding, drainage network evolution and valley incision during the Neogene in the Andean Precordillera of Northern Chile, *Geomorphology*, *65*(3-4), 279–300. [online] Available from: <Go to ISI>://000227347600007.

García, M., R. Riquelme, M. Farías, and R. He (2011), Late Miocene − Holocene canyon incision in the western Altiplano , northern Chile: tectonic or climatic forcing? Email alerting service Permission Late Miocene – Holocene canyon incision in the western Altiplano , north, *J. Geol. Soc. London.*, 1047–1060, doi:10.1144/0016-76492010-134.

Garzione, C. N., P. Molnar, J. C. Libarkin, and B. J. MacFadden (2006), Rapid late Miocene rise of the Bolivian Altiplano: Evidence for removal of mantle lithosphere, *Earth Planet. Sci. Lett.*, *241*(3-4), 543–556. [online] Available from: <Go to ISI>://000235289000016.

Gleadow, a. J. W., I. R. Duddy, P. F. Green, and J. F. Lovering (1986), Confined fission track lengths in apatite: a diagnostic tool for thermal history analysis, *Contrib. to Mineral. Petrol.*, *94*(4), 405–415, doi:10.1007/BF00376334. [online] Available from: http://www.springerlink.com/index/10.1007/BF00376334

Green, P. F., I. R. Duddy, A. J. W. Gleadow, P. R. Tingate, and G. M. Laslett (1986), Thermal annealing of fission tracks in apatite 1. A qualitative description, *Chemical Geology*, *59*, 237 – 253, doi:10.1016/ 0009-2541(86)90048-3.

Hall, S. R., D. L. Farber, L. Audin, R. C. Finkel, and A. S. Meriaux (2008), Geochronology of pediment surfaces in southern Peru: Implications for Quaternary deformation of the Andean forearc, *Tectonophysics*, *459*(1-4), 186–205, doi:10.1016/j.tecto.2007.11.073. [online] Available from: <Go to ISI>://000261369300013

Hoke, G. D., and C. N. Garzione (2008), Paleosurfaces, paleoelevation, and the mechanisms for the late Miocene topographic development of the Altiplano plateau, *Earth Planet. Sci. Lett.*, *271*(1-4), 192–201, doi:10.1016/j.epsl.2008.04.008. [online] Available from: http://linkinghub.elsevier.com/retrieve/pii/S0012821X08002446 (Accessed 22 July 2012)

Hoke, G. D., B. L. Isacks, T. E. Jordan, N. Blanco, A. J. Tomlinson, and J. Ramezani (2007), Geomorphic evidence for post-10 Ma uplift of the western flank of the central Andes 18°30′–22°S, *Tectonics*, *26*(5), 1–17, doi:10.1029/2006TC002082. [online] Available from: http://www.agu.org/pubs/crossref/2007/2006TC002082.shtml (Accessed 22 July 2012)

Isacks, B. L. (1988), Uplift of the central Andean Plateau and bending of the Bolivian Orocline, *J. Geophys. Res.*, *93*(B4), 3211–3231.

Jara, P., and R. Charrier (accepted), Nuevos antecedentes geocronológicos y estratigráficos en la Cordillera Principal de Chile central entre 32° y 32°30´S Implicancias paleogeográficas y estructurales, *Andean Geology*.

Jordan, T. E., P. L. Nester, N. Blanco, G. D. Hoke, F. Dávila, and A. J. Tomlinson (2010), Uplift of the Altiplano - Puna plateau : A view from the west, *Tectonics*, *29*(May), doi:10.1029/2010TC002661.

Jordan, T. E., B. L. Isacks, R. W. Allmendinger, J. A. Brewer, V. A. Ramos, and C. J. Ando (1983), Andean Tectonics Related to Geometry of Subducted Nazca Plate, *Geol. Soc. Am. Bull.*, *94*(3), 341–361, doi:10.1130/0016-7606(1983)94<341:atrtgo>2.0.co;2. [online] Available from: <Go to ISI>://WOS:A1983QN40400003.

Kay, S. M., and C. Mpodozis (2002), Magmatism as a probe to the Neogene shallowing of the Nazca plate beneath the modern Chilean flat-slab, *J. South Am. Earth Sci.*, *15*(1), 39–57, doi:Pii s0895-9811(02)00005-6. [online] Available from: <Go to ISI>://WOS:000175725400005.

Ketcham, R. A. (2005), Forward and Inverse Modeling of Low-Temperature Thermochronometry Data, *Rev. Mineral. Geochemistry*, *58*, 275–314, doi:10.2138/rmg.2005.58.11.

Litvak, V. D., S. Poma, S. M. Kay, and E. Valle (2007), Paleogene and Neogene magmatism in the Valle del Cura region: New perspective on the evolution of the Pampean flat slab , San Juan province , Argentina, *J. South Am. Earth Sci.*, *24*, 117–137, doi:10.1016/j.jsames.2007.04.002.

Maksaev, V., R. Moscoso, C. Mpodozis and C. Nasi (1984), Las unidades volcánicas y plutónicas del Cenozoico superior en la Alta Cordillera del Norte Chico (29°-31°S), Geología, alteración hidrotermal y mineralización. *Rev. Geo. Chile*, *21*,11-51.

Manea, V. C., M. Pérez-gussinyé, and M. Manea (2012), Chilean flat slab subduction controlled by overriding plate thickness and trench rollback, *Geology*, (1), 35–38, doi:10.1130/G32543.1.

Marot, M. (2013), Zones de subduction horizontale versus normale: Une comparaison basée sur la tomographie sismique en 3-D et de la modélisation pétrologique de la lithosphère continentale du Chili Central et de l'Ouest de l'Argentine (29°S-35°S), 224 pp., Phd Thesis, l'Université de Nice-Sophia Antipolis, Nice.

Martin, M., J. Clavero, C. Mpodozis, and L. Cutiño (1995), *Estudio geológico regional de la franja El Indio, Cordillera de Coquimbo*, Santiago, Chile.

Martin, M. W., J. Clavero, and C. Mpodozis (1999), Late Paleozoic to Early Jurassic tectonic development of the high, *J. South Am. Earth Sci.*, *12*, 33–49.

Martínez, F., C. Arriagada, C. Mpodozis, and M. Peña (2012), The Lautaro Basin: A record of inversion tectonics in northern Chile, *J. South Am. Earth Sci.*, *39*(2).

Martinez, F., C. Arriagada, M. Pena, I. Del Real, and K. Deckart (2013), The structure of the Chanarcillo Basin: An example of tectonic inversion in the Atacama region, northern Chile, *J. SOUTH Am. EARTH Sci.*, *42*, 1–16, doi:10.1016/j.jsames.2012.07.001.

Martinod, J., L. Husson, P. Roperch, B. Guillaume, and N. Espurt (2010), Horizontal subduction zones , convergence velocity and the building of the Andes, *Earth Planet. Sci. Lett.*, *299* (3-4), 299–309, doi:10.1016/j.epsl.2010.09.010. [online] Available from: http://dx.doi.org/10.1016/j.epsl.2010.09.010.

Mortimer, C. (1973), The Cenozoic history of the southern Atacama Desert, Chile, *J. Geol. Soc. London.*, *129*(5), 505–526, doi:10.1144/gsjgs.129.5.0505. [online] Available from: http://jgs.lyellcollection.org/cgi/doi/10.1144/gsjgs.129.5.0505 (Accessed 22 July 2012).

Mpodozis, C. and P. Cornejo (1988), Hoja Pisco Elqui, IV Región de Coquimbo, scale 1:50.000, Serv. Nac. de Geol. y Miner, Santiago.

Mpodozis, C., H. Brockway, C. Marquardt, J. Perelló (2009), Geocronología U/Pb y tectónica de la región de Los Pelambres-Cerro Mercedario: implicancias para la evolución cenozoica de Los Andes del centro de Chile y Argentina, paper presented at XII Congr. Geol. Chileno, Universidad de Chile, Santiago, Chile.

Munoz, M., M. Farias, R. Charrier, C. M. Fanning, M. Polve, and K. Deckart (2013), Isotopic shifts in the Cenozoic Andean arc of central Chile: Records of an evolving basement throughout cordilleran arc mountain building, *Geology*, *41*(8), 931–934, doi:10.1130/G34178.1.

Nasi, C., R. Moscoso V. and Maksaev (1990) Hoja Guanta, Regiones de Atacama y Coquimbo, scale 1:50.000, Serv. Nac. de Geol. y Miner, Santiago.

Pardo-Casas, F., and P. Molnar (1987), Relative motion of the Nazca (Farallon) and South American plates since late Cretaceous time, *Tectonics*, *6*(3), 233–248.

Pankhurst, R. J., I., Millar and F. Hervé (1996), A Permo-Carboniferous U-Pb age for part of the Guanta Unit of the Elqui-Limari Batholith at Rio del Transito, Northern Chile, *Rev. Geo. Chile*, *23*, 35-42.

Parada, M. A., and B. Levi (1999), Multiple sources for the Coastal Batholith of central Chile 31 – 34^{o}S : geochemical and Sr – Nd isotopic evidence and tectonic implications, *Lithos*, *46*, 505–521.

Pardo, M., D. Comte, and T. Monfret (2002), Seismotectonic and stress distribution in the central Chile subduction zone, *J. South Am. Earth Sci.*, *15*(1), 11–22, doi:10.1016/s0895-9811(02)00003-2. [online] Available from: <Go to ISI>://WOS:000175725400003.

Paskoff, R. (1970), *Recherches géomorphologiques dans le Chili semi-aride*, Biscaye Freres, Bordeaux.

Phillips, K., R. W. Clayton, P. Davis, H. Tavera, R. Guy, S. Skinner, I. Stubailo, L. Audin, and V. Aguilar (2012), Structure of the subduction system in southern Peru from seismic array data, *J. Geophys. Res. Earth*, *117*, doi:B11306 10.1029/2012jb009540. [online] Available from: <Go to ISI>://WOS:000311851700002.

Phillips, J. D. (2002), Erosion, isostatic response, and the missing peneplains, *GEOMORPHOLOGY*, *45*(3-4), 225–241, doi:10.1016/S0169-555X(01)00156-8.

Pilger, R. H. (1981), Plate reconstructions, aseismic ridges, and low-angle subduction beneath the Andes, *Geol. Soc. Am. Bull.*, *92*(7 pt 1), 448–456.

Pineda, G. and M. Calderón (2008), Geología del área Monte Patria-El Maqui, Región de Coquimbo. Servicio Nacional de Geología y Minería, scale 1:100.000, Serv. Nac. de Geol. y Miner, Santiago.

Pineda, G. and C. Emparán (2006), Geología del área Vicuña-Pichasca, Región de Coquimbo. Servicio Nacional de Geología y Minería, scale 1:100.000, Serv. Nac. de Geol. y Miner, Santiago.

Quang, C. X., A. H. Clark, J. K. W. Lee, and N. Hawkes (2005), Response of supergene processes to episodic Cenozoic uplift, pediment erosion, and ignimbrite eruption in the porphyry copper province of southern Peru, *Econ. Geol.*, *100*(1), 87–114, doi:10.2113/100.1.0087. [online] Available from: <Go to ISI>://WOS:000227707900006.

Ramos, V. A., E. O. Cristallini, and D. J. Perez (2002), The Pampean flat-slab of the Central Andes, *J. SOUTH Am. EARTH Sci.*, *15*(1), 59–78, doi:10.1016/S0895-9811(02)00006-8.

Riquelme, R., G. Hérail, J. Martinod, R. Charrier, and J. Darrozes (2007), Late Cenozoic geomorphologic signal of Andean forearc deformation and tilting associated with the uplift and climate changes of the Southern Atacama Desert (26°S–28°S), *Geomorphology*, *86*(3-4), 283–306, doi:10.1016/j.geomorph.2006.09.004. [online] Available from: http://linkinghub.elsevier.com/retrieve/pii/S0169555X06004089 (Accessed 28 January 2012).

Rivano, S., and P. Sepúlveda (1991), Hoja Illapel, Región de Coquimbo, scale 1:50.000, Serv. Nac. de Geol. y Miner, Santiago.

Rodríguez, M. P., G. Aguilar, C. Urresty and R. Charrier (accepted), Neogene landscape evolution in the Andes of north- central Chile between 28.5 and 32° S: Interplay between tectonic and erosional processes. *Geodynamic Processes in the Andes of Central Chile and Argentina, Geological Society, London*.

Somoza, R. (1998), Updated Nazca (Farallon) - South America relative motions during the last 40 My: implications for mountain building in the central Andean region, *J. South Am. Earth Sci.*, *11*(3), 211–215. [online] Available from: <Go to ISI>://000078067600001.

Sernageomin (2003), Carta Geológica de Chile, scale 1:1.000.000, Serv. Nac. de Geol. y Miner, Santiago.

Schildgen, T. F., K. V. Hodges, K. X. Whipple, P. W. Reiners, and M. S. Pringle (2007), Uplift of the western margin of the Andean plateau revealed from canyon incision history, southern Peru, *Geology*, *35*(6), 523, doi:10.1130/G23532A.1. [online] Available from: http://geology.gsapubs.org/cgi/doi/10.1130/G23532A.1 (Accessed 21 July 2011).

Thiele, R. (1964), *Reconocimiento geológico de la alta Cordillera de Elqui*, Santiago, Chile.

Tosdal, R. M., A. H. Clark, and E. Farrar (1984), Cenozoic Polyphase Landscape and Tectonic Evolution of the Cordillera Occidental, Southernmost Peru, *Geol. Soc. Am. Bull.*, *95*(11), 1318–1332. [online] Available from: <Go to ISI>://A1984TV75700006.

Winocur (2010), Geología y estructura del Valle del Cura y el sector central del Norte Chico, provincia de San Juan y IV Región de Coquimbo, Argentina y Chile, P.h. D thesis, pp, Univ. de Bs. Aires, Buenos Aires, Argentina.

Winocur D. A., V. D. Litvak, and V. A Ramos (accepted), Magmatic and Tectonic Evolution of the Oligocene Valle del Cura Basin, Main Andes of Argentina and Chile: Evidence for Generalized Extension, *Geodynamic Processes in the Andes of Central Chile and Argentina*, Geological Society, London.

Victor, P., O. Oncken, and J. Glodny (2004), Uplift of the western Altiplano plateau: Evidence from the Precordillera between 20 degrees and 21 degrees S (northern

Chile), *Tectonics*, *23*(4), doi:Tc4004 10.1029/2003tc001519. [online] Available from: <Go to ISI>://WOS:000222919100001.

Yáñez, G., C. R. Ranero, R. Von Huene, and J. Díaz (2001), Magnetic anomaly interpretation across the southern central Andes (32°-34°S): The role of the Juan Fernández Ridge in the late Tertiary evolution of the margin, *J. Geophys. Res. B Solid Earth*, *106*(B4), 6325–6345.

3.4. Final conclusions of this chapter

The key conclusions of this chapter are listed below for a better comprehension of the model of landscape evolution to be presented in chapter 6.

1. In the AFT samples collected for this work, the Dpar values for chlorine content higher than 1% are significantly lower than the Dpar predicted by the data of Carlson et al. (1999) and Barbarand et al. (2003). These differences could be explained by differences on how Dpar was measured or other sample properties that may affect etching and, therefore, Dpar size.

2. The huge gap between AHe ages and AFT ages with mean track values > 14 µm are mostly due to the generally high chlorine content of these apatites.

3. Thermochronometric data indicates that tectonic-related exhumation has been an active process since the Late Cretaceous- Early Paleogene in north-central Chile (Fig. 3.1a and b).

4. Late Cretaceous- Early Paleogene accelerated exhumation is related to inversion of Mesozoic extensional basins developed along the Coastal Cordillera, but also along the western border of the eastern Frontal Cordillera (Fig. 3.1a and b).

5. After the Late Cretaceous- Early Paleogene period of accelerated exhumation, the Coastal Cordillera has been little exhumed, which traduced in a long-term inhibition of incision from 45 Ma at least until 30 Ma (AHe ages) (Fig. 3.1b). Importantly, this is valid for the Coastal Cordillera to the south of 30°S. According to AFT and AHe data from the Coastal Cordillera just to the west of the Domeyko Depression to the north of 30°S, a last period of exhumation occurred in this area during the Eocene to Oligocene Incaic Orogeny (Fig. 3.1a, Maksaev et al., 2010).

6. After the Late Cretaceous- Early Paleogene period of accelerated exhumation the western border of the eastern Cordillera was reheated due to the development of the (Paleocene?) Eocene magmatic arc.

7. Since 35-30 Ma western border of the eastern Frontal Cordillera has been progressively exhumed probably due to the combined effects of the extensional tectonics related to the development of a Late Oligocene intra-arc extensional basin along the eastern Frontal Cordillera and the progressive tectonic inversion of this basin throughout the entire Miocene (Fig. 3.1 a). For simplicity, the Late Oligocene basin would be referred herein as the Tilito intra-arc basin, after the name of its related geological unit, the Tilito Formation.

8. North of 31°S, exhumation along the western Frontal Cordillera started before 30 Ma in the northern part of the Limarí valley and around 35 Ma in the Elqui valley according to Cembrano et al (2003) (Fig. 3.1a). Eocene to Oligocene exhumation may be related to contractional deformation along the Vicuña and Rivadavia Faults, previously related to the Incaic orogenic phase. Exhumation along the western Frontal Cordillera of the Limarí valley was progressive until after 20 Ma. This period of progressive exhumation overlaps with the period of accelerated exhumation in the central Frontal Cordillera of the Huasco and Elqui valleys around 22-18 Ma and the progressive exhumation since 35-30 Ma in the eastern Frontal Cordillera (Fig. 3.1a). Exhumation during the Early Miocene across the entire Frontal Cordillera may be related to contractional deformation associated to the tectonic inversion of the Tilito intra-arc basin along the eastern Frontal Cordillera. Finally, a new period of accelerated exhumation around 7 Ma (Fig. 3.1a), which relates to the progressive tectonic inversion of the Tilito Extensional Basin and uplift along the eastern Frontal Cordillera.

9. South of 31°S accelerated exhumation at the foot of the topographic front in the western Frontal Cordillera occurred around 22 -16 Ma, while in the areas of the Principal Cordillera to the east exhumation occurred until the Late Miocene (Fig. 3.1). Here, Early Miocene accelerated exhumation correlates with the tectonic inversion of the Abanico Extensional Basin throughout the Principal Cordillera at 32°S (Jara and Charrier, in press).

10. The Andean topographic front in north-central Chile was constructed progressively since the since the Eocene to Oligocene north of 31°S and the Early Miocene south of 31°S, including two episodes of accelerated exhumation during the Early and the Late Miocene, correlated with periods of increased contractional deformation widely recognized throughout the Central Andes.

11. During the Early Miocene widespread deformation, uplift and tectonic-related exhumation throughout the Frontal Cordillera in north-Central Chile may be the consequence of the considerable increase in the convergence rate occurring after breakup of the Farallon into the Nazca and Cocos Plates (Charrier et al., 2013; Pardo-Casas and Molnar 1987).

12. During the Late Miocene tectonic-related exhumation and uplift along the eastern Frontal Cordillera may be the consequence of the decrease in convergence rate after ~10 Ma and the concomitant westward underthrusting of the Precordillera basement.

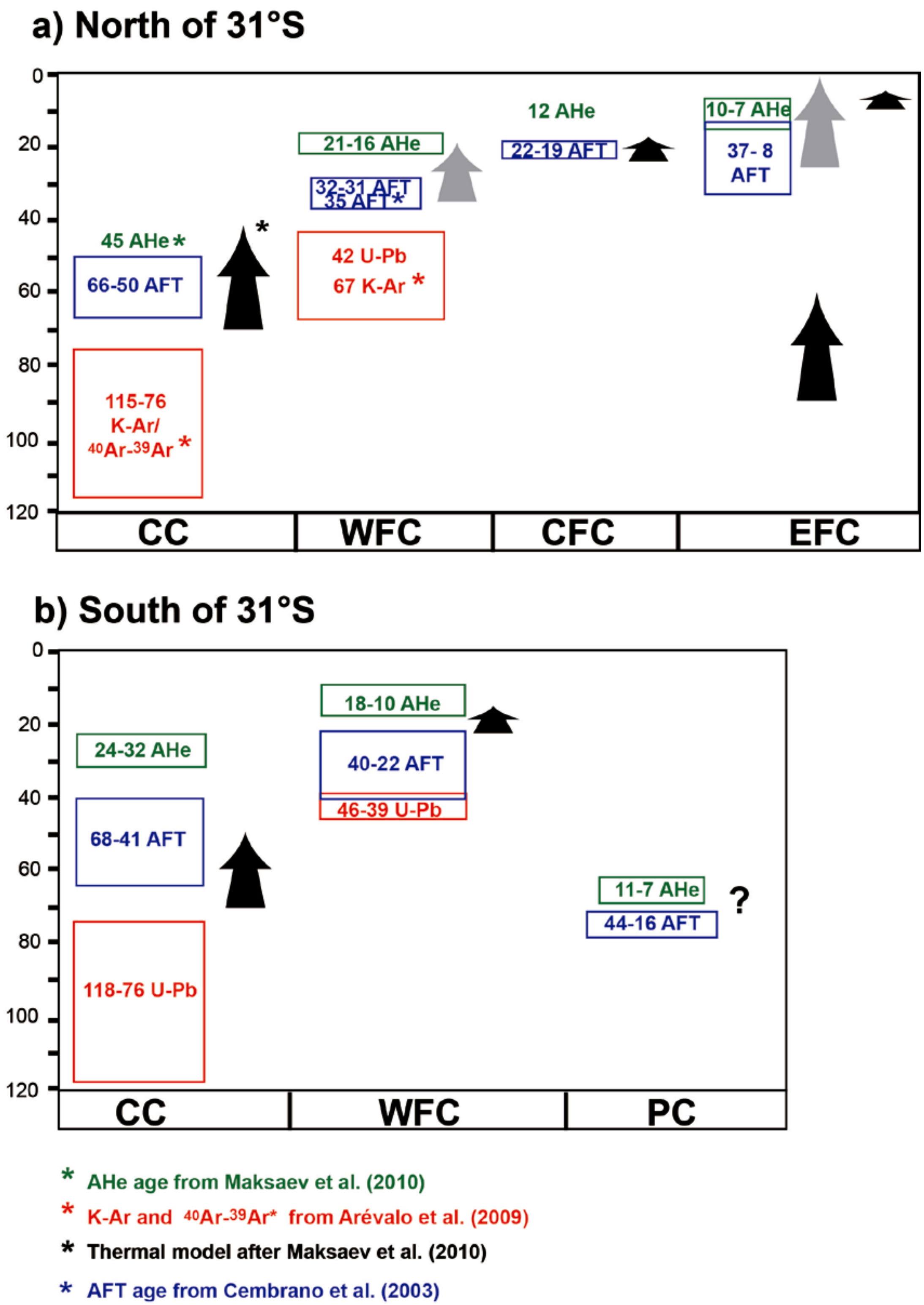

Fig. 3.1 Spatial and temporal variations of AFT and AHe ages and periods of progressive (grey arrows) or accelerated exhumation (black arrows) in north-central Chile a) north of 31°S and b) south of 31°S. CC=Coastal Cordillera, WFC= Western Frontal Cordillera, CFC= Central Frontal Cordillera, EFC= eastern Frontal Cordillera and PC= Principal Cordillera.

Chapter 4- QUATERNARY UPLIFT ALONG THE COASTAL CORDILLERA IN NORTH-CENTRAL CHILE

4.1. Introduction

This chapter includes in section 4.2 an article entitled “Geochronology of pediments and marine terraces in north-central Chile and their implications for Quaternary uplift in the Western Andes”, published in January 2013 in *Geomorphology*.

The article includes the results and the analysis of the geomorphic mapping and the ^{10}Be/ ^{26}Al cosmogenic dating of an extensive planation surface exposed within the river valleys and the coastal area, which is now uplifted ca.150-100 m above the present-day thalwegs and sea-level. Finally, the implications in terms of timing for Quaternary uplift along the Coastal Cordillera in north-central Chile are discussed.

4.2. Article: “Geochronology of pediments and marine terraces in north-central Chile and their implications for Quaternary uplift in the Western Andes”.

Geomorphology 180–181 (2013) 33–46

Contents lists available at SciVerse ScienceDirect

Geomorphology

journal homepage: www.elsevier.com/locate/geomorph

Geochronology of pediments and marine terraces in north-central Chile and their implications for Quaternary uplift in the Western Andes

María Pía Rodríguez [a,*], Sébastien Carretier [b], Reynaldo Charrier [a,1], Marianne Saillard [b,2], Vincent Regard [b], Gérard Hérail [b], Sarah Hall [c,3], Dan Farber [c], Laurence Audin [d]

[a] Departamento de Geología, Facultad de Ciencias Físicas y Matemáticas, Casilla 13518, Correo 21, Santiago, Chile
[b] Université de Toulouse, UPS, IRD, CNRS, GET, 14 Av. Edouard Belin, 31400, Toulouse, France
[c] Earth and Planetary Science Dept., University of California Santa Cruz, CA, CA 95060, USA
[d] Institut des Sciences de la Terre, IRD: UR219, CNRS: UMR5275, IFSTTAR, Université de Savoie, Université Joseph Fourier, Grenoble I, INSU, OSUG, France

ARTICLE INFO

Article history:
Received 15 March 2012
Received in revised form 1 September 2012
Accepted 12 September 2012
Available online 23 September 2012

Keywords:
CRN dating
Uplift
Chile
Fluvial terraces
Pediment
Shore platform

ABSTRACT

In north-central Chile, a wide shore platform is morphologically connected with a high fluvial terrace and a pediment. The eastward extension of Quaternary coastal uplift in the Southern Central Andes is poorly constrained since no age correlation between marine and continental landforms has been reported. We use ^{26}Al and ^{10}Be concentrations to constrain the geomorphic evolution of these marine and continental landforms near the Choapa valley (31.6° S). ^{10}Be ages for the shore platform indicate that this surface was repeatedly reoccupied during sea-level highstands between ~800 and 500 ka and uplifted after 500 ka. While 'zero erosion' ages for the pediment between ~600 and 300 ka only partly overlap the shore platform age range, more realistic exposure ages calculated for an erosion rate of 1 m/Ma are between ~945 and 475 ka, fitting the age range of the correlated shore platform. ^{10}Be concentrations of the high fluvial terrace are highly scattered evidencing vertical mixing of clasts probably due to slow lowering of the surface. Although it is not possible to determine an age for this landform, the scattering among its ^{10}Be concentrations implies that this marker is several hundreds of thousands of years old and that the high fluvial terrace began to form at ~1200 ka or after. Finally, ^{10}Be concentrations of the high fluvial terrace, the pediment and the shore platform are of the same order of magnitude, which is consistent with the clear morphologic correlation between these three types of landforms. These data suggest that the marine and continental landforms studied formed synchronously, with some local differences, during a long period of relative tectonic stability between ~(1200?) 800 and 500 ka and uplifted after 500 ka. Our results confirm recent studies showing a post-400 ± 100 ka renewal of uplift along the Pacific coast after a Lower to Middle Pleistocene period of slow uplift. Moreover, the extension of the surfaces suggests that a broad region of ~40 km has been uplifted ca. 150 m during the Quaternary.

1. Introduction

Near-coastal deformation in the Southern Central Andes is widely documented by the presence of marine sedimentary sequences and shoreline and fluvial geomorphic features uplifted along the Pacific coast. In particular, Quaternary coastal uplift has been inferred from the study of marine terraces and beach ridges (Paskoff, 1970; Leonard and Wehmiller, 1992; Ota et al., 1995; Ortlieb et al., 1996; Marquardt et al., 2004; Quezada et al., 2007; Saillard et al., 2009; Regard et al., 2010). Initially, the age of these surfaces was constrained through macrofossil biostratigraphy and through diverse dating techniques on shells such as U-series, electron spin resonance, amino-acid racemization and ^{14}C (e.g. Herm, 1969; Leonard and Wehmiller, 1992; Ota et al., 1995; Marquardt et al., 2004). However, many of the marine terraces along the Pacific margin of the Southern Central Andes correspond to shore platforms with little or no fossil content. Only recently, has the use of in-situ produced cosmogenic nuclides facilitated better constraint on the geomorphic evolution of these surfaces by providing exposure age dating of these marine landforms (Marquardt, 2005; Quezada et al., 2007; Saillard, 2008). In contrast to previous models of coastal uplift which assumed steady uplift in this region (e.g. Ota et al., 1995), recent data suggest that coastal uplift rates in the Southern Central Andes have been highly variable during the Pleistocene and that periods of rapid

* Corresponding author.
E-mail address: mariarod@ing.uchile.cl (M.P. Rodríguez).
[1] Current address: Escuela de Ciencias de la Tierra, Universidad Andres Bello, Campus República, Santiago, Chile.
[2] Current address: Géoazur, Université Nice Sophia-Antipolis, Centre National de la Recherche Scientifique (UMR 7329), Observatoire de la Côte d'Azur, La Darse B.P. 48, 06235 Villefranche sur-Mer Cedex, France.
[3] Current address: Earth and Planetary Sciences, McGill University, Quebec, Canada.

0169-555X/$ – see front matter © 2012 Elsevier B.V. All rights reserved.
http://dx.doi.org/10.1016/j.geomorph.2012.09.003

uplift alternate with periods of relatively slow uplift (Quezada et al., 2007; Saillard et al., 2009). Previous authors show that periods of slow uplift favor the development of particularly wide shore platforms (>1 km) due to superimposition of repeated sea-level highstands on a relatively stable rocky coast (Anderson et al., 1999; Quezada et al., 2007; Álvarez-Marrón et al., 2008; Saillard et al., 2009; Regard et al., 2010). This particular type of wide shore platform, named *rasa*, corresponds to a characteristic and relatively continuous feature of the coastal morphology along the Pacific margin in southern Peru and northern Chile (Fig. 1; Paskoff, 1970; Regard et al., 2010). In order to laterally correlate surfaces with similar cliff foot elevations and determine the timing of uplift, Regard et al. (2010) compiled cliff foot elevations and extrapolated cliff foot ages using the available chronological data for the *rasas* spanning the region from Atico, Peru to La Serena, Chile (Fig. 1). The data compiled thus include a range of diverse dating techniques on shells already mentioned above (e.g. Leonard and Wehmiller, 1992; Ota et al., 1995; Marquardt et al., 2004), the faunal assemblage (e.g. Herm, 1969) and cosmogenic nuclides to determine the age of the *rasas* (Marquardt, 2005; Quezada et al., 2007; Saillard, 2008). Regard et al. (2010) recognized three *rasa* levels in southern Peru and northern Chile, the main one of which has a cliff-foot formation age of 400±100 ka and lies at 110±20 m (above mean sea-level). They interpret the data as representing a coastal region spanning ~1500 km from Atico to La Serena that experienced renewed uplift since at least 400 ka, corresponding to marine isotopic stage (MIS) 11. This uplift followed a long period of relative quiescence, which is necessary to shape such a wide shore feature. Quaternary uplift could have also affected the coastal area located further south of La Serena as the presence of *rasas* has been reported from Nazca, Peru to Valparaíso, Chile (Paskoff, 1970; Fig. 1), however no geochronological data have been reported that would support this model. Importantly, it has also been proposed that subduction-related Quaternary uplift was not solely located at the coast but has affected all the forearc of southern Peru and northern Chile (Mortimer, 1973; Tosdal et al., 1984; Clark et al., 1990; Hartley et al., 2000, 2005; Hall et al., 2008). Recently a number of studies have applied cosmogenic nuclide dating to constrain the geomorphic evolution of planation surfaces located inland from the coast (Nishiizumi et al., 2005; Kober et al., 2007; Hall et al., 2008; Evenstar et al., 2009; Placzek et al., 2010). These studies have documented the existence of Neogene and Quaternary aged surfaces. However, many of these studies have interpreted cosmogenic concentrations to reflect surface erosion rates rather than the age of landform abandonment following surface uplift. Moreover, the planation surfaces studied in these works have no specific geomorphic correlation with marine landforms.

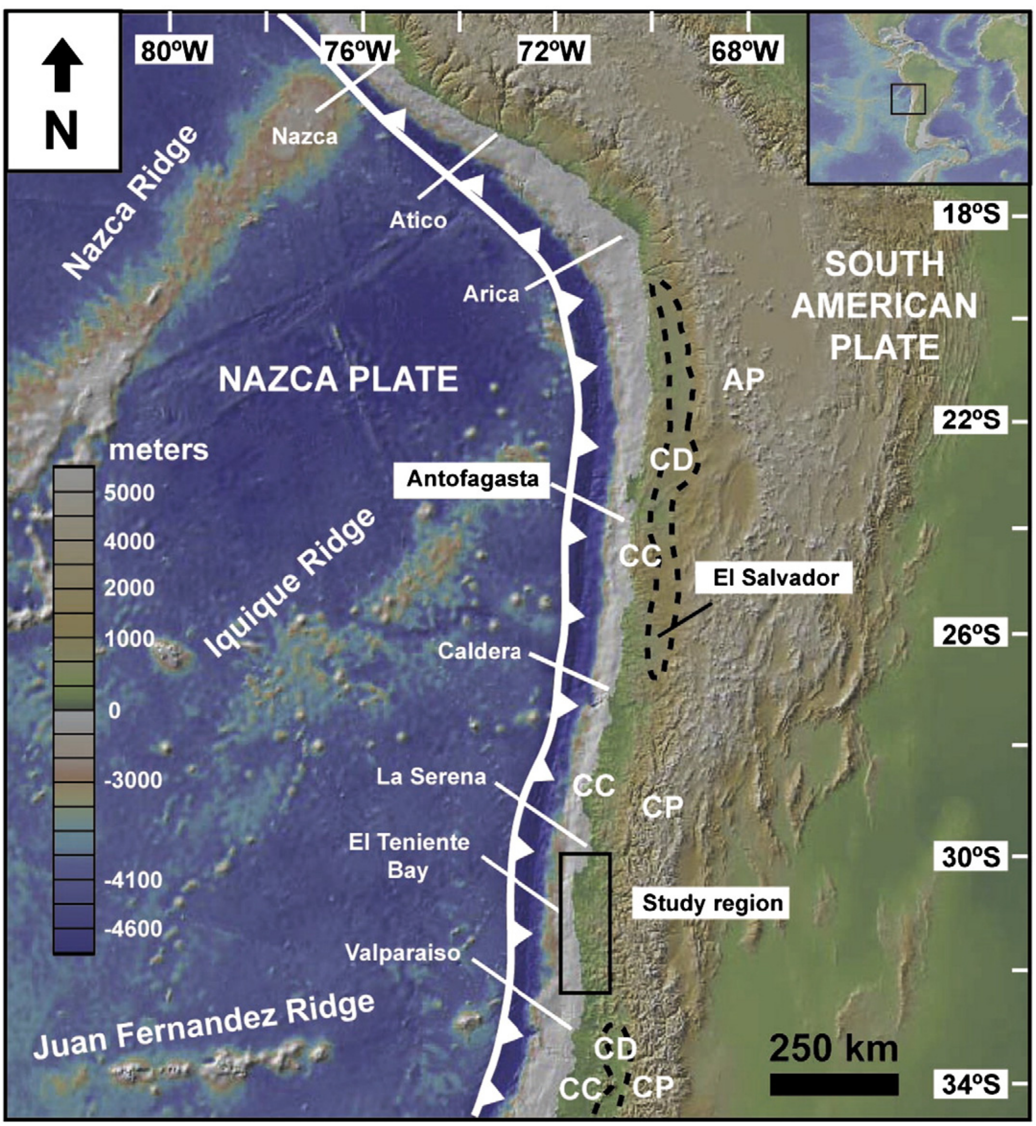

Fig. 1. Geodynamic setting of the study region. Dashed lines mark the limits of the Central Depression. Topography and bathymetry based in NASA elevation model with a resolution of 30 and 90 m respectively. CC = Coastal Cordillera; CD = Central Depression; CP = Principal Cordillera; AP = Altiplano-Puna.

Thus, it remains unclear whether the uplift documented by marine terraces corresponds to a local uplift of the coastal area or a more regional one involving planation surfaces inland. To address this issue, we have collected new data from a key location in north-central Chile between 30 and 32.5° S, which document the geomorphic connections of Quaternary tectonics in the western Andes. The study area is bounded to the north by the region studied by Saillard et al. (2009) and Regard et al. (2010) where *rasas* have been described in detail and, importantly, our geomorphic analysis suggests lateral connections between diverse geomorphic elements such as a shore platforms, a high fluvial terrace and a pediment uplifted in a west–east direction over a broad region (~40 km). We use ^{10}Be concentrations of the shore platform and $^{10}Be/^{26}Al$ concentrations of the high fluvial terrace and the pediment to constrain the geomorphic surface evolution and the timing of uplift near the Choapa valley (~31.6° S; Figs. 1, 2).

2. Regional setting

The study area between 30 and 32.5° S (Fig. 1) is located within a segment of the Southern Central Andes where the subduction angle between the Nazca and South American Plates is ~10°, usually referred as the Chilean or Pampean flat subduction segment (Cahill and Isacks, 1992). This segment is characterized by a strong interplate coupling between both tectonic plates, a highly compressed continental crust, and by the absence of Quaternary volcanism (Pardo et al., 2002). Yañez et al. (2001) suggest that flat subduction in this region is related to the subduction of the Juan Fernández aseismic ridge at 33° S which has been continuously subducting beneath South America at the same piercing point since 10 Ma. Therefore, it is not plausible that the Quaternary coastal uplift of the Tongoy region, north of 31° S, is related to subduction of this ridge (Saillard et al., 2009). Although major historical earthquakes, such as the 1647 AD (Mw = 8.5) and the 1730 AD (Mw = 8.7) events, have occurred at the subduction segment underlying the study region, no destructive megathrust earthquakes have occurred since the 1943 AD Illapel earthquake (Mw = 7.9) and this region is therefore known as the Illapel seismic gap (30–32.2° S) (Beck et al., 1998).

Climatically, this region of Chile is semiarid due to the year-round influence of the southeast Pacific anticyclone (SEP), with northward penetration of the southern hemisphere westerlies only possible when the SEP is weakened or displaced northwards (Veit, 1996). Mean annual precipitation at the coastal area is ~100 mm with high interannual variability strongly linked to ENSO (El Niño Southern Oscillation), where the warmer phase is generally associated with higher than average precipitation (Vicuña et al., 2010 and references therein).

The main north–south oriented morphostructural units within the western Andean margin of Chile generally consist of a Coastal Cordillera, a Central Depression and a Principal Cordillera (corresponding to the Altiplano-Puna in northern Chile) (Fig. 1). However, no Central Depression is developed along the margin from about 27° S to 30° S (Fig. 1) and the transition between Coastal Cordillera and Principal Cordillera is marked by a sharp increase in elevation of the topography. This study is focused on the coastal area and the middle and lower courses of the main valleys of the Coastal Cordillera (Fig. 1). The western side of the Coastal Cordillera preserves a series of shore platforms and is generally known as the Coastal Plain (Paskoff, 1970; Ota et al., 1995; Benado, 2000; Saillard et al., 2009); whereas towards the east the Coastal Cordillera develops as an area of higher topography known as the Medium Cordillera reaching ~3200 m in elevation (Paskoff, 1970). The Coastal Cordillera consists of Paleozoic metamorphic and sedimentary basement to the west, a Mesozoic volcano-sedimentary cover to the east and a Cenozoic marine to continental sedimentary cover exposed near the coast and within the main valleys (Fig. 2). North–south oriented Mesozoic plutonic belts that have ages increasing to the east have intruded both the Paleozoic basement and the Mesozoic volcano-sedimentary rocks (Fig. 2).

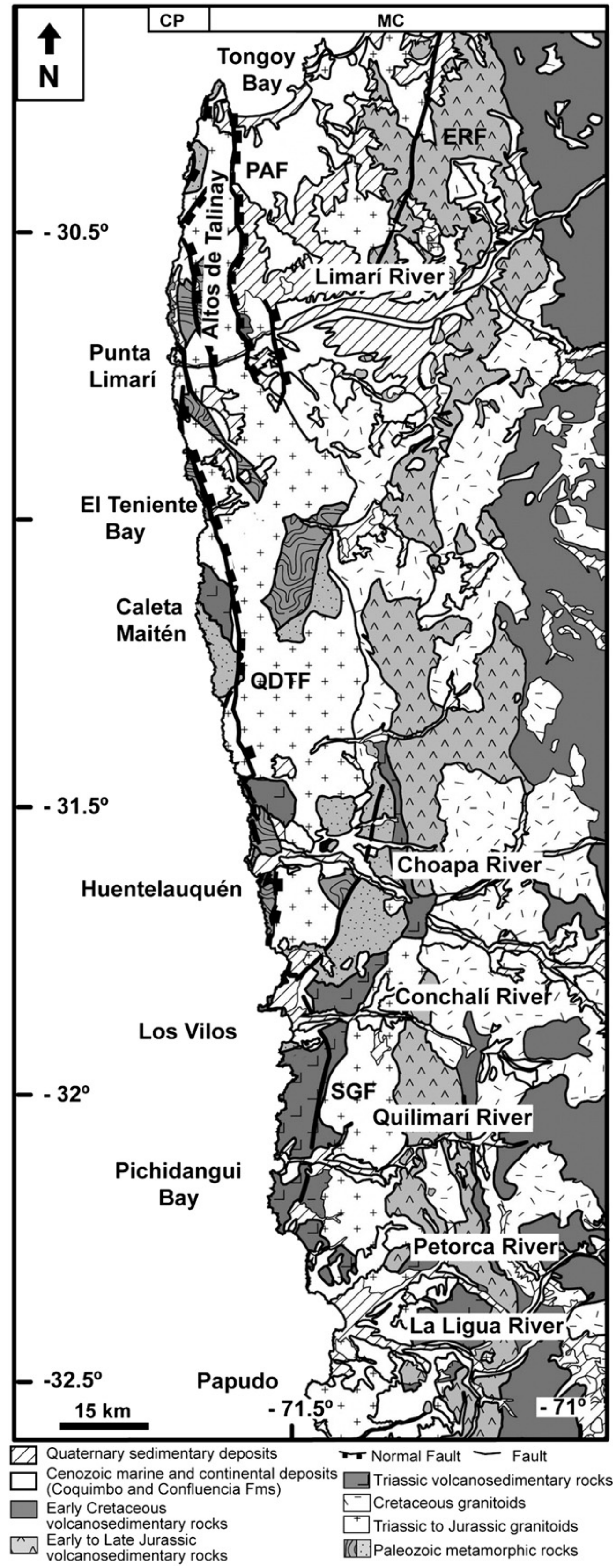

Fig. 2. Geological Map of Coastal Cordillera in the study area. CP = Coastal Plain, MC = Medium Cordillera, PAF = Puerto Aldea Fault, ERF = El Romeral Fault, QDT = Quebrada Del Teniente Fault, SDG = Silla Del Gobernador Fault.
Modified from Emparán and Pineda, 2006; Rivano and Sepúlveda, 1991 and SERNAGEOMIN, 2003.

The fluvial terraces studied here are most commonly developed cross-cutting the continental Cenozoic deposits of the Coastal Cordillera and are thought to be younger than the above-mentioned deposits (Paskoff, 1970). These Cenozoic deposits correspond to unconsolidated fluvial gravels and alluvial breccias of the Confluencia Formation (Paskoff, 1970; Rivano and Sepúlveda, 1991; Fig. 2). The Confluencia Formation changes laterally towards the west to marine-to-transitional mudstones, sandstones, coquinas and limestones of the Coquimbo Formation (Emparán and Pineda, 2006; Le Roux et al., 2006). Although no geochronological data for the Confluencia Formation are available from the study area, based on the interfingering between continental and marine deposits observed in the field (Rivano and Sepúlveda, 1991) its age is assumed to be similar to the Coquimbo Formation. $^{87}Sr/^{86}Sr$ dating of shells indicate the Coquimbo Formation was deposited during a series of transgressions and regressions related to regional and local tectonic movements combined with global sea-level variations during a broad timeframe between ~11 and 1.2 Ma in the Tongoy Bay area (Le Roux et al., 2006). Accordingly, the age of the Confluencia Formation is constrained between the Miocene and the Pleistocene (Emparán and Pineda, 2006).

Just north of the study region described here, in the Altos de Talinay area, a sequence of five shore platforms (Paskoff, 1970; Ota et al., 1995; Benado, 2000; Saillard et al., 2009) has been recognized and dated (Saillard et al., 2009; Fig. 3). The shore platforms from the ocean-facing side of the Altos de Talinay are morphologically connected with marine terraces related to the development of beach ridges within the Tongoy Bay (Paskoff, 1970; Saillard, 2008, Fig. 3). The shore platforms mapped and dated by Saillard et al. (2009) correspond to T_I, T_{II}, T_{III}, T_{IV} and T_V terraces, located at elevations of 425 ± 15, 170 ± 20, 55 ± 5, 25 ± 3 and 6 ± 1 m amsl. Saillard et al. (2009) collected two to three bedrock and cobble samples per platform yielding highly reproducible 'zero erosion' ^{10}Be surface exposure ages of 679 ± 8, 318 ± 1, 225 ± 12, 123 ± 14 and 11 ± 2 ka, respectively. Among these surfaces, T_I and T_{II} shore platforms are, in turn, morphologically connected with pediments and a high fluvial terrace at the Limarí river valley (Paskoff, 1970; Fig. 3).

The main faults in the study area are the NNW–SSE to NNE–SSW trending El Romeral, Puerto Aldea, Quebrada del Teniente and La Silla del Gobernador faults (Fig. 2). Previous authors proposed that these faults may correspond to the southern extension of the Atacama Fault System (AFS; Arabasz, 1971) referred to in this location as the El Romeral–La Silla del Gobernador segment of the AFS (Charrier et al., 2007). In northern Chile, a series of faults related to the AFS present late Cenozoic to Recent normal and reverse reactivations (Delouis et al., 1998; Riquelme et al., 2003; Allmendinger and González, 2010). Just north of the study region, near the city of Caldera (Fig. 1), the AFS is thought to produce the relative uplift of the western side of the Coastal Cordillera from the mid-Miocene onwards (Riquelme et al., 2003). Within the study area, normal and reverse movements along the Puerto Aldea Fault controlled deposition of the Coquimbo Formation (Le Roux et al., 2006). The shore platforms T_I and T_{II} from the Altos de Talinay area (~679 and 317 ka, respectively) (Figs. 2, 3) are cut by the Puerto Aldea and Quebrada del Teniente faults showing normal displacements (Saillard et al., 2009).

3. Geomorphic description

We have mapped the marine and continental landforms using field analyses, satellite images and digital elevation models (Fig. 3). We used the Landsat ETM panchromatic band (spatial resolution of 15 m) and digital elevation models based on the Shuttle Radar Topography Mission (SRTM) data, with a spatial resolution of 3 arc sec (90 m) and a vertical resolution of 10 m (Farr et al., 2007). We followed the procedure described by Regard et al. (2010) to determine the shoreline angle elevation of marine landforms. The procedure consists of using the SRTM digital elevation models (DEMs) to generate several topographic cross-sections perpendicular to the coast in locations where the shore platforms are devoid of sediment cover.

Within the study area between El Teniente Bay and Papudo, there is a sequence of four shore platforms (Paskoff, 1970; Saillard, 2008; this work, Fig. 3). Among these surfaces, the highest shore platform is continuous over 170 km and laterally connected with a high fluvial terrace and a pediment outcropping in the main river valleys including the Teniente, Choapa and Quilimarí valleys (images 1, 2 and 3 of Fig. 3, respectively).

3.1. Marine landforms

As previously mentioned, four shore platforms are preserved in the study region (Fig. 4 Profile B–B′), among which the highest one, herein named T_0, laterally connects with continental landforms throughout the main river valleys (Fig. 4). The T_0 surface is carved mainly onto Jurassic granitoids and Triassic marine and silicic volcanic rocks and secondarily onto Miocene to Pleistocene marine deposits and Paleozoic metamorphic and sedimentary rocks (Fig. 2). Although faulted and incised, this shore platform extends continuously, from El Teniente Bay in the north, to Papudo, in the south (Fig. 4). Between El Teniente Bay and Huentelauquén, T_0 width varies between ~6.5 and 3 km, narrowing towards the south and reaching a minimum of ~0.3 km at Pichidangui Bay (Fig. 4, Profiles A–A′ and B–B′, respectively). T_0 corresponds to a composite feature comprising two to three secondary levels, T_{0a}, T_{0b} and T_{0c} (Fig. 4, profiles B–B′ and A–A′ and Fig. 5a and b). The transition between T_{0a} and T_{0b} is marked by a smooth scarp (Fig. 4, profile A–A′). In contrast, the border between T_{0b} and T_{0c} is more abrupt south of Caleta Maitén to Punta Arena (Fig. 5a, b) and between Punta Blanca and Caleta Manso, becoming more gradual south of Caleta Manso (Fig. 5d). In the areas where the border between T_{0b} and T_{0c} is abrupt, this transition seems to be controlled by activity along NNW–SSE faults (Figs. 4, 5a, b). South of Huentelauquén the scarp between T_{0b} and T_{0a} disappears and T_{0a} is no longer recognized, except near the Pichidangui Bay where pieces of T_{0a} are preserved as erosional remnants (Fig. 5d). Landward, T_0 is limited by a series of NNW–SSE and N–S trending faults between El Teniente Bay and Punta Blanca (Figs. 4, 5a, b), whereas at the south of Punta Blanca it is usually backed by a cliff or directly connects with a high fluvial terrace or a pediment (Fig. 5c). Oceanwards, T_0 is limited by a former sea cliff and bounded by one to three lower levels of shore platforms (Fig. 4 Profiles B–B′ and A–A′). According to Paskoff (1970), the shore platforms to the west of T_0 would correlate with the three lower marine terraces in the Altos de Talinay area, corresponding to the shore platforms T_{III}, T_{IV} and T_V later described and dated by Saillard et al. (2009) (Fig. 4 Profiles B–B′). In particular, T_{III} corresponds to a distinct broad marine landform which based on its elevation between 30 and 60 m amsl, could also be correlated to the lower *rasa* level described by Regard et al. (2010) (Fig. 4 Profiles B–B′).

Although the shoreline angle of T_0 is often obscured by NNW–SSE and N–S faults and colluvial deposits at its inner edge, we measured the shoreline angle elevation where possible obtaining a highly variable value between 370 and 190 m amsl. Although the borders between the different secondary levels of the T_0 are not marked by a clear scarp, we measured the shoreline angle elevation of each level T_{0a}, T_{0b} and T_{0c} where possible. The value obtained for T_{0a} ranges from 370 to 300 m amsl between El Teniente Bay to Huentelauquén, whereas near the Pichidangui Bay the higher elevations reach by the erosional remnants of T_{0a} correspond to 300 m amsl. For the shoreline angle elevation of T_{0b} and T_{0c}, we obtained values ranging from 205 to 170 m amsl and 120 to 90 m amsl, respectively.

3.2. Continental landforms

A high fluvial terrace and a pediment outcropping at the lower and middle courses of the river valleys between the El Teniente and La

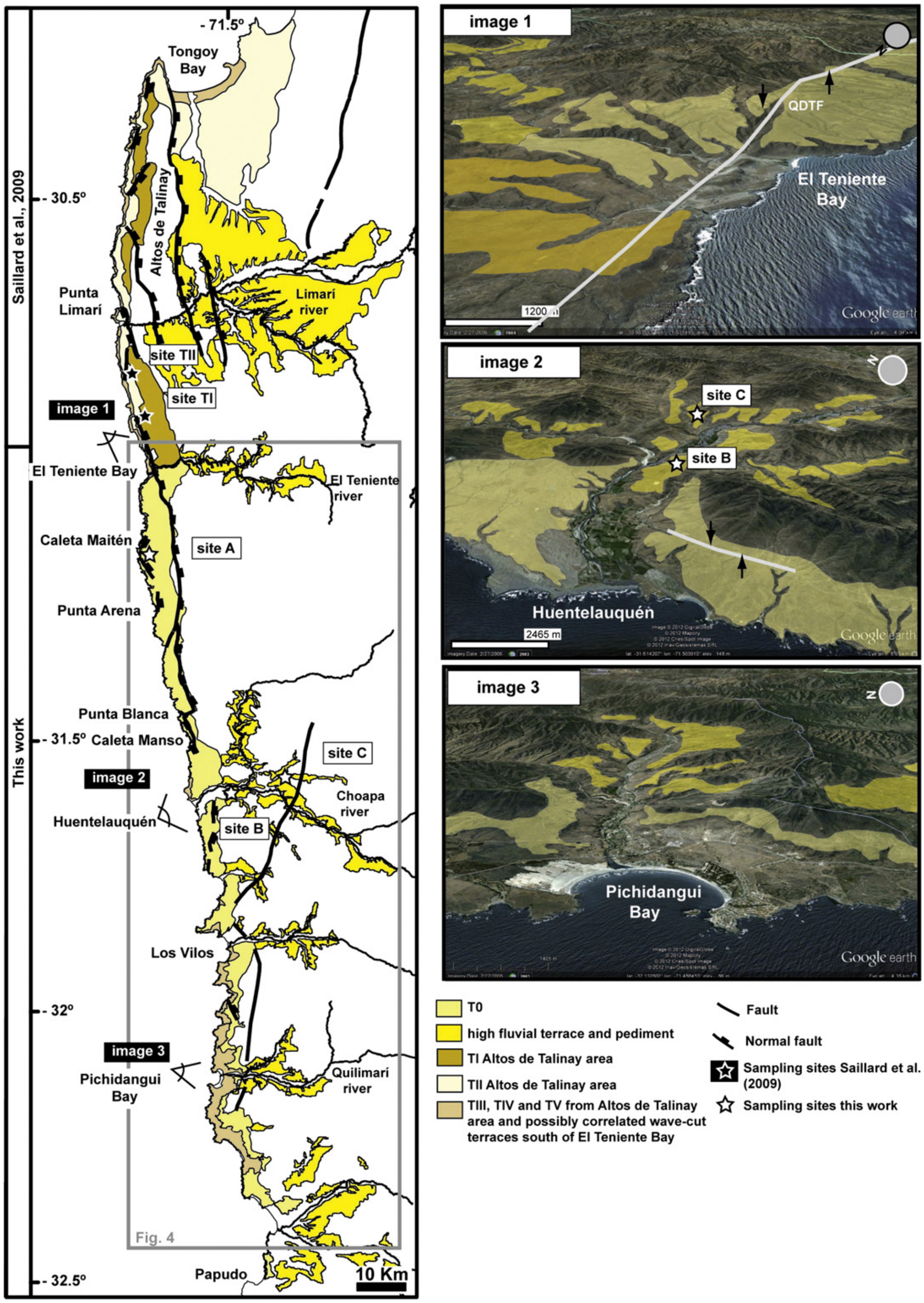

Fig. 3. Geomorphological map between the Tongoy Bay and Papudo. Between Tongoy and El Teniente Bay the map was modified from Saillard et al. (2009) and Paskoff (1970). From El Teniente Bay southwards the shore platforms and the continental planation surface formed by the high fluvial and pediment were mapped in this work. Images 1, 2 and 3 taken from Google Earth show the morphological connection between T_0 and the continental planation surface throughout El Teniente, Choapa and Quilimarí river valleys, respectively. White lines show the position of the main faults.

Ligua rivers, are systematically connected with the shore platform T_0 (Figs. 3, 6). Within each valley the high fluvial terrace is located close to the present-day river channel and grades into the pediment near the valley walls (Fig. 6). In the Tongoy Bay area, the high fluvial terrace is thought to correspond to an erosive rather than an aggradational feature, as its spans various lithological types, including the fluvial gravels of the Confluencia Formation (Paskoff, 1970; Heinze, 2003). Similarly, within the valleys of the study region south of Bahía Teniente, the high fluvial terrace corresponds to a planar surface carved into unconsolidated Miocene to Pleistocene gravels of the Confluencia Formation (Fig. 7c), Jurassic granitoids, Paleozoic metamorphic rocks (Fig. 7d) and Triassic volcanics. A discontinuous gravel cap rests on top of the planar surface, which is an usual feature in degradational fluvial terraces (e.g. Burbank and Anderson, 2001;

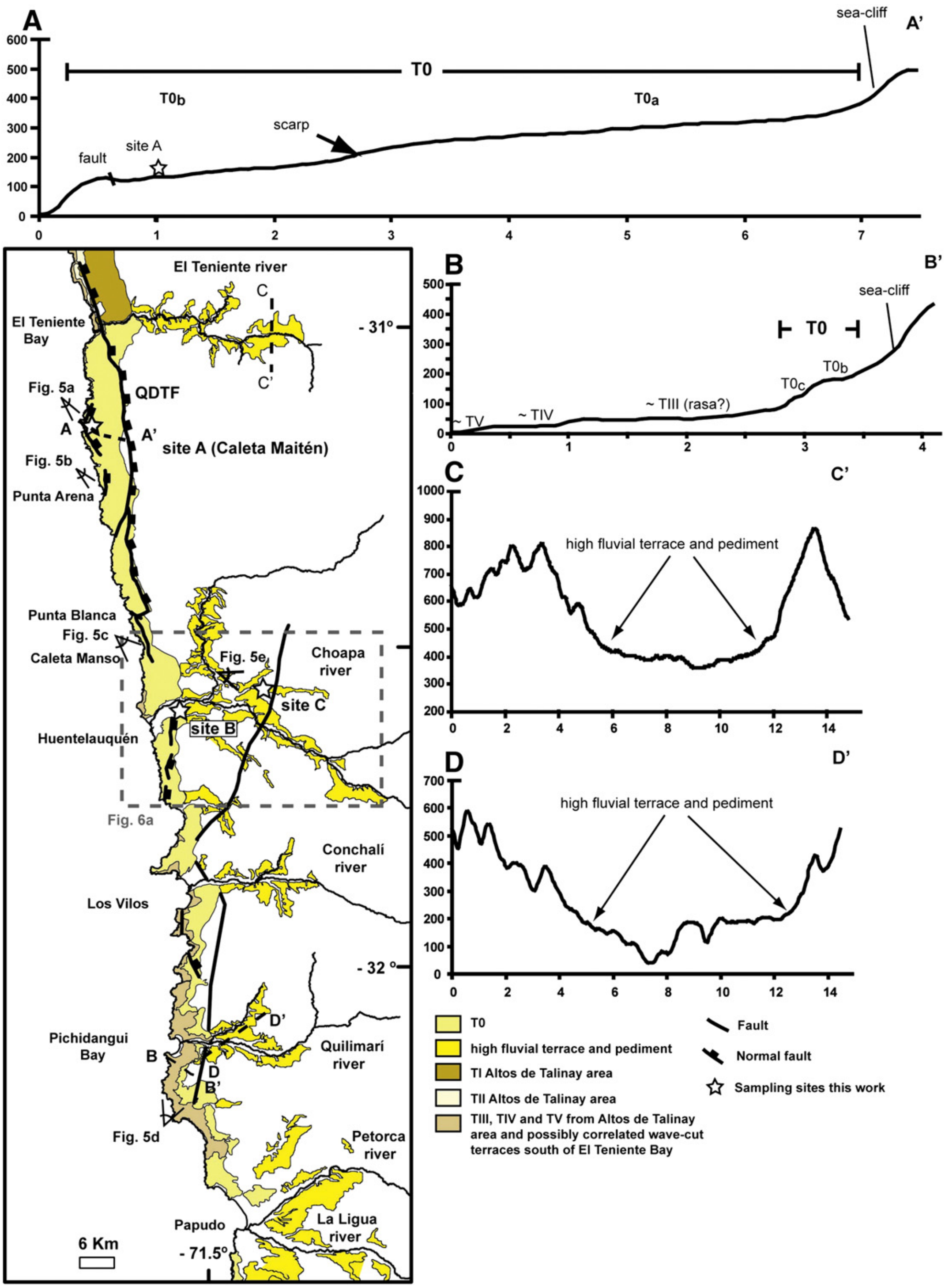

Fig. 4. Geomorphological map of the study region between El Teniente Bay and Papudo. Dashed lines mark the trace of topographic profiles. The horizontal scale in profiles A–A′ and B–B′ differs from the horizontal scale in profiles C–C′ and D–D′. QDTF = Quebrada del Teniente Fault.

DeVecchio et al., 2012; Karlstrom et al., 2012; Schildgen et al., 2012) (Fig. 7e). In turn, the pediment consists of granitic angular cobbles and boulders floating on a white to red weathered layer of a few tens of centimeters thick of Jurassic granitoids (Fig. 7a). This layer connects towards the center of the valleys with the gravel cap covering the high fluvial terrace (Fig. 5e, f). According to the geomorphic and sedimentological connection between the high fluvial terrace and the pediment we interpret them as corresponding to a single continental planation surface.

From El Teniente to La Ligua rivers, the highest elevation of the continental planation surface diminishes from ~400 m amsl in El Teniente valley (Fig. 4 Profile C–C′) to ~350 m amsl in the Choapa valley, ~200 m amsl in Quilimarí valley (Fig. 4 Profile D–D′), and ~180 m amsl in La Ligua valley. Within each river valley the elevation of the surface can be highly variable from the present-day channel towards the valley walls. This high variability is easily observed in the broad surfaces of the Choapa river valley, which range over ~100 m of relief from the present-day channel to the valley wall (Fig. 6a).

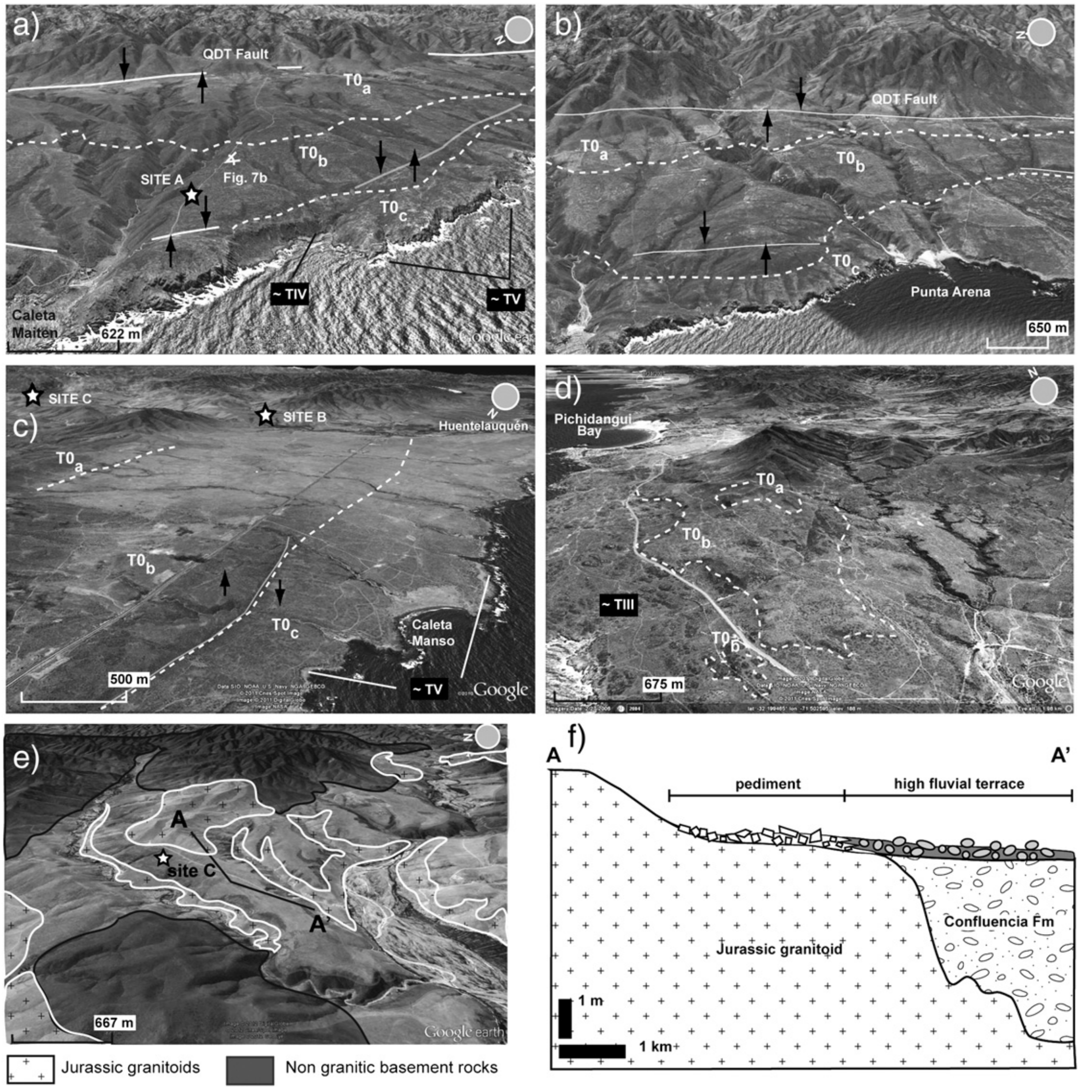

Fig. 5. Google Earth's images of T_0 and the pediment, location in Fig. 4. T_0 images looking from a) southward from Caleta Maitén b) southward from Punta Arena c) southward from Caleta Manso and d) northward towards the Pichidangui Bay. Dashed lines mark the scarp between secondary levels T_{0a}, T_{0b} and T_{0c} of T_0. White lines show the position of main faults after Rivano and Sepúlveda, 1991. White stars show the samples' locations. e) Image of the pediment in the vicinities of sampling site C. Basement outcrops shown in transparency. White stars show the samples' locations. f) Schematic profile showing the connection between the pediment and the high fluvial terrace. Location of profile A–A′ in Fig. 5e).

4. Methodology and sampling location

Cosmogenic nuclides formed in situ by the interaction of cosmic rays with the nucleus of atoms in minerals near the surface of the earth. Where quartz is abundant, cosmogenic ^{10}Be and ^{26}Al are useful radionuclides for determining surface exposure ages and rates of superficial processes during the ~Pleistocene to Recent (e.g. Nishiizumi et al., 2005; Álvarez-Marrón et al., 2008; Saillard et al., 2009). We collected bedrock, cobble and pebble samples at three different sites for the main shore platform in the study area T_0, the high fluvial terrace, and the pediment (Fig. 8). Samples were crushed and sieved to obtain the 250–1000 μm fraction. Mineral separation was obtained according to standard laboratory techniques in the Mineral Separation Laboratory of the Geology Department of University of Chile. Samples collected from T_0 (site A) were prepared at UCSC (USA) and measured at the AMS facility of the LLNL (USA). Samples collected from the high fluvial terrace and the pediment (sites B and C) were prepared and measured at the ASTER AMS facility of the CEREGE (France). All samples were calibrated directly against the National Institute of Standards and Technology standard reference material 4325 by using the values determined by Nishiizumi et al. (2007). We used the CRONUS-Earth online cosmogenic-nuclide calculator to calculate ^{10}Be zero erosion-exposure ages (Balco et al., 2008). Time-independent production rates were scaled using factors from Lal (1991) and Stone (2000), integrated over sample thickness and corrected for topographic shielding when necessary (for details on the parameters used for age calculation using the CRONUS-Earth calculator see the Supplementary data). The reported uncertainty in age calculation corresponds to the external error calculated by the CRONUS-Earth calculator. The external error includes both the analytical uncertainty in nuclide concentration measurement and the uncertainty in the nuclide production rate (Balco et al., 2008). When surfaces that are presumed to have been uplifted are dated using cosmogenic nuclides techniques, it is necessary to make a correction in age calculation related to the increase in the production rate of the radionuclide with elevation (Lal, 1991). The extreme case in which the surface spent a long time at low elevations and was only recently uplifted represents the largest production rate variation possible. Considering an uplift of ~150 m, the ^{10}Be production rate rises up ~12% with respect to the production rate used here in to calculate ^{10}Be exposure ages. However, as the ~12% increase in ^{10}Be production rate

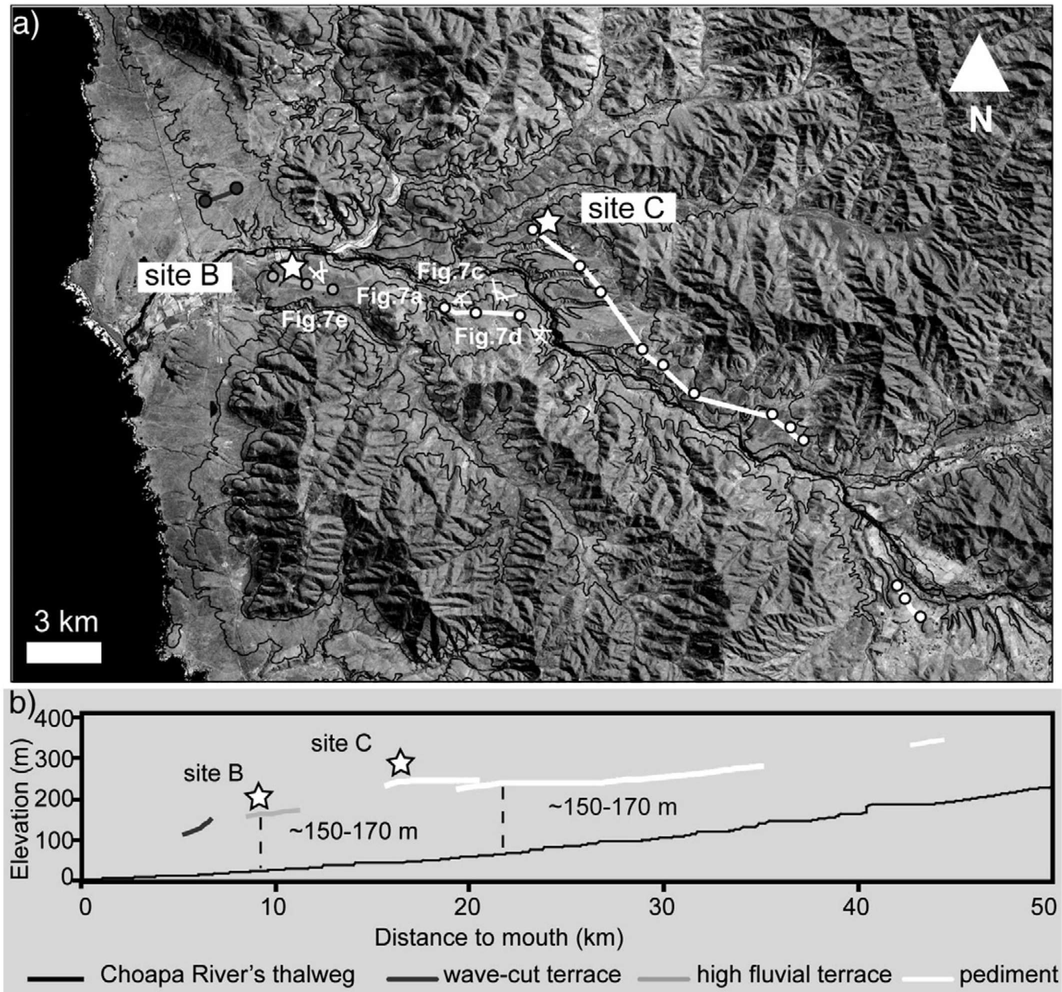

Fig 6. a) Enlarged portion of the Landsat ETM image (panchromatic band) showing the lower and middle courses of the Choapa river valley. White stars show sampling site locations. Dots show measured points use to construct elevation profiles of the rasa (dark gray line), the high fluvial terrace (pale gray line) and the pedimentation surface (white line) from Fig. 6b. The black thick solid line corresponds to Choapa river's thalweg, black thin solid lines are elevation curves every 100 m. b) Elevation profiles for the rasa, the high fluvial terrace, the pedimentation surface and the Chopa River's thalweg.

corresponds to a maximum value and as we have taken into account the external error that is generally higher than 10%, the uncertainty related to uplift is already considered in our age error bars.

Samples for cosmogenic dating of T_0 were collected at site A, near the locality of Caleta Maitén and ~17 km further south of El Teniente Bay. We followed the assumptions described by Saillard et al. (2009) for shore platforms of the Altos de Talinay area by which CRN accumulation starts after terrace abandonment and erosion rate affecting the shore platform is near zero. Therefore, only ^{10}Be concentrations were determined for T_0, as an $^{26}Al/^{10}Be$ approach is more useful when more complex histories including burial and re-exposure are expected (Lal, 1991). In Caleta Maitén the shore platform T_0 is ~6 km wide and is carved into granitic rocks (Fig. 4 Profile A–A′). The scarce sedimentary material associated to T_0 corresponds to angular quartz-rich granitic cobbles and boulders resting on top of the bedrock surface (Fig. 8a). Landwards, T_0 is limited by the east verging NNW–SSE trending Quebrada del Teniente Fault (Figs. 4, 5a, b; Paskoff, 1970; Saillard et al., 2009) that vertically offsets the platform by 40 m south of El Teniente Bay (Ota et al., 1995). This sampling site was chosen because the morphological correlation of T_I from the Altos the Talinay with T_0 at this site is clearer than with T_0 further south (Fig. 4). Here we could easily interpret the lateral connection of T_I with T_0. Samples from site A were collected from the secondary level T_{0b} at 120 m amsl and ~600 m towards the east of the outer edge of T_0 (Fig. 5a). Samples from the T_{0a} were also collected, but did not contain enough quartz to analyze. One sample from site A (MS18_1) is a collection of thin pieces (~5 cm thick) chiseled from the top of a bedrock outcrop (Fig. 7b) and the other two samples from this site (MS18_3 and MS18_4) are thin pieces (~5 cm thick) chiseled from the top of granitoid angular cobbles (~15 cm diameter) lying on top of T_0 (Fig. 8a). In turn, samples for ^{26}Al and ^{10}Be analysis from the high fluvial terrace and the pediment were collected within the Choapa river basin where the surfaces are best preserved (Fig. 6a). At site B, pebbles were sampled from the discontinuous gravel cap on top of the high fluvial terrace at ~150 m amsl carved into the Confluencia Formation (Fig. 3, Image 2 and Fig. 7e). Samples from site B correspond to individual spherical decimetric rounded pebbles (Table 1; CH1, CH2, CH6) and one amalgamated sample made up of a mix of twelve individual decimetric rounded pebbles (Fig. 8b, Table 1; CH0). Whereas the individual samples correspond to granitic pebbles, the amalgamated sample is formed by pebbles of volcanic and granitic origin. The individual pebbles were collected in order to evaluate the scattering in ^{10}Be and ^{26}Al concentrations. The amalgamated sample was collected for the purpose of obtaining an average ^{10}Be and ^{26}Al concentration for the surface. At site C, we sampled a bedrock pediment located at an elevation of ~220 m amsl and composed of a regolith layer ~50 cm

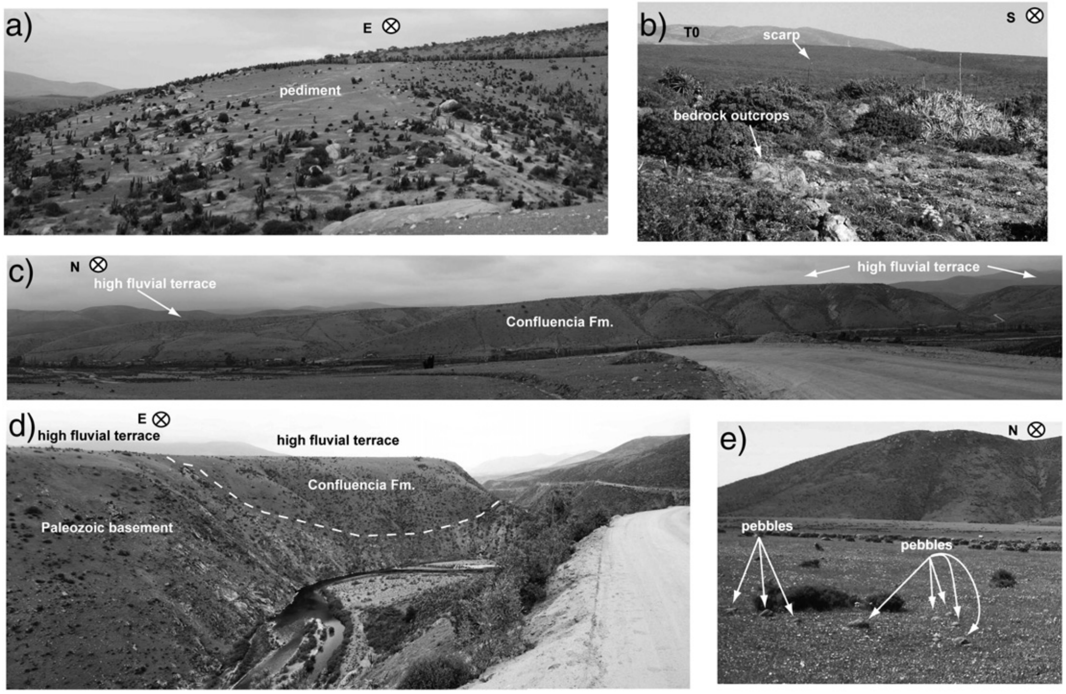

Fig. 7. Photos from continental and marine landforms in the Choapa river valley, photo locations in Figs. 6a and 5a. a) Pediment in the Choapa Valley. b) Sampled rasa at site A. c) Strath terraces from the Choapa Valley. d) High fluvial terrace carved into basement outcrops and gravels from the Confluencia Formation in the Choapa Valley. e) Sampled high fluvial terrace at site B.

thick into Jurassic granitoids (Fig. 6a, b). The samples collected from the pediment at site C are decimetric angular quartzite clasts from the regolith layer (Fig. 8c).

5. Results

The ^{10}Be concentrations range mainly between 1.4×10^6 and 3.6×10^6 atoms/g qz in the three sites with an average concentration of 2.19×10^6 atoms/g qz and a standard deviation of 6.01×10^5 (Table 1, Fig. 9). At site A, the ^{10}Be concentrations of the three samples from T_0 yield a similar age for two samples and a much older age for the third sample (Table 1). The sample from the bedrock yields a zero erosion model age of 523.8 ± 53 ka and the samples from the angular cobbles lying on top of T_0 yield zero erosion model ages of 550.8 ± 57 ka and 806.9 ± 88 ka (Table 1). At site B, ^{10}Be concentrations of the high fluvial terrace samples show great differences among the individual samples CH1, CH2 and CH6 and with the mean ^{10}Be concentration of the amalgamated sample CH0 (Table 1). The ^{10}Be concentration of CH0 is lower than those of the individual pebbles (Table 1). The scattering among the ^{10}Be concentrations of the terrace samples could have been produced either before deposition of the clasts at site B or after by mixing of the surface layer. In order to evaluate the complexity of the exposure histories for samples at site B, ^{26}Al/^{10}Be and ^{10}Be concentrations of these samples were plotted on a two nuclide diagram (Fig. 10). Samples plotting inside the "steady-state erosion island" of Lal (1991) are consistent with a model of continuous and constant exposure, corresponding to a balance between production and loss by erosion and radioactive decay. Samples plotting below the island have experienced a more complex history possibly including repeated episodes of burial and exposition, or unsteady erosion of the land surface. Two samples from site B show an unrealistic deficit in ^{26}Al compared to ^{10}Be (CH1, CH2). Such low ^{26}Al concentrations cannot be explained by any geological model. Even if these samples would have been buried very deep ($\gg 4$ m) for 10 Ma, they would have also experienced ^{10}Be loss which would yield a higher ^{26}Al/^{10}Be ratio than measured here (for further details see Supplementary data). Other unpublished studies have found unrealistic ^{26}Al concentrations (D. Bourlès and R. Braucher, personal communication), which remain to be explained. We present this ^{26}Al data only for future discussion about this problem. At site C, ^{10}Be concentrations of the pediment samples also show significant differences (Table 1). Except for sample CH7 which shows an unrealistically low ^{26}Al concentration, the five other samples are located within or slightly below the steady-state island shown in Fig. 10. According to their position inside the steady state island, samples CH11, CH12 and CH13 could have suffered a single stage exposure history. On the contrary, samples CH8 and CH10 from site C are located below the steady state island indicating a more complex exposure history and unsteady erosion. In accordance with the large spread in cosmogenic nuclide concentrations, the ^{10}Be zero erosion model ages calculated for the pediment samples range between 327.4 and 615.9 ka. The maximum erosion rates that the single stage exposure samples CH11, CH13 and CH12 could have suffered are 1.3, 1.7 and 2.0 m/Ma, respectively. To recalculate exposure ages for erosion rates higher than zero for these samples, we need to use erosion rates lower than the lowest value among these three, namely, 1.3 m/Ma. Thus, in order to visualize how much the exposure ages of the mentioned samples would change if erosion was greater than zero, we used erosion rates of 0.5 and 1 m/Ma that are lower than 1.3 m/Ma and higher than the erosion rates calculated for alluvial fans in the hyper-arid Atacama Desert (0.03 to 0.36 m/Ma, Nishiizumi et al., 2005) to calculate the exposure ages of the single stage exposure samples, obtaining ages ranging from 383.0 to 596.4 ka and from 475.4 to 944.5 ka, respectively (Table 1).

6. Discussion

6.1. Interpretation of surface ages

At site A, it would be expected that if the cobble had a significant pre-exposure prior to being deposited, it would have a significantly higher ^{10}Be inventory relative to the bedrock upon which it sits. Thus,

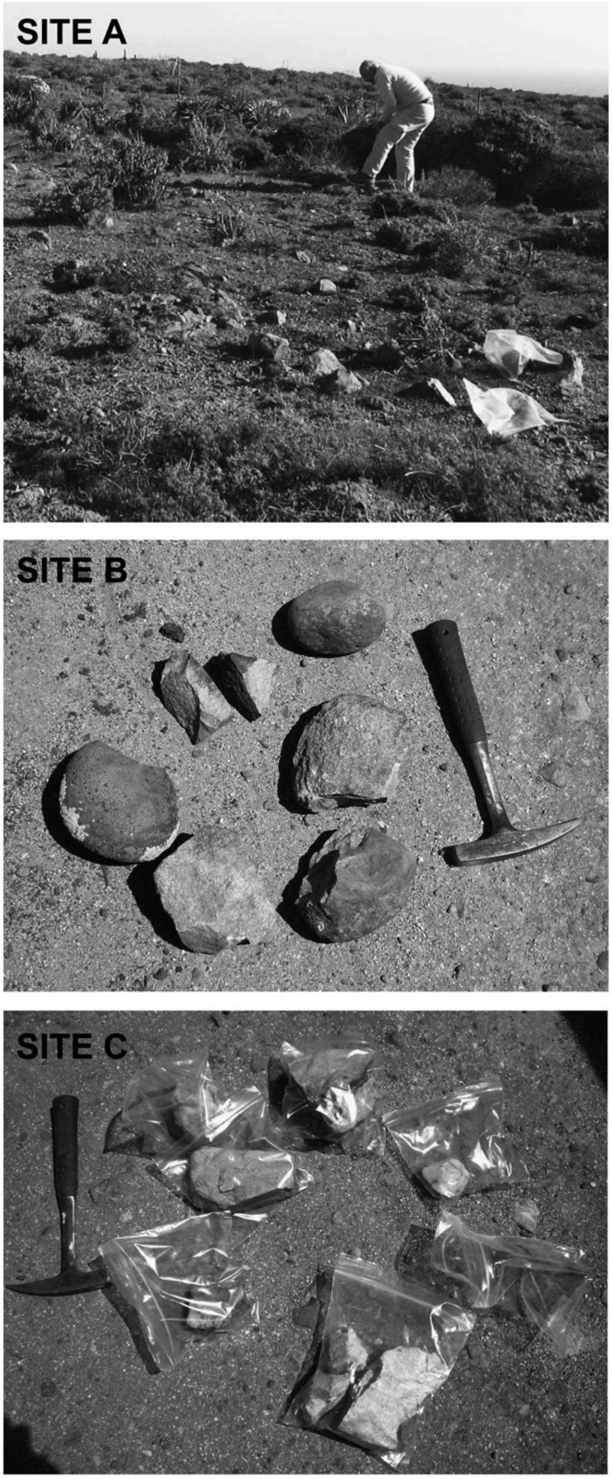

Fig. 8. Samples collected from T_0 at site A (only the cobbles, bedrock samples not shown), the high fluvial terrace at site B and the pediment at site C.

the concordance between the ages of the bedrock sample (MS18_1, 523.8 ± 53 ka) and one of the cobbles (MS18_3, 550.8 ± 57 ka), suggests that the inheritance in the cobble sample is insignificant. Importantly, under marine or continental erosion conditions, the cobble should be eroded more easily than the bedrock and the fact that both samples have similar ^{10}Be concentrations indicates erosion at the sampling site has been negligible since ~500 ka. The higher ^{10}Be content of the other cobble (MS18_4, 806.9 ± 88 ka) with respect to the other two samples indicates that this sample has a significant inherited component of ^{10}Be. This sample was collected several meters to the west of the inner edge of T_0 and away from any active channel (Figs. 5a, 8d), so it is unlikely that it was eroded and transported from a higher elevation after ~500 ka. However, its angular shape is consistent with a limited transport to the sampling locality. A more probable explanation may be that T_0 was eroded during several sea-level highstands and this ~800 ka cobble may have been deposited on the higher level (T_{0a}) during an older sea-level highstand. Following this older sea-level highstand, T_0 may have been reoccupied and eroded by the sea sometime between ~800 and 500 ka, cutting a new secondary level (T_{0b}) within the original surface. This interpretation is supported by the presence of a smooth scarp separating the secondary T_{0b} level from the higher secondary level T_{0a} (Fig. 4 Profile A–A′ and Fig. 5a, b) at the location where samples were collected. Thus, the ~800 ka cobble could have been remobilized, transported a short distance, which would explain its high angularity, and deposited at the sampling site by ~500 ka.

At site B, analyzed samples correspond to rounded clasts on top of a planar surface cut onto the Miocene–Pleistocene Confluencia Formation, a deposit consisting of sand to pebble sized clasts. Accordingly, scatter among the ^{10}Be concentrations may be related to remobilization of older Confluencia Formation clasts exposed during the Miocene–Pleistocene (high ^{10}Be concentrations) and/or to the re-exposure of older Confluencia Formation clasts that were buried and exhumed through erosion of the surface (low ^{10}Be concentrations). However, as samples were collected from a planar surface and away from gullies or any other indicator of channeled water flow (Figs. 6a, 7e), the remobilization or exhumation of older Confluencia Formation clasts by means of alluvial or fluvial erosion is unlikely. Thus, it is necessary to invoke an erosional process that could bring together in the same layer previously buried pebbles with surface pebbles preserving the planar morphology of the terrace. A probable explanation is that during the slow erosion of the surface finer sediments are blown by wind and washed out by infiltrated water while larger grain size particles in between are not removed but are mixed with similar grains originally located below and re-exposed due to removal of finer grains. Through time these processes finally lead to formation of a planar surface covered by a discontinuous gravel cap, which is morphologically similar to a desert pavement (Fig. 7e) (e.g. Matmon et al., 2009; Vassallo et al., 2011), but in a semiarid climate where more water is available. Consequently, pebbles with high ^{10}Be concentration exposed since the beginning of the fluvial terrace formation are mixed with pebbles with low ^{10}Be concentration exhumed recently. In this case, assuming no inheritance-related ^{10}Be concentrations, the clast presenting the highest ^{10}Be concentration gives the most accurate age of the geomorphological marker (Vassallo et al., 2011), namely 1120.2 ± 127 ka (Table 1). Our surface data do not allow us to be more conclusive, but our preferred scenario implies that this marker is several hundreds of thousand years old.

At site C, as previously stated, we have recognized two groups of samples according to their position inside the 'steady state island'. On one hand, samples CH11, CH12 and CH13 would have suffered a continuous and steady exhumation, and on the other hand, samples CH8 and CH10 would have suffered a more complex burial/exposure history (Fig. 10). Sampled pebbles are angular and located ~1 km downslope of a hill corresponding to the only outcrops of granitoids in the vicinities of site C (Fig. 5e). This implies that these samples have a local origin (no transport along a river system), and were probably detached from the granitic basement and incorporated into the thin (~50 cm) regolith layer covering it (Fig. 5e, f). Therefore, inheritance at this site would be negligible and cannot explain the scattering among ^{10}Be concentrations. One geological process that could explain the differences among the two groups of samples corresponds to soil creep within the regolith. Soil creep involves independent and random vertical displacements of grains that are reburied or

Table 1
^{26}Al and ^{10}Be concentrations and exposure ages for samples at sites A, B and C.

Sample name	Lithology/thickness (cm)	[^{10}Be] (atoms/g qz)	+/− (atoms/g qz)	[^{26}Al] (atoms/g qz)	+/− (atoms/g qz)	Minimum Be exposure age (ky)	External error (ky)	0.5 m/My Be exposure age (ky)	External Error (ky)	1 m/My Be exposure age (ky)	External error (ky)
Site A											
Rasa											
MS18_1	Granite/5 cm	1,900,000	34,000	–	–	523.8	53	–	–	–	–
MS18_3	Granite/5 cm	2,000,000	48,000	–	–	550.8	57	–	–	–	–
MS18_4	Granite/5 cm	2,700,000	49,000	–	–	806.9	88	–	–	–	–
Site B											
Strath terrace											
Amalgamated											
CHO	Granitic and andesitic pebbles/5 (media)	1,600,000	52,000	3,900,000	270,000	419.6	43	–	–	–	–
Individual clasts											
CH1	Granitic pebble/10	2,800,000	78,000	760,000	120,000	826.7	93	–	–	–	–
CH2	Granitic pebble/7	3,600,000	100,000	210,000	47,000	1120.2	137	–	–	–	–
CH6	Granitic pebble/10	2,200,000	84,000	3,400,000	710,000	630.6	70	–	–	–	–
Site C											
Pediment											
CH7	Granite/3	2,400,000	74,000	2,000,000	200,000	615.9	66	892.6	157	–	–
CH8	Granite/5	2,200,000	44,000	11,000,000	510,000	567.4	58	786.3	123	–	–
CH10	Granite/7	2,300,000	42,000	11,000,000	370,000	612.3	64	883.8	149	–	–
CH11	Granite/5	1,900,000	39,000	10,000,000	360,000	466.2	47	596.4	81	944.5	276
CH12	Granite/5	1,400,000	24,000	7,400,000	290,000	327.4	32	383.0	44	475.4	73
CH13	Granite/10	1,500,000	27,000	8,900,000	330,000	383.0	37	463.2	57	617.7	115

eroded by overland flow or other processes upon reaching the surface (Heimsath et al., 2002). Although this type of mechanism was originally described to affect quartz grains <1 mm within a mature soil profile (Heimsath et al., 2002), vertical mixing of decimeter-scale pebbles over a depth of 0.5 to 1 m have been observed at the surface of alluvial terraces using cosmogenic nuclide concentrations (e.g. Le Dortz et al., 2011). According to this process, the most concentrated samples have the longer burial-exhumation history. This is what is observed with the samples CH8 and CH10, which exhibit the higher ^{10}Be concentrations and also the more complex exposure history. For the complete sample suite the large range of zero erosion exposure ages (327.4 to 615.9 ka) and exposure ages with erosion rate of 1 m/Ma (475.4 to 944.5 ka) calculated for the single stage samples show that this surface has evolved during a long time span before being incised and abandoned.

6.2. Long period of tectonic stability

The large range of ^{10}Be concentrations obtained for each type of landform is consistent with the geomorphic characteristics we have previously described for each feature. We interpret the ^{10}Be ages between ~800 and 500 ka to indicate that T_0 is a polygenetic landform formed during several sea-level highstands. This conclusion is consistent with its composite nature and with the fact that a long time period is necessary to form such a broad erosional bedrock surface. Secondary levels within T_0 suggest that the coast was uplifted during T_0 formation, but the lack of secondary levels without sharp separations by scarps suggests that the uplift rate was slow, thus allowing marine reoccupation. Importantly, the dated samples were collected ~600 m towards the east of the outer edge of T_0 and in a locality where only the two higher secondary levels, T_{0a} and T_{0b}, are preserved. Therefore, T_0 was uplifted strictly after ~500 ka at site A and even later towards the south where the lower level T_{0c} is almost always preserved. The spread in the ^{10}Be concentrations from the high fluvial terrace samples is consistent with the geomorphic characteristics of this landform in the valleys of north central Chile. Indeed, a long period of undisturbed lateral erosion or slow surface lowering would be necessary to carve such a broad surface. Slow surface lowering is the most consistent explanation according to our interpretation of cosmogenic concentrations for the high fluvial terrace

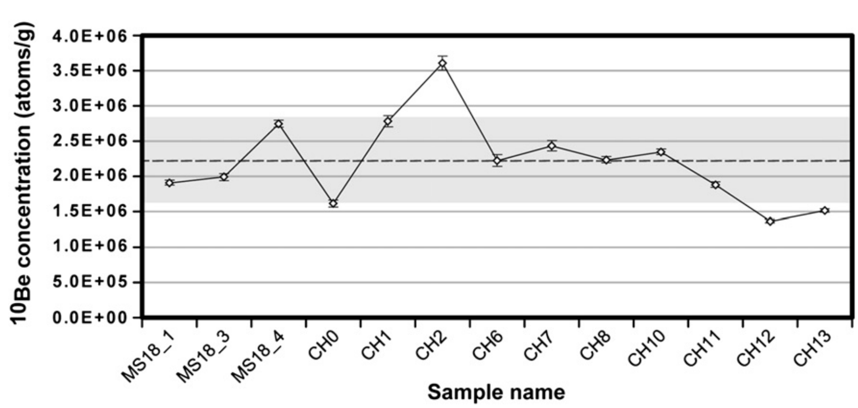

Fig. 9. ^{10}Be concentrations for the samples collected from T_0, the high fluvial terrace and the pediment. The dash line shows the average ^{10}Be concentration of all samples from the three sites. The gray fringe shows the standard deviation with respect to the average value.

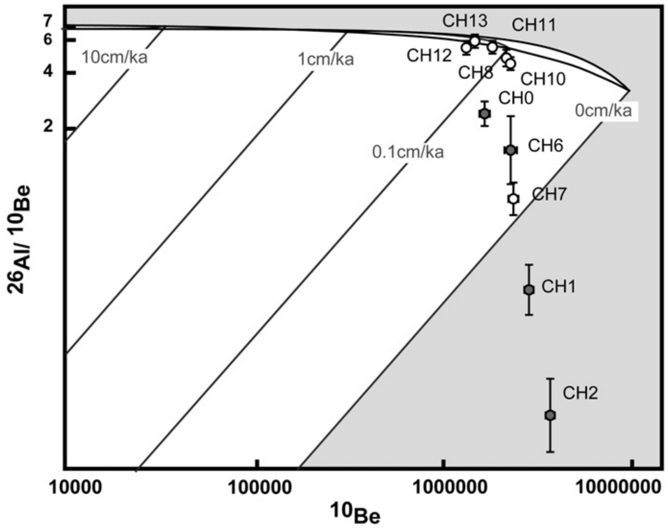

Fig. 10. $^{26}Al/^{10}Be$ diagram for samples from the high fluvial terrace (site B, dark gray) and from the pediment (site C, white) throughout the Choapa river basin. The steady state erosion island corresponds to the area between black solid lines. The forbidden zone for ^{26}Al and ^{10}Be concentrations is in light gray.

in Section 6.1. Although it is difficult to constrain the age of the high fluvial terrace at site B, it is interesting to note that the ^{10}Be concentrations are of the same order of magnitude as those obtained on T_0 at site A (Fig. 9, Table 1). ^{10}Be concentrations of the pediment at site C are also of the same order of magnitude as the ^{10}Be concentrations of T_0 at site A and the high fluvial terrace at site B (Fig. 10, Table 1). This similarity is consistent with the clear morphologic correlation between these three features and suggests that the marine and continental surfaces correspond to one regional geomorphic marker formed coevally during several hundreds of thousand years during the Pleistocene. This geomorphic marker possibly started to form after 1.2 Ma when deposition of the Coquimbo and Confluencia formations resumed (Le Roux et al., 2006) and based on the ages obtained for T_0 at site A and the minimum exposure ages ~300 ka obtained for the pediment at site C, was uplifted after ~500 ka southwards from El Teniente Bay. Considering an erosion rate of 1 m/Ma, that is close to the maximum erosion rate that the pediment samples could have experienced, the youngest age obtained for the pediment is ~475 ka (CH12). This age is very close to the lowest age of T_0 and reinforces the notion that the continental and marine landforms formed synchronously during the Lower and Middle Pleistocene between ~(1200?) 800 and 500 ka and uplifted post-500 ka.

Throughout the Choapa valley, the elevation of the continental planation surface formed by the high fluvial terrace and the pediment above the present-day river channel indicates that the post-500 ka uplift is around 150 m (Fig. 6b). The uplifted geomorphic marker composed of the continental planation surface and T_0 extends for over 40 km in a west–east direction (Fig. 6b). The uplifted area does not present any clear spatial relationship with the El Romeral–Silla del Gobernador segment of the AFS, which would have accommodated Quaternary uplift of the western area of the Coastal Cordillera north of study area (Riquelme et al., 2003) nor with any other main fault (Fig. 3).

6.3. Correlation with the rest of the Southern Central Andes

Correlating T_0 south of El Teniente Bay with the marine levels of Altos de Talinay is not straightforward. Image 1 in Fig. 3 shows how the shore platform T_I described by Saillard et al. (2009) north of El Teniente Bay is morphologically continuous with T_0 south of El Teniente Bay defined in this study. The continuity led the previous authors to correlate both landforms (see Fig. 4 in Saillard et al., 2009). However, the shoreline angle elevation recorded for T_I (425 ± 15 m) from the Altos de Talinay is higher than the one measured for T_{0a} and, consequently, the maximum age of ~800 for T_0 is larger than the exposure age of 679 ± 8 recorded for T_I (Saillard et al., 2009). However, T_I presents a maximum width of 7.5 km suggesting that it probably formed during more than one sea-level highstands (Saillard et al., 2009). Moreover, as samples for ^{10}Be dating of T_I in the Altos de Talinay area were collected at 241 m amsl and the shoreline elevation is at 425 ± 15 m amsl, T_I probably started to form earlier than 679 ± 8 ka, which could be consistent with the older age of ~800 ka for T_0 south of El Teniente Bay. According to the model of tectonic uplift in the Altos de Talinay area (Saillard et al., 2009), just after formation of T_I around 679 ± 8 ka (~MIS 17), coastal uplift rates were rapid compared to the magnitude of sea-level rise preserving this platform after the subsequent highstand. The T_{II} shore platform in the Altos de Talinay formed during MIS 9c (~321 ka; Saillard et al., 2009). We do not really know what happen between MIS 17 and MIS 9c (i.e. MIS 15 and 13) as no marine terraces are preserved, thus plausibly slow coastal uplift (Saillard et al., 2009) or subsidence occurred during this time. On the contrary, as no shore platform formed during MIS 9c south of El Teniente Bay, our data south of El Teniente Bay suggest that T_0 was probably continuously forming between ~800 and <500 ka at an uplift rate than was necessarily slower than in the Altos de Talinay. This suggests north–south variation of coastal uplift rates between the Altos de Talinay area and the region south of El Teniente Bay. The different tectonic histories in the two zones could be explained by the Quebrada del Teniente fault. The fault affects the T_{0a} level by 40 m near El Teniente Bay (Fig. 3; Ota et al., 1995; Saillard, 2008) and thus accommodated slip after T_{0a} formation. This is in good agreement with previous works suggesting that peninsulas, such as the Altos de Talinay, correspond to particular settings where the preservation of marine landforms is largely influenced by local tectonic forces (Delouis et al., 1998; Saillard, 2008; Saillard et al., 2009; Regard et al., 2010). However, despite local differences in shore platform preservation, both areas were uplifted after 400 ± 100 ka (later than ~321 ka in the Altos de Talinay area and later than 500 ka south of El Teniente Bay) after a period of slow uplift or subsidence extending between ~679 ka and ~321 ka in the Altos de Talinay and between ~800 and <500 ka south of El Teniente Bay. Consequently, the renewal of coastal uplift proposed by Regard et al. (2010) can be extended farther south of La Serena and into the study region, affecting the Central Andes forearc between 15 and 32.5° S.

In the Atacama Desert north of the study region, near El Salvador and Antofagasta (Fig. 1), Quaternary ages have also been obtained for continental landforms from the Central Depression (Nishiizumi et al., 2005; González et al., 2006). At Antofagasta, inactive alluvial fans from the eastern side of the Coastal Cordillera that yield an average ^{21}Ne age of 424 ± 151 ka are affected by several fault scarps associated with the AFS. Although these alluvial fans are not morphologically correlated with marine surfaces, deformation around ~400 ka is consistent with active tectonics affecting continental landforms located inland from the coast in the Antofagasta area as observed in the Choapa valley region. At El Salvador, samples collected from incised streams and bedrock samples from steep slopes within the Central Depression yield ^{10}Be exposure ages between 320 and 360 ka (Nishiizumi et al., 2005). Plausibly, these ages represent an erosive event in response to surface uplift around ~400 ka in the Central Depression of El Salvador area. Taken together, these ages suggest that the post-400 ka renewal of uplift could have also extended eastward from the coast in the Central Depression of northern Chile.

As explained earlier in the text, the uplifted area in the study region is not spatially related to major faults which could be responsible for surface uplift. We have also shown that Quaternary uplift of the marine and continental surfaces within the study region would be related to a regional coastal uplift recorded for the Central Andes forearc post-400 ka. Therefore, subduction-related processes such as underplating of subduction material and subduction erosion that have been usually used to explain uplift of shore platforms on a local extent cannot explain surface uplift within the study region. As stated by Regard et al. (2010), regional coastal uplift requires a mechanism operating at deep crustal or lithospheric levels such as subduction processes or lithospheric mantle dynamics. Therefore, in order to unravel the undersurface processes related to Quaternary uplift it is necessary to integrate the geomorphic data with geophysical data. Finally, as more data are needed to determine how the surfaces under study were uplifted, we can only generally refer to the uplift driving mechanism as subduction-related processes.

7. Conclusion

Regional geomorphic correlation between coastal and continental surfaces form a wide marker that has been uplifted ~150 m since formation. Given the similarity in the exposure ages of the three type of landforms studied here, these surfaces probably formed coevally along the coast and throughout the valleys between ~(1200?) 800–500 ka ago and could have been finally uplifted ca. 500 ka. Our results suggest that after a period of slow uplift or tectonic stability long enough to develop such a broad geomorphic marker, ~150 m of uplift occurred during the Pleistocene (post-500 ka). Our data extend farther south the results of Regard et al. (2010), and therefore extend the region of renewed or accelerated coastal uplift post-400 ± 100 ka southward for a continuous zone between 15° S and 32.5° S. In particular, in our studied region between 31° and 32.5° S, the geomorphic and chronologic correlation between marine and continental planation surfaces suggests that uplift affected not only the coast but also a wide band of ~40 km of the Western Andes.

Appendix A. Supplementary data

Supplementary data to this article can be found online at http://dx.doi.org/10.1016/j.geomorph.2012.09.003.

References

Allmendinger, R.W., González, G., 2010. Invited review paper: Neogene to Quaternary tectonics of the coastal Cordillera, northern Chile. Tectonophysics 495, 93–110.

Álvarez-Marrón, J., Hetzel, R., Niedermann, S., Menéndez, R., Marquínez, J., 2008. Origin, structure and exposure history of a shore platform more than 1 Ma in age at the coast of northern Spain: a multiple cosmogenic nuclide approach. Geomorphology 93, 316–334.

Anderson, R.S., Densmore, A.L., Ellis, M.A., 1999. The generation and degradation of marine terraces. Basin Research 11, 7–19.

Arabasz, W.J., 1971. Geological and Geophysical studies of the Atacama fault zone in northern Chile. Ph. D. Thesis, Geological and Planetary Science Department, California Institute of Technology, Pasadena, 275 p.

Balco, G., Stone, J., Lifton, N., Dunai, T., 2008. A complete and easily accessible means of calculating surface exposure ages or erosion rates from ^{10}Be and ^{26}Al measurements. Quaternary Geochronology 3, 174–195.

Beck, S., Barrientos, S., Kausel, E., Reyes, M., 1998. Source characteristics of historic earthquakes along the central Chile subduction zone. Journal of South American Earth Sciences 11, 15–129.

Benado, D.E., 2000. Estructuras y estratigrafía básica de terrazas marinas en sector costero de Altos de Talinay y Bahía Tongoy, implicancias neotectónicas. Departamento de Geología. Thesis, Departamento de Geología, Universidad de Chile, Santiago, 78 p.

Burbank, D., Anderson, R., 2001. Tectonic Geomorphology. Blackwell Science, Oxford.

Cahill, T., Isacks, B.L., 1992. Seismicity and shape of the Subducted Nazca Plate. Journal of Geophysical Research-Solid Earth 97, 17503–17529.

Charrier, R., Pinto, L., Rodríguez, M.P., 2007. Tectonostratigraphic evolution of the Andean Orogen in Chile. In: Moreno, T., Gibbons, W. (Eds.), The Geology of Chile. The Geological Society, London, pp. 21–114.

Clark, A.H., Tosdal, R.M., Farrar, E., Plazolles, A., 1990. Geomorphologic environment and age of supergene enrichment of the Cuajone, Quellaveco, and Toquepala Porphyry Copper-Deposits, Southeastern Peru. Economic Geology and the Bulletin of the Society of Economic Geologists 85, 1604–1628.

Delouis, B., Philip, H., Dorbath, L., Cisternas, A., 1998. Recent crustal deformation in the Antofagasta region (northern Chile) and the subduction process. Geophysical Journal International 132, 302–338.

DeVecchio, D.E., Heermance, R.V., Fuchs, M., Owen, L.A., 2012. Climate-controlled landscape evolution in the Western Transverse Ranges, California: insights from Quaternary geochronology of the Saugus Formation and strath terrace flights. Lithosphere 4, 110–130.

Emparán, C., Pineda, G., 2006. Geología del Area Andacollo-Puerto Aldea, Región de Coquimbo. Carta Geológica de Chile, Serie Geológica Básica

Farr, T.G., Rosen, P.A., Caro, E., Crippen, R., Duren, R., Hensley, S., Kobrick, M., Paller, M., Rodríguez, E., Roth, L., Seal, D., Shaffer, S., Shimada, J., Umland, J., Werner, M., Oskin, M., Burbank, D., Alsdorf, D., 2007. The shuttle radar topography mission. Antenna 1–33.

González, G., Dunai, T., Carrizo, D., Allmendinger, R., 2006. Young displacements on the Atacama Fault System, northern Chile from field observations and cosmogenic ^{21}Ne concentrations. Tectonics 25, 1–15.

Hall, S.R., Farber, D.L., Audin, L., Finkel, R.C., Mériaux, A.-S., 2008. Geochronology of pediment surfaces in southern Peru: Implications for Quaternary deformation of the Andean forearc. Tectonophysics 459, 186–205.

Hartley, A.J., May, G., Chong, G., Turner, P., Kape, S.J., Jolley, E.J., 2000. Development of a continental forearc: a Cenozoic example from the Central Andes, northern Chile. Geology 28, 331–334.

Hartley, A.J., Chong, G., Houston, J., Mather, A.E., 2005. 150 million years of climatic stability: evidence from the Atacama Desert, northern Chile. Journal of the Geological Society 162, 421–424.

Heimsath, A.M., Chappell, J., Spooner, N.A., Questiaux, D.G., 2002. Creeping soil. Geology 30, 111–114.

Heinze, B., 2003. Active intraplate faulting in the forearc of north central Chile (30°–31°S): implications from neotectonic field studies, GPS data, and elastic dislocation modelling. Geoforschungszentrum, Potsdam.

Herm, D., 1969. Marines Pliozän und Pleistozän in Nord und Mittel-Chile unter besonderer Berücksichtigung der Entwicklung der Mollusken-Faunen. Zitteliana 2 (159 p).

Karlstrom, K.E., Coblentz, D., Dueker, K., Ouimet, W., Kirby, E., Van Wijk, J., Schmandt, B., Kelley, S., Lazear, G., Crossey, L.J., Crow, R., Aslan, A., Darling, A., Aster, R., MacCarthy, J., Hansen, S.M., Stachnik, J., Stockli, D.F., Garcia, R.V., Hoffman, M., McKeon, R., Feldman, J., Heizler, M., Donahue, M.S., 2012. Mantle-driven dynamic uplift of the Rocky Mountains and Colorado Plateau and its surface response: Toward a unified hypothesis. Lithosphere 4, 3–22.

Kober, F., Ivy-Ochs, S., Schlunegger, F., Baur, H., Kubik, P.W., Wieler, R., 2007. Denudation rates and a topography-driven rainfall threshold in northern Chile: multiple cosmogenic nuclide data and sediment yield budgets. Geomorphology 83, 97–120.

Evenstar, L.A., Hartley, A.J., Stuart, F.M., Mather, A.E., Rice, C.M., Chong, G., 2009. Multiphase development of the Atacama Planation Surface recorded by cosmogenic 3He exposure ages: Implications for uplift and Cenozoic climate change in western South America. Geology 37, 27–30.

Lal, D., 1991. Cosmic ray labeling of erosion surfaces: in situ nuclide production rates and erosion models. Science 104, 424–439.

Le Dortz, K., Meyer, B., Sébrier, M., Braucher, R., Nazari, H., Benedetti, L., Fattahi, M., Bourlès, D., Foroutan, M., Siame, L., Rashidi, A., Bateman, M.D., 2011. Dating inset terraces and offset fans along the Dehshir Fault (Iran) combining cosmogenic and OSL methods. Geophysical Journal International 185, 1147–1174.

Le Roux, J.P., Olivares, D.M., Nielsen, S.N., Smith, N.D., Middleton, H., Fenner, J., Ishman, S.E., 2006. Bay sedimentation as controlled by regional crustal behaviour, local tectonics and eustatic sea-level changes: Coquimbo Formation (Miocene–Pliocene), Bay of Tongoy, central Chile. Sedimentary Geology 184, 133–153.

Leonard, E.M., Wehmiller, J.F., 1992. Low uplift rates and terrace reoccupation inferred from mollusk aminostratigraphy, Coquimbo Bay Area, Chile. Quaternary Research 38, 246–259.

Marquardt, C., 2005. Déformations néogènes le long de la côte nord du Chili (23°–27°S), avant-arc des Andes centrales. Ph.D Thesis, Université de Toulouse, Toulouse, 212 p.

Marquardt, C., Lavenu, A., Ortlieb, L., Godoy, E., Comte, D., 2004. Coastal neotectonics in Southern Central Andes: uplift and deformation of marine terraces in Northern Chile (27°S). Tectonophysics 394, 193–219.

Matmon, A., Simhai, O., Amit, R., Haviv, I., Porat, N., McDonald, E., Benedetti, L., Finkel, R., 2009. Desert pavement-coated surfaces in extreme deserts present the longest-lived landforms on Earth. Geological Society of America Bulletin 121, 688–697.

Mortimer, C., 1973. The Cenozoic history of the southern Atacama Desert, Chile. Journal of the Geological Society 129, 505–526.

Nishiizumi, K., Caffee, M.W., Finkel, R.C., Brimhall, G., Mote, T., 2005. Remnants of a fossil alluvial fan landscape of Miocene age in the Atacama Desert of northern Chile using cosmogenic nuclide exposure age dating. Earth and Planetary Science Letters 237, 499–507.

Nishiizumi, K., Imamura, M., Caffee, M.W., Southon, J.R., Finkel, R.C., McAninch, J., 2007. Absolute calibration of Be-10 AMS standards. Nuclear Instruments & Methods in Physics Research Section B-Beam Interactions with Materials and Atoms, 258, pp. 403–413.

Ortlieb, L., Zazo, C., Goy, J.L., HillaireMarcel, C., Ghaleb, B., Cournoyer, L., 1996. Coastal deformation and sea-level changes in the northern Chile subduction area (23°S) during the last 330 ky. Quaternary Science Reviews 15, 819–831.

Ota, Y., Miyauchi, T., Paskoff, R., Koba, M., 1995. Plio–Quaternary terraces and their deformation along the Altos de Talinay, North–Central Chile. Revista Geologica de Chile 22, 89–102.

Pardo, M., Comte, D., Monfret, T., 2002. Seismotectonic and stress distribution in the central Chile subduction zone. Journal of South American Earth Sciences 15, 11–22.

Paskoff, R., 1970. Recherches géomorphologiques dans le Chili semi-aride. Biscaye Freres, Bordeaux.

Placzek, C.J., Matmon, A., Granger, D.E., Quade, J., Niedermann, S., 2010. Evidence for active landscape evolution in the hyperarid Atacama from multiple terrestrial cosmogenic nuclides. Earth and Planetary Science Letters 295, 12–20.

Quezada, J., Gónzalez, G., Dunai, T., Jensen, A., Juez-Larre, J., 2007. Pleistocene littoral uplift of northern Chile: ^{21}Ne age of the upper marine terrace of Caldera–Bahia Inglesa area. Revista Geologica de Chile 34, 81–96.

Regard, V., Saillard, M., Martinod, J., Audin, L., Carretier, S., Pedoja, K., Riquelme, R., Paredes, P., Hérail, G., 2010. Renewed uplift of the Central Andes Forearc revealed by coastal evolution during the Quaternary. Earth and Planetary Science Letters 297, 199–210.

Riquelme, R., Martinod, J., Hérail, G., Darrozes, J., Charrier, R., 2003. A geomorphological approach to determining the Neogene to Recent tectonic deformation in the Coastal Cordillera of northern Chile (Atacama). Tectonophysics 361, 255–275.

Rivano, S., Sepúlveda, P., 1991. Hoja Illapel, Región de Coquimbo. Carta Geológica de Chile.

Saillard, M., 2008. Dynamique du soulèvement côtier Pléistocène des Andes centrales: Étude de l'évolution géomorphologique et datations (^{10}Be) de séquences de terrasses marines (Sud Pérou-Nord Chili). Ph.D Thesis, Université de Toulouse, Toulouse, 308 p.

Saillard, M., Hall, S.R., Audin, L., Farber, D.L., Hérail, G., Martinod, J., Regard, V., Finkel, R.C., Bondoux, F., 2009. Non-steady long-term uplift rates and Pleistocene marine terrace development along the Andean margin of Chile (31°S) inferred from ^{10}Be dating. Earth and Planetary Science Letters 277, 50–63.

Schildgen, T.F., Cosentino, D., Bookhagen, B., Niedermann, S., Yıldırım, C., Echtler, H., Wittmann, H., Strecker, M.R., 2012. Multi-phased uplift of the southern margin of the Central Anatolian plateau, Turkey: a record of tectonic and upper mantle processes. Earth and Planetary Science Letters 317–318, 85–95.

Sernageomin, 2003. Carta Geológica de Chile (escala 1:1.000.000). Servicio Nacional de Geología y Minería.

Stone, J.O., 2000. Air pressure and cosmogenic isotope production. Journal of Geophysical Research — Solid Earth 105, 23753–23759.

Tosdal, R.M., Clark, A.H., Farrar, E., 1984. Cenozoic polyphase landscape and tectonic evolution of the Cordillera Occidental, Southernmost Peru. Geological Society of America Bulletin 95, 1318–1332.

Vassallo, R., Ritz, J.F., Carretier, S., 2011. Control of geomorphic processes on ^{10}Be concentrations in individual clasts: complexity of the exposure history in Gobi-Altay range (Mongolia). Geomorphology 135, 35–47.

Veit, H., 1996. Southern westerlies during the Holocene deduced from geomorphological and pedological studies in the Norte Chico, northern Chile (27–33°S). Palaeogeography Palaeoclimatology Palaeoecology 123, 107–119.

Vicuña, S., Garreaud, R.D., McPhee, J., 2010. Climate change impacts on the hydrology of a snowmelt driven basin in semiarid Chile. Climatic Change 105, 469–488.

Yañez, G.A., Ranero, R., Huene, V., 2001. Magnetic anomaly interpretation across the southern central Andes (32°–34°S): The role of the Juan Fernández Ridge in the late Tertiary evolution of the margin. Journal of Geophysical Research 106, 6325–6345.

Chapter 5- NEOGENE TO QUATERNARY UPLIFT AND INCISION OF PEDIPLAINS ALONG THE COASTAL CORDILLERA AND THE WESTERN FRONTAL CORDILLERA IN NORTH-CENTRAL CHILE (28-32°S).

5.1. Introduction

The content of this chapter includes the results, the discussion and the implications in terms of uplift timing of the geomorphic analysis of paleosurfaces and the geochronological U-Pb zircon dating of overlying tuffs throughout the Coastal and western Frontal Cordilleras in north-central Chile. Based on the obtained results, a model of uplift and incision of these pediplains is proposed and the roles that tectonic and erosional processes may have played on the development of the present-day topography of north-central Chile are suggested.

The chapter includes:

1) A brief presentation of the paleosurfaces studied in this thesis (section 5.2).

2) An article accepted for publication in the Geological Society Special Publication: Geodynamic Processes in the Andes of central Chile and Argentina, which includes the results of Project IGCP 586-Y "Geodynamic processes in the Andes between 32º and 34ºS" of the International Geological Correlation Programme (IGCP-UNESCO) (see section 5.3). The article is entitled “Neogene to Quaternary landscape evolution to the west of the topographic front in north-central Chile (28-32°S): Interplay between tectonic and erosional processes” and

3) The results and a brief discussion regarding ^{21}Ne cosmogenic analysis of one of these paleosurfaces in section 5.4

Finally, in section 5.5 the main conclusions of this chapter are listed.

5.2. Pediplains in the Coastal Cordillera and the western Frontal Cordillera of north-central Chile (28-32°S).

An assemblage of five pediplains is observed throughout the entire studied region (Fig. 5.1, 5.2). From the highest to the lowest they correspond to the La Silla, the Corredores, the Algarrobillo, the Cachiyuyo and the Ovalle pediplains (Fig. 5.1, 5.2).

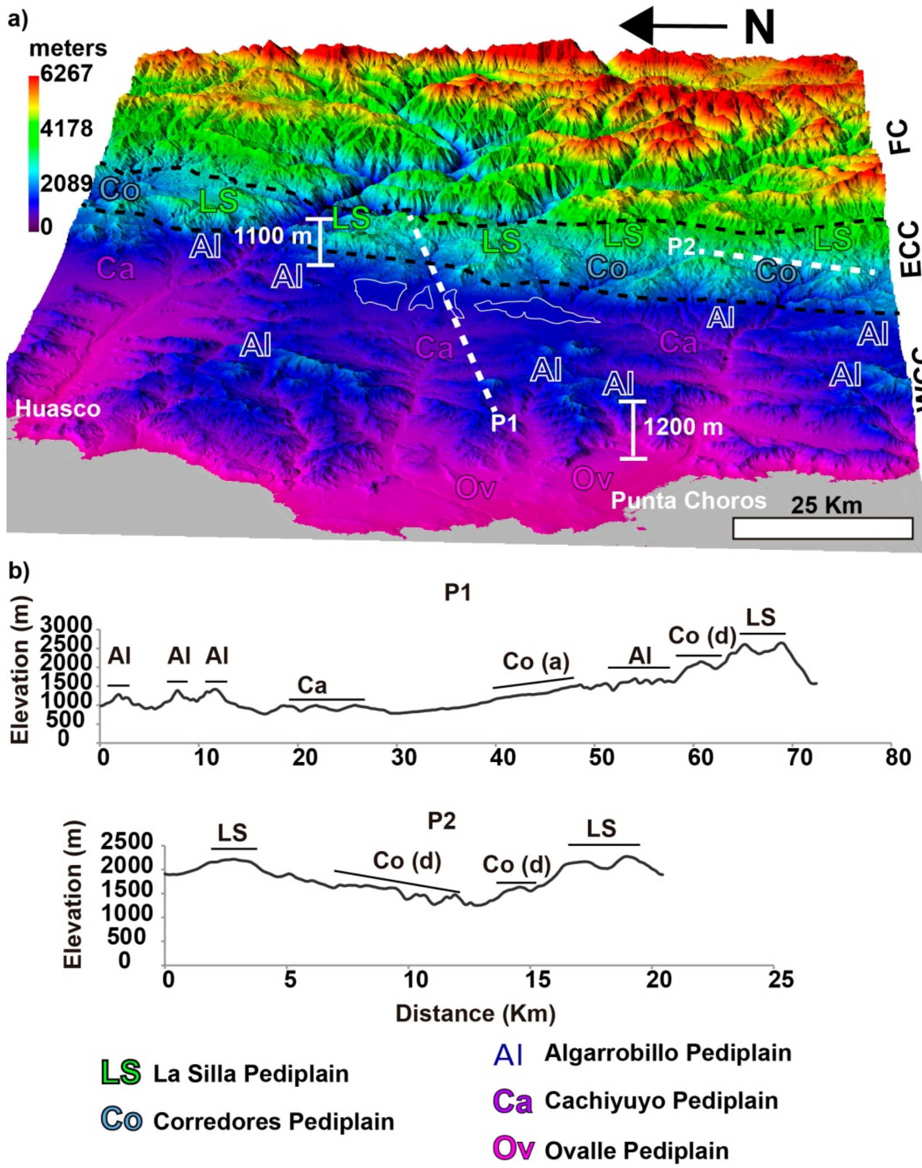

Fig. 5.1. a) 3D shaded relief image of pediplains remnant's throughout the Coastal Cordillera in north-central Chile to the north of 30°S. FC= Frontal Cordillera, ECC= Eastern Coastal Cordillera, WCC= Westerrn Coastal Cordillera. Black dashed lines mark the position of the main topographic front between the Frontal and the Coastal Cordilleras and the secondary topographic front separating the eastern from the western Coastal Cordillera. White dashed lines mark the trace of topographic profiles in Fig. 5.1b. White lines enclosed the aggradatinal part of the Corredores Pediplain. b) Topographic profiles showing the location of pediplains. Co (a)= aggradational part of the Corredores pediplain, Co (d)= degradational part of the Corredores pediplain. Trace of profiles in Fig. 5.1a.

The La Silla Pediplain is a bedrock surface that forms the highest summits of the Coastal Cordillera (Fig. 5.1, 5.2). The Corredores Pediplain is always incised within the La Silla Pediplain (Fig. 5.1a and b, 5.2) and it presents degradational and aggradational counterparts (Fig. 5.1a and b, 5.2). Its aggradational part is at generally lower elevations than its degradational part (Fig. 5.1a and b) and it is not preserved south of 30°S (Fig. 5.2a). Both the La Silla Pediplain and the degradational part of the Corredores Pediplain are separated from the Algarrobillo Pediplain by a topographic scarp that forms a secondary topographic front within the Coastal Cordillera. The Algarrobillo Pediplain is a bedrock surface that forms the highest summits of the western Coastal Cordillera (Fig. 5.1, 5.2). The secondary topographic front, i.e., the difference in elevation between the La Silla and the Algarrobillo pediplains is around ~1100 m throughout the studied region (Fig. 5.1, 5.2). The Cachiyuyo and the Ovalle pediplains are incised within the Algarrobilllo pediplain (Fig. 5.1, 5.2). The Cachiyuyo Pediplain presents both degradational and aggradational counterparts (Fig. 5.1, 5.2b). The Ovalle Pediplain corresponds to the planation surface formed by shore platforms, strath terraces and a pediment presented in chapter 4 and uplifted ~ 150 m post-500 ka. The difference in elevation between the Algarrobillo Pediplain and the Ovalle Pediplain is around 1200 m throughout the studied region (Fig. 5.1, 5.2).

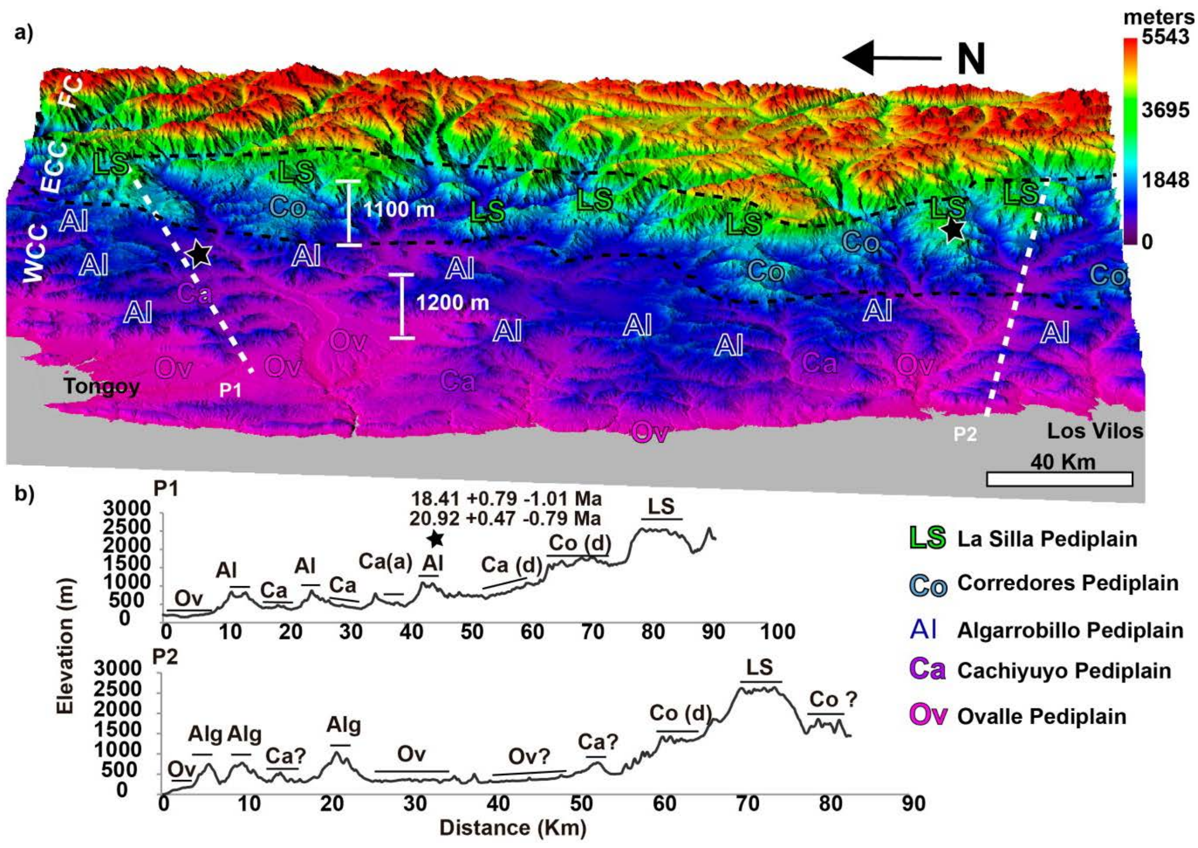

Fig. 5.2. a) 3D shaded relief image of pediplains remnant's throughout the Coastal Cordillera in north- central Chile to the south of 30°S. FC= Frontal Cordillera, ECC= Eastern Coastal Cordillera, WCC= Western Coastal Cordillera. Black dashed lines mark the position of the main topographic front between the Frontal and the Coastal Cordilleras and the secondary topographic front separating the eastern from the western Coastal Cordillera. White dashed lines mark the trace of topographic profiles in Fig. 5.1b.. b) Topographic profiles showing the location of pediplains. Ca (a)= aggradational part of the Cachiyuyo pediplain, Ca (d)= degradational part of the Cachiyuyo pediplain. Trace of profiles in Fig. 5.2a. Stars mark the position of the tuff overlying the La Silla and the Algarrobillo pediplains dated in this thesis.

5.3. Article: Neogene to Quaternary landscape evolution to the west of the topographic front in north-central Chile (28-32°S): Interplay between tectonic and erosional processes (manuscript accepted for publication in the Geological Society Special Publication "Geodynamic Processes in the Andes of central Chile and Argentina" IGCP Project 586-Y "Geodynamic processes in the Andes between 32º and 34ºS", International Geological Correlation Programme (IGCP-UNESCO).

María Pía Rodríguez[1,2], Germán Aguilar[2], Constanza Urresty[1] and Reynaldo Charrier[1,3].

[1] Departamento de Geología, Facultad de Ciencias Físicas y Matemáticas, Universidad de Chile, Santiago, Chile.

[2] Advanced Mining Technology Center (AMTC), Facultad de Ciencias Físicas y Matemáticas, Universidad de Chile, Santiago, Chile.

[3] Escuela de Ciencias de la Tierra, Universidad Andrés Bello, Campus República, Santiago, Chile.

Abstract

We combine geomorphological analysis of paleosurfaces and U-Pb zircon geochronology of overlying tuffs to reconstruct the Neogene to Quaternary landscape evolution in north-central Chile (28-32°S). Prior to the Early Miocene, a pediplain sloping down to sea-level dominated the landscape of the present-day Coastal Cordillera and some areas of the western Frontal Cordillera. This pediplain was offset during the Early Miocene, leading to uplift of the eastern Coastal Cordillera and the western Frontal Cordillera and the formation of a secondary topographic front. During the Late Miocene, the entire Coastal Cordillera was uplifted, with resulting deposition taking place within river valleys similar to those of the present-day. A new pediplain developed on top of these deposits between the Early to Middle Pleistocene and was finally uplifted post-500 ka. These three major uplift stages correlate with episodes of increased deformation, starting after a Late Oligocene-Early Miocene episode of increased plate convergence. The presence of an inherited paleotopography together with a strong decrease of precipitation to the north of 30°S would have determined differences in landscape development throughout the Coastal Cordillera between this area and the area to the south of 30°S since the Early Miocene.

1. Introduction

The morphology of active mountain belts results from the interplay between tectonic processes, which deform the lithosphere and result in uplifted regions of the Earth's surface; and erosional processes, which are mainly controlled by climate and rock type (Strecker et al., 2007). In the Central Andes (15-34°S, Fig. 1), along-strike variations of topography and the amount of shortening have been mostly related to north-to-south changing tectonic features. The most widely mentioned correspond to subduction geometry (Jordan et al., 1983; Isacks, 1988); the age of the Nazca Plate (Ramos et al., 2004) and interplate coupling (Lamb and Davis, 2003). It is thought that these tectonic factors together with the pre-Neogene geological history (Ramos et al., 1996; Lamb et al., 1997; Tassara and Yañez, 2003; Giambiagi et al., 2012) may have played a dominant role in the first order topography and structure of the Andes (Hilley and Coutand, 2010). However, it is also likely that erosional processes may influence the kinematics of deformation (Sobel and Strecker, 2003; Hilley et al., 2004) and control the response time to uplift (Aguilar et al., 2011; Carretier et al., this volume) at the scale of morphostructural segments (Fig.1; Hilley and Coutand, 2010).

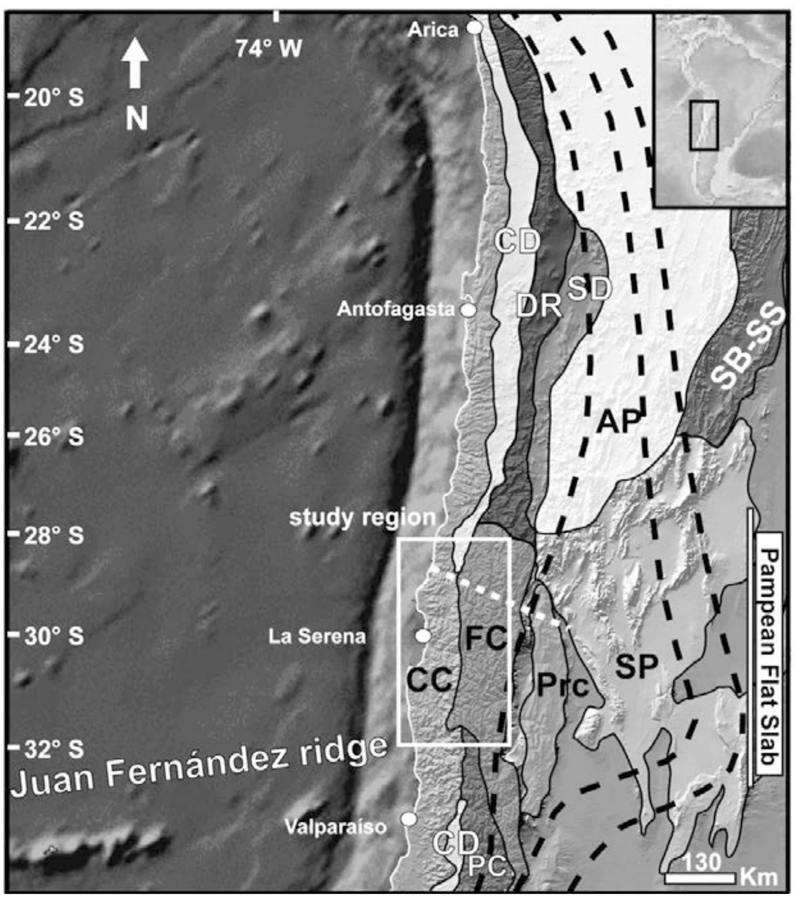

Fig. 1 Morphostructural units and tectonic setting of the Central Andes (15-34°S). Dashed black lines mark depth contour lines of the Nazca Plate underneath the South America Plate at 100, 150 and 200 km (Cahill and Isacks, 1992). Dashed white line marks the symmetry axis of the Vallenar Orocline (Arriagada et al., 2009). CC: Coastal Cordillera, CD: Central Depression, DR: Domeyko Cordillera, SD: Subandean Depression, AP: Altiplano-Puna (including the Western and Eastern Cordilleras), SB: Subandean Ranges, SS: Santa Bárbara System, FC: Frontal Cordillera, Pc: Precordillera, SP: Sierras Pampeanas, PC: Principal Cordillera.

Here, we present the case of the Central Andes of north-central Chile between 28° and 32°S, whose Neogene to Quaternary landscape evolution may have been influenced by several factors. On the one hand, this region is located on the Pampean or Chilean flat-slab segment (27-33°S). Within this segment the subduction angle between the Nazca and South American plates is ~ 10°, contrary to the adjacent regions of the Central Andes where this angle is ~ 30° (Cahill and Isacks, 1992). Slab flattening is thought to be related to the subduction of the buoyant Juan Fernández Ridge (Fig. 1), which migrated from the northern to the southern part of the study area between ~ 16 and 12 Ma (Yañez et al., 2001). However, it is unclear if Neogene crustal thickening and uplift are a consequence of the subduction of the Juan Fernández Ridge (Cembrano et al., 2003) or are better related to changes in the convergence parameters between the Nazca and South American Plates (Kay and Mpodozis, 2002; Charrier et al., 2013). The study area also records a transition in the pre-Neogene topography that is reflected in the presence of the Vallenar Orocline at this latitude of the Central Andes (Arriagada et al. 2009, Fig. 1). The Vallenar Orocline is thought to mark the southernmost extent of Eocene to Oligocene deformation (Arriagada et al., 2009), associated with the so-called Incaic relief (Steinmann, 1929; Charrier and Vicente, 1972; Cornejo et al., 2003). During the Eocene and Oligocene the Incaic relief was the main paleogeographic feature to the north of 31°S (Fig. 1; Maksaev and Zentilli, 1999; Pineda and Emparán, 2006; Pineda and Calderón, 2008; Arriagada et al., 2009, Bissig and Riquelme, 2010; Arriagada et al., in press), while an extensional volcano-sedimentary basin, known as the Abanico Basin (Charrier et al., 2002; Jara and Charrier, in press), developed south of 32°S. However, it is unclear how differences in the pre-Neogene paleotopography may have influenced the subsequent landscape evolution throughout north-central Chile. On the other hand, the region of north-central Chile has a semi-arid climate, which is transitional between the hyperarid conditions of the southern Atacama Desert north of 27°S and the more humid conditions of central Chile south of 33°S (Fig. 2a). The Southeast Pacific anticyclone (SEP) is the main factor responsible for the hyperaridity north of 27°S, whereas the penetration of the Southern Hemisphere westerlies results in the more humid conditions of central Chile (Veit, 1996). In particular, along the studied region a north-to-south rise in precipitation occurs at 30°S related to the influence of the SEP (Fig. 2a). During the Paleogene, the climate in north-central Chile was warmer and more humid than at present as indicated by the woody components of paleoflora from fossiliferous localities just south of La Serena (Fig. 2a, Villagrán et al., 2004). Since ~ 21 to 15 Ma subtropical vegetation was replaced by sclerophytic shrubs indicating a warm, seasonal climate receiving scarce rainfall from both the east and the west (Villagrán et al., 2004). The transition between a hyperarid climate to the north of 27°S and a humid climate south of 33°S occurred after the Middle Miocene (~ 15 Ma, Le Roux, 2012). During this period, the combination of a series of events including glaciations in West Antartica, formation of the Humboldt Current and uplift of the Andes are thought to have been responsible for the development of the latitudinal precipitation gradient throughout the study area (Le Roux, 2012). The roles, if any, that the present-day along-strike increase in precipitation and/or climatic changes throughout the Miocene could have played in shaping the landscape in north central Chile are largely unknown.

In this study we combine geomorphological analysis of subplanar paleosurfaces in the Coastal and the western Frontal Cordilleras (Fig. 1) with the U-Pb zircon geochronology of overlying tuffs to reconstruct the Neogene to Quaternary history of uplift and incision of these paleosurfaces

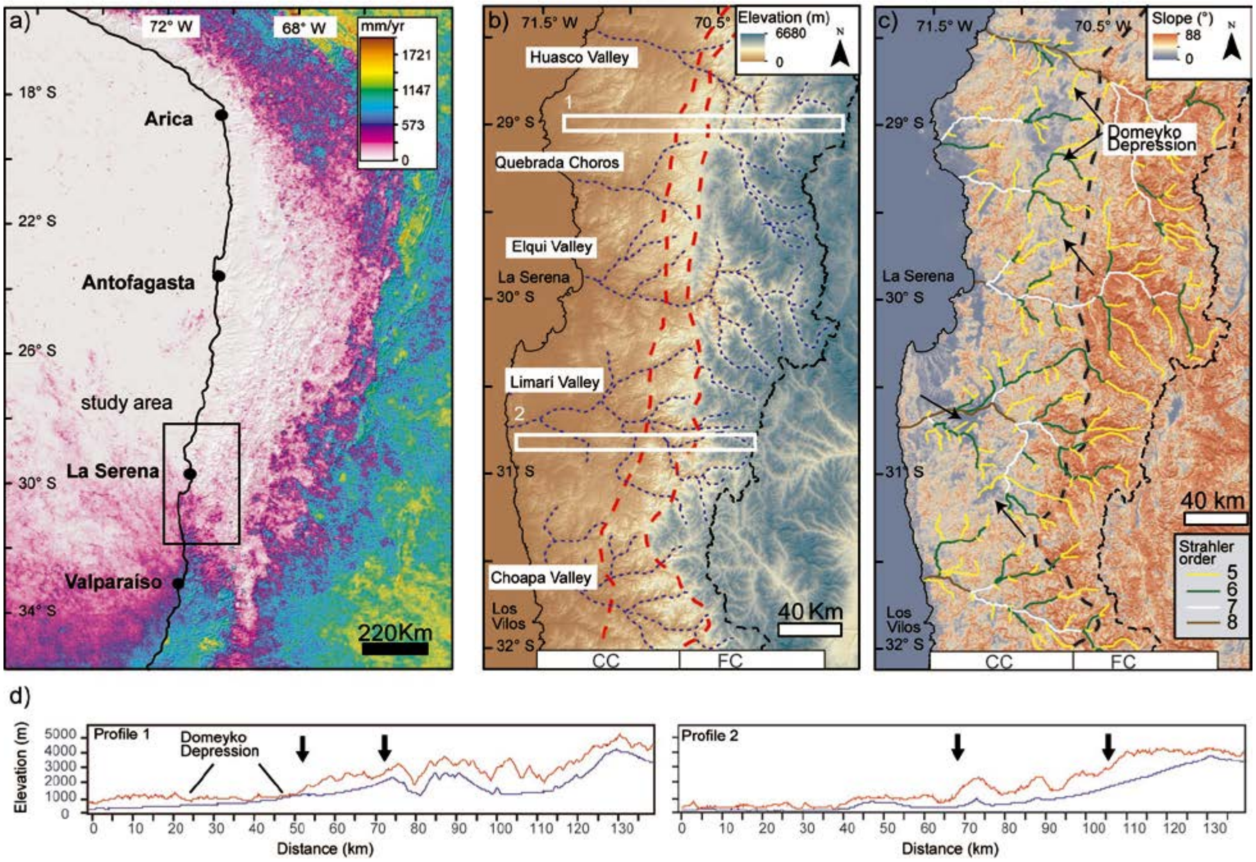

Fig. 2. a) Shaded relief image map color-coded for mean annual precipitation from Kenji Matsuura and Cort J. Willmott (2011) world database available at http://climate.geog.udel.edu/~climate/html_pages/download.html. b) Elevation map throughout study area based in the SRTM DEM. Dashed red lines mark the position of topographic fronts. Dashed blue lines mark the main rivers and tributaries. Dashed black line marks the international border. c) Slope map throughout study area derived from the SRTM DEM. Thick dashed black line marks the position of the main topographic front. Thin dashed line marks the position of the international border. Arrows mark depressed areas within the Algarrobillo pediplain south of 30° S c) Maximum (red) and minimum (blue) elevation profiles in a 5 km diameter swath. Arrows mark the position of topographic fronts. Trace of profiles in Fig. 2b.

in north-central Chile (28-32°S). Our results are discussed considering previous data on subplanar paleosurfaces in the Coastal Cordillera (Rodríguez et al., 2013) and the higher Frontal Cordillera along the international border between Chile and Argentina (e.g. Bissig et al., 2002; Nalpas et al., 2009). Finally, we discuss the roles that tectonic and erosional processes may have played in the development of the present-day topography in north- central Chile.

2. Regional framework

The large-scale geomorphology of the study area is characterized by a marked rise in mean elevation along west to east transects (Fig. 2b and d, Aguilar et al., 2011; 2013).

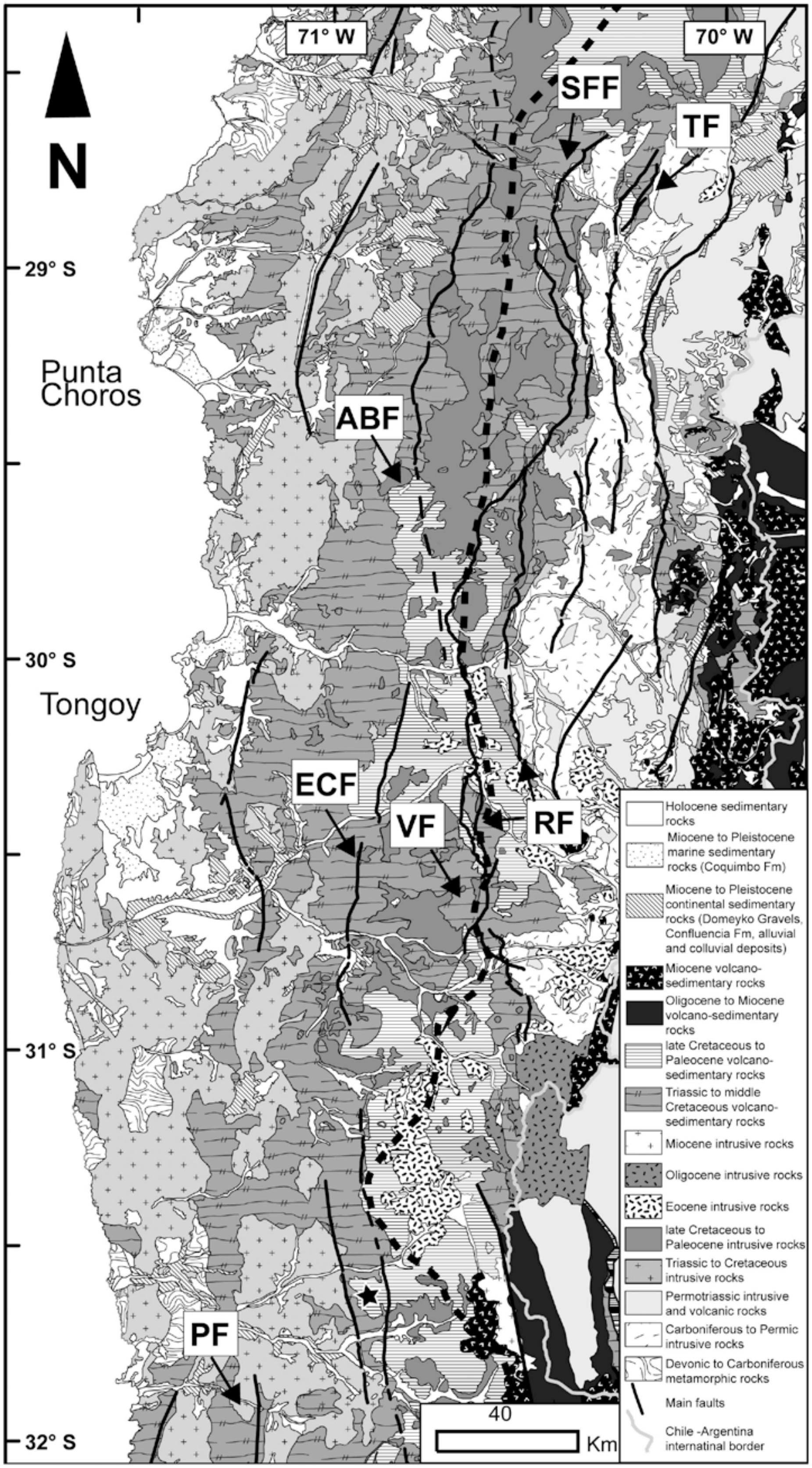

Fig. 3. Geological map of the study area, based on Sernageomin (2003). Black dashed line marks the main topographic front line that separates the Coastal Cordillera, to the west, from the Frontal Cordillera, to the east. Black stars show location of tuffs dated by U-Pb zircon geochronology on top of the La Silla Pediplain and the Algarrobillo Pediplain in this study. VF: Vicuña Fault, RV: Rivadavia Fault, SFF: San Félix Fault, TF: La Totora Fault, ABF: Agua de los Burros Fault, ECF: El Chaper Fault, PF: Pupio Fault.

This first-order geomorphological feature represents a topographic front separating two north-south elongated morphostructural units corresponding to the Coastal Cordillera and Frontal Cordillera from west to east (Fig. 2b and c). Contrary to what is observed in the Andean segments to the north of 27°S and to the south of 33°S, no continuous Central Depression is observed to the east of the Coastal Cordillera in the study region (Fig. 1 and 2c). Only in the area north of 30°S, the Domeyko Depression corresponds to an area of relatively lower topography within the Coastal Cordillera (Fig. 2c).

The Coastal Cordillera is characterized to the west by a series of shore platforms displaying low slopes values (< 20 °) (Fig. 2c; Paskoff, 1970; Ota et al.,1995; Benado, 2000; Saillard et al., 2009; Rodríguez et al., 2013). To the east, the Coastal Cordillera reaches a maximum elevation of ~ 3200 m a.m.s.l (Fig. 2b). The Coastal Cordillera mainly corresponds to an east-dipping homoclinal block of Triassic to Lower Cretaceous volcano-sedimentary rocks that unconformably cover a Devonian to Carboniferous (Permian?) metamorphic and sedimentary basement (Fig. 3; Rivano and Sepúlveda, 1991). Both features are intruded by Triassic to Early Cretaceous north-south elongated plutonic belts with increasing ages to east (Fig.3; Rivano and Sepúlveda, 1991; Emparán and Pineda, 2006; Arévalo et al., 2009). Towards the border with the Frontal Cordillera, the Lower Cretaceous rocks at the top of the east-dipping homoclinal block are unconformably covered by subhorizontal Upper Cretaceous to Paleocene volcano-sedimentary rocks and intruded by a plutonic belt of similar age (Fig. 3; Pineda and Emparán; 2006; Pineda and Calderón, 2008). Along the coast and within the main valleys, Neogene to Quaternary marine and continental sedimentary rocks are exposed (Fig. 4; Rivano and Sepúlveda, 1991; Le Roux et al., 2004, 2005, 2006; Emparán and Pineda, 2006; Arévalo et al., 2009). As it would be explained later these deposits are closely related to the development of the pediplains studied here. The Coquimbo Formation corresponds to a shallow marine to transitional sedimentary succession exposed along the coast near the localities of Punta Choros and Tongoy (Figs. 3 and 4). It records continuous marine deposition from the Early Miocene (~ 23 Ma) to the Early Pleistocene (~ 1 Ma) (Le Roux et al., 2004; 2005; 2006). South of 30°S, the Coquimbo Formation grades laterally towards the east into the continental Confluencia Formation (Figs. 3 and 4). The Confluencia Formation is composed of fluvial and alluvial facies exposed along the lower and middle courses of the main valleys (Figs. 3 and 4). The fluvial deposits change laterally towards the valley walls into the alluvial deposits (Fig. 4). In some areas the latter overlie the fluvial deposits (Fig. 4). No geochronological constraints exist for the Confluencia Formation, but based on its relationship with the Coquimbo Formation, a general Miocene to Pleistocene age can be assumed (Emparán and Pineda, 2006). The alluvial facies within the Confluencia Formation present an interbedded ash bed south of Tongoy (Figs. 3 and 4), which has been correlated with a similar level within the marine Coquimbo Formation exposed just to the west (Figs. 3 and 4, Emparán and Pineda, 2006) and dated at ~ 6 Ma (Emparán and Pineda, 2000). North of 30°S, the Domeyko Gravels are exposed within the Domeyko Depression (Figs. 3 and 4). The Domeyko Gravels are alluvial deposit interpreted to have accumulated in a closed basin with a local sediment source (Arévalo et al., 2009). There are no chronostratigraphic or geochronological constraints available for the Domeyko Gravels. However, they are thought to be of Middle Miocene age (Arévalo et al., 2009) according to regional correlations with the Atacama Gravels at ~ 27° (Mortimer, 1973). Deposition of the Atacama Gravels started ~ 17 Ma and ended by ~ 10 Ma (Cornejo et al., 1993), finally leading to regional pedimentation and development of the Atacama Pediplain on top. Also exposed within the Domeyko Depression are alluvial and colluvial deposits that crop out attached to relatively higher topographic areas and that overlie the Domeyko Gravels (Fig. 4; Arévalo et al., 2009). No direct geochronological contraints are available for these deposits, but they have been correlated with similar deposits at 27°S (Arévalo et al., 2009) presenting intercalated ash units with ages between ~ 7 and 3 Ma (Fig. 4; Arévalo et al., 2009). The alluvial and colluvial deposits exposed north of 30°S are correlated with the alluvial facies of the Confluencia Formation exposed south of 30°S.

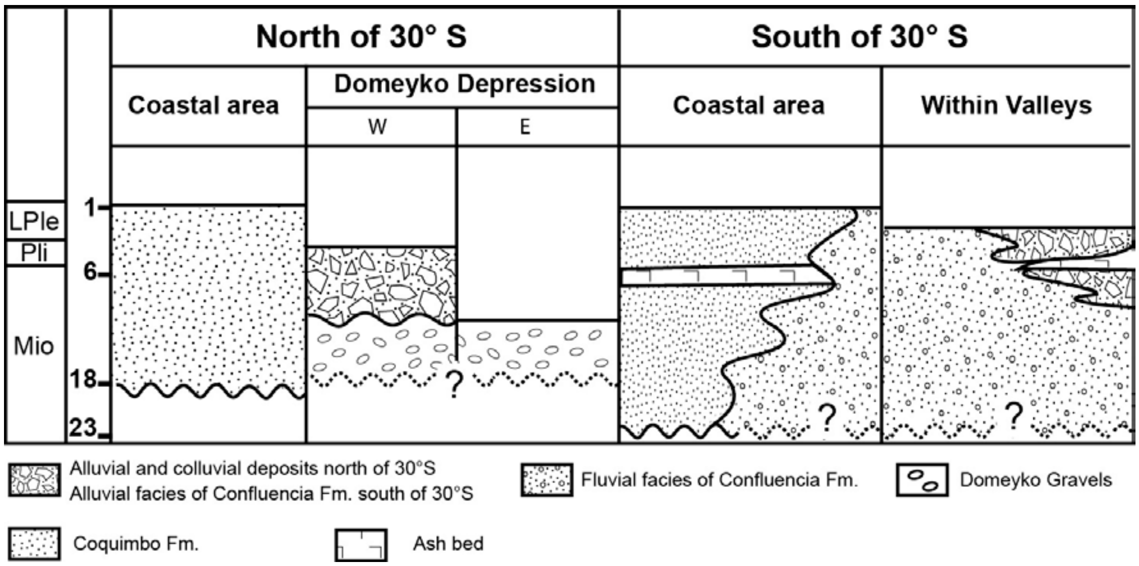

Fig. 4. Chronostratigraphic chart for Neogene and Quaternary sedimentary units exposed in the Coastal Cordillera north and south of 30ºS. Mio: Miocene, Pli: Pliocene, LPle: Lower Pleistocene.

The Frontal Cordillera reaches elevations as high as ~ 6700 m a.s.l. It is formed by a core of Carboniferous to Permian magmatic units (Fig. 3; Nasi et al., 1990; Pineda and Calderón, 2008), which is here referred to as the Central Frontal Cordillera (Fig. 5). The core is covered to the west by a dominantly west-dipping block of Triassic to Upper Cretaceous folded volcano-sedimentary rocks, intruded by a Late Cretaceous- Early Paleocene magmatic belt (Nasi et al., 1990; Mpodozis and Cornejo, 1988; Pineda and Emparán; 2006; Pineda and Calderón, 2008). This area will be referred to below as the western Frontal Cordillera (Fig. 5). To the east, the basement core is intruded or in faulted contact with a block composed mostly of Permo-Triassic magmatic and volcanic rocks unconformably overlain by Oligocene to Miocene folded volcano-sedimentary rocks (Fig. 3; Maksaev et al., 1984; Nasi et al., 1990; Martin et al., 1999; Bissig et al., 2001; Winocur et al., this volume). These rocks are unconformably covered by Miocene subhorizontal volcanics (Fig. 3; Maksaev et al., 1984; Nasi et al., 1990; Martin et al., 1999; Bissig et al., 2001; Winocur et al., this volume). The area of the Frontal Cordillera to the east of the basement core will be referred to as the eastern Frontal Cordillera (Fig. 5). Finally, a NNE-SSW trending magmatic belt of Eocene (-Oligocene?) age intrudes the areas of the central and western Frontal Cordillera (Figs. 2 and 5).

South of 31.5°S the area to the east of the main topographic front corresponds to the Principal Cordillera (Fig. 5), which is defined by a core of Oligocene to Miocene folded volcano-sedimentary rocks (Charrier et al., 2002; Mpodozis et al., 2009; Jara and Charrier, accepted) flanked to the east by a fold and thrust belt of Mesozoic sedimentary and volcanic rocks a (Fig. 5). These rocks are unconformably covered by Miocene subhorizontal volcanics and intruded by a north-south trending Miocene magmatic belt (Fig. 3; Mpodozis et al., 2009; Jara and Charrier, accepted).

Crustal thickening processes in the study area began with the Late Cretaceous tectonic inversion of volcano-sedimentary extensional basins of a (Late Triassic?) Jurassic-Lower Cretaceous arc-backarc system (Emparán and Pineda, 2000; Arancibia, 2004; Emparán and Pineda, 2006; Charrier et al., 2007; Salazar, 2012). Late Cretaceous inversion reactivated pre-existing normal faults along the Coastal and Frontal Cordilleras (Fig. 3) (Emparán and Pineda, 2000; Arancibia, 2004; Emparán and Pineda, 2006; Pineda and Emparán, 2006; Arévalo et al., 2009). Eocene to Oligocene compression throughout the study area is associated with the Incaic Orogenic Phase (Steinmann 1929; Charrier and Vicente, 1972; Cornejo et al., 2003). The Incaic Orogenic Phase corresponds to an important episode of shortening, uplift and exhumation widely recognized throughout the Domeyko Cordillera in northern Chile during the Eocene and Oligocene. Paleomagnetic data indicate that Eocene to Oligocene clockwise paleomagnetic rotations decreases from to 30°S to the south and become mostly zero south of 31°S (Arriagada et al., 2009; in press). Therefore, it has been interpreted that the study area includes the southern limit of Incaic deformation (Arriagada et al., 2009). According to structural and geochronological data, Eocene compression in the Huasco Valley was associated with inversion of previous Lower Cretaceous extensional basins by a series of low angle faults located between the San Félix and La Totora Faults in the western and central Frontal Cordillera (Fig. 3, Salazar, 2012). At the latitude of the Elqui and Limarí River valleys, the Eocene to Oligocene compression was related to a pop-up system formed by the closely spaced west-vergent Vicuña Reverse Fault and the east-vergent Rivadavia Reverse Fault in the western Frontal Cordillera (Fig. 3; Pineda and Emparán, 2006; Pineda and Calderón, 2009). Finally, contractional tectonics affected the eastern Frontal Cordillera and the Principal Cordillera from the Early Miocene to at least the Late Miocene (Nasi et al., 1990; Rivano and Sepúlveda., 1991; Bissig et al., 2001; Mpodozis et al., 2009; Winocur, 2010; Jara and Charrier, accepted; Winocur et al., this volume).

3. Large to medium scale geomorphological features

The topographic front that separates the Coastal Cordillera from the Frontal Cordillera defines two areas differing in their slope and hypsometry (Aguilar et al., 2013). The Frontal Cordillera presents contrasting slopes values, with very high values (> 45°) associated with canyons and low values (< 20°) mostly observed at the high elevations of watersheds in the eastern Frontal Cordillera along the international border between Chile and Argentina (Fig. 2c). The Coastal Cordillera has homogeneous and lower slope values compared with the Frontal Cordillera, although high slope values are observed locally within river valleys and along the edges of low-slope areas (Fig. 2c). Another abrupt rise in the mean elevation throughout west-to-east transects within the Coastal Cordillera defines a secondary topographic front (Fig. 2b). It is characterized by ~ 600-1000 m of relief (difference in elevations) and separates the Coastal Cordillera in two areas referred to here as the western Coastal Cordillera and the eastern Coastal Cordillera (Fig. 5). Hypsometric integral values show a progressive increase from the Coastal Cordillera to the Frontal Cordillera, revealing that the zone between the secondary and main topographic fronts is an ancient mountain front, which probably evolved as a degradational feature carved during the Neogene (Aguilar et al., 2013). The low slope areas throughout the Coastal and eastern Frontal Cordilleras are also generally characterized by low relief, forming sub-planar inter-river areas (i.e. the interfluves). These subplanar surfaces resemble the morphology of paleosurfaces widely described in the Central Andes forearc to the north and south of the study area (Mortimer, 1973; Tosdal et al., 1984; Clark et al., 1990; Farías et al., 2005; García and Hérail, 2005; Quang et al., 2005; Riquelme et al., 2007; Hoke et al., 2007; Farías et al., 2008; Hall et al., 2008; Hoke and Garzione, 2008). Their low relief and slope indicate that incision was mostly inhibited during landform formation. However, their present-day location at hundreds of meters above the river thalwegs implies that they were initially graded to a lower base level. Therefore, they are generally interpreted as paleosurfaces displaced from their original location due to regional forearc uplift or tilting (Mortimer, 1973; Tosdal et al., 1984; Farías et al., 2005; Riquelme et al., 2007; Hoke et al., 2007; Farías et al., 2008; Hoke and Garzione, 2008). These types of subplanar paleosurfaces have been mostly classified as pediplains (Mortimer et al., 1973; Tosdal et al., 1984), extensive surfaces formed due to the coalescence of multiple pediments. Pediments correspond to abraded bedrock surfaces covered by a thin veneer of alluvial debris or weathered material (Cooke et al., 1993). It has been recognized that pediplains may contain degradational and aggradational counterparts, with degradational parts corresponding to bedrock surfaces and aggradational parts corresponding generally to the top surface of fluvial and/or alluvial deposits representing the erosional material formed due to bedrock surface degradation (Mortimer, 1973; Tosdal et al., 1984; Riquelme et al., 2003; Riquelme et al., 2007).

In the Coastal Cordillera of the study area, four to six pediplains have already been mapped in the area of the Domeyko Depression (Urresty, 2009; Garrido, 2009). South of 30°S, a geomorphological marker formed by marine and continental landforms that have been uplifted ~ 150 m was dated using cosmogenic ^{10}Be (Rodríguez et al., 2013). The marine landforms correspond to shore platforms partly developed on top of the older Coquimbo Formation (Fig. 3 and 4; Le Roux et al., 2006). The continental landforms correspond to a high strath terrace and a pediment that form a single continental planation surface mostly carved into older fluvial gravels from the Miocene to Pleistocene Confluencia Formation (Fig. 4; Rivano and Sepúlveda, 1991; amend. Emparán and Pineda, 2006).

Pediplains have been identified throughout the western Frontal Cordillera (Aguilar et al., 2013) and were mapped and dated in the eastern Frontal Cordillera along the international border between Chile and Argentina (Bissig et al., 2002; Nalpas et al., 2009). No pediplains have been identified within the central Frontal Cordillera.

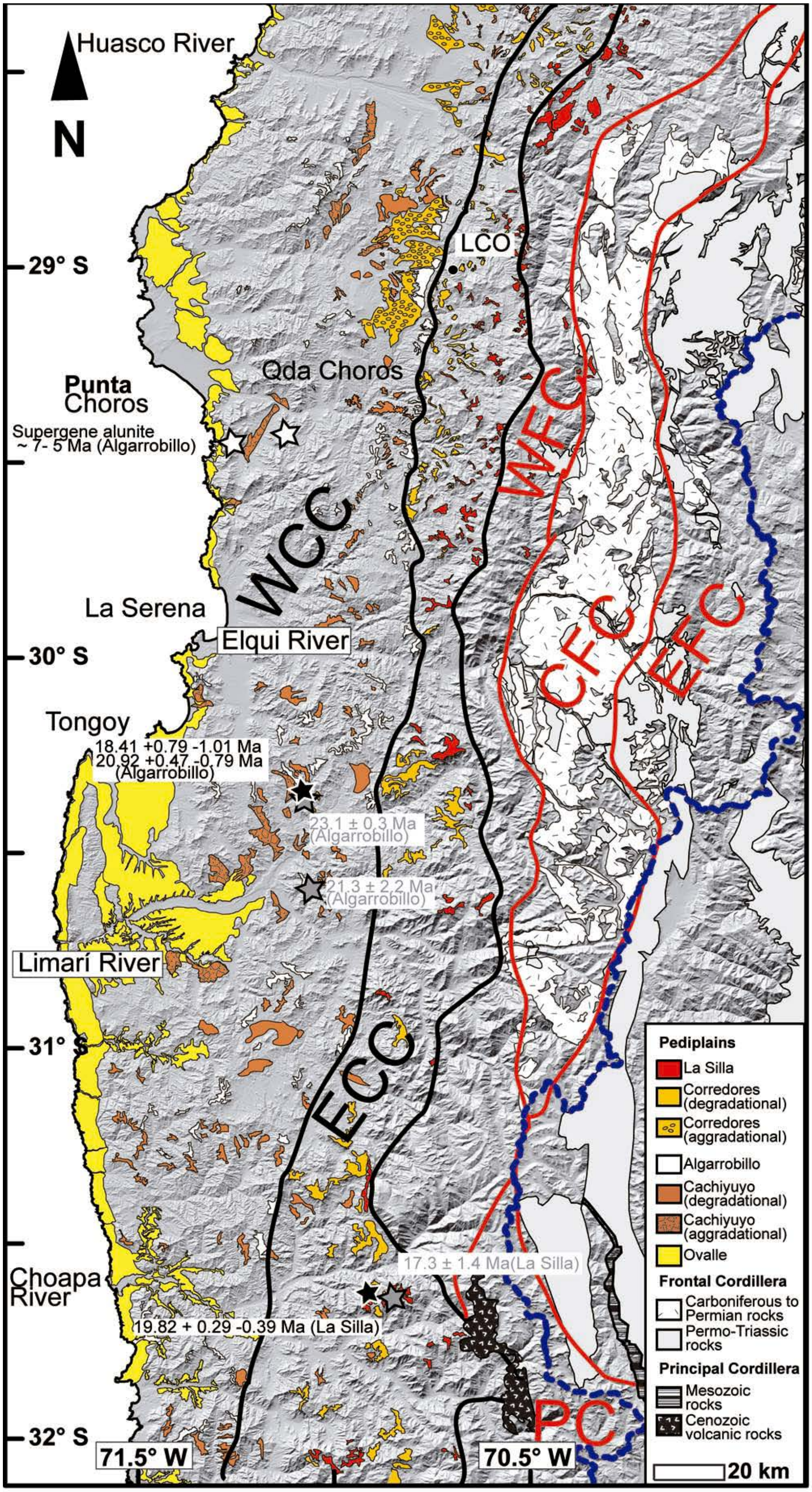
Huasco River
N
29° S
LCO
Qda Choros
Punta
Choros
Supergene alunite
~ 7- 5 Ma (Algarrobillo)
WCC
WFC
La Serena
Elqui River
30° S
CFC
EFC
Tongoy
18.41 +0.79 -1.01 Ma
20.92 +0.47 -0.79 Ma
(Algarrobillo)
23.1 ± 0.3 Ma
(Algarrobillo)
21.3 ± 2.2 Ma
(Algarrobillo)
Limarí River
31° S
ECC
17.3 ± 1.4 Ma(La Silla)
Choapa
River
19.82 + 0.29 -0.39 Ma (La Silla)
PC
32° S
71.5° W
70.5° W
Pediplains
La Silla
Corredores (degradational)
Corredores (aggradational)
Algarrobillo
Cachiyuyo (degradational)
Cachiyuyo (aggradational)
Ovalle
Frontal Cordillera
Carboniferous to Permian rocks
Permo-Triassic rocks
Principal Cordillera
Mesozoic rocks
Cenozoic volcanic rocks
20 km

Here we mapped pediplains in the Coastal Cordillera and the western Frontal Cordillera (Fig. 5 and 6a, b and c). Importantly, the present study is the first attempt to regionally map and correlate the pediplains of the Coastal and western Frontal Cordilleras in north-central Chile in order to characterize the processes involved in their formation, uplift and incision.

4. Methods

4.1. Geomorphological mapping

Satellite images and elevation, slope and geological maps together with field observations were used to map pediplains. The satellite images used include the panchromatic band of the Landsat 7 ETM+ presenting a resolution of 15 m per pixel. Elevation and slope maps were extracted from the SRTM digital elevation model (SRTM DEM, 90 m resolution per pixel) using ArcGis 9.3 and Envi 4.2 software packages. The geological maps used range in scale between 1:250,000 and 1:100,000. Flow grids were extracted from the SRTM DEM using the software RiverTools to visualize the drainage network and the thalweg profiles of the main channels that incise the pediplains. In order to standardize the geomorphological mapping, criteria for surface recognition were defined, which are similar to a protocol already used by Clark et al. (2006) to recognize remnant surfaces of an ancient landscape throughout the eastern Tibetan Plateau. As previously mentioned, the low relief and slope of the studied surfaces allow us to interpret that they formed graded to their respective original base level surfaces. Therefore, in order to map these surfaces it is necessary to establish maximum values for relief and slope. The maximum relief for surface recognition was established as ~ 600 m (Clark et al., 2006) whereas only surfaces presenting moderately low slopes < 20º were mapped. It is also necessary to put some constraints on other geomorphological or sedimentological features of these surfaces that indicate they were actually displaced from their original base levels, as they lack significant active sedimentation and that they are related to knickpoints downstream (Clark et al., 2006).

Three samples from tuff layers covering two different bedrock pediplains presented in the following section, the La Silla and the Algarrobillo Pediplains, were collected at the localities of Cerro Carrizo and Quebrada Higuerillas (Fig. 7). The samples were crushed

Fig. 5, Remnants of pediplains throughout the study area in shaded relief image of the SRTM DEM. Black stars show location of tuffs dated by U-Pb zircon geochronology overlying the La Silla Pediplain in Cerro Carrizo and the Algarrobillo Pediplain in Quebrada Higuerillas. Grey stars show location of volcanic deposits overlying the La Silla and Algarrobillo Pediplains dated in previous studies (Rivano and Sepùlveda, 1991; Bissig, 2010, Emparán and Calderón, in press). White stars show location of supergene alunite samples dated by ^{39}Ar- ^{40}Ar geochronology by Creixell et al. (2012). Black lines mark the position of topographic fronts. Red lines mark the boundaries between the different blocks composing the Frontal Cordillera. Blue dashed line mark the international border between Chile and Argentina. WCC: western Coastal Cordillera; ECC: eastern Coastal Cordillera; WFC: western Frontal Cordillera; CFC: central Frontal Cordillera; EFC: eastern Frontal Cordillera, PC: Principal Cordillera. LCO: Las Campanas Astronomical Observatory.

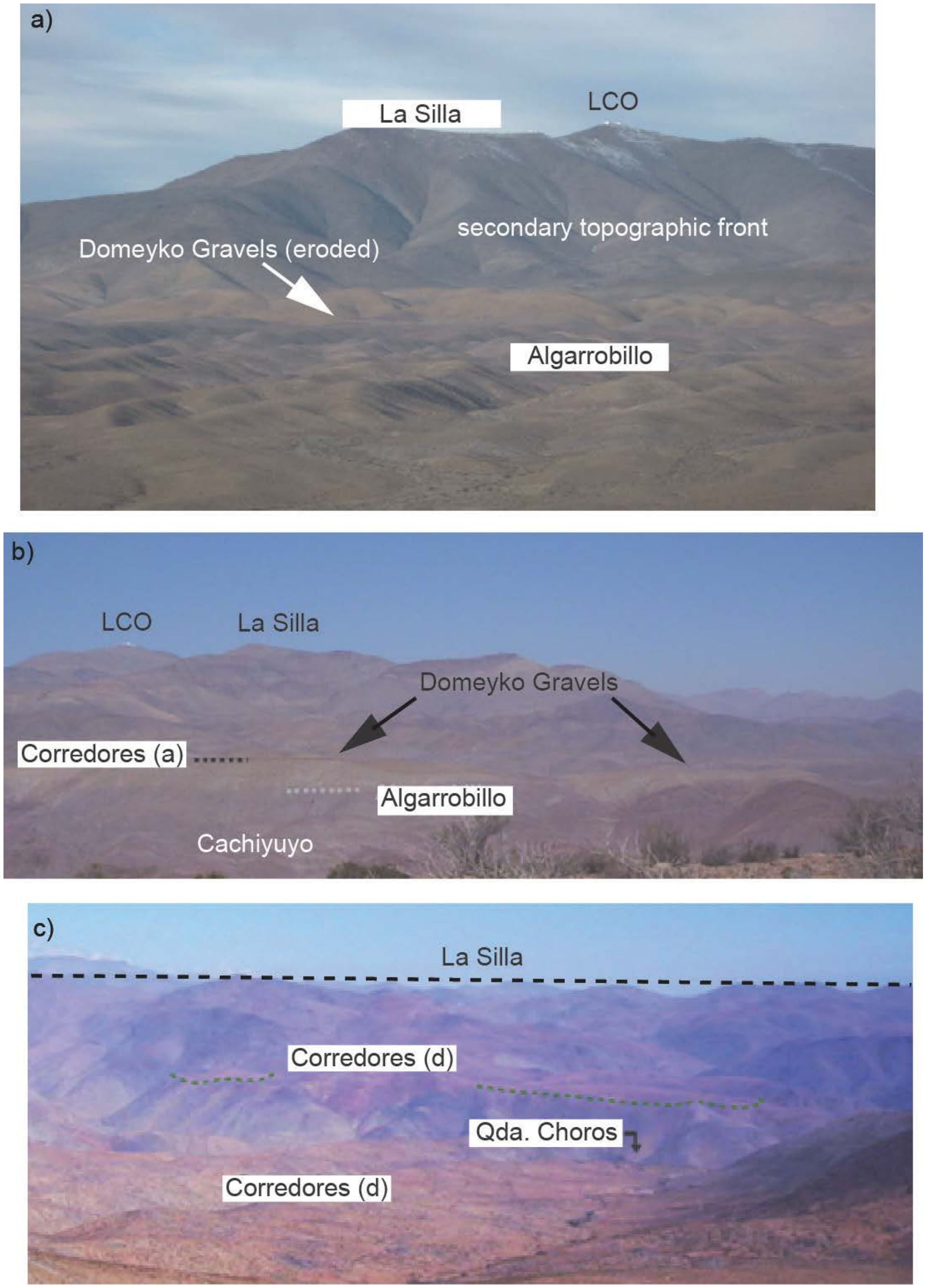

Fig. 6. a) View to the northeast of the secondary topographic front in the area of the Domeyko Depression. The Las Campanas Astronomical Observatory (LCO) (ca 2.300 m a.s.l.) is observed on top of remnants of the La Silla Pediplain. LCO location in Fig. 5. Remnants of the Algarrobillo Pediplain are exposed at the foot of the secondary topographic front underlying eroded exposures of the Domeyko Gravels b) View to the east of the secondary topographic front in the area of the Domeyko Depression. The Las Campanas Astronomical Observatory (LCO) (ca 2.300 m a.s.l.) is observed on top of remnants of the La Silla Pediplain. Remnants of the aggradational part of the Corredores Pediplain (on top of the Domeyko Gravels) are exposed at the foot of the secondary topographic front. Remnants of the Algarrobillo Pediplain underlying the Domeyko Gravels are also observed. c) View to the southeast of remnants of the degradational part of the Corredores Pediplain at both flanks Quebrada Choros.

4.2. Geochronology

and sieved to obtain the 250-1000 μm fraction. Mineral separation was obtained according to standard laboratory techniques in the Mineral Separation Laboratory of the Geology Department of the University of Chile. At least fifty zircons from each sample were mounted in epoxy and polished for laser ablation analyses at the University of Arizona. The U-Pb geochronology of zircons was carried out using by laser ablation-multicollector-inductively coupled plasma-mass spectrometry (LA-MC-ICP-MS) at the Arizona LaserChron Center (University of Arizona). Ages were calculated using the subroutine “Zircon Age extractor” of Isoplot (Ludwig, 2009), which implements an algorithm (“TuffZirc”) for extracting reliable ages and age-errors from suites of $^{206}Pb/^{238}U$ dates on complex single-zircon populations to finally provide a best estimate for the magmatic age of the tuff (Fig. 7).

5. Results

The pediplains studied here correspond to gently undulating bedrock and aggradational surfaces, which are exposed as patches that can be correlated based on their elevation and lateral connection. Furthermore, the pediplains must meet the criteria defined in the previous section. A total of five levels of pediplains are recognized within the study area (Fig. 5 and 8a and b). Despite differences in the pre-Neogene geological evolution between the regions located to the north and to the south of 30°S these five levels are systematically observed throughout the entire study area (Fig. 5). The two highest degradational pediplains; here named as La Silla and Corredores Pediplains, are located in the eastern Coastal Cordillera just to the east of the secondary topographic front (Fig. 5 and 8a and b). The Corredores Pediplain is also composed of an aggradational part exposed within the western Coastal Cordillera just to the west of the secondary topographic front north of 30°S (Fig. 5 and 8a). The Algarrobillo Pediplain is exposed within the western Coastal Cordillera just to the west of the secondary topographic front (Fig. 5 and 8a and b). The Algarrobillo Pediplain underlies the aggradational deposits related to the development of the Corredores Pediplain north of 30°S (Fig. 5, 8a and 6a and b). The Cachiyuyo Pediplain, which has a lower elevation in relation to the Algarrobillo Pediplain, is exposed in both the western and eastern Coastal Cordillera (Figs. 5 and 8a and b). It presents both degradational and aggradational counterparts (Fig. 5 and 8a and b). Finally, the lowest pediplain observed within the study area, the Ovalle Pediplain, occurs within the western Coastal Cordillera (Figs. 5 and 8a and b).

La Silla Pediplain

The La Silla Pediplain corresponds to a degradational bedrock surface always exposed just to the east of the secondary topographic front (Figs. 5, 8a and b and 6a, b and c). North of 30°S the pediplain is present in the western Frontal Cordillera and the eastern

Coastal Cordillera (Table 1, Fig. 5 and 8b). South of 30°S the pediplain forms the highest summits of the eastern Coastal Cordillera (Fig. 5 and 8b). The range of elevations of the La Silla Pediplain is constant throughout the study area lying between

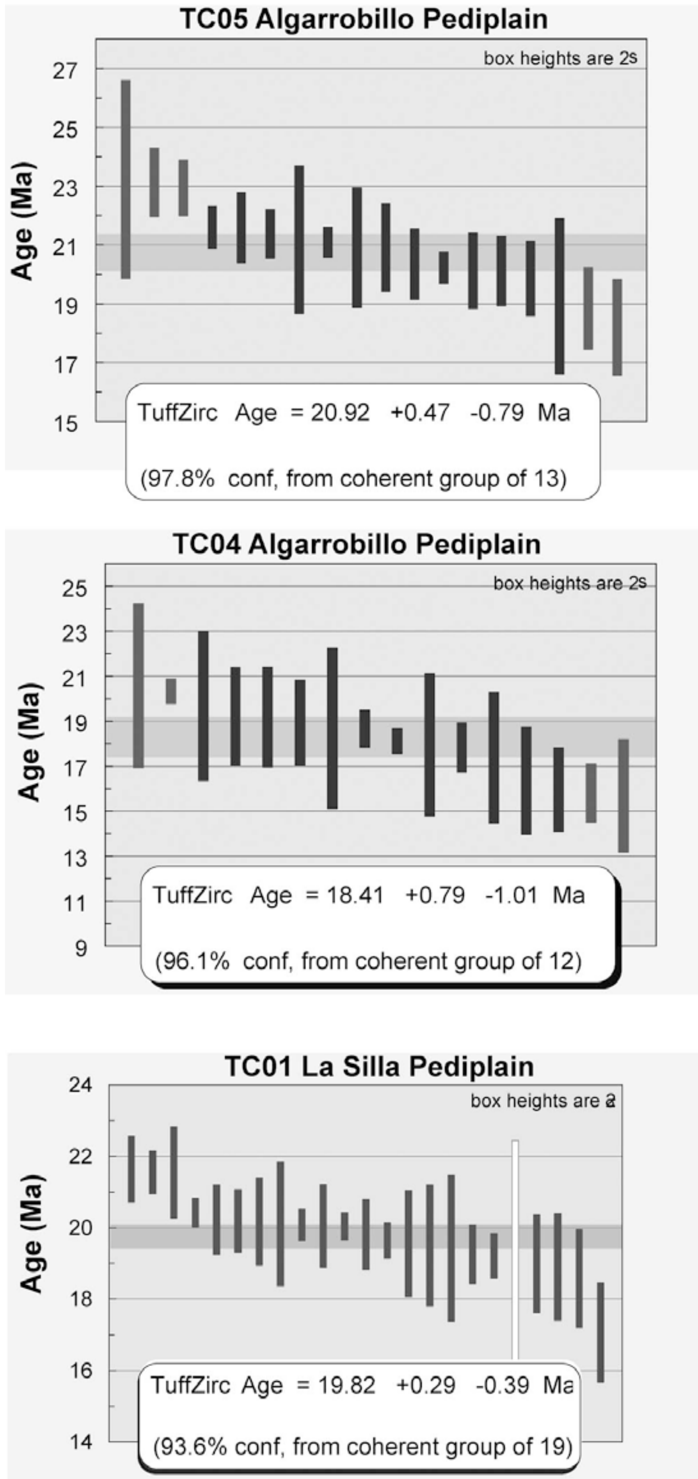

Fig. 7. LA-ICPMS U-Pb zircon ages obtained for tuffs covering the Algarrobillo and La Silla Pediplains. Errors are ±2σ.

3200-1800 m a.s.l. It is carved independent of the lithology into Upper Cretaceous and Paleocene volcano-sedimentary rocks and Paleocene to Eocene granitoids. Importantly, remnants of the La Silla Pediplain are exposed both west and east of the Vicuña Fault near the town of Hurtado (Fig. 9). The youngest rocks cross-cut by the La Silla Pediplain correspond to a granitoid with a U-Pb zircon age of 48.1±0.4 Ma (Table 1, Emparán and Pineda, 2006). One tuff sample interpreted as an ash fall overlying the La Silla Pediplain within the Choapa Valley was collected (Figs. 5, 7 and 8b). The U-Pb zircon age obtained for this tuff sample is 19.82*+0.29-0.39* Ma (Table 1, Fig. 5, 7 and 8b). Additionally, an andesitic lava with a K-Ar age of 17.3±1.4 Ma covers the dated tuff ~ 2 km south of the sampled site and within the same surface remnant (Table 1, Fig. 5 and 8b; Rivano and Sepúlveda, 1991).

Corredores Pediplain

The Corredores Pediplain is composed of both degradational and aggradational counterparts (Figs. 5 6b and c and 8a and b). Its degradational part is a bedrock surface only exposed in the eastern Coastal Cordillera and always incised into the La Silla Pediplain (Figs. 5 and 6c). The elevation of this bedrock surface ranges between 2000-1200 m a.s.l., throughout the entire study area. Similar to the La Silla Pediplain, it is mainly carved into the Upper Cretaceous and Paleocene volcanosedimentary rocks, but it is also well developed on top of Paleocene granitoids. The aggradational part of the Corredores Pediplain is exposed to the west of the secondary topographic front and only in the area located to the north of 30°S, within the Domeyko Depression (Figs. 5, 6b and 8a). It has an elevation range between 1400 and 800 m a.s.l., corresponding to the surface on top of the alluvial deposits of the Domeyko Gravels of probable Middle Miocene age (Table 1, Figs. 5, 6b and 8a). Importantly, the aggradational part of the Corredores Pediplain it is not observed south of 30º S (Figs. 5 and 8b).

Algarrobillo Pediplain

The Algarrobillo Pediplain is a degradational bedrock surface that is separated by the secondary topographic front from the La Silla Pediplain and the degradational part of the Corredores Pediplain throughout the entire study area (Figs. 5, 6a, 8 a and b). North of of 30° S, remnants of the Algarrobillo Pediplain are exposed on top of the NNE-NNW trending ranges of the Coastal Cordillera and within the Domeyko Depression (Fig. 5). Remnants exposed at the summits of the NNE-NNW trending ranges have elevations as high as 1800 m a.s.l. that diminishes seawards to 1200 m a.s.l. Within the Domeyko Depression the elevation of the Algarrobillo Pediplain is around ~ 1700 m at the foothills of the secondary topographic front just north of 30°S. Further north it diminishes to 1200 m a.s.l. and plunges underneath the Domeyko Gravels of probable Middle Miocene age (Figs.5, 6a and b and 8a). Remnants of the Algarrobillo Pediplain at the western border of the Domeyko Depression are at elevations that are slightly lower (~ 1500 - 1200 m a.s.l.), but within the same elevation range as those on top of the NNE-NNW trending ranges (~ 1800 - 1200 m a.s.l.). As no dislocation or encasement is observed between low relief/slope remnant surfaces of both areas, they are here in correlated as part of the

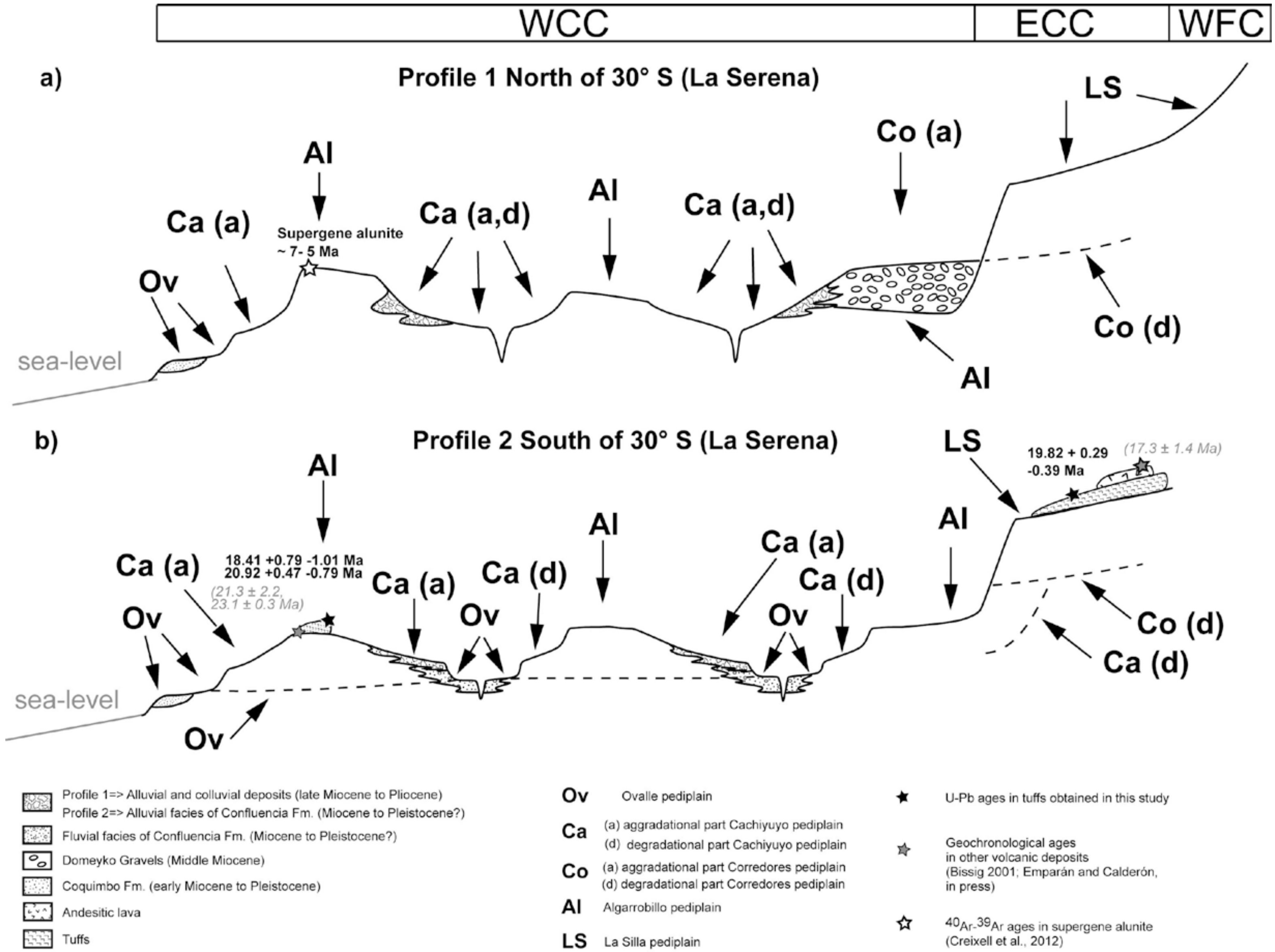

Fig. 8. a) Schematic profiles of pediplains from the Coastal and western Frontal Cordilleras north of 30ºS. b) Schematic profiles of pediplains from the Coastal Cordillera south of 30ºS.

same original pediplain. South of 30°S, the Algarrobillo Pediplain's remnants form the summits of the western Coastal Cordillera in a range of elevations between 1600 and 1100 m a.s.l. that diminish progressively seaward. Here, exposures of the Algarrobillo Pediplain are present as close as ~ 3 km to the present-day coastline (Fig. 5). The Algarrobillo Pediplain is carved mainly into Jurassic and Lower Cretaceous volcanosedimentary and intrusive rocks. Two samples were collected from an ignimbritic deposit at the top of the Algarrobillo Pediplain (Figs. 5, 7 and 8b). The U-Pb zircon geochronologic determinations for these samples give two similar ages of 20.92*+0.47-0.79* Ma and 18.41*+0.79-1.01* Ma (Fig. 5, 7 and 8b). In other studies two ages of 23.07±0.33 (^{40}Ar /^{39}Ar biotite) and 21.3±2.2 (K-Ar biotite) were obtained for tuffs overlying the Algarrobillo Pediplain just to the south of La Serena (Table 1, Figs. 5 and 8b; Bissig, 2001; Emparán and Calderón, in press). Additionally, the Algarrobillo Pediplain underlies the Domeyko Gravels of probably Middle Miocene age in the Domeyko Depression.

Cachiyuyo Pediplain

The Cachiyuyo Pediplain is composed of both aggradational and degradational bedrock counterparts (Figs. 5 and 8a and b). They are incised within north-to- south trending tributaries draining the Algarrobillo and Corredores Pediplains (Fig. 5, 8a and b). The

Name	Location	Description	Geochronological constrains
La Silla	ECC-WFC	Degradational	andesitic lava (other works)=> 17.3 ± 1.4 Ma (K-Ar whole rock) overlying tuffs (this work) => 19.82 +0.29 -0.39 Ma (U Pb zircon) youngest rocks crosscut (other works) => 48.1 ± 0.4 Ma U Pb zircon
Corredores	ECC	Degradational and aggradational (Domeyko Gravels)	probable middle Miocene age for Domeyko Gravels => probable late Miocene age for Corredores pediplain
Algarrobillo	WCC	Degradational	supergene alunite (incision timing) => ~ 7-5 Ma 40Ar-39Ar overlaid by Domeyko Gravels overlying tuffs (this work)=> 20.92 +0.47 -0.79 Ma and 18.41 +0.79 -1.01 Ma (U Pb zircon) overlying tuffs (other works)=> 23.07 ± 0.33 (40Ar /39Ar biotite) and 21.3 ± 2.2 (K-Ar biotite) Ma
Cachiyuyo	WCC-ECC	Degradational and aggradational (alluvial facies of Confluencia Fm. and Depósitos aluviales and coluviales antiguos)	probable late Miocene to early Pliocene age for "Depósitos aluviales and coluviales antiguos"=> probable late Pliocene age for Cachiyuyo pediplain
Ovalle	WCC	Degradational	^{10}Be cosmogenic ages between ~ (1200?) 800 and 500 ka (Rodríguez et al., 2013)

Table 1. Geochronological and relative ages used to constrain the development of pediplains from the Coastal and western Frontal Cordilleras in north-central Chile (28- 32º S).

elevation of the Cachiyuyo Pediplain mostly ranges between 1000 and 700 m a.s.l. north of 30°S and between 1100 and 500 a.s.l. south of 30°S. The degradational part of the Cachiyuyo Pediplain is carved mainly into Jurassic to Lower Cretaceous volcano-sedimentary and intrusive rocks and to a lesser degree into the Triassic succession of volcanic rocks and the Paleozoic metamorphic basement. Within the Domeyko Depression the aggradational part of the Cachiyuyo Pediplain corresponds to the surface on top of alluvial and colluvial sediments of probable Late Miocene to Pliocene age (Table 1, Figs. 8a and 9, Arévalo et al., 2009). South of 30°S, the aggradational part of the Cachiyuyo Pediplain corresponds to the surface on top of the alluvial facies within the Confluencia Formation (Table 1, Figs. 8b and 9, Emparán and Pineda, 2006), correlated with the alluvial and colluvial deposits exposed to the north of 30°S. In both areas the alluvial and colluvial deposits are adjacent to topographically higher areas corresponding mostly to remnants of the Algarrobillo and the aggradational part of the Corredores Pediplains (Fig. 8a and b).

Ovalle Pediplain

The Ovalle Pediplain is exposed south of 30°S as a single planation surface formed by morphologically continuous marine and continental landforms already described and dated using cosmogenic ^{10}Be (Rodríguez et al., 2013). These ^{10}Be cosmogenic age determinations indicate that the Ovalle Pediplain formed between ~ (1200?) 800 to 500 ka (Early to Middle Pleistocene, Table 1). Its elevation varies from ~100 m a.s.l. near the coast to ~ 400 m a.s.l. near the secondary topographic front. The Ovalle Pediplain is incised into the Algarrobillo and Cachiyuyo Pediplains (Figs. 5 and 8a and b) and has been uplifted ~150 m above the present-day thalwegs (Rodríguez et al., 2013). Whereas the marine landforms mainly correspond to a wide shore platform; the continental landforms correspond to a high fluvial terrace and a pediment morphologically connected and systematically exposed throughout the lower and middle courses of present-day river valleys in the area south of 30°S (Figs. 5 and 8b, Rodríguez et al., 2013). In this area, the Ovalle Pediplain crosscuts Jurassic granitoids and the Paleozoic metamorphic basement and the older alluvial and fluvial facies of the Confluencia Formation within the valleys. According to the interpretation of the concentration of cosmogenic ^{10}Be in samples from the high fluvial terrace, this landform corresponds to an older aggradational terrace related to fluvial deposition of the Confluencia Formation later modified during the pedimentation event leading to the development of the Ovalle Pediplain (Rodríguez et al., 2013). North of 30°S the Ovalle Pediplain is restricted to the coastal region (Fig. 5 and 8a) where it is exposed as a wide shore platform or *rasa* (Regard et al., 2010). Near the coast in both areas, the shore platform is carved into Jurassic and Triassic granitoids, the Miocene to Pleistocene marine deposits of the Coquimbo Formation (Fig. 8a and b) and the Paleozoic metamorphic basement.

6. Discussion

6.1. Age of formation and incision of pediplains

The age of pediplains are generally constrained by the youngest geological unit overlain by the pediment and the youngest unit covering the surface (e.g. Bissig et al., 2001). Whereas the age of the youngest geological unit eroded by the pediment constrains the maximum age of initiation of pediplain development, the age of the youngest unit covering this surface is used to constrain the minimum age of development of the pediplain. Finally, it is also important to consider the relative ages given by the relationship of incision between two pediplains (Table 1).

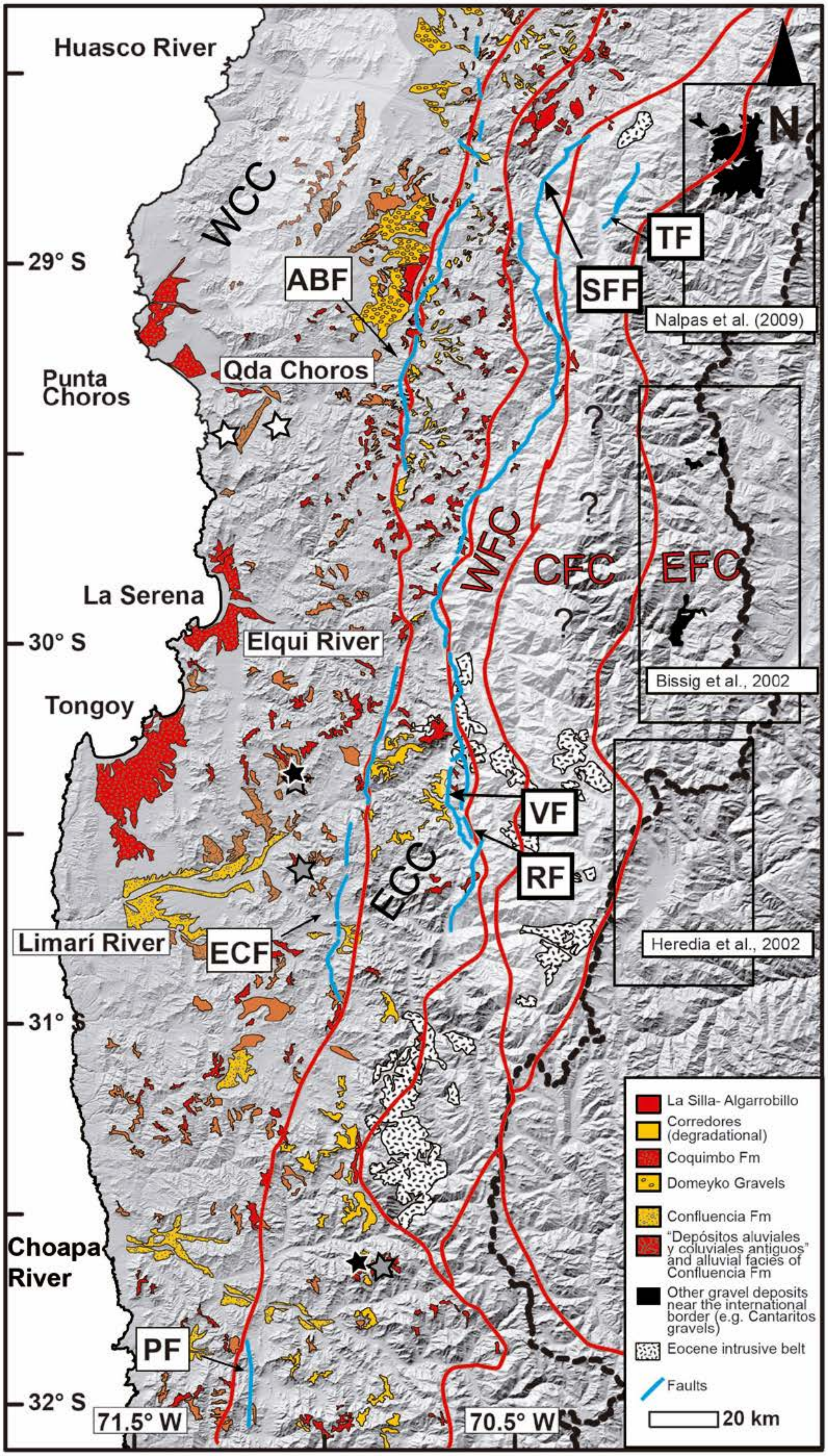
Huasco River
WCC
29° S
ABF
Qda Choros
Punta Choros
La Serena
30° S
Elqui River
Tongoy
Limarí River
ECF
ECC
31° S
Choapa River
PF
32° S
71.5° W
70.5° W
WFC
CFC
EFC
TF
SFF
VF
RF
N
Nalpas et al. (2009)
Bissig et al., 2002
Heredia et al., 2002
La Silla- Algarrobillo
Corredores (degradational)
Coquimbo Fm
Domeyko Gravels
Confluencia Fm
"Depósitos aluviales y coluviales antiguos" and alluvial facies of Confluencia Fm
Other gravel deposits near the international border (e.g. Cantaritos gravels)
Eocene intrusive belt
Faults
20 km

Regardless of the mechanism by which the tuffs were deposited on top of the Algarobillo and La Silla Pediplains, the ages obtained (Table 1) indicate that both surfaces were subplanar components of the landscape by the Early Miocene. However, it is known that ignimbritic flows or ash falls are able to surge up valley flanks. This could imply that the Algarobillo and La Silla Pediplains were not necessarily graded to base level when the tuffs were deposited on top. The La Silla Pediplain is also covered by an andesitic lava of ~ 17 Ma (Table 1, Figs. 5 and 8b; Rivano and Sepúlveda, 1991). As lava is not able to surge up valley flanks, the La Silla Pediplain was graded to its base level when both deposits covered this surface. The Early Miocene ages of several tuffs (Table 1, Figs. 5 and 8b) covering the Algarrobillo Pediplain are in good agreement with the underlying position of this surface with respect to the Domeyko Gravels of probable Middle Miocene age within the Domeyko Depression (Fig. 8a, see also Fig. 5.1a and b). The fact that the Algarrobillo Pediplain served as a depocenter for the Domeyko Gravels also suggests that it was graded to its base level by the Early Miocene, just before deposition of this unit. Importantly, exposures of the La Silla Pediplain are systematically separated from the Algarrobillo Pediplain remnants by a secondary topographic front of ~ 1100 m (Figs. 8a and b, see also Fig. 5.1, Fig 5.2). This scarp could present two different origins. One implies that both pediplains formed a once continuous surface that was displaced after ~ 17 Ma by a series of N-S faults, namely, the Agua de los Burros, El Chape and Pupio Faults (Fig. 10a; Moscoso et al., 1982; Rivano and Sepúlveda, 1991; Pineda and Emparán, 2006; Arévalo et al., 2009), which are spatially correlated with the secondary topographic front (Fig. 9). The other possibility is that this feature results from scarp retreat after regional uplift of a single surface (Fig. 10b). In such a case, the La Silla Pediplain would be older than the Algarrobilllo Pediplain (Fig. 10b). On the contrary, the ages between ~ 23 and 18 Ma of tuffs overlying the Algarrobilllo Pediplain are slightly older than the age of ~ 19-17 Ma of volcanic deposits overlying the La Silla Pediplain. Therefore, the geomorphological and geochronological data described here strongly suggest that the La Silla and the Algarrobilllo Pediplains once formed a single low relief/slope surface that was later offset by N-S faults that displaced the La Silla Pediplain to higher elevations (Fig. 10a).

According to the estimated age of the Domeyko Gravels, offset from the original La Silla - Algarrobilllo single surface would have occurred after ~ 17 Ma and prior to the Middle Miocene. After the offset of this original surface, the degradational and aggradational parts of the Corredores Pediplain developed on top of the La Silla and Algarrobillo

Fig. 9. Shaded relief image of the study area showing the trace of main faults and showing remnants of the Corredores and Algarrobillo Pediplains, as well as outcrops of Lower Miocene to Pleistocene continental and marine deposits. Black stars show location of tuffs dated by U-Pb zircon geochronology overlying the La Silla Pediplain in Cerro Carrizo and the Algarrobillo Pediplain in Quebrada Higuerillas. Grey stars show location of volcanic deposits overlying the La Silla and Algarrobillo Pediplains dated in previous studies (Rivano and Sepúlveda, 1991; Bissig, 2010, Emparán and Calderón, in press). White stars show location of supergene alunite samples dated by ^{39}Ar-^{40}Ar geochronology by Creixell et al. (2012). Black lines mark the position of topographic fronts. Red lines mark the boundaries between the different blocks composing the Frontal Cordillera. Blue lines mark the trace of main faults. Boxes show the areas of the Eastern Frontal Cordillera where Neogene pediplains have been described. The areas in transparent white indicate the probable extension of an Eocene positive relief in the western Coastal Cordillera and of the Main Incaic Range along the western and central Frontal Cordillera. WCC: western Coastal Cordillera; ECC: eastern Coastal Cordillera; WFC: western Frontal Cordillera; CFC: central Frontal Cordillera; EFC: eastern Frontal Cordillera, PC: Principal Cordillera. ABF: Agua de los Burros Fault; ECF; El Chape Fault, PF: Pupio Fault, VF: Vicuña Fault, RV: Rivadavia Fault, SFF: San Félix Fault, TF: La Totora Fault.

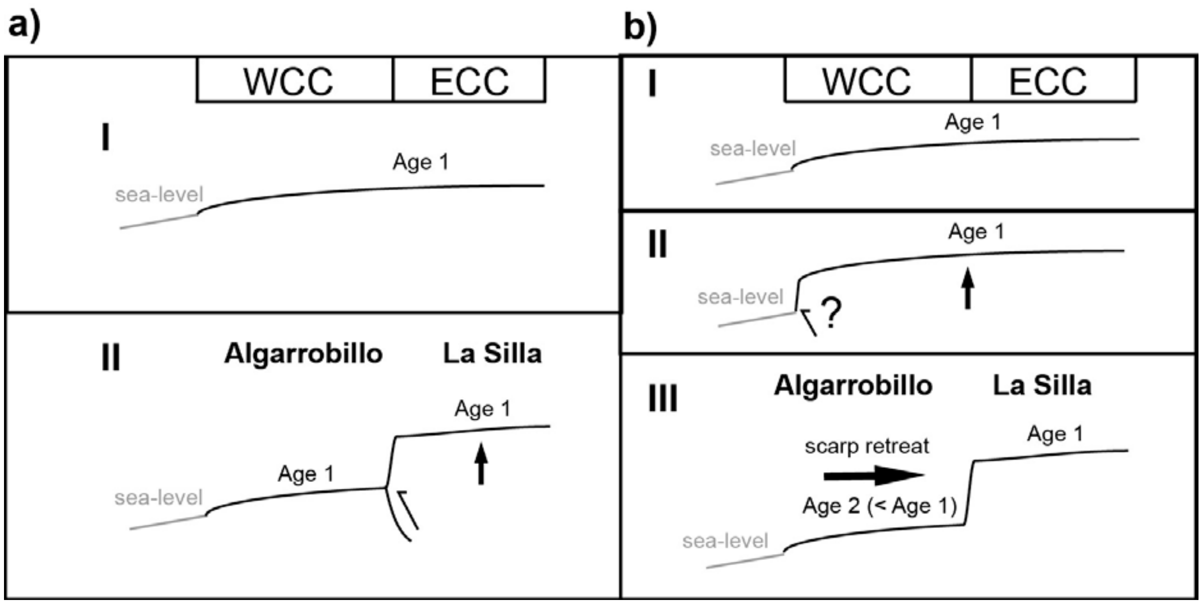

Fig. 10. Schematic profiles showing possible origins for the original La Silla- Algarrobillo Pediplain. a) Original La Silla-Algarrobillo Pediplain formed near sea-level and offset by N-S trending faults aligned with the secondary topographic front. b) Original La Silla- Algarrobillo Pediplain formed near sea-level with the secondary topographic front formed due to scarp retreat.

Pediplains, respectively (Figs. 11a and b). According to the probable Middle Miocene age of the Domeyko Gravels the Corredores Pediplain was already formed by the Late Miocene (Table 1, Figs. 11a and b). Presently the Corredores Pediplain's remnants are located several hundreds of meters above the river thalwegs (Figs. 8a and b). Similarly, the Algarrobillo Pediplain's remnants, which underlie the aggradational part of the Corredores Pediplain (Figs. 8a and b), are also located several hundreds of meters above present-day river's thalwegs (Fig. 8a and b). Thus, both surfaces were incised after the Late Miocene (Figs. 11a and b). ^{40}Ar-^{39}Ar ages on supergene alunite in the range ~ 7-5 Ma were obtained from samples collected from the Algarrobillo Pediplain and valleys incising this surface near Quebrada Choros (Table 1, Figs. 5 and 8a,Creixell et al., 2012). Episodes of supergene copper enrichment are thought to occur under semiarid conditions beneath pediplains due to abrupt descents in the water table and concomitant pediment incision (Sillitoe et al., 1968; Mortimer, 1973; Tosdal et al., 1984; Quang et al., 2005). It is not clear if such abrupt descents are related to tectonic uplift (Mortimer, 1973) or to changing climatic conditions (Arancibia et al., 2005). Regardless of the cause of water table descents, the ages of supergene alunite are consistent with incision of the Algarrobillo Pediplain taking place between ~ 7 and 5 Ma (Late Miocene to Early Pliocene, Table 1). With respect to the Cachiyuyo Pediplain, the estimated age for the alluvial to colluvial deposits related to the aggradational part of the Cachiyuyo Pediplain is Late Miocene to Early Pliocene (Table 1). Thus, the age of the Cachiyuyo Pediplain is younger than Early Pliocene, probably Late Pliocene (Table 1). Finally, the ^{10}Be cosmogenic age determinations made by Rodríguez et al. (2013) indicate the Ovalle Pediplain formed between ~ (1200?) 800 to 500 ka (Early to Middle Pleistocene, Table 1).

In the eastern Frontal Cordillera near the international border between 29 and 30°S at the head of the Huasco and Elqui Rivers, three once continuous levels of pediplains are well preserved (Bissig et al., 2002, Fig. 9). The higher pediplain, the Frontera-Deidad surface (4600–5300 m a.s.l.), intersects intrusive bodies with an ^{40}Ar-^{39}Ar age of ~ 18 Ma (Bissig et al., 2002), which constrains its maximum age. The minimum age of this surface is inferred to be 15 Ma (Bissig et al., 2002).Farther north within the Huasco River's headwaters a smooth surface (4350- 4500 m a.s.l.) is defined by the top of a package of gravels, informally named the Cantarito gravels, previously correlated with the Atacama Gravels (Fig. 9, Cancino, 2007, Nalpas et al., 2009) exposed within the Central Depression at 27°S (Mortimer, 1973). This surface probably corresponds to the aggradational part of the Frontera-Deidad surface as an ignimbrite at the base of the gravels was dated at 22 ± 0.6 Ma (K-Ar, Cancino, 2007). Entrenched into the Frontera-Deidad surface, the Azufrera-Torta is observed (4300–4600 m a.s.l.). The minimum age of the Azufrera-Torta surface is constrained by an overlying dacitic tuff with an ^{40}Ar-^{39}Ar age ~ 12.7 Ma (Bissig et al., 2002). Finally, the pedimentation process finished with the incision of the paleovalley formed by the Los Rios surface, whose minimum age is defined by an ignimbrite on top presenting an ^{40}Ar-^{39}Ar age of ~ 6 Ma (Bissig et al., 2002). The few peaks that arise on top of the Frontera-Deidad surface would correspond to vestiges of an older uplifted surface, the Cumbre surface, which represents a local backscarp of the Frontera-Deidad surface (Bissig et al., 2002). According to the rocks that cross-cut this surface and its relationship with the Frontera-Deidad surface (Bissig et al., 2002), the probable age of the Cumbre surface is Late Oligocene-Early Miocene. Between 30 and 31°S, Heredia et al. (2002) recognized an extensive planation surface on top of rocks of the Permo-Triassic basement and covered by Early Miocene lavas (~ 18 Ma), which may also be correlated with the Cumbre surface surface (Fig. 9).

Independently of the mechanisms involved in pediplain development at both locations, the similarity between the ages presented here and the ages obtained by Bissig et al (2002) indicates that tectonic and climatic conditions were favorable for pediplain formation in the Coastal Cordillera - western Frontal Cordillera and in the eastern Frontal Cordillera since the Early Miocene. *A priori*, some chronological correlations among the pediplains from the both areas can be suggested with the age information and regional correlations given here. The Early Miocene minimum age of the original La Silla-Algarrobillo Pediplain indicates that this surface formed coevally with the Late Oligocene-Early Miocene Cumbre surface. Deposition of the Domeyko Gravels and the development of the probable Late Miocene Corredores Pediplain would have outlasted the formation of both, the Frontera-Deidad and the Azufrera-Torta Pediplain, which formed after the Early Miocene (~ 22-18 Ma) and during the Late Miocene (~ 12 Ma), respectively. Importantly, the timing of incision of the Algarrobillo Pediplain (~ 7-5 Ma) coincides with the incision of the palleovalley of the Los Rios surface (~ 6 Ma). Finally, the age correlations between pediplains from the western Coastal Frontal Cordillera and the eastern Frontal Cordillera made here are only preliminary as further geomorphological and geochronological data are needed to support these correlations.

6.2. Location of pediplains with respect to the Incaic relief

Taking the constraints on Eocene to Oligocene upper plate deformation as indicators of the Main Incaic Range, it is possible to state that within the Huasco Valley the Main Incaic Range formed a NNE-NNW trending belt offset ~ 15 km to the east of the main topographic front (Fig. 9). Here, the Main Incaic Range would have extended throughout the present-day western Frontal Cordillera and central Frontal Cordilleras. Within the Elqui and the northern Limarí Valleys, constraints on Eocene deformation and fission track thermochronology indicate that the position of the Main Incaic Range was shifted to the west with respect to further north, forming a narrow N-S mountainous belt between the Vicuña and Rivadavia Faults (Fig. 9; Cembrano et al. 2003; Emparán and Pineda, 2006; Pineda and Calderón, 2009). However, exposures of Eocene (Oligocene?) arc-like stocks (Bocatoma unit, Mpodozis and Cornejo, 1988) are observed further to the east (Fig. 9). The geochemical signature of these rocks indicates that they developed in a compressional arc tectonic regime (Bissig et al., 2003, Winocur et al., this volume). Thus, the Main Incaic Range probably extended further to the east in this area (Fig. 9), occupying the present-day western Frontal Cordillera and central Frontal Cordilleras. Thus, from 31°S to the north, the Eocene to Oligocene paleotopography was mostly characterized by the presence of the Main Incaic Range along the western and central Frontal Cordillera (Fig. 9). No structural or thermochronological evidence exists of the presence of an Eocene to Oligocene mountainous range in the area to the south of 31°S (Fig. 9).

Importantly, apatite fission track and U-Th/He thermochronology indicate that rocks from the Coastal Cordillera to the west of the Domeyko Depression were exhumed in response to uplift by the Middle to Late Eocene (Maksaev et al., 2009, see Fig. 3.1). Thus, to the north of 30°S the Eocene to Oligocene paleotopography was characterized by the presence of a positive relief in the western Coastal Cordillera to the west of the Domeyko Depression (Fig. 9). To the south of 30°S, apatite fission track ages between ~ 120 and 80 Ma in the western Coastal Cordillera (Cembrano et al., 2003) and thermal modeling of apatite fission track and apatite (U-Th)/ He (Rodríguez et al., 2012a; see Fig. 3.1) indicate that this area was exhumed in response to uplift by the Early to Late Cretaceous, prior to the Incaic Orogenic Phase.

The mentioned constrains on Eocene to Oligocene contractional deformation and exhumation are in good agreement with the spatial distribution of Neogene pediplains described here for the Coastal Cordillera and described in previous works for the eastern Frontal Cordillera (Fig. 9). North of 31°S, the La Silla Pediplain seems to follow the western border of the Main Incaic Range as their remnants are exposed along the western Frontal Cordillera in the area of the Huasco Valley; whereas within the Elqui and Limarí Valleys the La Silla Pediplain is exposed farther to the west forming the highest summits of the eastern Coastal Cordillera (Fig. 5). Moreover, in the Elqui and the Limarí valleys, remnants of the La Silla Pediplain are observed both to the west and to the east of the Vicuña Fault trace, implying that this landform resulted from the scarp retreat of the already elevated Eocene-Oligocene Main Incaic Range exposed along the western and central Frontal Cordillera. In the high Frontal Cordillera of the same area (north of

31°S), previous works indicate that Neogene pediplains developed along the eastern Frontal Cordillera, to the east of the position of the Main Incaic Range inferred here (Fig. 9). Thus, Neogene pediplains developed to the west and east of the Main Incaic Relief (Fig. 9). No evidence of Incaic deformation has been described south of 31°S. However, remnants of the La Silla Pediplain are anyway located immediately to the west of the exposures of Eocene to Oligocene magmatic rocks that mark the position of the Eocene-Oligocene volcanic arc (Fig. 9). Finally, with respect to the pediplains of the western Coastal Cordillera, the differences on exhumation timing to the north and to the south of 30°S are in good agreement with the slight relief display by the Algarrobillo Pediplain north of 30°S and the absence of such relief south of 30°S (Fig.8 a and b, Fig. 9).

The spatial relationship between the La Silla Pediplain and the areas affected by Eocene to Oligocene deformation in the Frontal Cordillera suggests a strong control of the Incaic paleotopography on the Neogene landscape evolution of both the Coastal and Frontal Cordilleras in the study area (Fig. 9). This is consistent with the previous proposition of Charrier et al. (2007), which suggested that the Main Incaic Range may have acted as the Eocene to Oligocene water divide.

Finally, the fact that the La Silla Pediplain cuts across the Vicuña Fault indicates that the topographic front corresponds to a degradational feature inherited from previous orogenic phases rather than a Late Oligocene-Early Miocene deformation front as previously stated by Aguilar et al. (2013).

6.3. Constraints on the original base level and the timing of uplift in the Coastal and Frontal Cordilleras

Low relief/slope surfaces can develop at high elevations (above sea-level) if downstream aggradation occurs, allowing the establishment of a new and higher base level and the concomitant reduction of the erosive efficiency of the drainage system. All of that finally induces the progressive smoothing of the relief upstream (Babault et al., 2005).

The geomorphological and geochronological data described above strongly suggest that the La Silla and the Algarrobilllo Pediplains once formed a single low relief/slope surface. By the Early Miocene this single surface dominated the landscape of the present-day Coastal Cordillera throughout the entire study area, but also involved the present-day western Frontal Cordillera north of 30°S (Fig. 11a and b). Importantly, the La Silla- Algarrobillo surface displayed a slight relief north of 30° S, with NNE-NNW oriented ranges to the west of the Domeyko Depression at relatively higher elevations (Fig. 11a). The presence of a higher topography in this area prior to the Early Miocene is consistent with apatite fission track and U-Th/He thermochronology (Maksaev et al., 2009) indicating that rocks from the western Coastal Cordillera to the west of the Domeyko Depression were exhumed in response to uplift by the Middle to Late Eocene. Moreover, the sedimentology of the Domeyko Gravels also indicates that they accumulated in a closed basin with a local sediment source (Arévalo et al., 2009). According to Le Roux et al. (2004, 2005, 2006), shallow marine sedimentation related to the Coquimbo Formation was already taking place in the Tongoy Bay and at Punta Choros, immediately to the west of the La Silla- Algarrobillo Pediplain by the Early Miocene around ~ 23 and 18 Ma, respectively (Figs. 4 and 9; Coquimbo Formation). This indicates that the original base level for this surface would probably correspond to sea-level. Disruption of the original La Silla- Algarrobillo surface and relative uplift of the eastern Coastal Cordillera (and western Frontal Cordillera north of 30°S) with respect to the western Coastal Cordillera occurred after ~ 17 Ma. It is unclear if the Domeyko Gravels correspond or not to syn-tectonic deposits (Garrido, 2009). Therefore, more sedimentological and geochronological work is needed to establish if disruption of the original La Silla- Algarrobillo surface occurred during the Early Miocene or extended into the Middle Miocene. A similar Early to Middle Miocene period of uplift is interpreted from apatite fission track and U-Th/He data that indicate accelerated cooling affecting the central Frontal Cordillera between ~ 20 and 15 Ma (Cembrano et al., 2003; Rodríguez et al., 2012a). Moreover, Early to Middle Miocene contractional deformation and related uplift would have extended into the eastern Frontal Cordillera according to structural (Winocur, 2010; Winocur et al., this volume) and geomorphological data (Bissig et al., 2002).

After disruption of the original Algarrobillo-La Silla surface, the development at high elevation of the degradational part of the Corredores Pediplain is explained by the geomorphological connection with the top of the Domeyko Gravels. However, the Corredores Pediplain is not geomorphologically continuous with any aggradational surface south of 30°S. One possibility is that in this area the Corredores Pediplain was tectonically uplifted to its present-day elevation by the same N-S faults which previously displaced the La Silla Pediplain (Fig. 9). Nevertheless, south of 30°S the Corredores Pediplain usually presents the same range of elevations (2000-1200 m a.m.s.l.) as in the Domeyko Depression and it is also always entrenched within the La Silla Pediplain. Therefore, the most probable explanation is that the Corredores Pediplain was actually formed at high elevations due to aggradation to the west of the secondary topographic front throughout the entire study area, but these deposits were later removed south of 30°S. The presence of a topographic barrier to the west of the Domeyko Depression north of 30° S (Fig. 8a) would allow preservation of the Domeyko Gravels after incision of the Corredores Pediplain. In contrast, the absence of such a barrier south of 30°S (Fig. 8b) probably allowed erosion and remobilization of deposits associated with the Corredores Pediplain overlying the Algarrobilo Pediplain. South of 30°S the western border of the Corredores Pediplain coincides with the maximum extension to the east of the Miocene to Pleistocene fluvial facies of the Confluencia Formation (Fig. 9 and 8b; Rivano and Sepúlveda, 1991; amend. Emparán and Pineda, 2000). These deposits may correspond to the aggradational deposits related to the Corredores Pediplain, later remobilized from the top of the Algarrobillo Pediplain due to incision, and re-deposited within the river valleys that incised this surface (Fig. 8b and 11b). With respect to the Algarrobillo Pediplain, it is known that marine deposition of the Coquimbo Formation was still taking place to the west by the Late Miocene when incision on top of this pediplain started, as suggested by supergene alunite ages (Figs. 5 and 8a; Creixell et al., 2012). Since sea-level was the base-level for the Algarrobillo Pediplain during most of the Miocene, this surface was necessarily uplifted to its present-day high elevations.

Therefore, the incision ages between 7-5 Ma indicate that uplift of the Algarrobillo Pediplain started before 7 Ma. Thus, uplift of the Algarrobillo Pediplain probably occurred in the Late Miocene before 7 Ma (Fig.11a and b).

Importantly, the transition between a hyperarid climate to the north of 27°S and a humid climate south of 33°S occurred ~ 15 Ma (Le Roux, 2012). Thus, aggradation of the Middle Miocene Domeyko Gravels and development at high elevations of the degradational part of the Corredores Pediplain may be related, at least in part, to a climatically-driven decrease of the transport capacity of rivers (Fig. 11a and b). Most probably, later incision on top the aggradational/ degradational Corredores Pediplain is a consequence of the Late Miocene uplift of the underlying Algarrobillo Pediplain (Fig. 11a and b). Late Miocene uplift of these pediplain is consistent with chronostratigraphic analysis performed in the marine Coquimbo Formation evidencing a period of generalized uplift affecting the coastal areas next to the Algarrobillo Pediplain by the Late Miocene (Le Roux et al., 2005). Finally, uplift of the Algarrobillo and Corredores Pediplains indicates the entire present-day Coastal Cordillera was uplifted by the Late Miocene (Fig. 11b) south of 30°S, whereas north of 30°S Late Miocene uplift also involved areas of the western Frontal Cordillera (Fig. 11a).

By the Late Pliocene, the Cachiyuyo Pediplain developed at the foot of the Algarrobillo and Corredores Pediplains (Fig. 11a and b). The local base level for development of the Cachiyuyo Pediplain is given by the aggradation related to the alluvial and colluvial deposits north of 30°S (Arévalo et al., 2009) and the alluvial facies within the Confluencia Formation south of 30°S (Emparán and Pineda, 2006) (Fig. 8a and b and 9). South of 30°S these deposits interfinger towards the center of the present-day valleys with fluvial facies within the Confluencia Formation (Fig. 8b). Therefore, base-level for the Cachiyuyo Pediplain probably corresponded to the original surface on top of this facies of the Confluencia Formation that was later modified by the pedimentation event leading to formation of the Ovalle Pediplain (Fig. 8b; Rodríguez et al., 2013). The Cachiyuyo Pediplain was formed during the Late Pliocene (Table 1). There are no arguments to decide whether incision of the Cachiyuyo Pediplain has a tectonic or climatic origin. According to geohistorical analysis of the Coquimbo Formation strong uplift of the coastal area since ~ 2 Ma led to the emergence of the Tongoy Bay sediments (Fig. 9, Le Roux et al. 2006). Thus, one possibility is that uplift by ~ 2 Ma would have also affected the Coastal Cordillera to the west of the Tongoy Bay. However, there is no direct evidence pointing to tectonic-related incision of the Cachiyuyo Pediplain (Fig. 11a and b). Finally, according to Rodriguez et al. (2013) the Ovalle Pediplain was uplifted ~ 150 m, after ~500 ka (Fig. 11a and b).

6.4. Tectonic versus erosional controls

The similarity in elevation and the latitudinal continuity of the different levels of pediplans described here show that the timing of Neogene to Quaternary surface uplift was similar north and south of the city of La Serena (30°S). Nevertheless two main important differences in pediplain development and preservation are observed between both areas:

1. North of 30°S the Algarrobillo pediplan is covered by the Domeyko Gravels (Fig. 8a) that were probably deposited in the Middle Miocene within a basin disconnected from the sea and flanked to the west by NNE ranges. In contrast, south of 30°S the same pediplain is uncovered and more incised according to hypsometric analysis (Aguilar et al., 2013). In this area, the Miocene to Pleistocene continental deposits from the Confluencia Formation are encased within the broad valleys that incise the Algarrobillo Pediplain (Fig. 8b). Part of these deposits probably corresponds to material remobilized after the Middle Miocene from an original position on top of the Algarrobillo Pediplain, otherwise the Corredores Pediplain could not have developed at high elevations. Near the coast, the Confluencia Formation changes laterally towards the west in to the marine Coquimbo Formation (Fig. 4).

2. South of 30°S the Ovalle Pediplain is a wide Early to Middle Pleistocene planation surface composed of marine and continental erosion landforms, with the continental erosional surfaces developed on top of the older fluvial gravels of the Confluencia Formation (Fig. 8b). In contrast, to the north of 30°S the Ovalle Pediplain forms a much narrower strip next to the coast that is mainly composed of shore platforms mostly disconnected from continental erosion surfaces inland (Fig. 8a).

In summary, a morphologic and sedimentary connection between the river and the coastal systems is observed south of 30°S since at least the Early Miocene that is not detected further north. This indicates that the drainage system south of 30°S has presented a larger capacity to incise and transport material towards the sea than the drainage system to the north. According to the sedimentological features of the Domeyko Gravels (Arévalo et al., 2009) and the paleotopography of the Algarrobillo Pediplain, by the Early Miocene the ability of the river to incise and transport was inhibited by the blocking of the drainage exerted by high NNE trending ranges just to the west of the Domeyko Depression.

Presently, in spite of the lower elevation of N-S oriented ranges in the western Coastal Cordillera south of 30°S relative to the NNE-NNW oriented ranges to the north, low slope, depressed areas aligned with the Domeyko Depression are also locally observed within the Algarrobillo Pediplain south of La Serena (Fig. 2c). In Fig. 2c it is also shown how rivers draining these depressions are captured by higher order channels within the Elqui and Limarí Valleys. Therefore, the differences in pediplain development after the Early Miocene in both areas seem to be related to the ability of the main channels to capture lower order channels (Farías, 2007). There are three possible explanations for this: 1) the rocks are easier to erode south of 30°S (Farías, 2007), 2) the slope is higher south of 30°S (Carretier et al., 2013) or 3) the water flow is higher than further north (Whipple and Tucker, 1999). The first possibility is ruled out because depressions of both areas are developed on top of the same lithological units, Early Cretaceous granitoids to the west and Lower to Upper Cretaceous volcano-sedimentary rocks to the east. The second possibility is rejected because regional slope would depend on previous topography (before the Early Miocene) dominated by the Main Incaic Range, that according to structural and exhumation data diminishes in importance south of 31°S. The last possibility is the favored explanation because water flow depends on the drainage area and precipitation. Indeed, the areas drained by that of the Elqui, Limarí and Choapa Rivers are evidently higher than the one drained by the rivers in the Domeyko Depression as indicated by their higher Sthraler order (Fig. 2c). However, the high order of the main channel of the Huasco Valley indicates that its drainage area is also significant and similar to the Elqui, Limarí and Choapa rivers. This suggests that drainage area could be an important, but not dominant factor controlling landscape evolution in the study area. However, it is observed that precipitation rises from < 100 mm/yr to > 300-200 mm/yr south of 30°S (Fig. 2a). This latitude marks the northernmost penetration of the southern hemisphere westerlies, which bring moisture from southern latitudes, opposite to the effect of the Pacific Anticyclone, the main responsible for the hyperaridity of the Atacama Desert to the north. The latitudinal precipitation gradient was acquired after the Middle Miocene by the combination of a series of events including glaciations in West Antartica, formation of the Humboldt Current and uplift of the Andes (Le Roux, 2012). Thus, it is proposed here that a rise in water flow due to higher precipitation south of 30°S would have played an important role in determining the differences in geomorphological evolution observed along the Coastal Cordillera north and south of 30°S since the Middle Miocene. Such a precipitation gradient was superimposed on the previous pre-Neogene paleotopography that presented a strong inherited Incaic component. Thus, the paleotopography inherited from the Eocene to Oligocene (Incaic) phase of uplift and deformation in both the Coastal and Frontal Cordilleras would correspond to a dominant factor controlling Neogene landscape development in the study area.

Uplift timing throughout the study area closely correlates with episodes of increased contractional deformation recognized throughout the western flank of the Andes to the north of 27°S and to the south of 33°S. The Early (Middle?) Miocene uplift stage of the eastern Coastal Cordillera correlates with a period of intense deformation in the Altiplano of northern Chile (Pinto et al., 2004; Victor et al., 2004; Farías et al., 2005) that is also recognized in southern Perú (Mégard, 1984) and with the tectonic inversion of the extensional volcano-sedimentary Abanico Basin in central Chile south of 32°S (Charrier et al., 2002). In northern Chile, late Oligocene- Early Miocene uplift and deformation is thought to have been focused along the western border of the Altiplano and has not been identified throughout the Coastal Cordillera. However, in central Chile late Oligocene- Early Miocene contractional deformation and uplift extended into the present-day Central Depression in central Chile (Fock, 2005; Rodríguez et al, 2012b). Here, the west-vergent north-to-south trending Los Ángeles-Infiernillo Fault corresponding to the western border of the Abanico Basin (Charrier et al., 2002), uplifted the eastern part of the present-day Central Depression by the Early Miocene (Rodríguez et al, 2012b). The Los Ángeles-Infiernillo Fault is roughly aligned and can be correlated with the north-to-south Agua de los Burros and El Chape Faults that uplifted the eastern Coastal Cordillera with respect to the western Coastal Cordillera by the Early (Middle?) Miocene in north-central Chile.

The Late Miocene uplift stage of the western and eastern Coastal Cordillera correlates with regional uplift of the forearc region recognized in southern Perú (Tosdal et al., 1984; Clark et al., 1990; Quang et al., 2005; Schildgen et al., 2007), northern Chile (Hoke et al., 2007; Hoke and Garzione, 2009), the Southern Atacama Desert (Riquelme et al., 2007; Nalpas et al., 2008) and central Chile south of 33° S (Farías et al., 2008; Maksaev et al., 2009). The post-500 ka uplift of the Ovalle Pediplain correlates with a renewal of uplift of marine landforms along the Pacific coast post 400 ± 100 ka after an Early to Middle Pleistocene period of relatively slow uplift identified to the north of La Serena (30°S) by Regard et al. (2010). Uplift of the Ovalle Pediplain also correlates with Pleistocene to Holocene uplift of pediments and other continental landforms along the forearc of southern Peru and northern Chile (González et al., 2003, 2006; Kober et al., 2007; Hall et al., 2008; Saillard et al., 2008; Jordan et al., 2010).

Increased deformation by the Early (Middle?) Miocene would be explained by a more intense stress transmission and widespread strain due to an increased plate convergence rate (Charrier et al., 2009; 2013) after break-up of the Farallon into the Nazca and Cocos Plate (Pardo-Casas and Molnar, 1987). Paradoxically,the second period of major uplift along the Coastal Cordillera during the Late Miocene coincides with a period of deceleration of plate convergence (Pardo-Casas and Molnar, 1987), contrary to what is observed for the Early (Middle?) Miocene. The driving forces for Late Miocene and Middle Pleistocene uplift are still unclear and a matter of great debate in the case of the Late Miocene (Garzione et al., 2006; Barnes and Ehlers, 2009). To determine these driving forces is beyond the scope of the study. However, the fact that Late Miocene and Middle Pleistocene uplift is recognized for such a vast area from southern Perú to central Chile suggests that they were also controlled by first order tectonic features.

7. Conclusions

Prior to ~ 17 Ma an extensive pediplain sloping down to sea level dominated the landscape of the present-day Coastal Cordillera and some areas of the western Frontal Cordillera (Fig. 11a and b). North of 31°S the pediplain developed to the west of an inherited Main Incaic Range exposed in the present-day Frontal Cordillera, whereas south of 31°S it developed to the west of the Eocene to Oligocene magmatic arc. North of 30ºS, this pediplain was not completely subplanar as it already presented a slight inherited relief flanking the Domeyko Depression to the west (Fig. 11a). On the contrary, south of 30ºS the pediplain extended across the present-day Coastal Cordillera progressively diminishing in elevation towards the sea (Fig. 11b).

In the Early (Middle?) Miocene the pediplain was offset by a series of west-vergent north-to-south trending faults (Fig. 11a and b). The eastern Coastal Cordillera was uplifted with respect to the western Frontal Cordillera throughout the entire study area (Fig. 11a and b). North of 30°S the western Frontal Cordillera was also uplifted (Fig. 11a and b). Importantly, offset of the original pediplain is coeval with an important period of

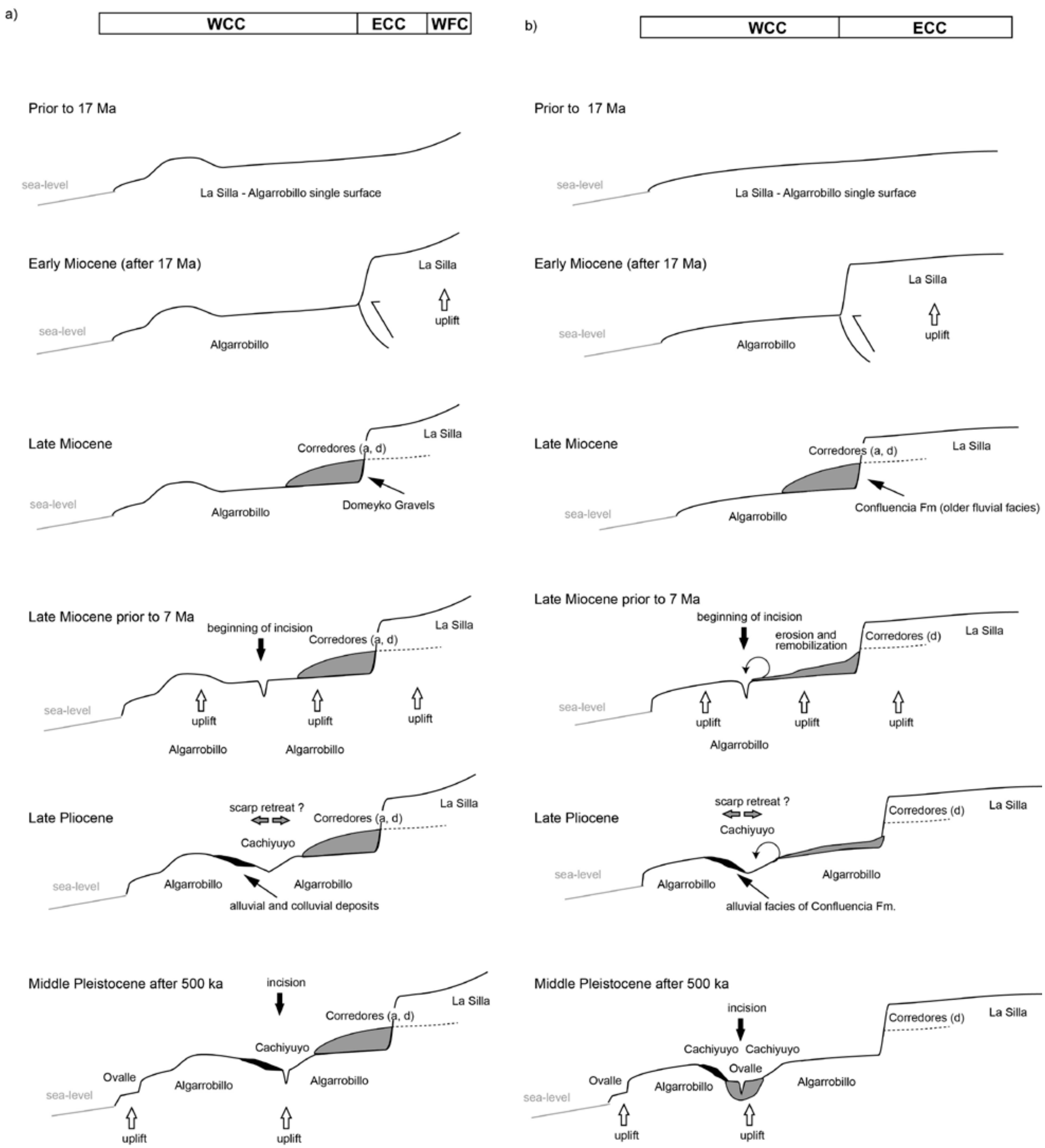

Fig. 11. Model of landscape evolution from the Early Miocene to the Middle Pleistocene. a) north of 30°S and b) south of 30°S.

uplift-related exhumation in the central Frontal Cordillera. Uplift leaded to the formation of a secondary topographic front within the present-day Coastal Cordillera and concomitant deposition next to the scarp. Aggradation to the west of the scarp and development of degradational pediplains at high elevations by the Late Miocene (Fig. 11a and b) may have been favored by the establishment of the observed latitudinal precipitation gradient throughout the study region after the Middle Miocene (Le Roux, 2012). North of 30ºS the aggradational deposits accumulated within the Domeyko Depression (Fig. 11a). On the contrary, to the south of 30ºS the absence of a topographic barrier to the west and the higher precipitation rate compared to the north prevented preservation of the aggradational deposits at their original depocenters (Fig. 11b).

8. Acknowledgements

This study was supported in part by the Chilean Government through the Comisión Nacional de Ciencia y Tecnología CONICYT (Anillo ACT-18 project, AMTC), the Advanced Mining Technology Center (AMTC) of the Facultad de Ciencias Físicas y Matemáticas-Universidad de Chile; FONDECYT Project 11085022 “Interacción Clima-Tectónica en el Alzamiento Andino de Chile Central durante el Neógeno”; Fondecyt N° 11121529, the Ecos -Conicyt proyect C11U02 "Levantamiento de la costa pacífica de Sud América y acoplamiento interplaca en la zona de subducción". Additional support was obtained by IRD Project “Erosión en los Andes”.

This study is part of the PhD thesis of M.P. Rodríguez, which was supported by a 4 year grant from CONICYT and the PhD thesis of G. Aguilar, which was supported by 4 year grant from CONICYT, the Universidad Católica del Norte and Égide-France (Bourse d’excellence Eiffel).

9. References

Aguilar, G., Riquelme, R., Martinod, J., Darrozes, J., and Maire, E., 2011, Variability in erosion rates related to the state of landscape transience in the semi-arid Chilean Andes: Earth Surface Processes and Landforms, v. 36, p. 1736–1748, doi:10.1002/esp.2194.

Aguilar, G., Riquelme, R., Martinod, J. and Darrozes, J. 2013. Role of climate and tectonics in the geomorphologic evolution of the Semiarid Chilean Andes between 27-32°S: Andean Geology 40 (1): 79-101. January, 2013, doi: 10.5027/andgeoV40n1-a04.

Arancibia, G. 2004. Mid-cretaceous crustal shortening: evidence from a regional-scale ductile shear zone in the Coastal Range of central Chile (328 S). Journal of South American Earth Sciences v. 17, p. 209–226.

Arévalo, C., Mourgues, F.A., Chávez, R. 2009. Geología del Área Vallenar-Domeyko, Región de Atacama. Servicio Nacional de Geología y Minería, Carta Geológica de Chile.

Arriagada, C., Mpodozis, C., Yañez, G., Roperch, P., Charrier, R., Farías, M. 2009. Rotaciones Tectónicas en Chile Central: El Oroclino de Vallenar y el “Megakink” del Maipo. XII Congreso Geológico Chileno, Santiago.

Babault, J., Van Den Driessche, J., Bonnet, S., Castelltort, S., Crave, A. 2005. Origin of the highly elevated Pyrenean peneplain: Tectonics 24, TC2010, doi:10.1029/2004TC001697.

Barnes, J.B. and Ehlers, T.A. 2009. End member models for Andean Plateau uplift. Earth Sci Rev 97:105–132

Benado, D.E. 2000. Estructuras y estratigrafía básica de terrazas marinas en sector costero de Altos de Talinay y Bahía Tongoy, implicancias neotectónicas. Thesis, Departamento de Geología, Universidad de Chile, Santiago, 78 p.

Bissig, T., Clark, A.H., Lee, J.K.W., and Hodgson, C.J. 2002. Miocene landscape evolution and geomorphologic controls on epithermal processes in the El Indio-Pascua Au-Ag-Cu belt, Chile and Argentina: Economic Geology and the Bulletin of the Society of Economic Geologists, v. 97, no. 5, p. 971–996, doi: 10.2113/97.5.971

Bissig, T., Lee, J.K.W., Clark, A.H., Heather, K.B. 2001. The Cenozoic History of volcanism and hydrothermal alteration in the Central Andes Flat-Slab Region: New 40Ar-39Ar constraints from the El Indio-Pascua Au (-Ag, Cu) Belt, 29°20’-30°30’S. International Geology Review 43: 1-29.

Bissig, T. and Riquelme, R. 2010. Andean uplift and climate evolution in the southern Atacama Desert deduced from geomorphology and supergene alunite-group minerals. Earth and Planetary Science Letters 299: 447-457.

Cahill, T. and Isacks, B.L. 1992. Seismicity and shape of the subdueted Nazca plate. Journal of Geophysical Research 97: 17503-17529.

Cancino, G. 2007. Hoja El Transito mapa de compilación, 1/250 000, SERNAGEOMIN.

Carretier, S., Regard, V., Vassallo, R., Aguilar, G., Martinod, J., Riquelme, R., Pepin, E., Charrier, R., Hérail, G., Farías, M., Guyot, J.-L., Vargas, G., and Lagane, C. 2013. Slope and climate variability control of erosion in the Andes of central Chile. Geology, v. 41, p. 195-198. doi:10.1130/G33735.

Cembrano, J., Zentilli, M., Grist, A., Yañez, G. 2003. Nuevas edades de trazas de fisión para Chile Central (30°-34°S): Implicancias en el alzamiento y exhumación de los Andes desde el Cretácico. 10° Congreso Geológico Chileno, Concepción-Chile.

Charrier, R. and Vicente, J.C. 1972. Liminary and geosynclinal Andes: major orogenic phases and synchronical evolution of the central and Magellan sectors of the Argentine-Chllean Andes. In Intemational Upper Mantle Project Conference on Solid Earth Problems, Proceedings, Vol. 2, p. 451-470. Buenos Aires.

Charrier, R., Baeza, O., Elgueta, S., Flynn, J.J., Gans, P., Kay, S.M., Muñoz, N., Wyss, A.R., Zurita, E., 2002. Evidence for Cenozoic extensional basin development and tectonic inversion south of the flat-slab segment, southern Central Andes, Chile (33º-36ºS.L.). Journal of South American Earth Sciences, Vol. 15, p. 117-139.

Charrier, R., Pinto, L., Rodríguez, M.P. 2007. Tectonostratigraphic evolution of the Andean Orogen in Chile. In: Moreno, T., Gibbons, W. (Eds.), The Geology of Chile. The Geological Society, London, pp. 21–114.

Charrier, R., Farias, M., Maksaev, V. 2009. Evolución tectónica, paleogeográfica y metalogénica durante el Cenozoico en los Andes de Chile norte y central e implicaciones para las regiones adyacentes de Bolivia y Argentina. Rev. Asoc. Geol. Argent. v.65 n.1.

Charrier, R., Herail, G., Pinto, L., Garcia, M., Riquelme, R., Farias, M., and Muñoz, N. 2013. Cenozoic tectonic evolution in the Central Andes in northern Chile and west central Bolivia: implications for paleogeographic, magmatic and mountain building evolution: International Journal of Earth Sciences, v. 102, no. 1, p. 235-264.

Clark, M. K., Royden, L.H., Whipple, K. X., Burchfiel, B. C., Zhang, X. and Tang, W. 2006. Use of a regional, relict landscape to measure vertical deformation of the eastern Tibetan Plateau. Journal of geophysical research, Vol. 111, F03002, doi:10.1029/2005JF000294.

Clark, A.H., Tosdal, R.M., Farrar, E., Plazolles, A. 1990. Geomorphologic environment and age of supergene enrichment of the Cuajone, Quellaveco, and Toquepala Porphyry Copper-Deposits, Southeastern Peru. Economic Geology and the Bulletin of the Society of Economic Geologists 85, 1604–1628.

Cooke, R., Warren, A., and Goudie, A. 1993. Desert geomorphology: London, UCL Press, 526 p.

Cornejo, P., Mpodozis, C., Ramírez, C.F., Tomlinson, A.J. 1993. Estudio geológico de la Región de Potrerillos y El Salvador (26°-27° Lat. S). Servicio Nacional de Geología y Minería - Corporación del Cobre, Informe Registrado IR-93-01, Vol. 1, 258 p. Santiago.

Cornejo, R., Matthews, S., Pérez de Arce, C. 2003. The 'K-T' compressive deformation event in northern Chile (24-27°S). In Congreso Geológico Chileno, No. 10, Actas, CD-Rom, Sesión Temática 1. Concepción.

Creixell, C., Ortiz, M., Arévalo, C. 2012. Geología del área Carrizalillo-El Tofo, Región de Atacama, Servicio Nacional de Geología y Minería, 1 mapa escala 1:100.000. Carta Geológica de Chile, Serie Geología Básica.

Emparán, C., Pineda, G., 2006. Geología del Area Andacollo-Puerto Aldea, Región de Coquimbo. Carta Geológica de Chile, Serie Geológica Básica.

Farías, M. 2007. Tectónica y erosión en la evolución del relieve de los Andes de Chile Central durante el Neógeno. Tesis Doctoral, Universidad de Chile y Université de Toulouse III, (inédito), 194 p., Santiago - Toulouse.

Farías, M., Charrier, R., Comte, D., Martinod, J., and Herail, G. 2005. Late Cenozoic deformation and uplift of the western flank of the Altiplano: Evidence from the depositional, tectonic, and geomorphologic evolution and shallow seismic activity (northern Chile at 19 degrees 30ºS): Tectonics, v. 24, no. 4, doi: Tc400110.1029/2004tc001667.

Farías, M., Charrier, R., Carretier, S., Martinod, J., Fock, A., Campbell, D., Caceres, J., and Comte, D. 2008. Late Miocene high and rapid surface uplift and its erosional response in the Andes of central Chile (33 degrees-35 degrees S): Tectonics, v. 27, no. 1, doi: Tc1005 10.1029/2006tc002046.

Farías, M., Charrier, R., Carretier, S., Martinod, J., Fock, A., Campbell, D., Caceres, J., and Comte, D. 2008 b. No subsidence in the development of the Central Depression along the Chilean margin. 7th Symposium on Andean Geodinamics, Nice-France.

García, M. and Hérail, G. 2005. Fault-related folding, drainage network evolution and valley incision during the Neogene in the Andean Precordillera of Northern Chile: Geomorphology 65: 279– 300.

Garzione, C.N., Molnar, P., Libarkin, J.C., MacFadden, B. 2006. Rapid late Miocene rise of the Andean plateau: evidence for removal of mantle lithosphere. Earth Planet Sci Lett 241:543–556.

Garrido, G. 2009. Evolución geomorfológica de la Depresión de Domeyko entre los 28º45’-29º00’S durante el Neógeno. Thesis, Departamento de Geología, Universidad de Chile.

Giambiagi, L., Mescua, J., Bechis, F., Tassara, A., and Hoke, G. 2012. Thrust belts of the southern Central Andes: Along-strike variations in shortening, topography, crustal geometry, and denudation: Geol. Soc. Am. Bull., v. 124, no. 7-8, p. 1339{1351, doi: 397 10.1130/B30609.1.

González, G., Cembrano, J., Carrizo, D., Macci, A., Schneider, H. 2003. Link between forearc tectonics and Pliocene-Quaternary deformation of the Coastal Cordillera, Northern Chile. Journal of South American Earth Sciences 16: 321-342.

González, G., Dunai T., Carrizo, D., Allmendinger, R. 2006. Young displacements on the Atacama Fault System, northern Chile from field observations and cosmogenic 21Ne concentrations. Tectonics 25 (TC3006), doi:10.1029/2005TC001846.

Hall, S.R., Farber, D.L., Audin, L., Finkel, R.C., Mériaux, A.-S. 2008. Geochronology of pediment surfaces in southern Peru: Implications for Quaternary deformation of the Andean forearc. Tectonophysics 459, 186–205.

Heredia N., Fernandez L. R. R., Gallastegui G., Busquets P. and Colombo F. 2002. Geological setting of the Argentine Frontal Cordillera in the flat-slab segment (30°`-31° 30’ S latitude), Journal of South American American Earth Sciences 15, 79–99, doi:10.1016/S0895-9811(02)00007-X.

Hilley, G. E., Strecker, M. R., and Ramos, V. A. 2004. Growth and erosion of fold-and-thrust belts, with an application to the Aconcagua Fold-and-Thrust Belt, Argentina. Journal of Geophysical Research, Solid Earth, 109, doi:10.1029/2002JB002282.

Hilley, G.E. and Coutand, I. 2010. Links between topography, erosion, rheological heterogeneity, and deformation in contractional settings: insights from the Central Andes, Tectonophysics, 95, 78-92.

Hoke, G.D., Isacks, B.L., Jordan, T.E., Blanco, N., Tomlinson, A.J., and Ramezani, J. 2007. Geomorphic evidence for post-10 Ma uplift of the western flank of the central Andes 18 degrees 30’-22 degrees S: Tectonics, v. 26, no. 5, doi: Tc502110.1029/2006tc002082.

Hoke, G.D., Garzione, C.N. 2008. Paleoelevation and geomorphic constraints on the late Miocene rise of the Andes. Earth and Planetary Science Letters 271, 192–201.

Isacks, B.1988. Uplift of the central Andean plateau and bending of the Bolivian orocline. Journal of Geophysical Research, B, Solid Earth and Planets 93, 3211–3231.

Jordan, T.E., Isacks, B.L., Allmendinger, R.W., Brewer, J.A., Ramos, V.A., y Ando, C.J., 1983. Andean tectonics related to geometry of subducted Nazca plate: Geological Society of America Bulletin, v. 94, p. 341-361.

Jordan, T.E., Nester, P.L., Blanco, N., Hoke, G.D., Dávila, F., Tomlinson, A.J. 2010. Uplift of the Altiplano-Puna plateau: a view from the west. Tectonics 29:TC5007. doi:10.1029/2010TC002661

Jara, P. and Charrier, R. In press. Nuevos antecedentes estratigráficos y geocronológicos para el Meso-Cenozoico de la Cordillera Principal de Chile entre 32° y 32°30´S Implicancias estructurales y paleogeográficas. Andean Geology.

Kay, S. Mahlburg and Mpodozis, C. 2002. Magmatism as a probe to the Neogene shallowing of the Nazca plate beneath the modern Chilean flatslab, Journal of South American Earth Science, 15, 39-59.

Kober, F., Ivy-Ochs, S., Schlunegger, F., Baur, H., Kubik, P.W., Wieler, R. 2007. Denudation rates and a topography-driven rainfall threshold in northern Chile: Multiple cosmogenic nuclide data and sediment yield budgets. Geomorphology 83 (2007) 97–120

Lamb, S. and Davis, P. 2003. Cenozoic climate change as a possible cause for the rise of the Andes: Nature 425: 792–797. DOI: 10.1038/nature02049.

Lamb, S., Hoke, L., Kennan, L., Dewey, J 1997. Cenozoic evolution of the Central Andes in Bolivia and northern Chile: en Burg, J., Ford, M., (eds.), Orogeny through time. J. Geol. Soc. Lond., Special Publication 121: 237-264.

Le Roux, J.P., Gómez, C., Fenner, J., Middleton, H. 2004. Sedimentological processes in a scarp-controlled rocky shoreline to upper continental slope environment, as revealed by unusual sedimentary features in the Neogene Coquimbo Formation, north-central Chile. Sedimentary Geology 165, 67–92.

Le Roux, J.P., Gómez, C., Venegas, C., Fenner, J., Middleton, H., Marchant, M., Buchbinder, B., Frassinetti, D., Marquardt, C., Gregory-Wodzicki, K.M., Lavenu. A. 2005. Neogene–Quaternary coastal and offshore sedimentation in north-central Chile: record of sea level changes and implications for Andean tectonism: Journal of South American Earth Sciences 19: 83– 98.

Le Roux, J.P., Olivares, D.M., Nielsen, S.N., Smith, N.D., Middleton, H., Fenner, J., Ishman, S.E. 2006. Bay sedimentation as controlled by regional crustal behaviour, local tectonics and eustatic sea-level changes: Coquimbo Formation (Miocene–Pliocene), Bay of Tongoy, central Chile. Sedimentary Geology 184, 133–153.

Le Roux, J. P. 2012. A review of Tertiary climate changes in southern South America and the Antarctic Peninsula. Part 2: continental conditions: Sedimentary Geology, v. 247, p. 21-38.

Litvak, V. D., S. Poma, S. M. Kay, and E. Valle (2007), Paleogene and Neogene magmatism in the Valle del Cura region : New perspective on the evolution of the Pampean flat slab , San Juan province , Argentina, , 24, 117–137, doi:10.1016/j.jsames.2007.04.002.

Ludwig, K.R. 2009. SQUID 2 (rev. 2.50), A User's Manual, Berkeley Geochronology Ctr. Special Publication vol. 5. 104 p.

Maksaev, V., Moscoso, R., Mpodozis, C. and Nasi, C., 1984. Las unidades volcánicas y plutónicas del Cenozoico superior entre la Alta Cordillera del Norte Chico (29°-31° S), Geología, alteración hidrotermal y mineralización. Revista Geológica de Chile, 21: 11-51.

Maksaev, V., Munizaga, F., Zentilli, M., and Charrier, R., 2009, Fission track thermochronology of Neogene plutons in the Principal Andean Cordillera of central Chile (33-35 ° S): Implications for tectonic evolution and porphyry Cu-Mo mineralization: v. 36, no. 2, p. 153–171.

Maksaev, V. and Zentilli, M. 1999. Fission track thermochronology of the Domeyko Cordillera, northern Chile: Implications for Andean tectonics and porphyry copper metallogenesis: Explor. Mining. Geol. 8: 65-89.

Martin, M.W., Kato, T.T., Rodriguez, C., Godoy, E., Duhart, P., McDonough, M. and Campos, A. 1999. Evolution of the late Paleozoic accretionary complex and overlying forearc-magmatic arc, south central Chile (38°- 41°S): Constraints for the tectonic setting along the southwestern margin of Gondwana. Tectonics 18: doi: 10.1029/1999TC900021. issn: 0278-7407.

Moscoso, R., Nasi, C., Salinas, P. 1982. Hoja Vallenar y parte norte de La Serena, geological map, 1/250 000, SERNAGEOMIN, 100 p.

Mortimer, C. 1973. The Cenozoic history of the southern Atacama Desert, Chile: Journal of the Geological Society, v. 129, no. 5, p. 505–526, doi: 10.1144/gsjgs.129.5.0505.

Montgomery, D.R.; Balco, G.; Willett, S.D. 2001. Climate, tectonics, and the morphology of the Andes. Geology 29: 579-582.

Mpodozis, C.; Cornejo, P. 1988. Hoja Pisco Elqui. IV Región de Coquimbo. Servicio Nacional de Geología y Minería, Carta Geológica de Chile, No. 68, 163 p. Santiago.

Mpodozis, C., Brockway, H., Marquardt, C., Perelló, J. 2009. Geocronología U/Pb y tectónica de la región de Los Pelambres-Cerro Mercedario: implicancias para la evolución cenozoica de Los Andes del centro de Chile y Argentina. In Congreso Geológico Chileno, No.12., Santiago.

Nalpas, T., Dabard, M.-P., Pinto, L., Loi, A. 2009. Preservation of the Miocene Atacama Gravels in Vallenar area, northern Chilean Andes: Climate, stratigraphic or tectonic control? XII Congreso Geológico Chileno, Santiago.

Nasi, C., Moscoso, R., Maksaev, V. 1990. Hoja Guanta, Regiones de Atacama y Coquimbo, escala 1:250.000, n°67, SERNAGEOMIN.

Ota, Y., Miyauchi, T., Paskoff, R., Koba, M. 1995. Plio–Quaternary terraces and their deformation along the Altos de Talinay, North–Central Chile. Revista Geologica de Chile 22, 89–102.

Pardo-Casas, F. and P. Molnar, 1987. Relative motion of the Nazca (Farallón) and South American plates since Late Cretaceous time, Tectonics, 6, 3, 233-248.

Paskoff, R. 1970. Recherches géomorphologiques dans le Chili semi-aride. Biscaye Freres, Bordeaux.

Pepin, E., Carretier, S., Guyot, J.L., and Escobar, F. 2010. Specific suspended sediment yields of the Andean rivers of Chile and their relationship to climate, slope and vegetation: Hydrological Sciences Journal, v. 55, p. 1190–1205, doi:10.1080/02626667.2010.512868.

Pineda, G., Calderón, M. 2008. Geología del área Monte Patria-El Maqui, región de Coquimbo, Escala 1:100.000. Carta Geológica de Chile, Serie Geología Básica, n.116, SERNAGEOMIN: 44 h. Santiago.

Pineda, G., and C. Emparán (2006), Geología del area Vicuña-Pichasca, Región de Coquimbo, Servicio Nacional de Geología y Minería, Santiago.

Pinto, L., Hérail, G. and Charrier, R., 2004. Sedimentación sintectónica asociada a las estructuras neógenas en el borde occidental del plateau andino en la zona de Moquella (19°15'S, Norte de Chile). Revista Geológica de Chile, Vol. 31 (Nº1), pp 19-44.

Quang, C.X., Clark, A.H., Lee, J.K.W., and Hawkes, N. 2005. Response of supergene processes to episodic Cenozoic uplift, pediment erosion, and ignimbrite eruption in the porphyry copper province of southern Peru: Economic Geology, v. 100, no. 1, p. 87–114, doi: 10.2113/100.1.0087.

Ramos, V; Cegarra, M.; Cristallini, E. 1996. Cenozoic tectonics of the High Andes of west-central Argentina (30-36°S latitude). Tectonophysics 259: 185-200.

Ramos, V.A.; Cristalline, E.O.; Peréz, D.J. 2002. The Pampean flat slab of the Central Andes. Journal of South American Earth Sciences 15: 59-78.

Ramos, V., Zapata, T., Cristallini, E., Intracaso, A. 2004. The Andean thrust system-latitudinal variations in structural styles and orogenic shortening. In: McClay, K.R. (Ed.), Thrust Tectonics and Hydrocarbon Systems: AAPG Memoir, pp. 30–50.

Regard, V., Saillard, M., Martinod, J., Audin, L., Carretier, S., Pedoja, K., Riquelme, R., Paredes, P., Hérail, G. 2010. Renewed uplift of the Central Andes Forearc revealed by coastal evolution during the Quaternary. Earth and Planetary Science Letters 297, 199–210.

Riquelme, R., Hérail, G., Martinod, J., Charrier, R., and Darrozes, J. 2007. Late Cenozoic geomorphologic signal of Andean forearc deformation and tilting associated with the uplift and climate changes of the Southern Atacama Desert (26°S–28°S): Geomorphology, v. 86, no. 3-4, p. 283–306, doi: 10.1016/j.geomorph.2006.09.004.

Riquelme, R., Martinod, J., Hérail, G., Darrozes, J., Charrier, R. 2003. A geomorphological approach to determining the Neogene to Recent tectonic deformation in the Coastal Cordillera of northern Chile (Atacama). Tectonophysics 361, 255–275.

Rivano, S., Sepúlveda, P. 1991. Hoja Illapel, Región de Coquimbo. Carta Geológica de Chile.

Rodríguez, M. P., Charrier, R., Carretier, S., Brichau, S. y Farías, M. 2012a. Alzamiento y exhumación Cenozoicos en el Norte Chico de Chile (30 a 33º S). XIII Congreso Geológico Chileno, Antofagasta-Chile.

Rodríguez, M.P., Carretier, S., Charrier, R., Saillard, M., Regard, V., Hérail, G., Hall, S., Farber, D., Audin, L. 2013. Geochronology of pediments and marine terraces in north-central Chile and their implications for Quaternary uplift in the Western Andes. Geomorphology 180–181 (2013) 33–46.

Saillard, M., Hall, S.R., Audin, L., Farber, D.L., Hérail, G., Martinod, J., Regard, V., Finkel, R.C., Bondoux, F. 2009. Non-steady long-term uplift rates and Pleistocene marine terrace development along the Andean margin of Chile (31°S) inferred from 10Be dating. Earth and Planetary Science Letters 277, 50–63.

Salazar, E. 2012. Evolución tectonica-estratigrafica post-Paleozoica de la Cordillera de Vallenar. Thesis, Departamento de Geología, Universidad de Chile.

Schildgen, T.F., Hodges, K.V., Whipple, K.X., Reiners, P.W., Pringle, M.S., 2007. Uplift of the western margin of the Andean plateau revealed from canyon incision history, southern Peru. Geology 35, 523–526.

Sernageomin (2003), Carta Geológica de Chile (escala 1:1.000.000), Servicio Nacional de Geología y Minería.

Sillitoe, R.H., Mortimer, C., Clark, A.H. 1968. A chronology of landform evolution and supergene mineral alteration, Southern Atacama Desert, Chile. Institute of Mining and Metallurgy Transactions (Section B) 27: 166-169.

Sobel, E.R., Strecker, M.R. 2003. Uplift, exhumation, and precipitation: tectonics and climatic control of Late Cenozoic landscape evolution in the northern Sierras Pampeanas, Argentina. Basin Research 15.

Somoza, R., 1998. Updated Nazca (Farallon)-South America relative motions during the last 40 My: implications for mountain building in the central Andean region. Journal of South American Earth Sciences, Vol. 11, p. 211-215.

Steinmann, G., 1929. Geologie von Peru. Kart Winter, Heidelberg, 448 pp.

Strecker, M.R., Alonso, R.N., Bookhagen, B., Carrapa, B., Hilley, G.E., Sobel, E.R., Trauth, M.H. 2007. Tectonics and climate of the southern central Andes. Annual Review of Earth and Planetary Sciences 35: 747–787. DOI:10.1146/annurev.earth.35.031306.140158.

Tassara, A. and Yañez, G. 2003. Relación entre el espesor elástico de la litosfera y la segmentación tectónica del margen andino (15-47°S). Revista Geológica de Chile 30 (2): 159-186.

Tosdal, R.M., Clark, A.H., and Farrar, E. 1984. Cenozoic Polyphase Landscape and Tectonic Evolution of the Cordillera Occidental, Southernmost Peru: Geological Society of America Bulletin, v. 95, no. 11, p. 1318–1332.

Urresty, C. 2009. Evolución geomorfológica de la parte sur de la Depresión de Domeyko (29º00’-29º40’S) durante el Neógeno. Thesis, Departamento de Geología, Universidad de Chile.

Veit, H. 1996. Southern westerlies during the Holocene deduced from geomorphological and pedological studies in the Norte Chico, northern Chile (27–33°S). Palaeogeography Palaeoclimatology Palaeoecology 123, 107–119.

Victor, P., Oncken, O. and Glodny, J., 2004. Uplift of the western Altiplano plateau (Northern Chile). Tectonics, Vol. 23, TC4004, doi:101029/2003TC001519.

Whipple, K.X., and Tucker, G.E. 1999, Dynamics of the stream-power river incision model: Implications for height limits of mountain ranges, landscape response timescales and research needs, J. Geophys. Res., 104, 17,661– 17, 674.

Winocur, D. 2010. Geología y estructura del Valle del Cura y el sector central del Norte Chico, provincia de San Juan y IV Región de Coquimbo, Argentina y Chile. Tesis doctoral. Universidad de Buenos Aires. (inédito) 354 p. Buenos Aires.

Winocur, D.A., Litvak, V. and Ramos, V. this volume. Magmatic and tectonic evolution of the Oligocene Valle del Cura basin, Main Andes of Argentina and Chile: Evidence for generalized extension. In Sepúlveda, S., Giambiagi, L., Pinto, L., Moreiras, S., Tunik, M., Hoke, G. and Farías, M. (Editors), Geodynamic Processes in the Andes of Central Chile and Argentina, Geological Society of London, Special Publications.

Yañez, G.A., Ranero, R., and Huene, V. 2001. Magnetic anomaly interpretation across the southern central Andes (32°-34°S): The role of the Juan Fernández Ridge in the late Tertiary evolution of the margin: v. 106, p. 6325–6345.

5.4. Quaternary ^{21}Ne cosmogenic ages obtained for the Corredores Pediplain in the Choapa River Valley: Implications in terms of cosmogenic data interpretation.

In the locality of “Altos de Llahuín”, in the northern area of the Choapa River drainage basin (Fig. 5.3), quartz samples were collected for cosmogenic age determinations from a bedrock surface remnant assigned to the Corredores Pediplain. (Fig. 5.2). Under the assumption of a Miocene age for the Corredores Pediplain, one of these samples was analyzed using a stable cosmogenic isotope, corresponding to ^{21}Ne.

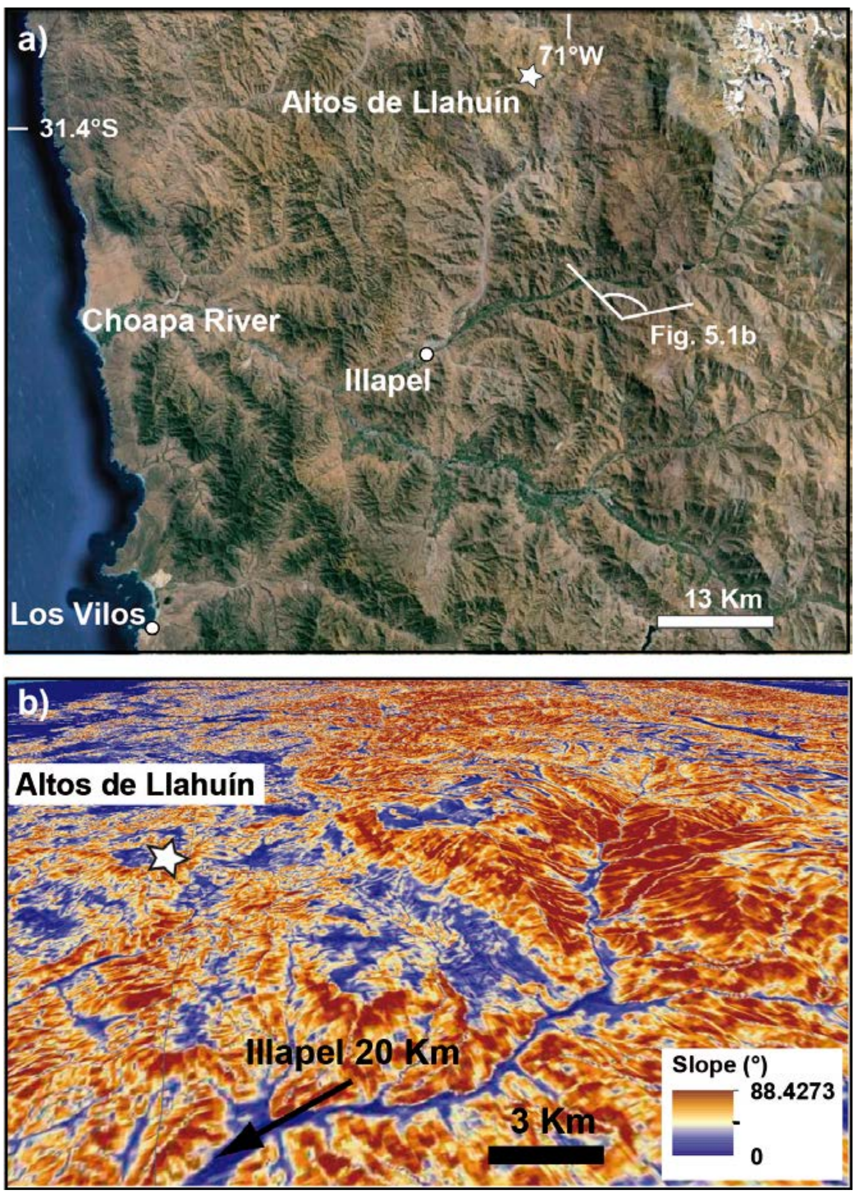

Fig. 5.3. a) Google Earth image of the Choapa River basin White star show the location of quartz samples collected for ^{21}Ne cosmogenic dating of a bedrock surface assigned to the Corredores Pediplain. b) 3D slope map showing low slopes surfaces at high elevations in the northern Choapa River basin. Location in Fig 5.3a.

Two quartz samples for neon analysis were crushed to 0.5 - 1 mm and prepared using standard sieving, heavy mineral and magnetic techniques in the "Laboratorio de Separación de Minerales" at the University of Chile. Neon analyses were performed in the Noble Gas Laboratory at Caltech. Ne was extracted using standard methods of HF dissolution and step heating using a laser. Results are summarized in Table 5.1.

A minimum exposure age was calculated using the time-dependent variation of the scaling scheme of Lal (1991)/ Stone (2000) for sample ESC-09 (the one with the highest ^{21}Ne amount). The age calculated was **18.6 ± 2 x10^{3} yrs**. This age is much younger than the Late Miocene age expected according to geomorphological and geochronological constrains in the article of section 5.2. There are two possible scenarios to explain the discrepancies between the Late Miocene age suggested by geological constrains and the Late Pleistocene cosmogenic age obtained for the Corredores Pediplain in the Choapa River Valley:

1. The bedrock surface dated was buried under a few meters of sediments (at least more than 3 meters) which prevented significant interaction between cosmic rays and quartz in sample ESC-09 before ~19 ka. Around ~19 ka, the sediments were removed and the bedrock surface was exposed to cosmic rays.

2. More than ~ 3 meters of bedrock were removed from the top of the Corredores Pediplain by the ~19 ka. Despite significant Late Pleistocene erosion, such erosion mechanism allowed the preservation of the original low slope/ relief morphology of the Corredores Pediplain remnants.

Table 5.1 Neon in quartz separates from the Corredores Pediplain in "Altos de Llahuín"

Sample	Lat/Long (degrees)	Elevation (m)	Weight (g)	^{20}Ne (pcc/g)	^{21}Ne/ ^{20}Ne	^{22}Ne/ ^{20}Ne	^{21}Ne (10^{6}at/g)
ESC-02	**-71.04/ -31.36**	**1922**	0,09922	2091,69	0,00305	0,10134	0,49
			0,09922	135,34	0,00293	0,10393	-0,01
			0,09922	1318,97	0,00301	0,10138	0,19
			0,09922	109,28	0,00292	0,10514	-0,01
TOTAL				**3655,29**			**0,65**
ESC-09	**-71.04/ -31.36**	**1824**	0,101	1764,55	0,00313	0,10149	0,82
			0,101	155,19	0,00288	0,10300	-0,03
			0,101	894,21	0,00311	0,10273	0,37
			0,101	89,53	0,00297	0,10492	0,00
TOTAL				**2903,48**			**1,16**

Throughout the entire studied region the Corredores Pediplain is one of the surfaces that display an aggradational counterpart. Thus, it is possible that bedrock surfaces may have been buried under a few meters of sedimentary material in the “Altos de Llahuín” area that were later remobilized from the top of bedrock surfaces. This is in good agreement with the interpretation made in section 5.2 by which aggradational deposits related to the Corredores Pediplain were remobilized and re-deposited within river valleys similar to those from the present-day after the Late Miocene south of 30°S (see Fig. 11 in section 5.2). Moreover, intuitively, it seems more unlikely to rip off more than three meters of bedrock than to remobilize a sedimentary package of more than three meters. More geomorphological and sedimentological field work is needed to understand the erosional processes that may have affect low relief/slope surfaces at high elevations in the “Altos de Llahuín” area. By now, the most probable scenario correspond to the first one mentioned.

Quaternary to Pliocene cosmogenic ages have been obtained for other uplifted paleosurfaces with overlying tuffs of Miocene age along the forearc of southern Perú (Hall et al., 2008) and northern Chile (Evenstar et al., 2009; Placzek et al., 2010). Given the probable multiphase development of pediplains, these ages have open the debate on whether these landforms should or should not be used as chronostratigraphic surfaces to constrain tectonic and/ or climatic development of the Andean forearc (Evenstar et al., 2009). One important thing to keep in mind regarding this debate corresponds to the scale of the processes under study. At the scale of orogenic processes pediplain surfaces may have been uplifted hundreds or even thousands of meters and may have developed during millions or tens of millions of years (see interpretation of thermal models from the Coastal Cordillera in section 3.3). Thus, erosional processes operating at the scale of a few meters during hundreds of thousands of years may not be significant to consider in the analysis of these surfaces. Cosmogenic ages record the last erosional event capable of remove a few meters of rocks or sediment from a surface that has suffered a single-exposure history. Thus, in order to obtain the older age from a surface using cosmogenic isotopes it is necessary to analyze samples collected from sites whose sedimentological and geomorphological characteristics strongly indicates negligible erosion (e.g. Dunai et al., 2005) or where erosion rates at the scale of millions of years can be constrain independently. Finally, despite later erosion, geochronological ages of overlying volcanic and/ or sedimentary units correspond to irrefutable evidence that the low relief surface under study was a subplanar component of landscape by the time these units were deposited.

5.5. Final conclusions of this chapter

1. Prior to ~ 17 Ma an extensive pediplain sloping down to sea level, the La Silla-Algarrobillo pediplain, dominated the landscape of the present-day Coastal Cordillera and some areas of the western Frontal Cordillera in north-central Chile (Fig. 5.3).

2. North of 30ºS, the La Silla-Algarrobillo pediplain extended across the present-day Coastal Cordillera, but also some areas of the western Frontal Cordillera. Here the La Silla-Algarrobillo pediplain was not completely subplanar as it already presented a slight inherited relief flanking the Domeyko Depression to the west. On the contrary, south of 30ºS the pediplain extended only across the present-day Coastal Cordillera, progressively diminishing in elevation towards the sea. (Fig.11).

3. In the Early (Middle?) Miocene the La Silla-Algarrobillo pediplain was offset by a series of west-vergent north-to-south trending faults. The eastern Coastal Cordillera was uplifted ~ 1.1 km (Fig. 5.4, elevation difference between La Silla and Algarrobillo pediplains see section 5.2) with respect to the western Coastal Cordillera, leading to the formation of a secondary topographic front -and concomitant deposition next to the scarp.

4. The Early (Middle?) Miocene offset of the La Silla-Algarrobillo Pediplain and uplift of the eastern Coastal Cordillera correlates to the east with a period of generalized tectonic-related exhumation recognized throughout the entire Frontal Cordillera and with the early stages of tectonic inversion of the Late Oligocene Tilito Extensional Basin (Winocur, 2010; Winocur et al., accepted) along the eastern Frontal Cordillera.

5. South of 32°S the north-to-south faults that offset the La Silla-Algarrobillo pediplain by the Early (Middle?) Miocene might correlate with the Los Ángeles – Infiernillo Fault which uplifted the present-day eastern Central Depression by the Early Miocene (see Fig.11 in section 2.4).

6. Aggradation to the west of the secondary topographic front and development of degradational pediplains at high elevations (Corredores Pediplain) by the Late Miocene may have been favored by the establishment of the observed latitudinal precipitation gradient throughout the study region after the Middle Miocene (Le Roux, 2012).

7. By the Late Miocene, the entire Coastal Cordillera was uplifted ~ 1.2 km (Fig. 5.3, elevation difference between Algarrobillo and Ovalle pediplains, see section 5.2).

Uplift triggering the rejuvenation of the drainage system (Fig.11). Deposits previously accumulated to the west of the secondary topographic front were remobilized and re-deposited by fluvial systems similar to the ones from the present-day in the region south of 30ºS (Fig.11).

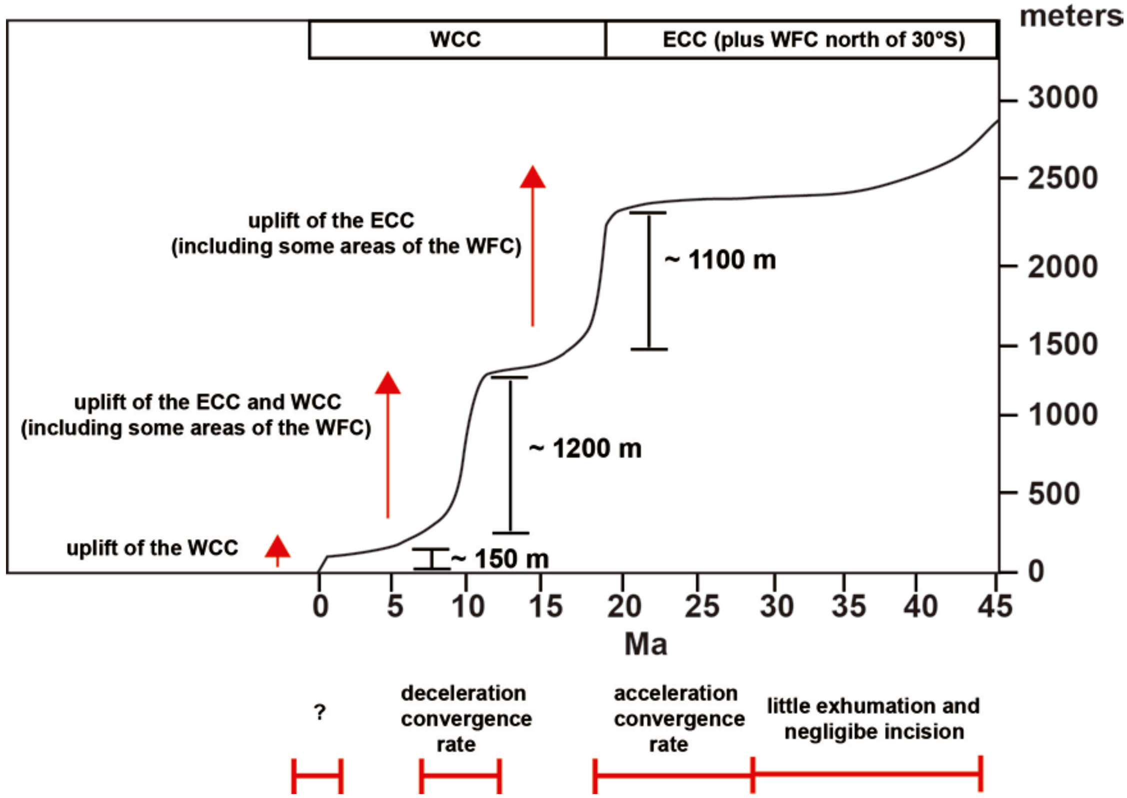

Fig. 5.4. Spatial and temporal variations of uplift throughout the Coastal Cordillera and correlated changes in plate convergence. ECC= eastern Coastal Cordillera, WCC= western Coastal Cordillera and WFC= western Frontal Cordillera.

8. According to the location of Neogene pediplains, the Main Incaic Range probably acted as the Eocene to Oligocene water divide in the area north of 31°S. The Early to Late Miocene ages of pediplains along the eastern Frontal Cordillera (Bissig et al. 2002) indicates these surfaces evolved in response to a different base level with respect to pediplains from the Coastal and western Frontal Cordillera throughout the entire Miocene.

9. Between the Early and Middle Pleistocene a new pediplain partly was carved on top of the deposits remobilized by Late Miocene incision south of 30°S. In this area, this surface connected with shore platforms towards the coast (Fig. 11). On the contrary, north of 30°S only the shore platforms developed during the Early and Middle Pleistocene (Fig. 11). Finally, this pediplain was uplifted post-500 ka (Fig. 11).

10. The three major uplift stages recognized for the Early (Middle?) Miocene, the Late Miocene and the Middle Pleistocene correlate with episodes of uplift and increased deformation recognized throughout the entire Central Andes, starting after a Late Oligocene-Early Miocene episode of increased plate convergence.

11. The presence of an inherited paleotopography together with a strong decrease of precipitation to the north of 30°S would have determined differences in landscape development throughout the Coastal Cordillera since the Early Miocene.

Chapter 6- FINAL DISCUSSIONS AND CONCLUSIONS

In this chapter, the results and interpretations from Chapters 3, 4 and 5 are combined in order to reconstruct landscape evolution in north-central Chile (28- 32°S).

In general terms, the results obtained here indicate that surface uplift and tectonic-related exhumation have occurred progressively since the Early Miocene throughout the entire studied region, including periods of accelerated uplift and/or exhumation during the Early Miocene, the Late Miocene and the Middle Pleistocene (Fig. 6.1). North-to-south variations in the Neogene to Quaternary landscape development are observed in both the Coastal and the Frontal Cordilleras. These variations occur at 30°S along the Coastal Cordillera and at 31°S along the Frontal Cordillera. The distribution and geomorphic characteristics of Cenozoic paleosurfaces combined with the thermochronological data from this and from previous works suggest that variations in landscape development are strongly influenced by the presence of an inherited “Incaic” topography along the western Coastal Cordillera in the area to the north of 30°S, and along the western and central Frontal Cordillera, in the area to the north of 31°S (Fig. 6.1). Along the Coastal Cordillera a strong latitudinal precipitation gradient was superimposed on the previous pre-Neogene paleotopography to determine differences in landscape development to the north of 30°S and to the south of 30°S since the Middle Miocene.

Prior to the Early Miocene, an early period of accelerated exhumation took place along the Coastal and Frontal Cordilleras during the Late Cretaceous to Early Paleogene. Late Cretaceous to Early Paleogene accelerated exhumation correlates with the tectonic inversion of Mesozoic extensional basins previously developed along these areas. After the Early Paleogene to at least 30 Ma, the Coastal Cordillera suffered little exhumation, which traduced in negligible incision during tens of millions of years. This would have favored the development of an extensive pediplain sloping down to sea-level, named here as the La Silla- Algarrobillo pediplain (Fig. 6.1a). Prior to the Early Miocene, the La Silla- Algarrobillo pediplain dominated the landscape of the present-day Coastal Cordillera and some areas of the present-day Frontal Cordillera to the north of 30°S (Fig. 6.1a). The main topographic front separating the Coastal from the Frontal Cordillera was constructed since the Eocene to Oligocene to the north of 31°S (Fig. 6.1a) and since the Early Miocene south of 31°S (Fig. 6.1b). The La Silla- Algarrobillo pediplain developed at the foot of the Main Incaic Range in the former area and at the foot of the Eocene magmatic arc in the last area (Fig. 6.1a). The Main Incaic Range probably acted as the Eocene to Oligocene water divide, as to the east of this mountainous range planation surfaces or pediplains also developed prior to the Early Miocene (Bissig et al., 2001; Heredia et al., 2002; Nalpas et al., 2009) along the eastern Frontal Cordillera north of 31°S. Since Eocene arc magmatism resumed around 35-30

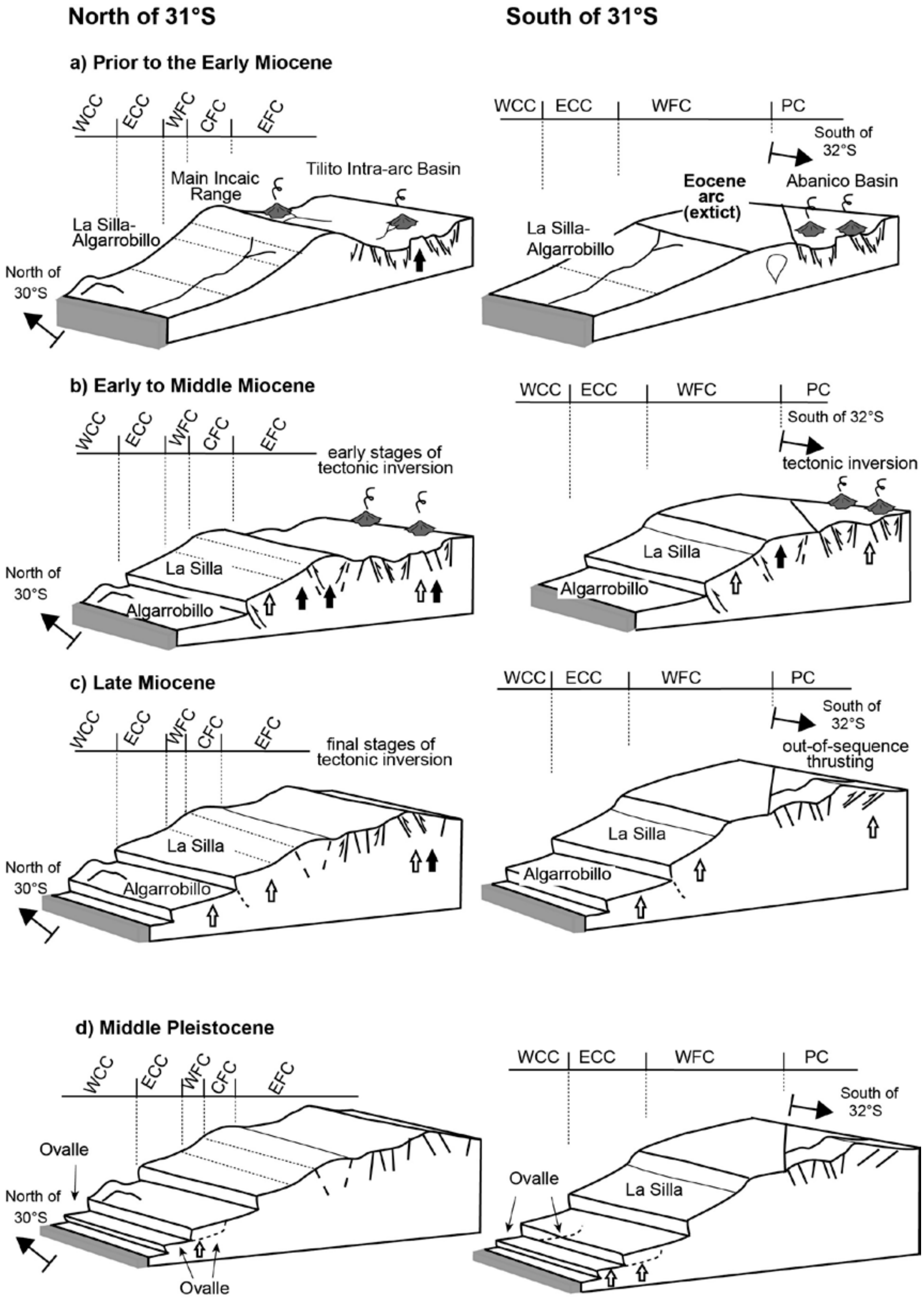

Fig.6.1. Short to long-term landscape evolution in north-central Chile (28- 32°S).White arrows indicate surface uplift and deformation, black arrows indicate tectonic-related exhumation. CC=Coastal Cordillera, WFC= western Frontal Cordillera, CFC=central Frontal Cordillera, EFC= eastern Frontal Cordillera, PC= Principal Cordillera.

Ma, the eastern Frontal Cordillera in the Elqui valley north of 31°S has been exhumed progressively, including an episode of accelerated exhumation around 7 Ma (Fig. 6.1). Exhumation in this area probably records the effects of extensional tectonics leading to the development of an Oligocene intra-arc basin, named here as the Tilito Intra-arc basin (Fig 6.1a) and of the progressive tectonic inversion of this basin starting in the Early Miocene and extending until the Late Miocene (Fig 6.1b and c; Winocur, 2010). North of 31°S, the Early Miocene contractional deformation related to the early stages of inversion of the Tilito Basin also involved the central Frontal Cordillera to the west, where tectonic-related accelerated exhumation is recorded ~ 20 Ma (Fig 6.1b), and the western Frontal Cordillera, where exhumation was continuous from before 30 to shortly after 20 Ma (Fig 6.1b). South of 31°S, a similar Early Miocene episode of tectonic-related accelerated exhumation between ~ 22 and 16 Ma took place in the western Frontal Cordillera along the foot of the topographic front (Fig 6.1b). In this area, Early Miocene accelerated-exhumation correlates with the tectonic inversion of the Abanico Extensional Basin (Charrier et al., 2002), that took place between ~ 21 and 18 Ma along the Principal Cordillera at 32°S (Mpodozis et al., 2009; Jara and Charrier, in press). During the same period, the La Silla- Algarrobillo pediplain was offset by a series of west-vergent north-to-south faults throughout the entire studied region (Fig 6.1b). As a result, the present-day eastern Coastal Cordillera was uplifted ~ 1.1 km with respect to the western Coastal Cordillera. Offset of the La Silla- Algarrobillo pediplain led to the development of a secondary topographic front that separates the present-day western and eastern Coastal Cordillera (Fig 6.1b). The mentioned faults can be correlated to the south of 32°S with the Los Ángeles-Infiernillo Fault that uplifted the present-day eastern Central Depression by the Early Miocene (see section 2.4.3 in chapter 2).

By the Late Miocene, tectonic-related accelerated exhumation and uplift of paleosurfaces (Bissig et al., 2001) in the Frontal Cordillera north of 31°S focused along the eastern Frontal Cordillera (Fig 6.1c). There, these processes can be related to the progressive tectonic inversion of the Tilito intra-arc basin (Winocur, 2010). South of 31°S, exhumation at the foot of the Principal Cordillera occurred until the Late Miocene – Early Pliocene. However, it is unclear if exhumation here records the effects of Late Miocene contractional deformation and uplift affecting this area. Moreover, structural and geochronological data at 32°S indicates that after 18 Ma shortening along the Chilean versant of the Andes was related to out-of-sequence thrusting along the international border between Chile and Argentina, to the east of the topographic front (Fig 6.1c, Jara and Charrier, in press). To the west, the entire present-day Coastal Cordillera was uplifted ~ 1.2 km in the areas to the north and to the south of 31°S during the Late Miocene (Fig 6.1c).

Finally, the western Coastal Cordillera was uplifted ~ 150 m post-500 ka throughout the entire studied region (Fig 6.1d).

The timing for Andean uplift and main tectonic-related exhumation interpreted here is in good agreement with the proposal of Charrier et al. (2013) by which uplift and related exhumation throughout the Central Andes has occurred continuously since the Eocene-Oligocene, but with periods of increased contractional deformation by the Late Oligocene-Early Miocene and the Late Miocene. Importantly, north-to-south variations on the initiation of development of the Andean topographic front are observed throughout north-central Chile, as no significant exhumation occurred at the foot of this topographic front before the Early Miocene in the area south of 31°S. As pointed out in chapter 3, these differences are in good agreement with structural and paleomagnetic data indicating that the western Frontal Cordillera in the area north of 31°S was affected by Eocene to Oligocene contractional deformation (Pineda and Calderón, 2008; Arriagada et al., in press), whereas the Principal Cordillera around 32°S was subjected to contractional deformation mostly during the Early Miocene (Mpodozis et al., 2009; Jara and Charrier, in press). Thus, two major stages for Andean evolution are recognized throughout the study region, one occurred during the Early Miocene and the other one during the Late Miocene (Fig. 6.1b and c). During the Early Miocene mostly the entire Chilean Andes were uplifted and/or tectonically-exhumed, including the eastern Coastal Cordillera and the western, central and eastern Frontal Cordillera north of 31°S and the eastern Coastal Cordillera, the western Frontal Cordillera and the Principal Cordillera south of 31°S (Fig. 6.1b). On the contrary, during the Late Miocene uplift and/or tectonically-induced exhumation only focused in the external portions of the Chilean Andes, i.e., the Coastal Cordillera and the eastern Frontal Cordillera.

The Early Miocene stage of uplift and exhumation may be explained by a more intense stress transmission and widespread strain due to the major change in the relative movement and a considerable increase in the convergence rate between the oceanic and continental plates that occurred after breakup of the Farallon into the Nazca and Cocos Plates (Charrier et al., 2013; Pardo-Casas and Molnar 1987). On the contrary, the Late Miocene episode of increased deformation correlates with a strong decreased of the convergence velocity of the Nazca plate around 10 Ma (Pilger 1983; Pardo-Casas and Molnar 1987). It is believed that coupling along subduction zones would increase during periods of deceleration of plate convergence (Yañez and Cembrano, 2004). In chapter 3, I hypothesize that the crustal scale east-verging ramp detachment structure recognized for the entire Central Andes (Isacks, 1988; Farías et al., 2010; Muñoz et al., 2013), including the study region (Alvarado et al., 2010 and references therein; Marot, 2013), may have favored the westward underthrusting of the Precordillera basement during the Late Miocene decrease in convergence rate due to a higher coupling between the Frontal Cordillera (Chilenia) and the Precordillera (Cuyania). This would have induced lower crustal deformation below the eastern Frontal Cordillera and uplift of this area. However, this does not explain why the western and central Frontal Cordillera to the west was not uplifted and/or considerable exhumed during the Late Miocene, while the Coastal Cordillera was uplifted ~ 1.2 km. One possibility is that the western and central Frontal Cordillera was in fact uplifted together with the eastern Frontal Cordillera, but that uplift was insufficient to exhume rocks throughout a new PAZ and PRZ. In this case, the entire Frontal Cordillera and Coastal Cordillera would have been uplifted in response to the lower crustal deformation induced by the westward underthrusting of the Precordillera basement. However, such scenario is inconsistent with the geometry of the inferred ramp-detachment structure below the Andes, which is located immediately to the east of the Coastal Cordillera. On the contrary, the Coastal Cordillera is located directly above the seismogenic contact between the Nazca and the South American Plates (Farías et al., 2010). Thus, processes occurring at the interplate contact should be invoked to account for the Late Miocene uplift of the Coastal Cordillera. One possibility is that, similar to what has been suggested for the eastern Frontal Cordillera, the Late Miocene deceleration of plate convergence leaded to higher coupling along the interface between the Nazca and South American plates. As a result, the slab may have been underthrusted along the subduction zone following Late Miocene deceleration of plate convergence, leading to uplift of the Coastal Cordillera. Finally, I suggest that coupling increased along the subduction zone and the border between the Frontal Cordillera (Chilenia) and the Precordillera (Cuyania) during the Late Miocene deceleration of plate convergence. This would have favored the underthrusting of the slab and of the Precordillera basement (Cuyania) along the subduction zone and the Frontal Cordillera-Precordillera border, respectively; leading to uplift at the external portions of the Chilean Andes, namely, the Coastal Cordillera and the eastern Frontal Cordillera.

7. References

Abre, P., C. Cingolani, U. Zimmermann, B. Cairncross, and F. Chemale Jr (2011), Provenance of Ordovician clastic sequences of the San Rafael Block (Central Argentina), with emphasis on the Ponón Trehué Formation, *Gondwana Res.*, *19*(1), 275–290, doi:DOI: 10.1016/j.gr.2010.05.013. [online] Available from: http://www.sciencedirect.com/science/article/B7XNB-507BHYP-4/2/29ed1f0b7315f8239fcdee4ba7d30c66

Aguilar, G., R. Riquelme, J. Martinod, and J. Darrozes (2013), Role of climate and tectonics in the geomorphologic evolution of the Semiarid Chilean Andes between 27-32 degrees S, *ANDEAN Geol.*, *40*(1), 79–101, doi:10.5027/andgeoV40n1-a04.

Aguirre, L. and Egert, E., 1965. Cuadrángulo Quebrada Marquesa, Provincia de Coquimbo. Instituto de Investigaciones Geológicas, Santiago, *Carta Geológica de Chile*, escala 1:50.000, Carta Nº 15, 92 p.

Allmendinger, R. W., D. Figueroa, D. Snyder, J. Beer, C. Mpodozis, and B. L. Isacks (1990), Foreland shortening and crustal balancing in the Andes at 30-degrees-s latitude, *Tectonics*, *9*(4), 789–809, doi:10.1029/TC009i004p00789.

Álvarez, J., C. Mpodozis, I. Blanco-Quintero, A. García-Casco, C. Arriagada, and D. Morata (2013), U–Pb ages and metamorphic evolution of the La Pampa Gneisses: Implications for the evolution of the Chilenia Terrane and Permo-Triassic tectonics of north Central Chile, *J. South Am. Earth Sci.*, *47*(0), 100–115, doi:http://dx.doi.org/10.1016/j.jsames.20 13.07.001.

Arancibia, G. (2004), Mid-cretaceous crustal shortening: evidence from a regional-scale ductile shear zone in the Coastal Range of central Chile (32� S), *J. South Am. Earth Sci.*, *17*(3), 209–226, doi:10.1016/j.jsames.2004.06.001. [online] Available from: http://linkinghub.elsevier.com/retrieve/pii/S0895981104000537 (Accessed 28 January 2012)

Arévalo, C., F. Mourgues, Francisco and R. Chávez (2009), Geología del Área Vallenar-Domeyko, Región de Atacama, scale 1:100.000, Serv. Nac. de Geol. y Miner, Santiago.

Argent, J. D., S. A. Stewart, P. F. Green, and J. R. Underhill (2002), Heterogeneous exhumation in the Inner Moray Firth, UK North Sea: constraints from new AFTA (R) and seismic data, *J. Geol. Soc. London.*, *159*(6), 715–729, doi:10.1144/0016-764901-141.

Arriagada, C; R. Ferrando, L. Córdova, D. Morata and P. Roperch (accepted), The Maipo Orocline: a first scale structural feature in the Miocene to Recent geodynamic evolution in the central Chilean Andes., *Andean* Geol.

Astini, R. A., J. L. Benedetto, and N. E. Vaccari (1995), The Early Paleozoic evolution of the argentine precordillera as a laurentian rifted, drifted, and collided terrane - a geodynamic model, *Geol. Soc. Am. Bull.*, *107*(3), 253–273, doi:10.1130/0016 7606(1995)107<0253:TEPEOT>2.3.CO;2.

Astini, R. A., J. L. Benedetto, and N. E. Vaccari (1996), The early Paleozoic evolution of the Argentine Precordillera as a Laurentian rifted, drifted, and collided terrane: A geodynamic model: Reply, *Geol. Soc. Am. Bull.*, *108*

Astini, R. A., and F. M. Davila (2004), Ordovician back arc foreland and Ocloyic thrust belt development on the western Gondwana margin as a response to Precordillera terrane accretion, *TECTONICS*, *23*(4), doi:10.1029/2003TC001620.

Babault, J., J. Van den Driessche, S. Bonnet, S. Castelltort, and A. Crave (2005), Origin of the highly elevated Pyrenean peneplain, *Tectonics*, *24*(2), TC2001, doi:10.1029/2004TC001697. [online] Available from: <Go to ISI>://000228856300002

Barbarand, J. (2003), Compositional and structural control of fission-track annealing in apatite, *Chem. Geol.*, *198*(1-2), 107–137, doi:10.1016/S0009-2541(02)00424-2. [online] Available from: http://linkinghub.elsevier.com/retrieve/pii/S0009254102004242 (Accessed 1 August 2012)

Barnes, J. B., and T. a. Ehlers (2009), End member models for Andean Plateau uplift, *Earth-Science Rev.*, *97*(1-4), 105–132, doi:10.1016/j.earscirev.2009.08.003. [online] Available from: http://linkinghub.elsevier.com/retrieve/pii/S0012825209001342 (Accessed 22 July 2012).

Beaumont, C., R. A. Jamieson, M. H. Nguyen, and B. Lee (2001), Himalayan tectonics explained by extrusion of a low-viscosity crustal channel coupled to focused surface denudation, *Nature*, *414*(6865), 738–742, doi:10.1038/414738a.

Bissig, T., J. K. W. Lee, A. H. Clark, and K. B. Heather (2001), The Cenozoic History of Volcanism and Hydrothermal Alteration in the Central Andean Flat-Slab Region: New 40

Ar- 39 Ar Constraints from the El Indio–Pascua Au (-Ag, Cu) Belt, 29°20′–30°30′ S, *Int. Geol. Rev.*, *43*(4), 312–340, doi:10.1080/00206810109465016. [online] Available from: http://www.tandfonline.com/doi/abs/10.1080/00206810109465016 (Accessed 30 August 2012)

Bissig, T., A. H. Clark, J. K. W. Lee, and C. J. Hodgson (2002), Miocene landscape evolution and geomorphologic controls on epithermal processes in the El Indio-Pascua Au-Ag-Cu belt, Chile and Argentina, *Econ. Geol.*, *97*(5), 971–996, doi:10.2113/97.5.971. [online] Available from: <Go to ISI>://WOS:000178050500003

Bissig, T., and R. Riquelme (2010), Andean uplift and climate evolution in the southern Atacama Desert deduced from geomorphology and supergene alunite-group minerals, *Earth Planet. Sci. Lett.*, *299*(3-4), 447–457, doi:DOI: 10.1016/j.epsl.2010.09.028. [online] Available from: http://www.sciencedirect.com/science/article/B6V61-518F0CS-3/2/bb88a23fa1f480e57b22ff13837997b7.

Burbank, D. W. (2002), Rates of erosion and their implications for exhumation, *Mineral. Mag.*, *66*(1), 25–52, doi:10.1180/0026461026610014. [online] Available from: <Go to ISI>://WOS:000174412700004

Burbank, D., and R. Anderson (2001), *Tectonic Geomorphology*, Blackwell Science, Oxford.

Cahill, T., and B. L. Isacks (1992), Seismicity and Shape of the Subducted Nazca Plate, *J. Geophys. Res. Earth*, *97*(B12), 17503–17529. [online] Available from: <Go to ISI>://A1992JY18900019.

Carlson, W. D., R. A. Donelick, and R. A. Ketcham (1999), Variability of apatite fission-track annealing kinetics: I. Experimental results, *Am. Mineral.*, *84*(9), 1213–1223. [online] Available from: <Go to ISI>://WOS:000082349700001

Cembrano, J., M. Zentilli, A. Grist, G .Yáñez (2003), Nuevas edades de trazas de fisión para Chile Central (30-34°S): Implicancias en el alzamiento y exhumación en los Andes desde el Cretácico, paper presented at *X Congr. Geol. Chileno*, Universidad de Concepción, Concepción, Chile.

Charrier, R. and Vicente, J.-C., (1972), Liminary and geosyncline Andes: major orogenic phases and synchronical evolutions of the central and Magellan sectors of the Argentine-Chilean Andes, *Solid Earth Probl. Conf.*, Upper Mantle Project, Buenos Aires, 2, 451-470.

Charrier, R. (1979), El Triásico de Chile y regiones adyacentes en Argentina: Una reconstrucción paleogeográfica y paleoclimática, *Comunicaciones*, *26*(1-47).

Charrier, R., O. Baeza, S. Elgueta, J. J. Flynn, P. Gans, S. M. Kay, N. Munoz, A. R. Wyss, and E. Zurita (2002), Evidence for Cenozoic extensional basin development and tectonic inversion south of the flat-slab segment, southern Central Andes, Chile (33 degrees-36 degrees SL), *J. South Am. Earth Sci.*, *15*(1), 117–139, doi:10.1016/s0895-9811(02)00009-3. [online] Available from: <Go to ISI>://WOS:000175725400009.

Charrier, R., L. Pinto, and M. P. Rodríguez (2007), Tectonostratigraphic evolution of the Andean Orogen in Chile, in *Geological Society Special Publication: The Andes of Chile*, pp. 21–114, Londres. [online] Available from: http://www.scopus.com/scopus/inward/record.url?eid=2-s2.0-34347336467&partnerID=40&rel=R6.5.0.

Charrier, R., G. Herail, L. Pinto, M. Garcia, R. Riquelme, M. Farias, and N. Munoz (2013), Cenozoic tectonic evolution in the Central Andes in northern Chile and west central Bolivia: implications for paleogeographic, magmatic and mountain building evolution, *Int. J. Earth Sci.*, *102*(1), 235–264, doi:10.1007/s00531-012-0801-4. [online] Available from: <Go to ISI>://WOS:000313487700011

Clark, A. H., R. M. Tosdal, E. Farrar, and A. Plazolles (1990), Geomorphologic Environment and Age of Supergene Enrichment of the Cuajone, Quellaveco, and Toquepala Porphyry Copper-Deposits, Southeastern Peru, *Econ. Geol.*, *85*(7), 1604–1628. [online] Available from: <Go to ISI>://A1990EU00800016.

Clark, M. K., B. C. B. L. M. Schoenbohm, L. H. Royden, K. X. Whipple, and and L. C. X. Zhang, W. Tang, E. Wang (2004), Surface uplift, tectonics, and erosion of eastern Tibet from large-scale drainage patterns, *Tectonics*, *23*(1), 1–21, doi:10.1029/2002TC001402. [online] Available from: http://www.agu.org/pubs/crossref/2004/2002TC001402.shtml (Accessed 22 July 2012).

Clark, M. K., L. H. Royden, K. X. Whipple, B. C. Burchfiel, X. Zhang, and W. Tang (2006), Use of a regional , relict landscape to measure vertical deformation of the eastern Tibetan Plateau, *Tectonics*, *111*(December 2005), 1–23, doi:10.1029/2005JF000294.

Coira, B., J. Davidson, C. Mpodozis, and V. Ramos (1982), Tectonic and Magmatic Evolution of the Andes of Northern Argentina and Chile, *Earth-Science Rev.*, *18*(3-4), 303–332, doi:10.1016/0012-8252(82)90042-3. [online] Available from: <Go to ISI>://WOS:A1982PT37300007

Cornejo, P., S Matthews and C.Pérez,(2003). The “K-T” compressive deformation event in northern Chile (24º-27ºS). Proceeedings 10th Congreso Geológico Chileno, Concepción, 10 p., CD Rom volume.

Crowhurst, P. V, P. F. Green, and P. J. J. Kamp (2002), Appraisal of (U-Th)/He apatite thermochronology as a thermal history tool for hydrocarbon exploration: An example from the Taranaki Basin, New Zealand, *Am. Assoc. Pet. Geol. Bull.*, *86*(10), 1801–1819.

Davis, J. S., S. M. Roeske, W. C. McClelland, and S. M. Kay (2000), Mafic and ultramafic crustal fragments of the southwestern Precordillera terrane and their bearing on tectonic models of the early Paleozoic in western Argentina, *Geology*, *28*(2), 171–174, doi:10.1130/0091-7613(2000)28<171:MAUCFO>2.0.CO;2.

Dedios, P.(1967), Cuadrángulo Vicuña, provincia de Coquimbo, Instituto de Investigaciones Geológicas, Santiago, *Carta Geológica* Nº 16.

Desilets, D., M. Zreda, and T. Prabu (2006), Extended scaling factors for in situ cosmogenic nuclides: New measurements at low latitude, *Earth Planet. Sci. Lett.*, *246*(3-4), 265–276, doi:10.1016/j.epsl.2006.03.051.

Dunai, T. J. (2001), Influence of secular variation of the geomagnetic field on production rates of in situ produced cosmogenic nuclides, *Earth Planet. Sci. Lett.*, *193*(1-2), 197–212, doi:10.1016/S0012-821X(01)00503-9.

Dunai, T. J., G. a. González López, and J. Juez-Larré (2005), Oligocene–Miocene age of aridity in the Atacama Desert revealed by exposure dating of erosion-sensitive landforms, *Geology*, *33*(4), 321, doi:10.1130/G21184.1. [online] Available from: http://geology.gsapubs.org/cgi/doi/10.1130/G21184.1 (Accessed 23 July 2012).

Emparán, C., and G. Pineda (2006), Geología del Area Andacollo-Puerto Aldea, Región de Coquimbo, *Cart. Geológica Chile, Ser. Geológica Básica*.

Evenstar, L. a., a. J. Hartley, F. M. Stuart, a. E. Mather, C. M. Rice, and G. Chong (2009), Multiphase development of the Atacama Planation Surface recorded by cosmogenic 3He exposure ages: Implications for uplift and Cenozoic climate change in western South

America, *Geology*, *37*(1), 27–30, doi:10.1130/G25437A.1. [online] Available from: http://geology.gsapubs.org/cgi/doi/10.1130/G25437A.1 (Accessed 22 July 2012)

Farias, M., R. Charrier, D. Comte, J. Martinod, and G. Herail (2005), Late Cenozoic deformation and uplift of the western flank of the Altiplano: Evidence from the depositional, tectonic, and geomorphologic evolution and shallow seismic activity (northern Chile at 19 degrees 30 ' S), *Tectonics*, *24*(4), doi:Tc4001 10.1029/2004tc001667. [online] Available from: <Go to ISI>://WOS:000230484000001.

Farías, M. (2007), Tectónica y erosión en la evolución del relieve de los Andes de Chile central durante el Neógeno, 194 pp., Phd Thesis, Universidad de Chile.

Farias, M., R. Charrier, S. Carretier, J. Martinod, A. Fock, D. Campbell, J. Caceres, and D. Comte (2008), Late Miocene high and rapid surface uplift and its erosional response in the Andes of central Chile (33 degrees-35 degrees S), *Tectonics*, *27*(1), doi:Tc1005 10.1029/2006tc002046. [online] Available from: <Go to ISI>://WOS:000252572200001.

Farias, M., D. Comte, R. Charrier, J. Martinod, C. David, A. Tassara, F. Tapia, and A. Fock (2010), Crustal-scale structural architecture in central Chile based on seismicity and surface geology: Implications for Andean mountain building, *Tectonics*, *29*, 22, doi:Tc3006 10.1029/2009tc002480. [online] Available from: <Go to ISI>://000278249500001.

Farley, K. A., R. A. Wolf, and L. T. Silver (1996), The effects of long alpha-stopping distances on (U-Th)/He ages, *Geochim. Cosmochim. Acta*, *60*(21), 4223–4229, doi:10.1016/S0016-7037(96)00193-7.

Finger, K. L., A. Encinas, and S. N. Nielsen (2013), Comment on `Evidence for an Early-Middle Miocene age of the Navidad Formation (central Chile): Paleontological, paleoclimatic and tectonic implications' of Gutierrez et al. (2013, Andean Geology 40 (1): 66-78), *ANDEAN Geol.*, *40*(3), 571–579, doi:10.5027/andgeoV40n3-a10.

Fleischer RL, Price PB, Walker RM (1975) Nuclear Tracks in Solids: Principles and Applications. University of California Press, Berkeley.

Flowers, R. M., R. A. Ketcham, D. L. Shuster, and K. A. Farley (2009), Apatite (U – Th)/ He thermochronometry using a radiation damage accumulation and annealing model, *Geochim. Cosmochim. Acta*, *73*(8), 2347–2365, doi:10.1016/j.gca.2009.01.015. [online] Available from: http://dx.doi.org/10.1016/j.gca.2009.01.015

Garrido, G. 2009. Evolución geomorfológica de la Depresión de Domeyko entre los 28º45’-29º00’S durante el Neógeno. Thesis, Departamento de Geología, Universidad de Chile.

Garzione, C. N., P. Molnar, J. C. Libarkin, and B. J. MacFadden (2006), Rapid late Miocene rise of the Bolivian Altiplano: Evidence for removal of mantle lithosphere, *Earth Planet. Sci. Lett.*, *241*(3-4), 543–556. [online] Available from: <Go to ISI>://000235289000016

Giambiagi, L. B., P. P. Alvarez, E. Godoy, and V. A. Ramos (2003), The control of pre-existing extensional structures on the evolution of the southern sector of the Aconcagua fold and thrust belt, southern Andes, *Tectonophysics*, *369*(1-2), 1–19, doi:Doi: 10.1016/s0040-1951(03)00171-9. [online] Available from: http://www.sciencedirect.com/science/article/B6V72-48Y6RTD-2/2/019b1b6fc002c098b871f007e594befe

Giambiagi, L., J. Mescua, F. Bechis, A. Tassara, and G. Hoke (2012), Thrust belts of the southern Central Andes: Along-strike variations in shortening, topography, crustal geometry, and denudation, *Geol. Soc. Am. Bull.*, *124*(7-8), 1339–1351, doi:10.1130/B30609.1.

Gleadow, a. J. W., I. R. Duddy, P. F. Green, and J. F. Lovering (1986), Confined fission track lengths in apatite: a diagnostic tool for thermal history analysis, *Contrib. to Mineral. Petrol.*, *94*(4), 405–415, doi:10.1007/BF00376334. [online] Available from: http://www.springerlink.com/index/10.1007/BF00376334

Gosse, J. C., and F. M. Phillips (2001), Terrestrial in situ cosmogenic nuclides: theory and application, *Quat. Sci. Rev.*, *20*(14), 1475–1560, doi:10.1016/S0277-3791(00)00171-2. [online] Available from: http://linkinghub.elsevier.com/retrieve/pii/S0277379100001712

Green, P. F., I. R. Duddy, A. J. W. Gleadow, P. R. Tingate, and G. M. Laslett (1986), Thermal annealing of fission tracks in apatite 1. A qualitative description, *Chemical Geology*, *59*, 237 – 253, doi:10.1016/ 0009-2541(86)90048-3.

Gripp, A. E., and R. G. Gordon (2002), Young tracks of hotspots and current plate velocities, *Geophys. J. Int.*, *150*(2), 321–361. [online] Available from: <Go to ISI>://000176921500001

Gutierrez, N. M., L. F. Hinojosa, J. P. Le Roux, and V. Pedroza (2013), Evidence for an Early-Middle Miocene age of the Navidad Formation (central Chile): Paleontological, paleoclimatic and tectonic implications, *ANDEAN Geol.*, *40*(1), 66–78, doi:10.5027/andgeoV40n1-a03.

Hall, S. R., D. L. Farber, L. Audin, R. C. Finkel, and a.-S. Mériaux (2008), Geochronology of pediment surfaces in southern Peru: Implications for Quaternary deformation of the Andean forearc, *Tectonophysics*, *459*(1-4), 186–205, doi:10.1016/j.tecto.2007.11.073. [online] Available from: http://linkinghub.elsevier.com/retrieve/pii/S0040195108001534 (Accessed 28 January 2012)

Heather, K. B., and Diaz, D., 2000, El Indio-Tambo District regional geological mapping program 1997-1999: Barrick Chile Ltda, internal report, 2 vols., 284 p., 16 maps.

Hervé, F. (1988), Late Paleozoic subduction and accretion in Southern Chile, *Episodes*, *11*, 183–188.

Hilley, G. E., M. R. Strecker, and V. A. Ramos (2004), Growth and erosion of fold-and-thrust belts with an application to the Aconcagua fold-and-thrust belt, Argentina, *J. Geophys. Res. Earth*, *109*(B1), doi:B01410 10.1029/2002jb002282. [online] Available from: <Go to ISI>://000188673200001

Hilley, G. E., and I. Coutand (2010), Links between topography, erosion, rheological heterogeneity, and deformation in contractional settings: Insights from the central Andes, *Tectonophysics*, *495*(1-2), 78–92, doi:10.1016/j.tecto.2009.06.017. [online] Available from: http://linkinghub.elsevier.com/retrieve/pii/S0040195109003503 (Accessed 30 August 2012)

Hoke, G. D., B. L. Isacks, T. E. Jordan, N. Blanco, A. J. Tomlinson, and J. Ramezani (2007), Geomorphic evidence for post-10 Ma uplift of the western flank of the central Andes 18°30′–22°S, *Tectonics*, *26*(5), 1–17, doi:10.1029/2006TC002082. [online] Available from: http://www.agu.org/pubs/crossref/2007/2006TC002082.shtml (Accessed 22 July 2012).

Hoke, G. D., and C. N. Garzione (2008), Paleosurfaces, paleoelevation, and the mechanisms for the late Miocene topographic development of the Altiplano plateau, *Earth Planet. Sci. Lett.*, *271*(1-4), 192–201, doi:10.1016/j.epsl.2008.04.008. [online] Available from: http://linkinghub.elsevier.com/retrieve/pii/S0012821X08002446 (Accessed 22 July 2012)

Hovius, N., P. Meunier, L. Ching-Weei, C. Hongey, C. Yue-Gau, S. Dadson, H. Ming-Jame, and M. Lines (2011), Prolonged seismically induced erosion and the mass balance of a large earthquake, *Earth Planet. Sci. Lett.*, *304*(3-4), 347–355, doi:10.1016/j.epsl.2011.02.005. [online] Available from: <Go to ISI>://WOS:000290839000006

Iroume, A., A. Huber, and K. Schulz (2005), Summer flows in experimental catchments with different forest covers, Chile, *J. Hydrol.*, *300*(1-4), 300–313, doi:10.1016/j.jhydrol.2004.06.014. [online] Available from: <Go to ISI>://WOS:000226223400020

Isacks, B. L. (1988), Uplift of the central Andean Plateau and bending of the Bolivian Orocline, *J. Geophys. Res.*, *93*(B4), 3211–3231.

Jara, P., and R. Charrier (in press), Nuevos antecedentes geocronológicos y estratigráficos en la Cordillera Principal de Chile central entre 32° y 32°30´S Implicancias paleogeográficas y estructurales, *Andean Geol.*

Jordan, T. E., B. L. Isacks, R. W. Allmendinger, J. A. Brewer, V. A. Ramos, and C. J. Ando (1983), Andean Tectonics Related to Geometry of Subducted Nazca Plate, *Geol. Soc. Am. Bull.*, *94*(3), 341–361, doi:10.1130/0016-7606(1983)94<341:atrtgo>2.0.co;2. [online] Available from: <Go to ISI>://WOS:A1983QN40400003

Jordan, T. E., P. L. Nester, N. Blanco, G. D. Hoke, F. Dávila, and A. J. Tomlinson (2010), Uplift of the Altiplano - Puna plateau : A view from the west, *Tectonics*, *29*(May), doi:10.1029/2010TC002661.

Kay, S. M., V. A. Ramos, C. Mpodozis, and P. Sruoga (1989), Late Paleozoic to Jurassic silici magmatism at the Gondwana margin, anology to the Middle Proterozoic in North America?, *Geology*, *17*(4), 324–328.

Kay, S. M., and C. Mpodozis (2002), Magmatism as a probe to the Neogene shallowing of the Nazca plate beneath the modern Chilean flat-slab, *J. South Am. Earth Sci.*, *15*(1), 39–57, doi:Pii s0895-9811(02)00005-6. [online] Available from: <Go to ISI>://WOS:000175725400005

Ketcham, R. A., R. A. Donelick, and W. D. Carlson (1999), Variability of apatite fission-track annealing kinetics: III. Extrapolation to geological time scales, *Am. Mineral*., 84, 1235 – 1255.

Ketcham, R. a. (2005), Forward and Inverse Modeling of Low-Temperature Thermochronometry Data, *Rev. Mineral. Geochemistry*, *58*(1), 275–314, doi:10.2138/rmg.2005.58.11. [online] Available from: http://rimg.geoscienceworld.org/cgi/doi/10.2138/rmg.2005.58.11 (Accessed 25 July 2012)

Lal, D. (1991), Cosmic ray labeling of erosion surfaces — in situ nuclide production rates and erosion models, *Earth Planet. Sci. Lett.*, *104*, 424–439.

Lamb, S., L. Hoke, L. Kennan, and J. Dewey (1997), Cenozoic evolution of the central Andes in Bolivia and northern Chile, in *Orogeny through time*, edited by J.-P. Burg and M. Ford, pp. 237–264.

Lamb, S., and P. Davis (2003), Cenozoic climate change as a possible cause for the rise of the Andes, *Nature*, *425*(6960), 792–797. [online] Available from: <Go to ISI>://000186118500035

Le Roux, J. P. et al. (2005), Neogene-Quaternary coastal and offshore sedimentation in north central Chile: Record of sea-level changes and implications for Andean tectonism, *J. South Am. Earth Sci.*, *19*(1), 83–98, doi:10.1016/j.jsames.2003.11.003. [online] Available from: <Go to ISI>://000231583800007

Le Roux, J. P., D. M. Olivares, S. N. Nielsen, N. D. Smith, H. Middleton, J. Fenner, and S. E. Ishman (2006), Bay sedimentation as controlled by regional crustal behaviour, local tectonics and eustatic sea-level changes: Coquimbo Formation (Miocene-Pliocene), Bay of Tongoy, central Chile, *Sediment. Geol.*, *184*(1-2), 133–153, doi:10.1016/j.sedgeo.2005.09.023. [online] Available from: <Go to ISI>://000235100200004.

Le Roux, J. P. (2012), A review of Tertiary climate changes in southern South America and the Antarctic Peninsula. Part 2: continental conditions, *Sediment. Geol.*, *247-248*, 21–38, doi:10.1016/j.sedgeo.2011.12.001. [online] Available from: http://linkinghub.elsevier.com/retrieve/pii/S003707381100279X (Accessed 22 July 2012)

Le Roux, J. P., N. M. Gutierrez, L. F. Hinojosa, V. Pedroza, and J. Becerra (2013), Reply to Comment of Finger et al. (2013) on: `Evidence for an Early-Middle Miocene age of the Navidad Formation (central Chile): Paleontological, paleoclimatic and tectonic implications' of Gutierrez et al. (2013, Andean Geology 40 (1): 66-78), *ANDEAN Geol.*, *40*(3), 580–588, doi:10.5027/andgeoV40n3-a11.

Lifton, N. A., J. W. Bieber, J. M. Clem, M. L. Duldig, P. Evenson, J. E. Humble, and R. Pyle (2005), Addressing solar modulation and long-term uncertainties in scaling secondary cosmic rays for in situ cosmogenic nuclide applications, *Earth Planet. Sci. Lett.*, *239*(1-2), 140–161, doi:10.1016/j.epsl.2005.07.001.

Litvak, V. D., S. Poma, and S. M. Kay (2007), Paleogene and Neogene magmatism in the Valle del Cura region: New perspective on the evolution of the Pampean flat slab, San Juan province, Argentina, *J. South Am. Earth Sci.*, *24*(2-4), 117–137, doi:10.1016/j.jsames.2007.04.002. [online] Available from: http://linkinghub.elsevier.com/retrieve/pii/S0895981107000570 (Accessed 30 August 2012)

Maksaev, V., R. Moscoso, C. Mpodozis and C. Nasi (1984), Las unidades volcánicas y plutónicas del Cenozoico superior en la Alta Cordillera del Norte Chico (29°-31°S), Geología, alteración hidrotermal y mineralización. *Rev. Geo. Chile*, *21*,11-51.

Manea, V. C., M. Pérez-gussinyé, and M. Manea (2012), Chilean fl at slab subduction controlled by overriding plate thickness and trench rollback, *Geology*, (1), 35–38, doi:10.1130/G32543.1.

Marot, M. (2013), Zones de subduction horizontale versus normale: Une comparaison basée sur la tomographie sismique en 3-D et de la modélisation pétrologique de la lithosphère continentale du Chili Central et de l'Ouest de l'Argentine (29°S-35°S), 224 pp., Phd Thesis, l'Université de Nice-Sophia Antipolis, Nice.

Martin, M., J. Clavero, C. Mpodozis, and L. Cutiño (1995), *Estudio geológico regional de la franja El Indio, Cordillera de Coquimbo*, Santiago, Chile.

Martin, M. W., J. Clavero, and C. Mpodozis (1999), Late Paleozoic to Early Jurassic tectonic development of the high, *J. South Am. Earth Sci.*, *12*, 33–49.

Martinez, F., C. Arriagada, M. Pena, I. Del Real, and K. Deckart (2013), The structure of the Chanarcillo Basin: An example of tectonic inversion in the Atacama region, northern Chile, *J. SOUTH Am. EARTH Sci.*, *42*, 1–16, doi:10.1016/j.jsames.2012.07.001.

Martinod, J., L. Husson, P. Roperch, B. Guillaume, and N. Espurt (2010), Horizontal subduction zones, convergence velocity and the building of the Andes, *Earth Planet. Sci. Lett.*, *299*(3-4), 299–309, doi:10.1016/j.epsl.2010.09.010. [online] Available from:

http://linkinghub.elsevier.com/retrieve/pii/S0012821X10005856 (Accessed 6 August 2012).

McQuarrie, N. (2002), The kinematic history of the central Andean fold-thrust belt, Bolivia: Implications for building a high plateau, *Geol. Soc. Am. Bull.*, *114*(8), 950–963.

McQuarrie, N., B. K. Horton, G. Zandt, S. Beck, and P. G. Decelles (2005), Lithospheric evolution of the Andean fold – thrust belt , Bolivia , and the origin of the central Andean plateau, , *399*, 15–37, doi:10.1016/j.tecto.2004.12.013.

Molnar, P., and P. England (1990), Late Cenozoic Uplift of Mountain-Ranges and Global Climate Change - Chicken or Egg, *Nature*, *346*(6279), 29–34, doi:10.1038/346029a0. [online] Available from: <Go to ISI>://WOS:A1990DM39600049

Montecinos, A., Aceituno, P., 2003. Seasonality of the ENSO-related rainfall variability in central Chile and associated circulation anomalies. Journal of Climate 16, 281–296.

Montgomery, D. R., G. Balco, and S. D. Willett (2001), Climate, tectonics, and the morphology of the Andes, *Geology*, *29*(7), 579, doi:10.1130/0091-7613(2001)029<0579:CTATMO>2.0.CO;2. [online] Available from: http://geology.gsapubs.org/cgi/doi/10.1130/00917613(2001)029<0579:CTATMO>2.0.CO;2

Morata, D., and L. Aguirre (2003), Extensional Lower Cretaceous volcanism in the Coastal Range (29820 0 – 308S), Chile : geochemistry and petrogenesis, , *16*, 459–476, doi:10.1016/j.jsames.2003.06.001.

Mortimer, C. (1973), The Cenozoic history of the southern Atacama Desert, Chile, *J. Geol. Soc.*, *129*(5), 505–526.

Mpodozis, C. and P. Cornejo (1988), Hoja Pisco Elqui, IV Región de Coquimbo, scale 1:50.000, Serv. Nac. de Geol. y Miner, Santiago.

Mpodozis, C., and V. A. Ramos (1989), The Andes of Chile and Argentina. In Geology of the Andes and its relation to Hydrocarbon and Mineral Resources, in *Circumpacific Council for Energy and Mineral Resources*, vol. 11, edited by G. E. Ericksen, M. T. Cañas, and J. A. Reinemud, pp. 59–90.

Mpodozis, C., and S. M. Kay (1990), Provincias Magmaticas acidas y evolucion tectonica de Gondwana: Andes Chilenos (28-31 S), *Rev. Geológica Chile*, *17*(2), 153–180.

Munoz, M., M. Farias, R. Charrier, C. M. Fanning, M. Polve, and K. Deckart (2013), Isotopic shifts in the Cenozoic Andean arc of central Chile: Records of an evolving basement throughout cordilleran arc mountain building, *Geology*, *41*(8), 931–934, doi:10.1130/G34178.1.

Nalpas, T., Dabard, M.-P., Pinto, L., Loi, A. 2009. Preservation of the Miocene Atacama Gravels in Vallenar area, northern Chilean Andes: Climate, stratigraphic or tectonic control? XII Congreso Geológico Chileno, Santiago.

Nasi, C., R. Moscoso V. and Maksaev (1990) Hoja Guanta, Regiones de Atacama y Coquimbo, scale 1:50.000, Serv. Nac. de Geol. y Miner, Santiago.

Nishiizumi, K., M. W. Caffee, R. C. Finkel, G. Brimhall, and T. Mote (2005), Remnants of a fossil alluvial fan landscape of Miocene age in the Atacama Desert of northern Chile using cosmogenic nuclide exposure age dating, *Earth Planet. Sci. Lett.*, *237*(3-4), 499–507. [online] Available from: http://www.sciencedirect.com/science/article/B6V61-4GTVYTK-1/2/e308f93f532d165361ee0c2abfb09d08.

Ortega, C., G. Vargas, J. A. Rutllant, D. Jackson, and C. Mendez (2012), Major hydrological regime change along the semiarid western coast of South America during the early Holocene, *Quat. Res.*, *78*(3), 513–527, doi:10.1016/j.yqres.2012.08.002..

Parada, M.A., S. Rivano, P. Sepúlveda, M Hervé,.F. Hervé, A Puig, F. Munizaga, M. Brook, R. Pankhurst and N. Snelling, (1988), Mesozoic and Cenozoic plutonic development in the Andes of Central Chile (30º 30'-32º30' S), Journal of South American Earth Sciences, 1 (3), 249-260.

Parada, M. A., and B. Levi (1999), Multiple sources for the Coastal Batholith of central Chile 31 – 34^{o}S : geochemical and Sr – Nd isotopic evidence and tectonic implications, *Lithos*, *46*, 505–521.

Pardo-Casas, F., and P. Molnar (1987), Relative motion of the Nazca (Farallon) and South American plates since late Cretaceous time, *Tectonics*, *6*(3), 233–248.

Paskoff, R. (1970), *Recherches géomorphologiques dans le Chili semi-aride*, Biscaye Freres, Bordeaux.

Pineda, G. and M. Calderón (2008), Geología del área Monte Patria-El Maqui, Región de Coquimbo. Servicio Nacional de Geología y Minería, scale 1:100.000, Serv. Nac. de Geol. y Miner, Santiago.

Pineda, G. and C. Emparán (2006), Geología del área Vicuña-Pichasca, Región de Coquimbo. Servicio Nacional de Geología y Minería, scale 1:100.000, Serv. Nac. de Geol. y Miner, Santiago.

Piracés, R., 1976. Estratigrafía de la Cordillera de la Costa entre la Cuesta Melón y Limache, Provincia de Valparaiso, Chile. Proceedings 1st. Congreso Geológico Chileno, Santiago, 1, A65-A82.

Porcher, C. C., L. A. D. Fernandes, G. I. Vujovich, and C. J. Chernicoff (2004), Thermobarometry, Sm/Nd ages and geophysical evidence for the location of the suture zone between Cuyania and the western proto-Andean margin of Gondwana, *GONDWANA Res.*, *7*(4), 1057–1076, doi:10.1016/S1342-937X(05)71084-4.

Quang, C. X., A. H. Clark, J. K. W. Lee, and N. Hawkes (2005), Response of supergene processes to episodic Cenozoic uplift, pediment erosion, and ignimbrite eruption in the porphyry copper province of southern Peru, *Econ. Geol.*, *100*(1), 87–114, doi:10.2113/100.1.0087. [online] Available from: <Go to ISI>://WOS:000227707900006

Ramos, V. A., T. E. Jordan, R. W. Allmendinger, C. Mpodozis, S. M. Kay, J. M. Cortes, and M. Palma (1986), Paleozoic terranes of the central argentine-chilean ANDES, *Tectonics*, *5*(6), 855–880, doi:10.1029/TC005i006p00855.

Ramos, V. A. (1994), Terrains of southern Gondwanaland and their control in the Andean structure (30^{o}-33^{o}S), in *Tectonics of the Southern Central Andes, Structure and Evolution of an Active Continental Margin*, edited by K. J. Reutter, E. Scheuber, and P. J. Wigger, pp. 249–261, Springer Verlag, Berlin.

Ramos, V. A., M. Cegarra, and E. Cristallini (1996), Cenozoic tectonics of the High Andes of west-central Argentina (30-36^{o}S latitude), *Tectonophysics*, *259*(1-3), 185–200. [online] Available from: <Go to ISI>://A1996VB37400014.

Ramos, V. A., M. Escayola, D. I. Mutti, and G. I. Vujovich (2000), Proterozoic-early Paleozoic ophiolites of the Andean basement of southern South America, in *OPHIOLITES AND OCEANIC CRUST: NEW INSIGHTS FROM FIELD STUDIES AND OCEAN DRILLING PROGRAM*, edited by Dilek, Y and Moores, EM and Elthon, D and Nicolas, A, pp. 331–349.

Ramos, V. A., E. O. Cristallini, and D. J. Perez (2002), The Pampean flat-slab of the Central Andes, *J. SOUTH Am. EARTH Sci.*, *15*(1), 59–78, doi:10.1016/S0895-9811(02)00006-8.

Ramos, V. A., E. Zapata, E. Cristallini, and A. Introcaso (2004), The Andean thrust system-Ltitudinal variations in structural stylesand orogenic shortening, edited by K. R. McClay, *Thrust tectonics Hydrocarb. Syst.*, *Memoir 82*, 30–50.

Ramos, V. A. (2009), Anatomy and global context of the Andes: Main geologic features and the Andean orogenic cycle, in *BACKBONE OF THE AMERICAS: SHALLOW SUBDUCTION, PLATEAU UPLIFT, AND RIDGE AND TERRANE COLLISION*, vol. 204, edited by Kay, SM and Ramos, VA and Dickinson, WR, pp. 31–65.

Rapela, C. W., R. J. Pankhurst, C. Casquet, E. Baldo, J. Saavedra, and C. Galindo (1998), Early evolution of the Proto-Andean margin of South America, *Geology*, *26*(8), 707–710, doi:10.1130/0091-7613(1998)026<0707:EEOTPA>2.3.CO;2.

Raymo, M. E., and W. F. Ruddiman (1992), Tectonic forcing of Late Cenozoic climate, *Nature*, *359*(6391), 117–122, doi:10.1038/359117a0.

Rebolledo, S. and R. Charrier, (1994), Evolución del basamento paleozoico en el área de Punta Claditas, Región de Coquimbo, Chile (31-32ºS). Revista Geológica de Chile, 21 (1), 55-69.

Regard, V., M. Saillard, J. Martinod, and L. Audin (2010), Renewed uplift of the Central Andes Forearc revealed by coastal evolution during the Quaternary, *Earth Planet. Sci. Lett.*, *297*(1-2), 199–210, doi:10.1016/j.epsl.2010.06.020. [online] Available from: http://dx.doi.org/10.1016/j.epsl.2010.06.020.

Reiners, P. W., and M. T. Brandon (2006), Using Thermochronology To Understand Orogenic Erosion, *Annu. Rev. Earth Planet. Sci.*, *34*(1), 419–466, doi:10.1146/annurev.earth.34.031405.125202. [online] Available from: http://www.annualreviews.org/doi/abs/10.1146/annurev.earth.34.031405.125202 (Accessed 13 July 2012)

Reutter, K.-J., 1974. Entwicklung und Bauplan der chilenischen Hochkordillere im Bereich 29º südlicher Breite. Neues Jahrbuch für Geologie und Paläontologie, Vol. 146, Nº 2, p. 153-178.

Riquelme, R., G. Hérail, J. Martinod, R. Charrier, and J. Darrozes (2007), Late Cenozoic geomorphologic signal of Andean forearc deformation and tilting associated with the uplift and climate changes of the Southern Atacama Desert (26°S–28°S), *Geomorphology*, *86*(3-4), 283–306, doi:10.1016/j.geomorph.2006.09.004. [online] Available from: http://linkinghub.elsevier.com/retrieve/pii/S0169555X06004089 (Accessed 28 January 2012)

Rivano, S., and P. Sepúlveda (1991), Hoja Illapel, Región de Coquimbo, *Cart. Geológica Chile*.

Roe, G. H. (2005), Orographic precipitation, *Annu. Rev. Earth Planet. Sci.*, *33*, 645–671, doi:10.1146/annurev.earth.33.092203.122541.

Ruddiman, W. F. (1997), *Tectonic Uplift and Climate Change*, Plenum Press, New York.

Rutllant, J., Fuenzalida, H., 1991. Synoptic aspects of the central Chile rainfall variability associated with the Southern Oscillation. International Journal of Climatology 11, 63–76.

Rutllant, J., Fuenzalida, H., Torres, R., Figueroa, D., 1998. Interacción océano atmósferatierra en la Región de Antofagasta (Chile, 23°S): Experimento DICLIMA. Revista Chilena de Historia Natural 71, 405–427.

Saillard, M., S. R. Hall, L. Audin, D. L. Farber, G. Hérail, J. Martinod, V. Regard, R. C. Finkel, and F. Bondoux (2009), Non-steady long-term uplift rates and Pleistocene marine terrace development along the Andean margin of Chile (31°S) inferred from 10Be dating, *Earth Planet. Sci. Lett.*, *277*(1-2), 50–63, doi:10.1016/j.epsl.2008.09.039. [online] Available from: http://linkinghub.elsevier.com/retrieve/pii/S0012821X08006584 (Accessed 15 June 2011).

Salazar, E. 2012. Evolución tectonica-estratigrafica post-Paleozoica de la Cordillera de Vallenar. Thesis, Departamento de Geología, Universidad de Chile.

Schellart, W. P., J. Freeman, D. R. Stegman, L. Moresi, and D. May (2007), Evolution and diversity of subduction zones controlled by slab width, *Nature*, *446*(7133), 308–311, doi:10.1038/nature05615.

Schildgen, T. F., K. V Hodges, K. X. Whipple, P. W. Reiners, and M. S. Pringle (2007), Uplift of the western margin of the Andean plateau revealed from canyon incision history, southern Peru, *Geology*, *35*(6), 523–526. [online] Available from: <Go to ISI>://000247628200011

Sdrolias, M., and R. D. Muller (2006), Controls on back-arc basin formation, *Geochemistry Geophys. Geosystems*, *7*, doi:Q04016 10.1029/2005gc001090. [online] Available from: <Go to ISI>://WOS:000237411300002.

Segerstrom, K., 1960. Cuadrángulo Quebrada Paipote, Provincia de Atacama. Instituto de Investigaciones Geológicas, Santiago, Carta Geológica de Chile, 1:50.000, Vol. 2, Nº 1, 35 p.

Sernageomin (2003), Carta Geológica de Chile, scale 1:1.000.000, Serv. Nac. de Geol. y Miner, Santiago.

Shuster, D. L., R. M. Flowers, and K. A. Farley (2006), The influence of natural radiation damage on helium diffusion kinetics in apatite, *Earth Planet. Sci. Lett.*, *249*(3-4), 148–161, doi:10.1016/j.epsl.2006.07.028.

Silver, P. G., R. M. Russo, and C. Lithgow-Bertelloni (1998), Coupling of South America and African plate motion and plate deformation, *Science (80-.).*, *279*(5347), 60–63.

Smart, D.F., Shea, M.A., (1985). Galactic cosmic radiation and solar energetic particles. Handbook of Geophysics and the Space Environment. Air Force Geophysics Laboratory, 6-1}6-29 pp.

Somoza, R. (1998), Updated Nazca (Farallon) - South America relative motions during the last 40 My: implications for mountain building in the central Andean region, *J. South Am. Earth Sci.*, *11*(3), 211–215. [online] Available from: <Go to ISI>://000078067600001.

Soler, P., Bonhomme, M., 1990. Relations of Magmatic Activity to Plate Dynamics in Central Peru from Late Cretaceous to Present. In: Kay, S., Rapela, C. (Eds.), Plutonism from Antarctica to Alaska: Geol. Soc. Am. Mem. , pp. 173–191.

Spikings, R., M. Dungan, J. Foeken, A. Carter, L. Page, and F. Stuart (2008), Tectonic response of the central Chilean margin (35-38 degrees S) to the collision and subduction of heterogeneous oceanic crust: a thermochronological study, *J. Geol. Soc. London.*, *165*(5), 941–953, doi:10.1144/0016-76492007-115.

Steinman, G., 1929. Geologie von Peru. Karl Winter, Heidelberg. 448 pp.

Strecker, M. R., R. N. Alonso, B. Bookhagen, B. Carrapa, G. E. Hilley, E. R. Sobel, and M. H. Trauth (2007), Tectonics and Climate of the Southern Central Andes, *Annu. Rev. Earth Planet. Sci.*, *35*(1), 747–787, doi:10.1146/annurev.earth.35.031306.140158. [online] Available from: http://www.annualreviews.org/doi/abs/10.1146/annurev.earth.35.031306.140158 (Accessed 13 July 2012).

Tassara, A., and G. Yanez (2003), Relationship between elastic thickness and the tectonic segmentation of the Andean margin, *Rev. Geol. Chile*, *30*(2), 159–186. [online] Available from: <Go to ISI>://000187878900002.

Thiele, R. (1964), *Reconocimiento geológico de la alta Cordillera de Elqui*, Santiago, Chile.

Thomas, H. (1958), Geología de la Cordillera de la Costa entre el Valle de La Ligua y la Cuesta de Barriga, *Inst. Investig. Geológicas, Boletín*, *2*, 1–86.

Thomas, W. A., and R. A. Astini (2003), Ordovician accretion of the Argentine Precordillera terrane to Gondwana: a review, *J. South Am. Earth Sci.*, *16*, 67–79. [online] Available from:http://www.ingentaconnect.com/content/els/08959811/2003/00000016/00000001/art00019

Tosdal, R. M., A. H. Clark, and E. Farrar (1984), Cenozoic Polyphase Landscape and Tectonic Evolution of the Cordillera Occidental, Southernmost Peru, *Geol. Soc. Am. Bull.*, *95*(11), 1318–1332. [online] Available from: <Go to ISI>://A1984TV75700006

Urresty, C., (2009) Evolución geomorfológica de la parte sur de la Depresión de Domeyko (29º00'-29º40'S) durante el Neógeno. Thesis, Departamento de Geología, Universidad de Chile.

Valdés, C. (2009), “Erosión neógena de la cordillera de los Andes en el segmento del flat-slab (28º-31”s): basado en el estudio de minerales pesados detríticos neógenos”, 196pp, Univesidad de Concepción, Concepción

Varas, M.I., (2011). Naturaleza, distribución espacial e implicaciones petrogenéticas de los enclaves máficos microgranulares del complejo plutónico illapel, Cordillera de la Costa, Chile Central Thesis, Departamento de Geología, Universidad de Chile.

Veit, H., and U. Bayreuth (1996), Southern Westerlies during the Holocene deduced from geomorphological and pedological studies in the Norte Chico, Northern Chile (27-33°S), , *123*.

Vergara, M., D. De Geologı, J. O. Nystro, and A. Cancino (1995), Jurassic and Early Cretaceous island arc volcanism , extension , and subsidence in the Coast Range of central Chile, *Geol. Soc. Am. Bull.*, *706*(12), 1427–1440.

Vérges, J., V. A. Ramos, A. Meigs, E. Cristallini, F. H. Bettini, and J. M. Cortés (2007), Crustal wedging triggering recent deformation in the Andean thrust front between 31^{o}S and 33^{o}S: Sierras Pampeanas-Precordillera interaction, *J. Geophys. Res.*, *112*(B3), B03S15, doi:doi:10.1029/2006JB004287. [online] Available from: <Go to ISI>://000244709500004.

Villagran, C., A. Leon, and F. A. Roig (2004), Paleodistribution of the alerce and cypres of the Guaitecas during the interstadial stages of the Llanquihue glaciation: Llanquihue and Chiloe provinces, Los Lagos Region, Chile., *Rev. Geol. CHILE*, *31*(1), 133–151.

Von Huene, R., W. Weinrebe, and F. Heeren (1999), Subduction erosion along the North Chile margin, *J. Geodyn.*, *27*(3), 345–358.

Whipple, K. X., E. Kirby, and S. H. Brocklehurst (1999), Geomorphic limits to climate-induced increases in topographic relief, *Nature*, *401*(6748), 39–43, doi:10.1038/43375.

Willett, S. D. (1999), Rheological dependence of extension in wedge models of convergent orogens, , *305*, 419–435.

Willett, S. D., M. T. Brandon, N. Haven, and D. M. Fisher (2006), Geological Society of America Special Paper 398 Penrose Conference Proceedings : Tectonics , Climate and Landscape Evolution Introduction Niels Hovius Cambridge CB2 3EQ.

Winocur (2010), Geología y estructura del Valle del Cura y el sector central del Norte Chico, provincia de San Juan y IV Región de Coquimbo, Argentina y Chile, P.h. D thesis, pp, Univ. de Bs. Aires, Buenos Aires, Argentina.

Winocur D. A., V. D. Litvak, and V. A Ramos (accepted), Magmatic and Tectonic Evolution of the Oligocene Valle del Cura Basin, Main Andes of Argentina and Chile: Evidence for Generalized Extension, *Geodynamic Processes in the Andes of Central Chile and Argentina*, Geological Society, London.

Yáñez, G., C. R. Ranero, R. Von Huene, and J. Díaz (2001), Magnetic anomaly interpretation across the southern central Andes (32°-34°S): The role of the Juan Fernández Ridge in the late Tertiary evolution of the margin, *J. Geophys. Res. B Solid Earth*, *106*(B4), 6325–6345.

Zech, R., C. Kull, and H. Veit (2006), Late Quaternary glacial history in the Encierro Valley, northern Chile (29°S), deduced from 10Be surface exposure dating, *Palaeogeogr. Palaeoclimatol. Palaeoecol.*, *234*(2-4), 277–286, doi:10.1016/j.palaeo.2005.10.011. [online] Available from: http://linkinghub.elsevier.com/retrieve/pii/S0031018205005870 (Accessed 9 January 2012)

APPENDIX I

(Supplementary data for article: “Thermochronometric contraints on the development of the Andean topographic front in north central Chile (28.5-32ºS)” from chapter 3)

Single-grain (U-Th-Sm)/He apatite analyses

Sample	Lat/Long (S degrees º)	Elevation (m)	U (ppm)	Th (ppm)	eU	He (nmol/g)	mass (μg)	Ft	radius (μm)	lenght (μm)	Sm (ppm)		Raw Age (Ma)		± 2σ (*) (Ma)		Corr Age (Ma)		± 2σ (Ma)
LE05 a	29.975/ 70.102	2050	16,0	59,4	29,7	0,8	4,4	0,74	56	210	133,9		4,9		0,3		6,6		0,4
LE05 b	29.975/ 70.102	2050	15,1	44,5	25,3	0,6	3,7	0,71	51	166	164,3		4,5		0,3		6,3		0,4
LE05 c	29.975/ 70.102	2050	18,1	76,2	35,6	1,0	2,6	0,72	59	119	177,9		5,3		0,3		7,3		0,5
LE05 d	29.975/ 70.102	2050	13,1	12,5	16,0	0,5	4,4	0,78	71	174	12,3		5,9		0,4		7,5		0,5
		Average	15,6	48,2		0,7		0,74	59		122,1	**Average Age**	**5,1**	Final analitical error	0,2	**Average Age**	**6,9**	Final analitical error	0,2
												Standard Deviation	0,6			Standard Deviation	0,6		
												Final Error	**0,6**			**Final Error**	**0,6**		
LE06	no data																		
LE04	no data																		
LE03 a	29.913/ 70.301	1432	8,0	21,5	12,9	0,5	1,9	0,68	50	115	301,0		6,7		0,6		9,7		0,8
LE03 b	29.913/ 70.301	1432	6,3	25,7	12,2	0,4	1,8	0,70	52	131	301,2		6,3		0,5		9,0		0,8
LE03 c	29.913/ 70.301	1432	5,1	16,4	8,9	0,4	2,3	0,71	57	111	243,9		8,4		0,7		11,7		1,0
LE03 d	29.913/ 70.301	1432	9,0	19,7	13,5	0,5	2,6	0,73	58	133	215,5		6,9		0,5		9,4		0,7
		Average	7,1	20,8		0,5		0,70	54		265,4	**Average Age**	**7,1**	Final analitical error	0,3	**Average Age**	**10,0**	Final analitical error	0,4
												Standard Deviation	0,9			Standard Deviation	1,2		
												Final Error	**0,9**			**Final Error**	**1,2**		
LE02 a	29.846/ 70.392	1208	32,7	82,0	51,5	3,7	2,9	0,73	55	163	182,0		13,2		0,8		18,1		1,1
LE02 b	29.846/ 70.392	1208	18,8	48,4	30,0	1,3	2,8	0,71	50	164	130,4		7,7		0,5		10,8		0,7
LE02 c	29.846/ 70.392	1208	18,0	48,0	29,1	0,6	2,5	0,71	54	128	165,2		3,7		0,3		5,3		0,4
LE02 d	29.846/ 70.392	1208	73,3	162,3	110,6	5,0	0,6	0,59	35	101	496,5		8,2		0,7		13,8		1,1
		Average	35,7	85,2		2,6		0,68	48		243,5	**Average Age**	**8,2**		0,3	**Average Age**	**12,0**		0,4
												Standard Deviation	3,9			Standard Deviation	5,4		
												Final Error	**3,9**			**Final Error**	**5,4**		
LL08 a	30.378/ 70.592	2173	46,7	45,3	57,1	3,1	1,9	0,68	42	161	111,7		9,8		0,7		14,4		1,0
LL08 b	30.378/ 70.592	2173	43,6	50,9	55,3	3,6	2,7	0,73	56	146	146,0		11,9		0,7		16,3		1,0
LL08 c	30.378/ 70.592	2173	38,2	26,1	44,2	2,2	1,1	0,63	39	112	154,4		9,2		0,7		14,5		1,2
LL08 d	30.378/ 70.592	2173	46,2	50,7	57,8	4,1	2,3	0,69	45	155	134,1		13,1		0,8		18,9		1,2
		Average	43,7	43,2		3,3		0,68	46		136,5	**Average Age**	**11,0**	Final analitical error	0,4	**Average Age**	**16,0**	Final analitical error	0,5
												Standard Deviation	1,8			Standard Deviation	2,1		
												Final Error	**1,8**			**Final Error**	**2,1**		
LL07 b	30.765/ 70.713	1182	45,6	97,0	68,0	5,0	1,7	0,71	56	124	516,7		13,4		0,8		18,7		1,2
LL07 c	30.765/ 70.713	1182	37,4	131,6	67,7	6,4	3,5	0,77	68	193	435,4		17,0		0,9		21,9		1,2
LL07 d	30.765/ 70.713	1182	40,7	177,6	81,6	8,0	3,5	0,75	62	169	465,1		17,6		1,0		23,5		1,3
		Average	41,3	135,4		6,5		0,74	62		472,4	Average Age	16,0	Final analitical error	0,4	Average Age	21,4	Final analitical error	0,7
												Standard Deviation	2,3			Standard Deviation	2,5		
												Final Error	2,3			Final Error	2,5		
LL06 a	30.764/ 70.703	1069	3,7	10,1	6,1	0,4	15,8	0,73	61	130	101,1		10,8		0,7		14,7		0,9
LL06 b	30.764/ 70.703	1069	33,7	97,9	56,2	4,3	3,4	0,74	57	187	362,6		13,9		0,8		18,8		1,1
LL06 c	30.764/ 70.703	1069	31,3	110,0	56,6	4,7	3,2	0,75	64	157	396,2		14,9		0,9		19,8		1,1
LL06 d	30.764/ 70.703	1069	58,1	96,6	80,3	7,6	3,8	0,75	59	183	346,3		17,2		0,9		22,8		1,2
		Average	31,7	78,6		4,2		0,74	60		301,5	**Average Age**	**14,2**	Final analitical error	0,4	**Average Age**	**19,0**	Final analitical error	0,5
												Standard Deviation	2,6			Standard Deviation	3,4		
												Final Error	**2,6**			**Final Error**	**3,4**		
LL01 a	31.176/ 70.817	1754	29,0	28,5	35,6	2,5	2,9	0,71	50	162	254,5		12,9		0,8		17,9		1,1
LL01 b	31.176/ 70.817	1754	29,7	33,3	37,4	2,5	3,5	0,73	53	177	247,1		12,1		0,7		16,6		1,0
LL01 c	31.176/ 70.817	1754	19,4	27,5	25,8	2,0	3,9	0,73	51	214	249,7		14,3		0,9		19,5		1,2
LL01 d	31.176/ 70.817	1754	29,5	34,1	37,4	2,9	5,4	0,77	66	201	229,5		14,3		0,8		18,4		1,0
		Average	26,9	30,9		2,5		0,74	55		245,2	**Average Age**	**13,4**	Final analitical error	0,4	**Average Age**	**18,1**	Final analitical error	0,5
												Standard Deviation	1,1			Standard Deviation	1,2		
												Final Error	**1,1**			**Final Error**	**1,2**		
LL02 a	31.170/70.826	1520	22,9	20,2	27,5	1,8	3,1	0,73	53	166	206,1		11,8		0,8		16,2		1,0
LL02 b	31.170/70.826	1520	20,3	22,4	25,5	1,6	3,3	0,73	51	193	197,4		11,7		0,8		16,1		1,0
LL02 c	31.170/70.826	1520	22,4	21,9	27,5	1,9	3,3	0,75	58	168	217,2		12,3		0,8		16,4		1,0
LL02 d	31.170/70.826	1520	22,0	27,4	28,3	2,5	2,8	0,73	56	148	212,4		15,8		1,0		21,6		1,4
		Average	21,9	23,0		1,9		0,73	54		208,3	**Average Age**	**12,9**	Final analitical error	0,4	**Average Age**	**17,6**	Final analitical error	0,6
												Standard Deviation	1,9			Standard Deviation	2,7		
												Final Error	**1,9**			**Final Error**	**2,7**		
LC05 a2	31.464/ 70.807	2097	50,2	68,6	66,0	3,6	2,3	0,67	41	166	273,9		10,0		0,7		14,9		1,0
LC05 b2	31.464/ 70.807	2097	28,1	39,2	37,1	2,4	2,2	0,68	47	123	177,1		12,0		0,8		17,5		1,2
LC05 a	31.464/ 70.807	2097	18,9	31,1	26,1	1,4	2,7	0,72	54	156	299,6		9,7		0,6		13,3		0,9
LC05 b	31.464/ 70.807	2097	10,1	18,0	14,3	0,7	2,1	0,73	62	120	70,8		8,7		0,7		11,9		0,9
LC05 c	31.464/ 70.807	2097	28,1	42,1	37,8	2,9	1,5	0,67	43	135	337,2		13,7		1,0		20,5		1,5
LC05 d	31.464/ 70.807	2097	46,3	59,3	59,9	4,3	2,7	0,73	54	171	216,8		13,0		0,8		17,7		1,0
		Average	30,3	43,1		2,6		0,70	50		229,2	**Average Age**	**11,2**	Final analitical error	0,4	**Average Age**	**16,0**	Final analitical error	0,5
												Standard Deviation	2,0			Standard Deviation	3,2		
												Final Error	**2,0**			**Final Error**	**3,2**		
LC07 a	31.476/ 70.726	2062	0,3	3,7	1,2	0,1	5,3	0,77	71	193	36,1		11,9		1,8		15,3		2,3
LC07 b	31.476/ 70.726	2062	15,8	28,5	22,4	1,6	2,9	0,78	79	153	192,7		12,6		0,8		16,0		1,0
LC07 d	31.476/ 70.726	2062	19,8	20,7	24,6	1,6	5,0	0,79	79	153	66,6		12,0		0,7		15,2		0,9
		Average	12,0	17,6		1,1		0,78	76		98,5	**Average Age**	**12,2**	Final analitical error	0,5	**Average Age**	**15,5**	Final analitical error	0,8
												Standard Deviation	0,4			Standard Deviation	0,4		
												Final Error	**0,5**			**Final Error**	**0,8**		
LC17 a	31.464/ 70.762	1832	4,9	26,4	11,0	0,5	2,4	0,69	46	186	29,8		7,9		1,3		11,5		2,0
LC17 b	31.464/ 70.762	1832	4,0	23,1	9,4	0,4	2,9	0,70	47	210	31,0		7,0		1,3		10,0		1,8
LC17 c	31.464/ 70.762	1832	4,2	21,8	9,2	0,3	3,6	0,74	64	141	26,4		6,5		1,0		8,7		1,4
		Average	4,4	23,8		0,4		0,71	52		29,1	**Average Age**	**7,1**	Final analitical error	0,5	**Average Age**	**10,1**	Final analitical error	1,0
												Standard Deviation	0,7			Standard Deviation	1,4		
												Final Error	**0,7**			**Final Error**	**1,4**		

LC16 a2	31.467/ 70.765		1586	15,9	34,8	23,9	1,7	5,4	0,75	59	191	80,5		13,0		0,8		17,3		1,0
LC16 b	31.467/ 70.766		1586	30,9	40,4	40,2	3,3	1,1	0,71	48	165	127,1		15,1		1,1		21,3		1,6
LC16 c	31.467/ 70.766		1586	27,8	47,8	38,8	2,3	2,1	0,79	75	199	97,6		10,7		0,7		13,5		0,8
		Average		24,9	41,0		2,4		0,75	61		101,7	**Average Age**	**12,9**	Final analitical error	0,4	**Average Age**	**17,4**	Final analitical error	0,7
													Standard Deviation	2,2			Standard Deviation	3,9		
													Final Error	**2,2**			**Final Error**	**3,9**		
LC18 a	31.471/ 70.765		1469	36,5	98,0	59,1	3,0	5,6	0,77	69	193	140,7		9,3		0,5		12,0		0,6
LC18 b	31.471/ 70.765		1469	10,1	33,5	17,8	1,1	2,7	0,69	52	122	159,1		10,6		0,9		15,2		1,3
LC18 c	31.471/ 70.765		1469	30,2	87,8	50,4	3,3	2,7	0,72	54	159	165,6		11,7		0,7		16,2		1,0
LC18 d	31.471/ 70.765		1469	19,0	65,7	34,1	0,9	3,9	0,73	57	157	167,0		4,6		0,3		6,3		0,5
		Average		24,0	71,3		2,1		0,73	58		158,1	**Average Age**	**9,1**	Final analitical error	0,3	**Average Age**	**12,5**	Final analitical error	0,5
													Standard Deviation	3,1			Standard Deviation	4,5		
													Final Error	**3,9**			**Final Error**	**4,5**		
LC08 a	31.505/ 70.800		1341	18,3	88,3	38,6	1,6	1,3	0,65	44	122	246,0		7,6		0,6		11,6		0,9
:LC08 b	31.505/ 70.800		1341	30,1	40,9	39,5	2,1	2,9	0,74	57	156	189,5		9,6		0,6		13,1		0,8
LC08 c	31.505/ 70.800		1341	20,7	40,0	29,9	1,4	4,0	0,76	63	198	177,9		8,5		0,5		11,1		0,7
LC08 d	31.505/ 70.800		1341	32,8	56,3	45,7	2,0	3,6	0,69	44	211	203,5		8,1		0,5		11,6		0,7
		Average		25,4	56,4		1,8		0,71	52		204,2	**Average Age**	**8,4**	Final analitical error	0,3	**Average Age**	**11,8**	Final analitical error	0,4
													Standard Deviation	0,9			Standard Deviation	0,8		
													Final Error	**0,9**			**Final Error**	**0,8**		
LC11 a	31.988/ 70.588		1260	28,4	48,8	39,6	1,4	2,8	0,89	152	309	294,8		6,5		0,4		7,4		0,4
LC11 b	31.988/ 70.588		1260	20,2	64,8	35,1	0,2	5,1	0,88	135	341	180,5		1,3		0,1		1,5		0,1
LC11 c	31.988/ 70.588		1260	8,8	33,4	16,5	0,5	3,1	0,89	147	362	292,5		5,8		0,4		6,5		0,4
LC11 d	31.988/ 70.588		1260	27,3	57,8	40,6	1,4	2,0	0,89	177	281	371,7		6,1		0,4		6,9		0,4
		Average		21,2	51,2		0,9		0,89	153		284,9	**Average Age**	**4,9**	Final analitical error	0,2	**Average Age**	**5,6**	Final analitical error	0,2
													Standard Deviation	2,5			Standard Deviation	2,8		
													Final Error	**2,5**			**Final Error**	**2,8**		
LC15 a	31.889/ 70.732		867	21,2	46,6	32,0	1,0	1,9	0,68	50	107	101,2		5,7		0,4		8,3		0,6
LC15 b	31.889/ 70.732		867	92,7	110,6	118,1	5,7	2,8	0,71	51	137	130,7		8,9		0,5		12,6		0,7
LC15 c	31.889/ 70.732		867	12,8	46,2	23,4	0,8	2,6	0,70	51	138	101,5		6,3		0,4		9,0		0,6
LC15 d	31.889/ 70.732		867	8,1	27,6	14,4	0,7	5,7	0,75	65	153	139,0		9,3		0,6		12,3		0,8
		Average		33,7	57,7		2,1		0,71	54		118,1	**Average Age**	**7,5**	Final analitical error	0,2	**Average Age**	**10,5**	Final analitical error	0,3
													Standard Deviation	1,8			Standard Deviation	2,2		
													Final Error	**1,8**			**Final Error**	**2,2**		
LC01 a2	31.607/ 70.974		1261	46,8	105,1	70,9	9,2	17,4	0,82	83	311	450,8		23,5		1,0		28,5		1,2
LC01 b2	31.607/ 70.974		1261	26,7	55,6	39,5	5,0	11,3	0,80	79	225	390,6		22,9		1,1		28,3		1,4
LC01 a	31.607/ 70.974		1261	25,8	32,8	33,3	3,8	5,5	0,77	61	244	243,2		20,4		1,1		26,5		1,5
LC01 b	31.607/ 70.974		1261	23,2	39,4	32,3	4,6	4,0	0,74	54	199	292,9		25,6		1,5		34,6		2,1
LC01 d	31.607/ 70.974		1261	21,9	35,0	30,0	4,4	5,7	0,77	67	196	240,3		26,8		1,5		34,5		1,9
		Average		28,9	53,6		5,4		0,78	69		323,5	**Average Age**	**23,9**	Final analitical error	0,7	**Average Age**	**30,5**	Final analitical error	0,8
													Standard Deviation	2,5			Standard Deviation	3,8		
													Final Error	**2,5**			**Final Error**	**3,8**		
LC02 a	31.609/ 70.981		1139	24,7	62,8	39,2	5,1	6,3	0,79	91	134	184,1		23,4		1,2		29,5		1,5
LC02 b	31.609/ 70.981		1139	37,6	70,8	53,9	7,6	9,5	0,80	74	260	156,2		25,5		1,2		31,8		1,5
LC02 c	31.609/ 70.981		1139	79,5	76,4	97,0	14,4	9,0	0,81	77	232	172,2		27,0		1,2		33,4		1,5
LC02 d	31.609/ 70.981		1139	52,9	62,8	67,4	10,0	21,7	0,87	118	309	90,0		27,2		1,1		31,3		1,3
		Average		48,7	68,2		9,3		0,82	90		150,6	**Average Age**	**25,8**	Final analitical error	0,6	**Average Age**	**31,5**	Final analitical error	0,7
													Standard Deviation	1,7			Standard Deviation	1,6		
													Final Error	**1,7**			**Final Error**	**1,6**		
LC03 a2	31.612/ 70.987		1010	67,1	71,0	83,4	8,1	2,8	0,68	40	221	463,2		17,6		1,1		25,8		1,6
LC03 b2	31.612/ 70.987		1010	3,9	13,0	6,9	0,6	4,1	0,72	51	197	274,1		15,6		1,2		21,4		1,7
LC03 a	31.612/ 70.987		1010	67,1	78,4	85,1	7,7	3,0	0,74	58	147	274,5		16,5		0,9		22,3		1,2
LC03 b	31.612/ 70.987		1010	40,7	55,5	53,4	5,4	3,4	0,74	53	209	256,4		18,4		1,1		24,9		1,4
LC03 c	31.612/ 70.987		1010	2,5	11,3	5,1	0,3	3,0	0,71	53	167	23,2		9,5		2,3		13,3		3,2
LC03 d	31.612/ 70.987		1010	13,5	27,2	19,8	2,8	5,5	0,77	62	220	223,5		25,6		1,5		33,3		2,0
		Average							0,72				**Average Age**	**17,2**	Final analitical error	0,8	**Average Age**	**23,5**	Final analitical error	1,1
													Standard Deviation	5,2			Standard Deviation	6,5		
													Final Error	**5,2**			**Final Error**	**6,5**		
LC04 a	31.621/ 70.991		836	12,6	39,1	21,6	2,7	4,4	0,77	69	177	223,9		22,5		1,4		29,1		1,8
LC04 b	31.621/ 70.991		836	9,0	24,9	14,8	1,6	5,9	0,77	66	205	235,3		18,8		1,2		24,2		1,5
LC04 d	31.621/ 70.991		836	9,3	37,3	17,9	2,5	3,5	0,75	60	218	313,3		24,4		1,7		32,2		2,2
		Average		10,3	33,8		2,2		0,76	65		257,5	**Average Age**	**21,9**	Final analitical error	0,6	**Average Age**	**28,5**	Final analitical error	1,1
													Standard Deviation	2,9			Standard Deviation	4,0		
													Final Error	**2,9**			**Final Error**	**4,0**		
LC09 c	31.751/ 70.959		590	16,5	50,6	28,1	4,2	4,1	0,72	50	203	167,2	**Average Age**	**26,9**	Final analitical error	1,7	**Average Age**	**37,3**	Final analitical error	2,4
													Standard Deviation				Standard Deviation			
													Final Error	**1,7**			**Final Error**	**2,4**		

APPENDIX II

(Supplementary data for article: "Geochronology of pediments and marine terraces in north-central Chile and their implications for Quaternary uplift in the Western Andes" from chapter 4)

														CRONUS online calculator results									
Parameters used to calculate zero erosion exposure ages														Be					Al				
	Sample name	Latitude (DD)	Longitude (DD)	Elevation (m)	Elv/pressure flag	Thickness (cm)	Density (g cm-2)	[^{10}Be] (atoms/g qz)	+/- (atoms/g qz)	[^{26}Al] (atoms/g qz)	+/- (atoms/g qz)	Thickness scaling factor	Shielding scaling factor	Production rate (muons) (atoms/g/yr)	Production rate (spallation) (atoms/g/yr)	Exposure age (yr)	Internal uncertainty (yr)	External uncertainty (yr)	Production rate (spallation) (atoms/g/yr)	Production rate (muons) (atoms/g/yr)	Exposure age (yr)	Internal uncertainty (yr)	External uncertainty (yr)
Strath Terrace																							
Amalgamated																							
	CHO	-31,595	-71,499	150	std	5,0	2,65	1614198	51521	3885018	267626	0,9597	1	0,188	4,08	419559	14900	43196	27,5	1,572	146505	10854	17469
Individual clasts																							
	CH1	-31,598	-71,500	152	std	10	2,65	2781892	77660	760256	116269	0,9216	1	0,188	3,92	826669	28574	93387	26,45	1,566	28091	4357	5010
	CH2	-31,598	-71,500	152	std	7	2,65	3607014	100129	208443	46882	0,9442	1	0,188	4,02	1120177	41667	136908	27,1	1,57	7449	1682	1803
	CH6	-31,598	-71,500	152	std	10	2,65	2222220	84071	3405824	705028	0,9216	1	0,188	3,92	630554	28044	70224	26,45	1,566	132373	29262	31734
Pediment																							
	CH7	-31,574	-71,400	223	std	3	2,65	2431749	74126	2038718	195859	0,9756	1	0,193	4,39	615895	21983	66388	29,65	1,614	68876	6847	9230
	CH8	-31,574	-71,400	223	std	5	2,65	2231304	43535	10705623	508228	0,9597	1	0,193	4,32	567399	12803	58402	29,16	1,611	437097	25910	54043
	CH10	-31,574	-71,400	223	std	7	2,65	2344881	42194	10501548	374569	0,9442	1	0,193	4,25	612311	12888	63541	28,69	1,608	434773	19353	50937
	CH11	-31,574	-71,400	223	std	5	2,65	1878456	38910	10314422	356142	0,9597	1	0,193	4,32	466203	10877	46879	29,16	1,611	416905	17798	48168
	CH12	-31,574	-71,400	223	std	5	2,65	1364394	23984	7432884	293796	0,9597	1	0,193	4,32	327441	6254	31527	29,16	1,611	282407	12866	31062
	CH13	-31,574	-71,400	223	std	10	2,65	1514439	26914	8949593	333793	0,9216	1	0,192	4,15	383031	7503	37427	28,01	1,603	367763	16523	41879
Average Pediment																							
	CHP	-31,574	-71,400	223	std	6	2,65	1960871	41611	8323798	343731	0,9519	1	0,193	4,29	493915	11887	50091	28,93	1,609	325157	15820	36847
Rasa	MS18-1	-31,152	-71,661	120,0	std	5	2,7	1905192	34348	-	-	0,9590	0,9998	0,186	3,95	523799	10796	53116	-	-	-	-	-
	MS18-2	-31,152	-71,661	121,0	std	5	2,7	1992154	43215	-	-	0,9590	0,9998	0,188	3,95	550823	15705	57273	-	-	-	-	-
	MS18-4	-31,152	-71,661	120,0	std	5	2,7	2744604	48954	-	-	0,9590	0,9998	0,187	3,95	806940	17725	88132	-	-	-	-	-

Explanation of $^{26}Al/^{10}Be$ ratios.

We tried to model data in order to explain the low $^{26}Al/^{10}Be$ ratio from several samples. To explain low ^{26}Al content, the model must incorporate a long stay at depth of the clasts. We modelled the $^{26}Al/^{10}Be$ ratio following a 3-stage clast history: (1) First, the clast is exhumed with erosion rate e and production P_alt., (2) Then it is stocked for a long time (T) in a sediment pile at depth z (100 m in the model). This allows the $^{26}Al/^{10}Be$ ratio to diminish, (3) Finally, it is removed from the sediment pile and stayed during theta=300-500 kyr at its current position, on top a terrace surface, which has been eroded at a rate E. Results are drawn in Figure 4. This figure shows that the very low ^{26}Al content in samples from the terrace cannot be geologically explained.

Parameter	Stage	Symbol	Range of variation
Initial erosion rate	1	e	0-10^{-4} m/yr
Production where exhumed	1	P_alt	Fixed to 25 at/g/yr
Time stocked	2	T	0-10 My
Depth into the alluvium	2	z	Fixed to 100 m
Age of present-day formation	3	Theta	300-500 ky
Erosion of present-day formation	3	E	Fixed to 1.10-6 m/yr

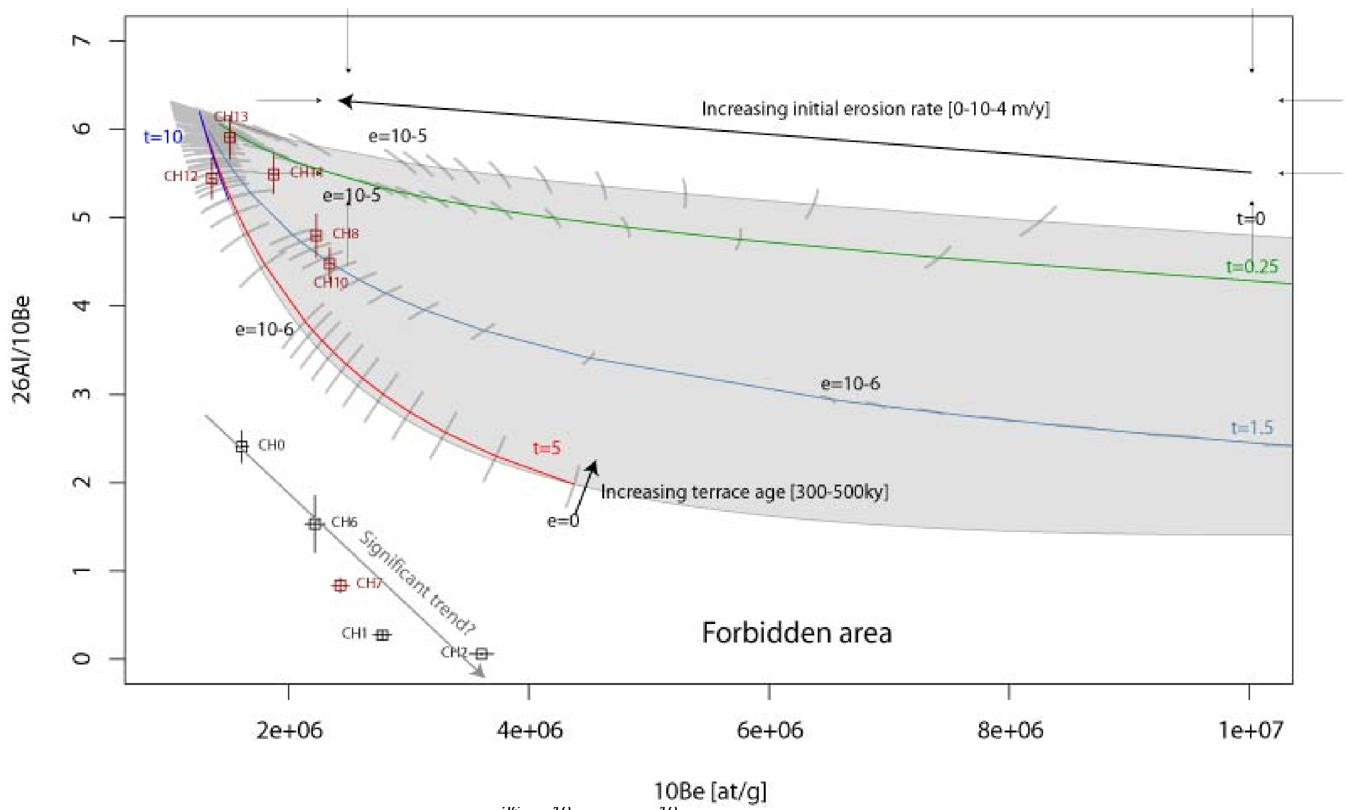

Figure 4. Graph illustrating the $^{26}Al/^{10}Be$ vs. ^{10}Be content. Theoretical values must fall into the grey-shaded area. Coloured lines represent different stocking times: 0, 0.25, 1.5, 5 and 10 My (black, green, blue, red and dark blue respectively). The position along the line is defined by the initial erosion rate (the higher the erosion rate, the more to the left the position); some of them are indicated in m/yr. The grey segments represent the evolution trend for varying terrace age (300 to 500 ky): An increase of the age leads to a greater $^{26}Al/^{10}Be$. Samples from the present study are plotted (CH0, CH1, CH2, CH6, CH7, CH8, CH10, CH12, CH13, CH14).

We have also compared samples from the pediment with the model, although there is no evidence of a deep alluvial cover on the pediment and the samples are not rounded, this suggests that exhumation occurred in the pediment itself. Even for such an extreme model, the very low ^{26}Al concentration of sample CH7 does not fit in the model. Samples with low ^{26}Al content (CH0, CH1, CH2, CH6, CH7) show a decrease of ^{26}Al/^{10}Be while the ^{10}Be concentration increases. This might reflect a progressive loss of ^{26}Al due to weathering or other processes acting near the surface. Further work and data are required to give an explanation to the ^{26}Al depletion.